PROCEEDINGS OF THE ISOTOPE SEPARATOR ON-LINE WORKSHOP

HELD AT
BROOKHAVEN NATIONAL LABORATORY
OCTOBER 31-NOVEMBER 1, 1977

R.E. CHRIEN, Editor

BROOKHAVEN NATIONAL LABORATORY
ASSOCIATED UNIVERSITIES, INC.
UNDER CONTRACT NO EY-76-C-02-0016 WITH THE
UNITED STATES DEPARTMENT OF ENERGY

DISCLAIMER

CONF-771078--

BNL 50847

PROCEEDINGS OF THE ISOTOPE SEPARATOR ON-LINE WORKSHOP

HELD AT
BROOKHAVEN NATIONAL LABORATORY
OCTOBER 31-NOVEMBER 1, 1977

R.E. CHRIEN, Editor

BROOKHAVEN NATIONAL LABORATORY
UPTON, NEW YORK 11973

NOTICE

Printed in the United States of America
Available from
National Technical Information Service
U.S. Department of Commerce
5285 Port Royal Road
Springfield, VA 22161
Price: Printed Copy $12.50; Microfiche $3.00

July 1978 250 copies

WORKSHOP ON ISOTOPE SEPARATOR ON-LINE SYSTEMS

Brookhaven National Laboratory, Upton, New York 11973

October 31-November 1, 1977

Foreword

A Workshop on Isotope Separator On-Line (ISOL) Systems was held at Brookhaven Monday, October 31 and Tuesday, November 1, 1977. The workshop was the initial step in a review leading to the establishment of an ISOL system for the study of mass separated fission products at the BNL High Flux Beam Reactor.

This system is called "TRISTAN-II", and is virtually identical to the separator which had been operational at the Ames Research Reactor up to its shutdown at the end of 1977. The review has led to a positive decision concerning the installation of TRISTAN at the HFBR, and the installation will be completed before the summer of 1979.

In this set of proceedings are contained most of the papers presented at the workshop. They cover a wide range of topics including delayed neutron emission, tunable dye-laser spectroscopy, perturbed angular correlations, solid state applications, nuclear theory, and nuclear spectroscopy. It is hoped that they will convey to the reader a feeling for the exciting new physics research opened up by ISOL systems.

We are indebted to John C. Hill, Iowa State University, for his energetic leadership in establishing the planning for the workshop and in contacting prospective speakers. The success of the meeting was further enhanced by the capable Public Relations staff at Brookhaven in making arrangements for the workshop, and by the expert assistance of Mrs. Cora Feliciano.

Robert E. Chrien

Robert E. Chrien

Schedule for BNL Workshop on ISOL Systems

Sunday, October 30, 1977

Registration 2:00 p.m. Brookhaven Center

Reactor Tour 2:30 p.m. from Brookhaven Center

Evening Reception 6:00 p.m. Brookhaven Center

Chemistry Conference Room

Monday, October 31, 1977

		Page
Greeting and Conference Details	9:00-9:15	
Session Chairman: R. Naumann, Princeton University		
"TRISTAN I - Techniques, Capabilities and Accomplishments" W. L. Talbert, Jr. (LASL)	9:15-9:45	1
"TRISTAN II - Extension of Capabilities to Non-Gaseous Fission Products" F. K. Wohn (Ames - Iowa State)	9:50-10:20	23
"Initial Results with the Berkeley On-Line Mass Separator - RAMA" J. Cerny (LBL - Berkeley)	10:30-11:00	57
"Studies of Fission Fragments Using the Gas Filled Recoil Separator JOSEF" T. A. Khan (KFA - Jülich)	11:10-11:40	67
"Recent Results from Delayed-Neutron Studies"† S. G. Prussin (Berkeley)	11:50-12:20	--
Lunch		
Session Chairman: G. Friedlander, BNL		
"Current Research on Delayed Neutron Emission at the SOLAR Facility" P. L. Reeder (Battelle Northwest)	2:00-2:30	87
"Applications of Fission-Product Decay Data" C. W. Reich (INEL)	2:40-3:10	109
"High-Resolution Hyperfine Spectroscopy Using Dye Lasers"† G. W. Greenlees (Minnesota)	3:20-3:50	--
"The UNISOR Project: Techniques and Results" E. H. Spejewski (ORNL)	4:00-4:30	149
User's Group Discussion R. E. Chrien (BNL) Panel (R. E. Chrien, J. C. Hill, F. K. Wohn)	5:00-5:15 5:15-6:00	
Cocktails	6:00	
Dinner	7:30	

† Manuscript not available.

Tuesday, November 1, 1977

† Manuscript not available.

†† Not presented at meeting.

OPENING REMARKS

R. A. Naumann

Electromagnetic isotope separation apparatus has been playing an important role in experimental nuclear physics for over sixty five years. Today this technique is permitting the nuclear investigator to begin the study of the large class of nuclei lying near the nucleonic binding limits. With the aid of recently developing experimental advances in mass separators themselves as well as related areas such as optical and solid state nuclear hyperfine spectroscopy, nuclear orientation methods and nuclear mass determinations, it is now possible to determine properties of the very unstable nuclei with a detail fairly recently available only for the stable species. These studies are yielding important information in such diverse areas as charge independence of nuclear forces, beta decay sum rules, new types of radioactivity and new regions of nuclear deformation.

The upcoming sessions include reports concerning several important and differing approaches to the problem of isolating and studying the shortest lived nuclei.

TITLE: TRISTAN I - TECHNIQUES, CAPABILITIES AND ACCOMPLISHMENTS

AUTHOR(S): W. L. Talbert, Jr.

SUBMITTED TO: Ames - Brookhaven Workshop on ISOL Systems, Brookhaven National Laboratory, Upton, New York, October 31 - November 1, 1977.

TRISTAN I - Techniques, Capabilities and Accomplishments

W. L. Talbert, Jr.
Los Alamos Scientific Laboratory
Los Alamos, NM 87545

ABSTRACT

Following a brief description of the TRISTAN facility, the techniques developed for on-line nuclear spectroscopy of short-lived fission products, the studies possible, and the activities studied are presented. All journal publications relating to the development of the facility and the studies carried out using it are referenced, and co-workers identified.

I. INTRODUCTION

In 1965, the Ames Laboratory research reactor became available for experiments in nuclear, materials, and chemical sciences. In 1966, the TRISTAN on-line isotope separator facility became operational, with the observation of mass-separated gaseous fission products in October. For nearly ten years, the TRISTAN facility (to be referred to below as TRISTAN I) set the stage for a series of successful spectroscopic studies and developments of techniques. On July 1, 1976, a new in-beam ion source was successfully operated which gave rise to non-gaseous fission products, thus extending significantly the coverage of short-lived neutron-rich nuclei. With this new approach, the TRISTAN facility became known as TRISTAN II.

Due to funding priorities in the Division of Physical Research of ERDA (now DoE), operation of the Ames Laboratory research reactor will cease at the end of calendar year 1977. Thus, the question of continuance of the existing research facilities at the reactor, such as TRISTAN II, arises and constitutes the underlying theme of this workshop. We are thus participating in discussions which are critical to the consideration of the future of studies possible with TRISTAN II, relocated to the High Flux Beam Reactor at Brookhaven.

There will be three talks on TRISTAN; this one, on the past achievements, both technical and scientific, of TRISTAN I; Fred Wohn will discuss the future promises of a continuance of TRISTAN II; and John Hill will speak to the studies which have been made during the short span of TRISTAN II.

Rather than repeat much of the information which has appeared in print, I would like to present a complete listing of pertinent references and discuss some of the philosophy behind the development of the capabilities and studies with TRISTAN I. The references are divided into system description and instrumentation development,[1-11] and the studies carried out,[12-48] essentially in chronological order except for the unpublished work (which, hopefully, will make its way into print). The definitive description of the system is Ref. 10.

I should like to emphasize at the outset that the development of the TRISTAN facility has been the product of the efforts of many people, and I will acknowledge their contributions now rather than at the end of my talk, to underscore my dependence upon them for the activities which resulted in the highly productive program at TRISTAN I. Table I illustrates what has not been properly appreciated up to now, in my opinion: that the number of students who received their training and did their research, compared to the number of dedicated staff (which at any one time numbered about 4 FTE's), is very large indeed.

II. TECHNIQUES ASSOCIATED WITH TRISTAN I

The initial concepts envisioned with TRISTAN were derived from two facts of the ^{235}U thermal fission process, both observable from the fission yields shown in Fig. 1. First of all, when viewing the mass yield profile, there are essentially two well-defined mass regions for study, and these regions are separated by roughly a chemical period. Secondly, when viewing the chemical yield profile, the gaseous products, Kr and Xe, both have yields close to the peak chemical yields. The accented individual chemical yields for Kr and Xe illustrate, moreover, that decay products of the high-yield gaseous activities would be produced in higher abundance through decay than by direct fission yield.

Given these facts in combination with the unique physical properties of the noble gases (high volatility and low chemical activity), the development of a system which would make available the gaseous fission products would not only be highly tractable, but also result in a scientifically significant coverage of neutron-rich activities. Coupled with these considerations is the need to concentrate on the techniques which are to be employed in looking at short-lived activities at an on-line facility. The latter effort was needed to be able to anticipate and address the procedures necessary for on-line studies of short-lived

TABLE I. List of co-workers

STAFF: 2 years or more

J. R. McConnell
F. K. Wohn
W. C. Schick, Jr.
J. C. Hill
K. L. Malaby
A. R. Landin
M. A. Cullison
J. J. Eitter
G. H. Carlson
J. C. Pacer

Less than 2 years

B. Anderberg
K. B. Nielsen
G. M. Day
A. B. Tucker
B. R. Erdal

STUDENTS:

C. L. Duke
D. Thomas
J. T. Larsen
G. H. Carlson
D. I. Haddad
J. E. Solecki
J. R. Clifford
R. J. Olson
J. W. Cook
J. K. Halbig
J. H. Norman
E. A. Henry
J. J. Eitter
J. P. Adams
M. A. Lee
J. A. Morman
R. S. Weinbeck
G. J. Basinger
L. J. Alquist
R. L. Bunting
M. D. Glascock
W. R. Western
R. L. Gill
C. J. Bischof
G. A. Sheppard
K. A. Burke
J. F. Wright

COLLABORATORS:

R. J. Hanson
H. H. Hsu
S. T. Hsue
C. L. Duke
D. M. Roberts
J. W. Layman
A. F. Voigt

VISITORS:

P. Paris
H. K. Carter
J. P. Zirnheld
J. Lin
T. A. Khan
S. Amiel
J. C. Wells, Jr.

ENCOURAGEMENT AND ADVICE:

I. Bergström
A. Kjellberg
S. Borg
G. Rudstam
R. D. Macfarlane
R. A. Naumann
S. Raman
B. J. Dropesky
G. Herrmann
M. E. Bunker
A. A. Bartlett
P. G. Hansen
S. Sundell
R. A. Meyer
G. B. Holm

SPONSORSHIP:

G. L. Rogosa (AEC and ERDA)

F. H. Spedding
D. J. Zaffarano
R. S. Hansen
} Ames Laboratory and Iowa State University

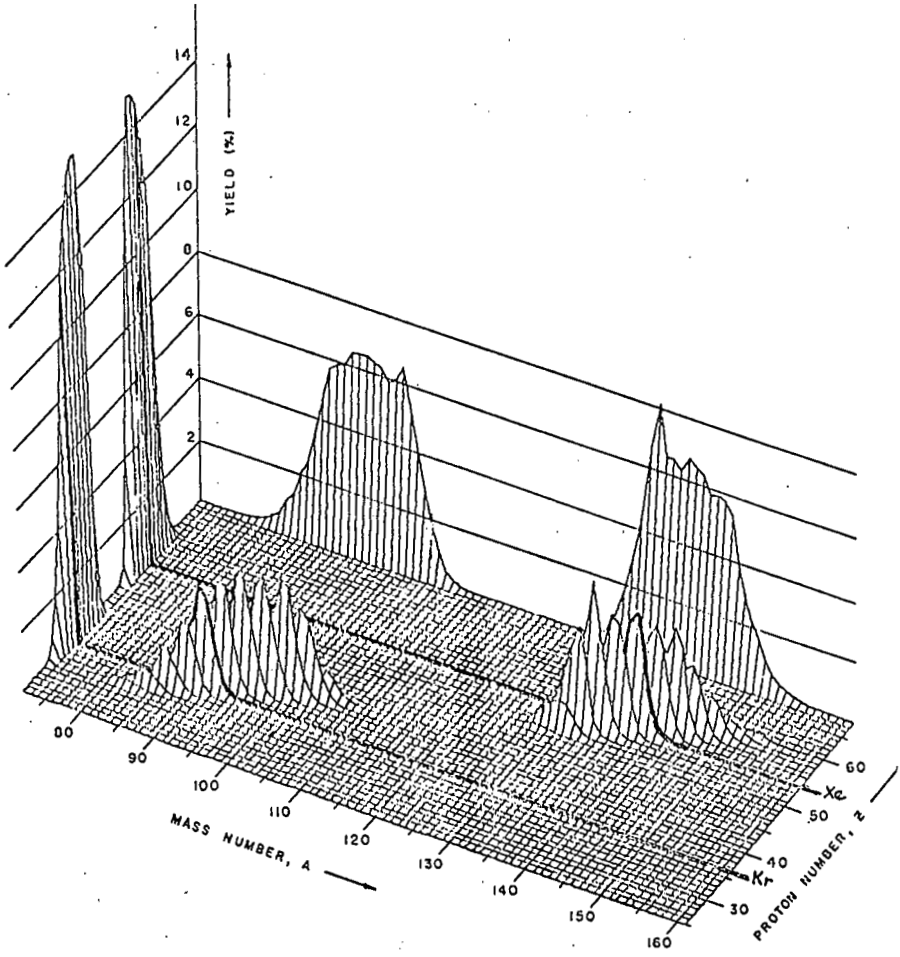

Figure 1. Isometric view of the yields for thermal fission of ^{235}U.

nuclei where the daughter activities are also short-lived.

The resulting system configuration is shown in Fig. 2, which shows the layout of TRISTAN I as it was used from 1969 until 1976. A detailed description of the system is given in Ref. 10; for the purpose of this talk, a short description will suffice. The sample of ^{235}U (in the form of the stearate or tetra-fluoride) was placed in a neutron beam from the reactor, of nominal diameter 5 cm and flux 3×10^9 n/cm^2/sec. The sample size was nominally 10 g of ^{235}U. Operation of the sample chamber and transport line at ambient room temperature resulted in the availability of predominantly the Kr and Xe fission products, with small amounts of Br and I. The two-stage separation provided by the separator followed by the switch magnet resulted in mass separation factors which were not measurable; that is, despite an estimated detection sensitivity of 10^7 to 1, no (A+1) activity could be detected at the (A) deposit after the switch magnet. The same statement did not hold true for (A-1) contaminants; the presence of KrH^+ and XeH^+ ions represented a real contribution to the deposit under study, and resulted in a (A-1) contamination level which was significant in the higher-mass studies. The combination of lower fission yield and shorter half-life (resulting in larger loss in transport) for the high-mass products compared to the (A-1) activities, resulted in an enhancement of the KrH^+ and XeH^+ deposition rates for these studies, even though the hydride activities were typically 10^{-4} the ionic activities for the same isotope.

Despite the above problem of hydride contamination, the principal concern in the studies of short-lived fission products was that of the interference from short-lived daughter activities. Accordingly, considerable effort was made in the development and analysis of moving tape collector technology, which provided a mechanical means of discrimination between activities of an isobaric decay chain. The principle of the moving tape collector can be seen in Fig. 3. In the collection of the separated ion beam, the ions are actually imbedded in the collecting surface. If this surface should be a tape which is capable of motion, the motion will carry the deposit from one place

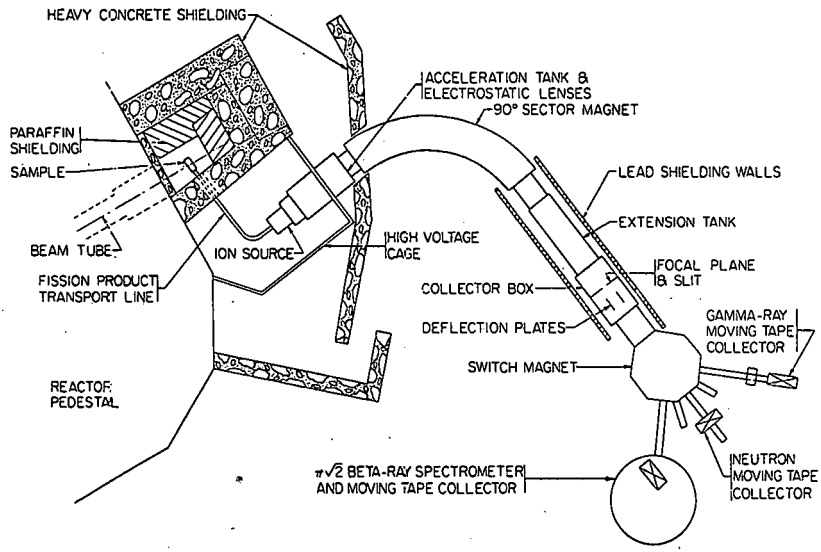

Figure 2. Layout of the TRISTAN I facility.

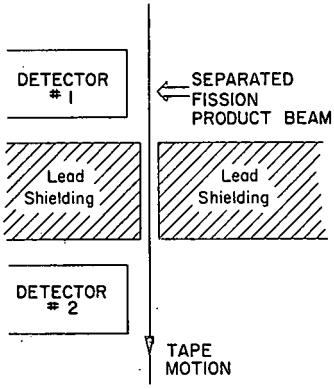

Figure 3. Moving tape collector principle.

to another. In considering the situation pictured in Fig. 3, with the tape in continuous motion, only the shortest activities in the deposition will decay before being moved into the lead shielding and away from detector #1. Thus, detector #1 will not see the longer-lived activities in the deposit. On the other hand, by the time the deposit has moved through the lead shielding to detector #2, the shortest-lived activities have decayed away, leaving only the longer-lived activities to be viewed by detector #2. In an isobaric decay chain of a Kr or Xe separated isotope deposit, the parent decays (Kr or Xe) are generally the shortest-lived activities and the daughter activities which build in as the parent decays are longer-lived. Detector #1 can thus be made sensitive to the parent decays and detector #2 to the daughter decays by appropriate choice of tape speed. We have found that the discontinuous motion of the tape is a preferred mode of operation, with selection of deposition, delay, and data acquisition times to optimize the temporal conditions for a selected activity within the isobaric decay chain.[4]

The moving tape collector principle has been applied to all the studies carried out. The "Gamma-Ray Moving Tape Collector" shown on the layout (Fig. 2) has been designed to accommodate electron spectrometers, as well as angular correlation detectors. Separate moving tape collectors were constructed for use with a neutron spectrometer and a $\pi\sqrt{2}$ spectrometer.

Among the other techniques developed for TRISTAN, without elaboration, are: the on-line $\pi\sqrt{2}$ beta-ray spectrometer,[8] an absolute beta counter for ground-state branching,[37] and a multiple-detector angular correlation detector array.[9] In addition, beta-ray and electron spectrometers were developed for decay energy and conversion electron studies.[6,30] Taken in total, the complement of experimental techniques available at TRISTAN represented perhaps the most complete spectroscopic capability at a single experimental facility. Still, the use of the facility was mainly limited by the available manpower.

III. CAPABILITIES

While the discussion on techniques gives an indication of the capabilities which result, a few comments can be made using the help of the stylized gamma-ray spectrum and decay scheme shown in Figs. 4 and 5, respectively. Apologizing in advance for being simplistic to those in the audience who are accomplished level scheme builders, let me explain that the analysis of the spectrum shown in Fig. 4 reveals that five gamma rays are emitted in the decay of the observed activity, and that these five gamma rays can be placed into the level scheme of Fig. 5 by using the energy-sum relationships evident from the analysis. The placement of γ_2 and γ_4 can be verified, in a general study, by showing them in coincidence with γ_1 (assuming a very short lifetime for the first excited state).

The existence of the beta branches, including that to the ground state, can be inferred from the intensity imbalances for feeding and depopulating the excited states, as observed from the gamma-ray intensities. For the ground-state branch, an additional piece of information is required, the total beta decay intensity (obtainable using a 4π beta detector). As frequently happens for short-lived fission products, the decay energy may exceed the neutron binding energy for the daughter nucleus. In this case, direct neutron emission may occur after beta decay, even in competition with gamma de-excitation. This phenomenon, referred to as delayed neutron emission, is of great interest from reactor control studies and also from the point of view that such emission constitutes observable information on the nature of highly excited states in nuclei.

Then, in view of the decay scheme shown in Fig. 5, the capabilities which should be covered are: half-life determination, delayed neutron emission, decay energy, ground-state beta branching, conversion coefficient measurements (to more fully characterize the de-excitation parameters), gamma-ray spectroscopy, coincidence studies, level lifetimes, and angular correlation studies (to measure de-excitation spin sequences). All of these capabilities were available at TRISTAN. The only nuclear

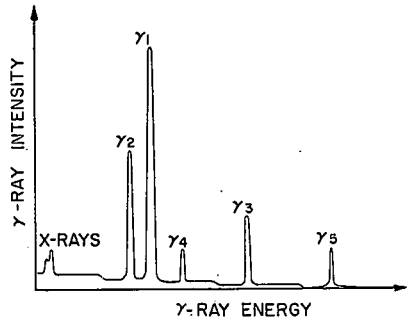

Figure 4. A simple gamma-ray spectrum.

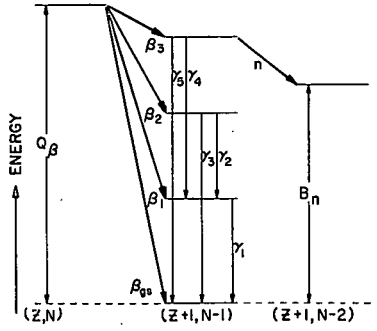

Figure 5. Generic decay scheme of a short-lived neutron rich nuclide.

parameters not unambiguously determined with these capabilities are the spins and moments of the ground states, for which a technique employing the nuclear hyperfine interaction seems feasible and is, indeed, under development. The determination of decay energy could also be accomplished using an on-line high-resolution mass spectrometer for direct mass measurement of the ground-state. It should be noted, however, that development of the latter two techniques is considerably more involved than for those at hand, with larger manpower resources inevitably required.

A word of caution: In considering the continuance of TRISTAN II, it would be advisable to install a further capability, essentially unrelated to the techniques described thus far. This is the on-line, interactive analysis capability afforded through an expanded-memory minicomputer system. If TRISTAN I had any real shortcomings, it was in the time required to analyze the data. An interactive analysis system, on-line or off-line, would have reduced the time spent on gaseous fission products considerably.

The last capability which should be required of a general facility to study neutron-rich fission products is that of greater coverage of the available elements than just the gaseous products. Although TRISTAN II represents just that capability, I would like to unveil the fact that as far back as 1968, I had attempted to summon additional support for the facility to investigate the possibilities for increased elemental availability. Given the lack of such support, we proceeded to do the best we could with the activities available until, about 1974, it was evident that we had to invest our current effort into the developments which eventually proved successful two years later. This was at the expense of completing the possible studies with the gaseous activities, and is at least partly responsible for the unpublished status of some of the studies which were carried out.

A summary of the capabilities, as well as the studies carried out, is shown in Table II. References are provided for the activities and studies made, and the techniques employed are described in the individual cases.

TABLE II. Spectroscopic capabilities and studies at TRISTAN

Type of study	Spectroscopic technique	Activities studied	References*
$T_{½}$	Ge(Li) spectrum multiscaling	^{85m}Kr; ^{89}Kr,Rb; ^{90}Kr,Rb; ^{91}Kr,Rb; ^{92}Kr,Rb; ^{93}Kr,Rb,Sr; (^{94}Kr,Rb); ^{136}I; ^{137}Xe; ^{138}Xe,Cs; ^{139}Xe,Cs; ^{140}Xe,Cs; ^{141}Xe,Cs,Ba; ^{142}Xe,Cs,Ba	14, 18, 41
P_n	BF_3 long counter	^{92}Kr,Rb; ^{93}Kr,Rb; ^{141}Xe,Cs; ^{142}Xe,Cs	12, 13
Q_β	$\pi\sqrt{2}$ mag. spect.	^{85m}Kr; ^{87}Kr; ^{88}Rb; ^{89}Sr; ^{91}Sr	17, 18, 22 24, 43
	Plastic scint.-Ge(Li)	^{88}Kr,Rb; ^{89}Kr; ^{90}Kr,Rb; ^{91}Kr,Rb; ^{92}Kr,Rb,Sr; ^{93}Kr,Rb; ^{138}Xe,Cs; ^{139}Xe,Cs; ^{140}Xe,Cs; ^{141}Xe,Cs,Ba; ^{142}Xe,Cs	25, 26
β_{gs}	$\pi\sqrt{2}$ mag. spect.	^{85m}Kr; ^{87}Kr; ^{91}Sr	18, 22, 24
	4π plastic scint.	^{88}Kr,Rb; ^{89}Kr,Rb; ^{90}Kr,Rb; ^{91}Kr,Rb	37
	Ge(Li) relative activity	^{89}Kr; ^{91}Kr,Rb; ^{92}Kr,Rb; ^{138}Xe,Cs; ^{139}Xe,Cs	21, 23, 28 36, 44
ICC	$\pi\sqrt{2}$ mag. spect.	^{85m}Kr; ^{88}Kr; ^{90}Kr,Rb; ^{91}Kr,Rb,Sr; ^{92}Kr	18, 24, 32 43
	Si(Li)	^{140}Xe	30
	LEPS	^{91}Kr,Rb	32
γ	Ge(Li) and LEPS	^{85m}Kr; ^{88}Kr,Rb; ^{89}Kr,Rb; ^{90}Kr,Rb; ^{91}Kr,Rb,Sr; ^{92}Kr,Rb,Sr,Y; ^{93}Kr,Rb,Sr,Y; (^{94}Kr,Rb); ^{136}I; ^{137}I,Xe; ^{138}I,Xe,Cs; ^{139}Xe,Cs; ^{140}Xe,Cs; ^{141}Xe,Cs,Ba,La; ^{142}Xe,Cs,Ba,La; ^{143}Ba; (^{143}Xe,Cs,La); (^{144}Xe,Cs)	15, 15, 18 19, 20, 21 23, 27, 28 29, 35, 36 38, 39, 40 42, 44, 45 46, 48

TABLE II. (Continued)

Type of study	Spectroscopic technique	Activities studied	References*
$\gamma\gamma$	Ge(Li)-Ge(Li)	^{88}Kr,Rb; ^{89}Kr,Rb; ^{90}Kr,Rb; ^{91}Kr,Rb,Sr; ^{92}Kr, Rb,Sr; ^{93}Kr,Rb,Sr,Y; ^{136}I; ^{137}I,Xe; ^{138}I,Xe,Cs; ^{139}Xe,Cs; ^{140}Xe,Cs; ^{141}Xe,Cs,Ba,La; ^{142}Xe,Cs,Ba,La; ^{143}Ba	15, 16, 19 20, 21, 23 27, 28, 29 35, 36, 38 39, 40, 41 42, 44, 45 46, 48
$\gamma(t)$	LEPS-plastic scint.	^{91}Kr,Rb; ^{136}I; ^{140}Xe; ^{141}Xe	26, 31
$\gamma\gamma(\theta)$	Ge(Li)-NaI(Tl)	^{90}Rb; ^{138}Cs; ^{140}Xe,Cs; ^{142}La	9, 33, 34 47

*Activities in parentheses have been studied, but preliminary data have not been analyzed.

IV. ACCOMPLISHMENTS

An idea of the scope of the accomplishments of TRISTAN I, as well as the capabilities, may be obtained from studying Table II. There yet remain some areas of study which render the picture incomplete; in particular, the ground-state beta branching intensities are unfortunately not available for mass numbers higher than 91, from direct measurement. What studies are presented, however, represent detail which is unlikely to be improved upon for the foreseeable future. The results contained in the references are, in many cases, significant improvements over prior studies, and for other activities, are the only definitive results available.

Another way of summarizing the accomplishments from the use of TRISTAN I is to present the nuclei studied on a portion of the chart of nuclides. This is done in Figs. 6 and 7, in combination with the fission chain yield and an indication of the approximate half-life regions. The shaded boxes represent the activities studied at TRISTAN I. It is obvious that there are many high-yield fission products not studied at TRISTAN I, and that the as yet unstudied regions represent a challenge for years to come. It is heartening that an approach such as TRISTAN II promises to fill in the gaps of our knowledge of short-lived nuclei produced in fission, given the resources and manpower for the near-term future.

To conclude this brief, yet comprehensive, review of TRISTAN I, I would like to inject a personal note. It was my great pleasure and honor to have been a part of the scientific strides made through the development of this facility. I appreciate especially the willing and effective support I received from my co-workers during the time of development and operation of TRISTAN. It saddens me to see the work halted, however momentarily it may turn out to be, in response to fiscal pressures which are imposed just at the instant that the facility is responding fully to its potential. I can only hope that the value of the past efforts will continue to be realized by the community so that the potentials which have been built up are not forfeited.

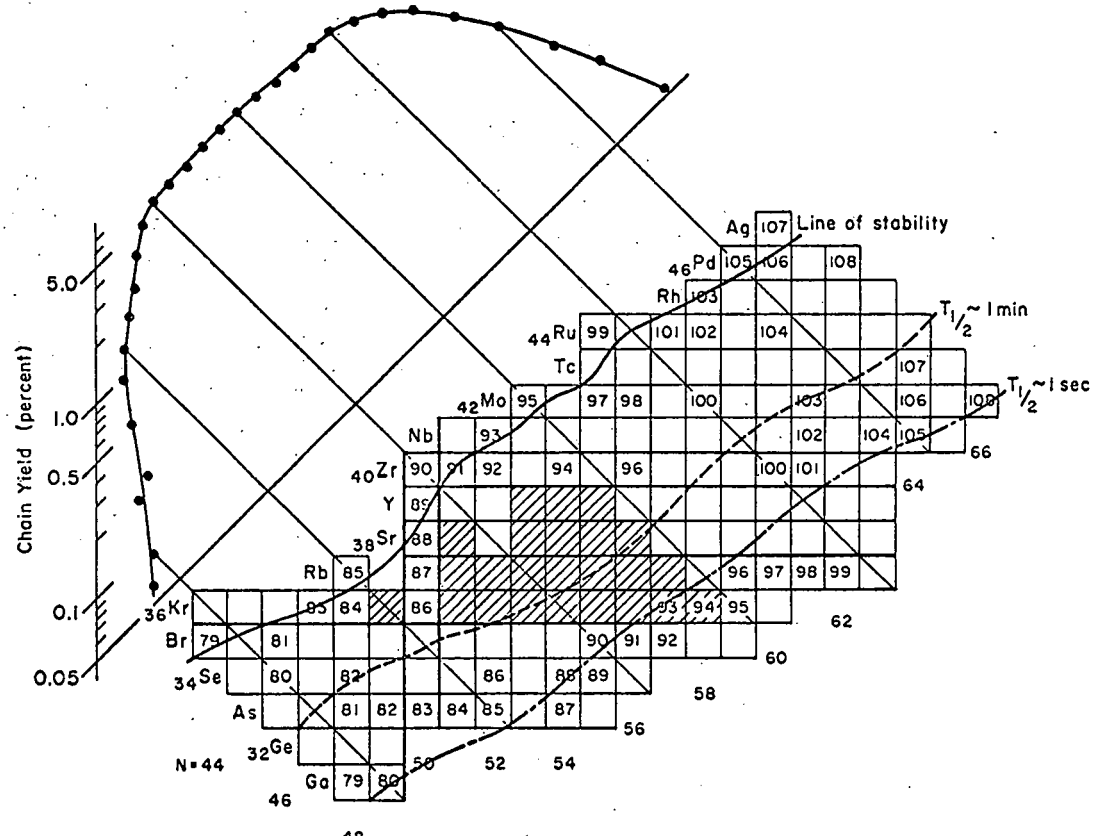

Figure 6. Partial chart of nuclides showing low-mass fission product region. Mass chain yields are also indicated. The shaded boxes are decays observed at TRISTAN I.

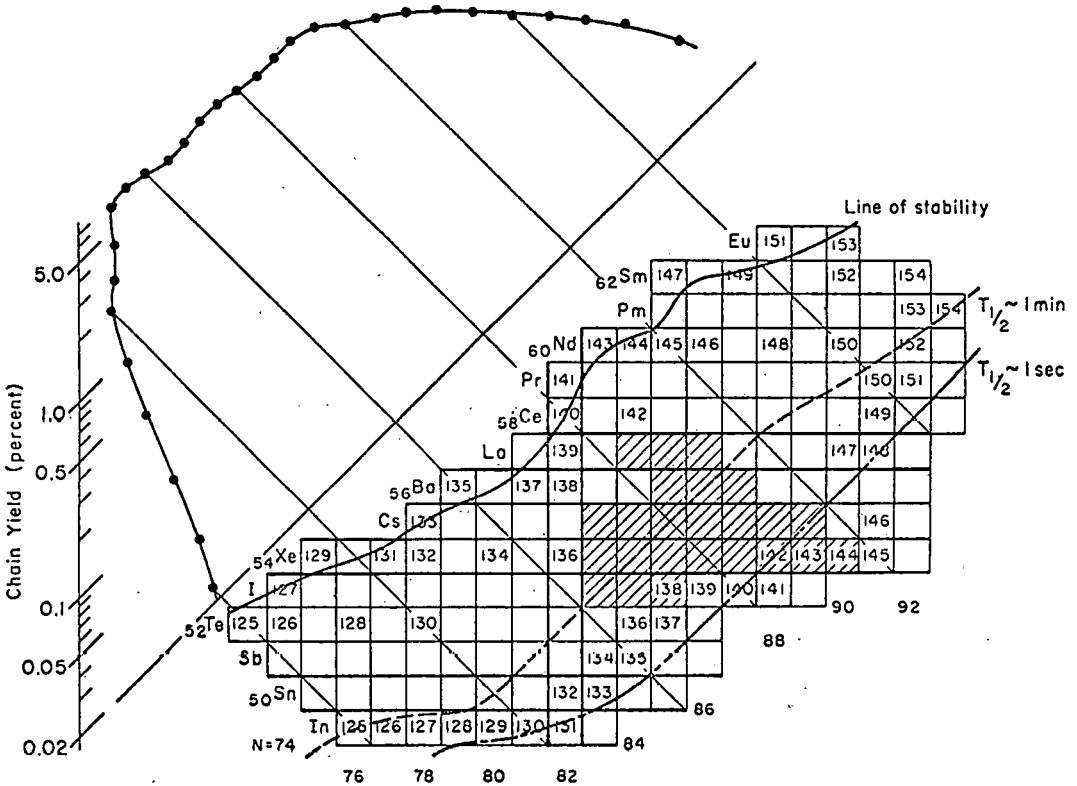

Figure 7. Partial chart of nuclides showing high-mass fission product region. The shaded boxes are decays observed at TRISTAN I.

References

1. W. L. Talbert, Jr. and D. Thomas, Nucl. Instrum. Methods 38, 306(1965).
2. W. L. Talbert, Jr. and J. R. McConnell, Arkiv for Fysik 36, 99(1967).
3. J. T. Larsen, J. W. Layman, and W. L. Talbert, Jr., Nucl. Instrum. Methods 55, 333(1967).
4. J. H. Norman, W. L. Talbert, Jr., and D. M. Roberts, USAEC Report IS-1893(1968).
5. J. T. Larsen, W. C. Schick, Jr., W. L. Talbert, Jr., and D. I. Haddad, Nucl. Instrum. Methods 69, 229(1969).
6. F. K. Wohn, J. R. Clifford, G. H. Carlson, and W. L. Talbert, Jr. Nucl. Instrum. Methods 101, 434(1972).
7. W. L. Talbert, Jr., J. R. McConnell, J. K. Halbig, and G. A. Sleege, Proc. 8th International Conference on Low Energy Ion Accelerators and Mass Separators, Skovde, Sweden, 12-15 June, 1973.
8. J. K. Halbig, F. K. Wohn, and W. L. Talbert, Jr., Rev. Sci. Instrum. 45, 789(1974).
9. G. J. Basinger, W. C. Schick, Jr., and W. L. Talbert, Jr., Nucl. Instrum. Methods 124, 381(1975).
10. J. R. McConnell and W. L. Talbert, Jr., Nucl. Instrum. Methods 128, 227(1975).
11. W. L. Talbert, Jr., F. K. Wohn, A. R. Landin, J. C. Pacer, R. L. Gill, M. A. Cullison, G. A. Sheppard, K. A. Burke, K. L. Malaby, and A. F. Voigt, Nucl. Instrum. Methods 139, 257(1976).
12. W. L. Talbert, Jr., A. B. Tucker, and G. M. Day, Phys. Rev. 177, 1805(1969).
13. W. L. Talbert, Jr., Phys. Rev. C 1, 1135(1970).
14. G. H. Carlson, W. C. Schick, Jr., W. L. Talbert, Jr., and F. K. Wohn, Nucl. Phys. A125, 267(1969).
15. J. D. Knight, O. E. Johnson, A. B. Tucker, and J. E. Solecki, Nucl. Phys. A130, 433(1969).
16. W. L. Talbert, Jr., F. K. Wohn, H. H. Hsu, and S. T. Hsue, Nucl. Phys. A146, 149(1970).
17. F. K. Wohn and W. L. Talbert, Jr., Nucl. Phys. A146, 33(1970).
18. F. K. Wohn, W. L. Talbert, Jr., and J. K. Halbig, Nucl. Phys. A152. 561(1970).
19. J. T. Larsen, W. L. Talbert, Jr., and J. R. McConnell, Phys. Rev. C 3, 1372(1971).
20. W. C. Schick, Jr., W. L. Talbert, Jr., and J. R. McConnell, Phys. Rev. C 4, 507(1971).
21. R. J. Olson, W. L. Talbert, Jr., and J. R. McConnell, Phys. Rev. C 6, 2095(1972).

22. F. K. Wohn, J. K. Halbig, W. L. Talbert, Jr., ard J. R. McConnell, Phys. Rev. C 7, 160(1973).

23. E. A. Henry, W. L. Talbert, Jr., and J. R. McConnell, Phys. Rev. C 7, 222(1973).

24. J. K. Halbig, F. K. Wohn, W. L. Talbert, Jr., J. J. Eitter, and J. R. McConnell, Nucl. Phys. A203. 532(1973).

25. J. R. Clifford, W. L. Talbert, Jr., F. K. Wohn, J. P. Adams, and J. R. McConnell, Phys. Rev. C 7, 2535(1973).

26. J. P. Adams, G. H. Carlson, M. A. Lee, W. L. Talbert, Jr., F. K. Wohn, J. R. Clifford, and J. R. McConnell, Phys. Rev. C 8, 767(1973).

27. W. L. Talbert, Jr. and R. J. Hanson, Phys. Rev. C 8, 1945(1973).

28. G. H. Carlson, W. L. Talbert, Jr., and J. R. McConnell, Phys. Rev. C 9, 283(1974).

29. W. C. Schick, Jr. and W. L. Talbert, Jr., Phys. Rev. C 9, 2328(1974).

30. J. P. Adams, F.K. Wohn, W. L. Talbert, Jr., W. C. Schick, Jr., and J. R. McConnell, Phys. Rev. C 10, 1467(1974).

31. J. A. Morman, W. C. Schick, Jr., and W. L. Talbert, Jr., Phys. Rev. C 11, 913(1975).

32. F. K. Wohn, W. L. Talbert, Jr., R. S. Weinbeck, M. D. Glascock, and J. K. Halbig, Phys. Rev. C 11, 1455(1975).

33. G. J. Basinger, W. C. Schick, Jr., and W. L. Talbert, Jr., Phys. Rev. C 11, 1755(1975).

34. L. J. Alquist, W. C. Schick, Jr., W. L. Talbert, Jr., and S. A. Williams, Phys. Rev. C 13, 1277(1976).

35. R. L. Bunting, W. L. Talbert, Jr., J. R. McConnell, and R. A. Meyer, Phys. Rev. C 13, 1577(1976).

36. M. D. Glascock, W. L. Talbert, Jr., and C. L. Duke, Phys. Rev. C 13, 1630(1976).

37. F. K. Wohn, M. D. Glascock, W. L. Talbert, Jr., S. T. Hsue, and R. J. Hanson, Phys. Rev. C 13, 2492(1976).

38. W. R. Western, John C. Hill, W. C. Schick, Jr., and W. L. Talbert, Jr., Phys. Rev. C 14, 275(1976).

39. W. R. Western, John C. Hill, W. L. Talbert, Jr., and W. C. Schick, Jr., Phys. Rev. C 15, 1024(1977).

40. C. J. Bischof and W. L. Talbert, Jr., Phys. Rev. C 15, 1047(1977).

41. W. R. Western, John C. Hill, W. L. Talbert, Jr., and W. C. Schick, Jr., Phys. Rev. C 15, 1822(1977).

42. J. C. Pacer, John C. Hill, D. G. Shirk, and W. L. Talbert, Jr., Phys. Rev. C 17, (1978).

43. J. K. Halbig, Ph.D. thesis, Iowa State University, 1973(unpublished).

44. M. A. Lee, Ph.D. thesis, Iowa State University, 1973 (unpublished), and
L. R. Greenwood, Nucl. Data Sheets 12, 139(1974).

45. C. L. Duke, F. K. Wohn, and W. L. Talbert, Jr., private communication, and
D. C. Kocher, Nucl. Data Sheets 16, 55(1975).

46. J. W. Cook and W. L. Talbert, Jr., private communication.

47. L. J. Alquist, Ph.D. thesis, Iowa State University, 1975(unpublished).

48. J. F. Wright, Ph.D. thesis, Iowa State University, 1974 (unpublished).

TRISTAN II - Extension of Capabilities to Non-Gaseous Fission Products

F. K. WOHN

Ames Laboratory-DOE and Department of Physics,
Iowa State University, Ames, Iowa 50011

ABSTRACT: The ISOL facility TRISTAN II is described and its expected capabilities on-line to the High Flux Beam Reactor at Brookhaven National Laboratory are discussed. In particular, the range of isotopes expected to be available and possible experimental studies of the short-lived fission-product isotopes are described.

1. Introduction

In the preceding talk by Talbert,[1] the story of the TRISTAN facility was told from its conception up to the birth of TRISTAN II in July 1976. In the talk to come by Hill,[2] the nuclear spectroscopic studies made with TRISTAN II during the past year will be described. One could label Talbert's talk as TRISTAN-past and Hill's talk as TRISTAN-present. In this vein the present talk can be regarded as TRISTAN-future. In the following, the general features of TRISTAN II are presented with the emphasis on the new capabilities for non-gaseous fission products and the future possibilities for studies of such activities on-line to the HFBR. The material in the following has been extracted from the more comprehensive report[3] which has been distributed to the participants of this meeting.

2. The TRISTAN II Facility

Schematic diagrams of the TRISTAN II facility in its present configuration at the ALRR in Ames are shown in Fig. 1 and 2. This configuration is the third in the history of TRISTAN. The two earlier versions of TRISTAN I have been described in detail by McConnell and Talbert.[4] Since most of the operating properties of the separator were unchanged in the conversion from TRISTAN I to TRISTAN II and are well described in Ref. 4, they will not be described here. Pertinent aspects of the present ion-source target configuration are given by Talbert et al.[5] Table 1 lists some of the characteristic properties of the three TRISTAN configurations, the last being TRISTAN II.

The closeup view of Fig. 3 shows the in-beam ion source of oscillating electron (Nielsen) type with a cylindrical anode made of graphite impregnated on its inner surface with 2g of ^{235}U in the form UO_2. (At the operating temperature of about 1500-1700°C, some of the UO_2 may be converted into UC.[6,7]) The target activity of 0.2 Curies is produced by the ALRR thermal neutron flux of $2.5 \times 10^9/cm^2/sec$. Fission products diffuse from the relatively open-structured graphite matrix into the ion source plasma, where they become ionized, then are extracted from the ion source and accelerated through 50 kV. The 50 kV ions are focused through a 100° electrostatic sector, followed by the 90° mass-separator magnet. At the focal plane of the separator magnet the ions of selected mass pass through a slit and are then directed by a switching magnet to one of the detection stations. Moving tape collectors at each detection station provide isobaric enhancement of the activity of interest.

Figure 4 shows a new in-beam ion source presently under construction at the Ames Laboratory. The design is based on the FEBIAD (Forced Electron Bombardment Induced Arc Discharge) ion source of Kirchner and Roeckl.[8] The FEBIAD ion source offers many advantages over the conventional oscillating-electron or Nielsen ion source, particularly for ISOL use. Among the advantages are low-pressure operation, very stable discharge conditions, long lifetime and high ionization efficiency. In addition, the end cap or outlet plate potential can be selected so as to maximize either resolving power or output intensity.[9] The ion source of Fig. 4 has the same graphite liner impregnated with UO_2 as the presently used ion source of Fig. 3. Since this modification should not affect the high-efficiency characteristics of the FEBIAD concept, it is hoped that higher activities will result with the new in-beam ion source.

A schematic diagram of the TRISTAN facility relocated at the HFBR at BNL is shown in Fig. 5. This layout differs significantly from the ALRR layout, as no electrostatic deflection is required before mass separation in the HFBR layout. The magnetic spectrometer shown in Fig. 1 is replaced in Fig. 5 by a planned atomic spectroscopic system using a tunable dye laser. Figure 5 indicates the addition of a second mass line to the facility, which could essentially double the potential use of the facility by allowing simultaneous measurements on two masses. (A second mass line, although also possible at ALRR, was not needed for the scale of the research program at Ames.) Thus the HFBR layout has three distinct differences compared to the ALRR layout: simpler ion optics, a second mass line, and a higher neutron flux (by a factor of 16). The third difference is by far the most advantageous.

3. Performance of TRISTAN II

The overall efficiency of an isotope (the fraction of the isotope produced in the target that is delivered after mass separation to a detection station) must be known to calculate the amount of activity available for study at any mass. For a similar in-beam ion source containing a target of UO_2 in graphite, such efficiencies are known. The OSIRIS facility in Studsvik was the first to develop (in 1970) such a system,[10] which was subsequently improved[6] and has been used extensively ever since. A similar system was also used at PINGIS in Stockholm for the ^{238}U (α, fission) reaction with 43-MeV α-particles;[11] see Table 2 for characteristics. In both cases, a target of UO_2 impregnated graphite was located within an oscillating-electron ion source and overall efficiencies in the range 10^{-4}-10^{-2} were measured.

The overall efficiencies for 18 elements were determined with good accuracy at OSIRIS using longer-lived isotopes ($T_{1/2}$ > 3s) with well-established decay schemes.[6] The same 18 elements have been separated at TRISTAN II; Fig. 6 shows these 18 elements and gives a comparison with TRISTAN I. Such a systematic determination of overall efficiencies has not been made at PINGIS nor with the new TRISTAN II configuration. However, a mass scan at TRISTAN II of β activity was found to agree well with a similar mass scan done at OSIRIS. The OSIRIS and TRISTAN II mass scans are shown in Fig. 7 together with the mass-yield curve for ^{235}U fission. Both mass scans were obtained with a 4π β dectector. For the OSIRIS scan the mass-separated activity was collected for 10 sec then immediately counted for 10 sec;[7] the corresponding times were 30 sec and 30 sec for the TRISTAN II scan, with a 1 sec delay before beginning the

counting. The OSIRIS scan was done with 3 g of U and a neutron flux of $4 \times 10^{10}/cm^2/sec$;[7] the TRISTAN II scan was done with about 8 g of U and a flux of $3 \times 10^9/cm^2 sec$. Although the effect of different time conditions on the various lifetimes renders a detailed comparison meaningless, the general agreement between the two mass scans indicates that the two facilities have quite comparable overall efficiencies for fission products. Thus it is quite reasonable to use the OSIRIS overall efficiency results shown in Table 4 to predict the activities to be expected for the very similar in-beam ion source of TRISTAN II at the HFBR. Before proceeding to make such specific predictions, it is worthwhile to first take a more global look at the isotopes produced in fission.

3.1 Thermal-Neutron Fission of ^{235}U

Contours of independent fission cross sections in barns are presented in Fig. 8 for thermal neutron fission of ^{235}U. The contours were calculated under the assumption of pure Gaussian charge dispersion with the same Gaussian width of $\sigma = 0.56$ (FWHM = 1.32) for all mass chains.[12,13] The values of Z_p (the most probable charge for a mass chain) were taken from the report of Wahl et al.[12] Mass yield values for thermal-neutron fission were taken from the compilation of Nethaway and Barton.[13] The odd-even fluctuations in fission yields[14] were not included in the calculation of the contours of Fig. 8. For the low-yield fission products in the valley and on the wings, Fig. 8 slightly underestimates the yields to be expected for the fission-neutron spectrum of the external beam of the HFBR. However, for the present purpose of estimating the quantities of fission products produced with TRISTAN II at the HFBR, the cross-sections of Fig. 8 are quite adequate.

The background for Fig. 8 consists of a section of the chart of the nuclides. The solid squares indicate stable or naturally-occuring radionuclides and the squares contained within the dashed outline are presently known nuclides. The solid outline contains nuclei for which some nuclear structure information exists. Only nuclei with at least a few energy levels known are included within the solid outline; for a substantial fraction of these nuclei the level structure information is far from comprehensive. For example, even such a basic quantity as the β-decay Q-value has not been measured for nearly 40% of these nuclei. For the nuclei lying between the solid and dashed outlines, the present state of our knowledge is extremely poor, with only the half-life and perhaps some γ rays known. Figure 8 makes it very clear that a large number of fission products are inadequately studied.

The half-lives of nuclides in the fission product region are shown in Fig. 9, which also shows the neutron drip line.[15,16] The half-life contours were calculated from a gross theory of β decay by Takahashi et al.[17] Agreement with experimental values is generally within an order of magnitude for nuclei with half-lives of 10 sec or longer. For half-lives less than 10 sec, the predictions appear to be more reliable and often are smaller than the measured half-lives.[18] Figure 3 shows that the nuclides lying within the dashed outline are expected to have half-lives of about 1 sec or longer. Many undiscovered nuclei (lying outside the dashed line) are predicted to have half-lives of the order of 1 sec; as Fig. 8 shows, many of these nuclei have sufficient fission yield to enable them to be studied with an ISOL system with the capabilities of TRISTAN II.

Before making specific predictions of mass-separated fission-product activities available with TRISTAN II at the HFBR, a general estimate of activities produced can be made. With a 2 g target of ^{235}U in the H-2 external beam thermal flux of $4 \times 10^{10}/cm^2/s$, the total activity in the target would be 1.1×10^{11} fissions/sec or 3 Curies. For an isotope on the minimum cross-section contour of 1 mbarn shown in Fig. 8, the production rate in the target would be 2×10^5/sec. Even at this minimum rate, mass-separated activities of about 10^3/sec would be available for isotopes with an overall efficiency of about 1%--more than adequate for the discovery of new isotopes.

3.2 Estimated Activities at the HFBR

Figures 10 and 11 present, in different formats, the results of a prediction of expected activities for fission-product nuclei in two mass regions. These two regions were chosen because they lie near single or double shell closure and because good element efficiencies exist in these two regions. Rare-gas or alkali-metal fission products were not included since studies of such products are not anticipated for TRISTAN II at BNL due to past and current comprehensive studies of these products at many ISOL facilities. The left-hand scales in Fig. 10 involve an effective yield which takes into account overall element efficiencies. The effective yield $Y_e(Z,A)$ represents the yield to be expected at a detector station after mass separation. For each nuclide the following expression was used to calculate $Y_e(Z,A)$:

$$Y_e(Z,A) = Y_e(Z-1,A) + \varepsilon(Z)[Y_c(Z,A) - 10\varepsilon(Z-1)Y_c(Z-1,A)],$$

where $Y_c(Z,A)$ represents cumulative yield and $\varepsilon(Z)$ is overall efficiency. The $Y_c(Z,A)$ values were taken from the recent compilation by Voigt[19] and the OSIRIS results[6] were used for $\varepsilon(Z)$.

The first term in the preceeding expression gives the yield due to the mass-separated precursor in the decay chain. The second term gives the extractable fraction of the cumulative yield in the target. The third term is a correction needed because some of the cumulative yield of the precursor does not decay within the target, having been lost as either extracted precursor or pumped out of the ion source as neutral atoms. The factor of 10 in the third term is used to estimate this loss and is based on the observation that only about 1 ion in 10 is extracted for rare-gas fission products introduced directly into the ion source. Since the third term is of second order in efficiencies and is expected to be much less than unity, the estimate given above for this term is adequate for the present discussion. In the right-hand scales of Fig. 10 (and for Fig. 11), the effective yields are converted into activities by selecting a ^{235}U mass of 2g and the 4 x $10^{10}/cm^2/sec$ thermal neutron flux of the H-2 external beam line at the HFBR.

A few comments are in order concerning the independent and cumulative effects on the shapes of the curves in Fig. 10. The curves for Zn and Ag are Gaussian since the efficiencies of their respective precursors were assumed to be zero. The curves for the other elements reflect the mass-separated cumulative effect. The curves for Br and In show clearly separated regions of cumulative and independent domination. The seemingly large shift in the peak of the Br curve is due to the rather sharp increase of efficiency for Br compared to its immediate precursors.

Half-life effects on the activities expected were not taken into account in the preceding calculation because the delay time distributions between production and ionization are not known. The OSIRIS efficiencies,

which were measured in such a manner that only longer-lived activities could be used, should be valid when the half-life is as long or longer than the verage delay time. For half-lives short compared to the delay time, however, the predictions shown in Fig. 10 would be too large due to neglect of decay in the target. Delay time distributions have both prompt and slow components, and little is known about the shape of the distributions for such a target system. For elements with efficiencies of 10^{-4}-10^{-3} the delay times may be in the range 10^{1}-10^{3} sec; for elements with efficiencies of 10^{-2}-10^{-3}, the delay time range is probably 1-10 sec.[20] Both target thickness and target temperature affect the delay time distribution of each element. Diffusion times decrease rapidly with increasing temperature, hence slightly higher operating temperatures (1700-1900°C) could cause a significant increase in the efficiency for a very short-lived isotope. For example, it has been observed at OSTIS[21] that the yield of 0.1-sec ^{98}Rb increases by more than an order of magnitude when the temperature is increased from 1700°C to 1900°C. Operating temperatures above the 1500°C of the OSIRIS target could well compensate for possible overestimations of expected activities of very short-lived isotopes given in Fig. 10 and 11 due to half-life effects. Furthermore, the higher ionization efficiencies anticipated with the modified-FEBIAD ion source could also compensate in part for the neglect of half-life effects in the predicted activities.

Possible Studies with TRISTAN II at the HFBR

In spite of the undertainties in the preceding calculation of activities due to possible half-life effects for the shorter lifetime nuclei, the numbers in Fig. 10 and 11 provide a useful estimation of the activities available with TRISTAN II at the HFBR. Detailed decay scheme studies, including coincidence measurements, are possible with activities of 10^{3}-10^{4}/sec; singles

studies of intense γ rays require minimum rates of $\sim 10^2$/sec; half-life measurements or identification of new isotopes can be made with lower activities provided background rates are low enough. Many nuclei (60-80) lying outside the solid outlines of Fig. 11 might be expected to have activities above about 10^3-10^4/sec, which would be adequate for detailed decay scheme studies. Also, for many of the nuclei within the solid outlines, additional or more comprehensive studies are well worthwhile. A large number (20-25) of new isotopes outside the dashed outlines might be identifiable with activities of about 10^2-10^3/sec.

The preceding estimates of the numbers of nuclei lying outside the solid or dashed outlines of Fig. 11 could be regarded as upper limits since losses due to half-life effects were not included in the estimated activities. The estimate of about 20-25 (for isotopes lying outside the dashed outlines) should be most affected by half-life effects since these nuclei are expected to have short half-lives of the order of seconds.[17] Nevertheless, a substantial number of new isotopes should be available with sufficient activities to permit identification or more comprehensive study. Furthermore, when one considers the diversity of possible studies (see Table 5) that could be done with TRISTAN II at the HFBR, one must recognize that many of the previously studied nuclei that lie within the solid outlines have not been sufficiently studied. In particular, atomic spectroscopic studies have been made for very few fission products. This is also true even for the rare gases, alkali metals and daughters (which were not included in Figs. 10 and 11 since nuclear spectroscopic studies are quite advanced at present for these fission products). Thus, of the nuclei expected to be available with TRISTAN II at the HFBR, a

grand total of more than 100 (perhaps closer to 200) would be candidates for one or more of the types of studies listed in Table 5.

4.1 Competition from other ISOL Facilities

With a grand total in the range 100-200, it would be clearly too time consuming to mention all of the studies that would be interesting. Some choice or selection must be made before more detailed comments are given. One consideration to be made in selecting nuclei for study with TRISTAN II is competition from other ISOL facilities engaged in the study of neutron-rich activities. In the following, this consideration for selecting the nuclide regions of Fig. 11 is discussed.

As stated previously, the rare gases Kr and Xe and their daughter activities have been studied for years at TRISTAN I, ARIEL, SOLIS, and IALE (see Tables 1 and 2). The alkali metals Rb and Cs and their daughter activities are still being studied at SOLIS, SOLAR, OSTIS and the ISOL facilities at Mainz and McGill. Although these studies are not complete (some of the studies have only recently begun), it is clear that investigations of these nuclei at TRISTAN II could not constitute the major thrust of the research program.

The direct ISOL facilities JOSEF and LOHENGRIN must also be considered as possible competitors. In addition to the direct fission-product and microsecond-isomer studies for which these two facilities have no competitors, nuclear spectroscopic studies have been made, but the main concentrations have not been in the nuclide regions of Fig. 11. At JOSEF, the major concentration in nuclear spectroscopy has been in the nuclear shape-transition region around mass 100, involving primarily Sr, Y and Zr nuclei.[22] At

LOHENGRIN, nuclear spectroscopic studies have concentrated in two regions -- near mass 150 (Cs, Ba, La, Ce, Pr) and near mass 100 (Rb, Sr, Y, Zr, Nb),[23] with the later studies often done in coordination with JOSEF.

The SIRIUS facility at Strasbourg could also be considered as a possible future competitor. Although SIRIUS is presently an operating facility, the thrust has mainly been in improving the interconnection of the helium jet and ion source. Identification of the isotopes available and determination of overall efficiencies have been initiated only recently. The goal of the project is to establish a facility for on-line studies of the lanthanide fission products, for which there would be little competition. Thus the emphasis in the research program, which is only beginning to be established, should not involve the nuclides of Fig. 11.

The OSIRIS facility at Studsvik separates the same fission-product elements as TRISTAN II, as the mass scans in Fig. 7 show. An excellent review of the OSIRIS facility and the experimental program was recently given by Rudstam.[7] More than half of the research program has been devoted to systematic studies such as beta decay properties, total decay energies, delayed neutron properties, and independent fission yields. As a consequence, detailed spectroscopic studies have constituted only a relatively minor part of the research program. Of the spectroscopic studies at OSIRIS, the light fission products have nearly been neglected, with one joint experiment (JOSEF, LOHENGRIN and OSIRIS) published. Several spectroscopic studies of the heavy fission products have been made in the region near Z=50, extending up to doubly magic ^{132}Sn. (See Ref. 7 for the list of reports on nuclear spectroscopic studies at OSIRIS.) In addition to continuing the present

projects, future plans at OSIRIS involve projects to expand the range of elements processed. Even if the number of elements available at OSIRIS does not expand, with the elements now available at OSIRIS (and TRISTAN II), to quote Rudstam in Ref. 7, "The field is still far from being fully explored, and we forsee a long period of fruitful research."

From the preceding brief discussion of areas of concentration at other ISOL facilities engaged in the study of fission products, it should be clear that the nuclide regions shown in Fig. 11 are the regions in which TRISTAN II would have minimal competition. This statement is particularly true for nuclear spectroscopic studies, as only a minor part of the research program at OSIRIS has involved studies in this region. Although such studies in the nuclide regions of Fig. 11 have been shown to have minimal competition, the question of whether these nuclei are worth studying should be addressed.

4.2 Nuclear Structure Studies

For the light fission-product region of Fig. 11, the nuclear structures of the nuclei near the N=50 shell could be systematically explored. Although the nucleus ^{78}Ni, which is expected to be doubly magic, is beyond reach, nuclei with a few particles or holes relative to a ^{78}Ni core could be studied. For the N=50 isotones, proton particle states could be explored in nuclei with three or more protons beyond the Z=28 shell, i.e. ^{81}Ga, ^{82}Ge, ^{83}As, etc. Neutron hole states in the N=50 shell and neutron particle states beyond N=50 could be studied in odd-A nuclei of Ge and Se. The behavior of collective states in even-even nuclei on either side of the N=50 shell could be systematically studied. For the low-lying levels in even-even Ge, Se and Kr nuclei, the trends near N=50 would reveal whether the closed shells at N=50 and Z=28 affect the level spacings in the same manner as closed shells

do nearer stability. Nuclear structure studies in the light fission-product region of Fig. 11 would allow our knowledge of the structure of nuclei around the N=50 and Z=28 shells, which was obtained near stability, to be extended towards ^{78}Ni. This could thus shed light on the unanswered question of whether these magic numbers remain magic as ^{78}Ni is approached.

For the heavy fission-product region of Fig. 11, both the Z=50 shell, N=82 shell and doubly magic ^{132}Sn regions could be systematically studied. The nuclei near ^{132}Sn are especially interesting. As Fig. 11 indicates, activities should be sufficient to study level structures of the single neutron-hole nucleus ^{131}Sn and the single proton nucleus ^{133}Sb through the decays of ^{131}In and ^{133}Sn, respectively. It might also be possible to study levels in both ^{132}Sn and ^{133}Sn through the decays of ^{132}In and ^{133}In, respectively, if the activities realized are not too far below the upper-limit estimations of Fig. 11. The proton-hole nucleus ^{131}In, however, seems to be beyond reach through the decay of ^{131}Cd. In terms of "valence" nucleons or nucleon holes relative to ^{132}Sn, possible studies could involve the following nuclei: valence-0 ^{132}Sn, 2 or 3 of the 4 valence-1 nuclei, 4 or 5 of the 8 valence-2 nuclei, 6 or 7 of the 12 valence-3 nuclei, 8 or 9 of the 16 valence-4 nuclei, etc. Thus at least half of the low-valence nuclei near ^{132}Sn could be systematically studied with TRISTAN II at the HFBR. Of the 21-25 nuclei listed above as possible, some nuclear structure information exists, particularly for the proton-particle neutron-hole nuclei nearer stability. As ^{132}Sn is approached, the information becomes more scarce, with most of the existing information coming from studies at OSIRIS. Comprehensive studies have not been made for the large majority of these nuclei.

TRISTAN II and OSIRIS both have the opportunity to make substantial contributions to our knowledge of nuclear structure in this especially interesting region.

In addition to shell-model oriented studies in the heavy fission-product region of Fig. 11, collective properties of even-even nuclei could also be explored with TRISTAN II. Even-even isotopes of Cd, Sn, Te and Xe, whose expected activities can be obtained from Fig. 11, could be studied. Also, even-even Ba and Ce isotopes would be available. A large number of these nuclei have not yet been studied in sufficient detail to provide the information needed to test the collective models. In addition to the behavior of collective states as the two shells Z=50 and N=82 are approached, trends in collective behavior as the nuclei approach the nuclear shape-transition regions below the Z=50 shell and above the N=82 shell could be systematically mapped.

In the preceding discussion of interesting studies to be made with TRISTAN II for the nuclide regions of Fig. 11, the emphasis was directed towards nuclear structure studies. In addition to the nuclear spectroscopic and atomic spectroscopic measurements required to obtain the nuclear structure information outlined above, many other interesting studies would clearly be possible for the nuclei in Fig. 11, as a glance at the possible studies in Table 5 shows. Although the other types of studies could also be discussed in some detail, the preceding limited discussion is sufficient to indicate the large number of interesting studies of the nuclei far from stability that would be possible with TRISTAN II at the HFBR.

REFERENCES

1. W. L. TALBERT, JR., "TRISTAN I - Techniques, Capabilities, and Accomplishments," these Proceedings.
2. J. C. HILL, "Recent Results from Studies of Non-Gaseous Fission Products with TRISTAN II," these Proceedings.
3. F. K. WOHN, "The Study of Nuclei Far from Stability with TRISTAN II at the High Flux Beam Reactor at Brookhaven," Ames Laboratory report IS-4270 (1977).
4. J. R. McCONNELL and W. L. TALBERT, JR., Nucl. Instr. and Meth. 128, 227 (1975).
5. W. L. TALBERT et al., Nucl, Instr. and Meth. 139, 257 (1976).
6. Ch. ANDERSON et al., Swedish Research Councils' Laboratory report LF-45 (1973); also LF-47 (1973).
7. G. RUDSTAM, Nucl. Instr. and Meth. 139, 239 (1976).
8. R. KIRCHNER and E. ROECKL, Nucl. Instr. and Meth. 127, 307 (1975).
9. R. KIRCHNER, Proc. Inter. Conf. on Low Energy Ion Beams, Salford, 1977; to be publ. by Institute of Physics, London, April, 1978.
10. S. BORG et al., Nucl. Instr. and Meth. 91, 109 (1971).
11. K. FRANSSON et al., Nucl. Instr. and Meth. 113, 157 (1973).
12. A. C. WAHL, et al., Proc. 2nd IAEA Symposium on Physics and Chemistry of Fission, Vienna, 1969; publ. by IAEA, 1969, p. 813.
13. D. R. NETHAWAY and G. W. BARTON, Lawrence Livermore Laboratory report UCRL-51458 (1973); see also D. R. NETHAWAY, UCRL-51640 (1974) and UCRL-51538 (1974).
14. S. AMIEL and H. FELDSTEIN, Phys. Rev. C 11, 845 (1975).

15. P. A. SEEGER and W. M. HOWARD, Nucl. Phys. A238, 491 (1975).

16. G. T. GARVEY et al., Rev. Mod. Phys. 41, S1 (1969).

17. K. TAKAHASHI et al., Atom. Data and Nucl. Data Tables 12, 101 (1973).

18. B. GRAPENGIESSER et al., J. Inorg. Nucl. Chem. 36, 2409 (1974).

19. A. F. VOIGT, Ames Laboratory report IS-4052 (1976).

20. G. RUDSTAM, private communication (1976).

21. K. WÜNSCH and H. WOLLNIK, private communication (1977).

22. H. LAWIN et al., Nucl. Instr. and Meth. 139, 227 (1976).

23. P. ARMBRUSTER et al., Nucl. Instr. and Meth. 139, 213 (1976).

24. Proc. 7th Inter. EMIS Conf. on Electromagnetic Isotope Separators and the Techniques of Their Application, Marburg, 1970; BMBW-FB K 70-28 (1970).

25. Proc. 8th Inter. EMIS Conf. on Low Energy Ion Accelerators and Mass Separators, Skövde, 1973; publ. by Chalmers University of Technology (1973).

26. Proc. Inter. Conf. on Target Techniques for On-Line Isotope Separators, Aarhus, 1975; abstracts publ. by University of Aarhus (1975).

27. Proc. 9th Inter. EMIS Conf. on Electromagnetic Isotope Separators and Related Ion Accelerators, Kiryat Anavim, 1976; Nucl. Instr. and Meth. 139, 1 (1976).

28. J. P. BOCQUET et al., Nucl. Instr. and Meth. 88, 51 (1970).

29. S. AMIEL, Ark. Fys. 36, 9 (1967).

30. S. AMIEL, Nucl. Instr. and Meth. 139, 305 (1976).

31. Proc. 3rd Inter. Conf. on Nuclei Far From Stability, Cargèse, 1976; report CERN 76-13 (1976).

32. E. O. ACHTERBERG et al., Nucl. Instr. and Meth. 101, 555 (1972).

33. K. SISTEMICH et al., Nucl. Instr. and Meth. 130, 491 (1975).

34. J. P. ZIRNHELD, Nucl. Instr. and Meth. 114, 517 (1974).

35. J. J. STOFFELS, Nucl. Instr. and Meth. 119, 251 (1974).

36. R. L. REEDER et al., Nucl. Instr. and Meth. 133, 501 (1976).

37. K. WÜNSCH, Ph.D. thesis, Technische Hochschule München, 1974 (unpublished).

38. K. L. KRATZ and E. ROECKL, private communication (1976).

39. A. KJELLBERG and G. RUDSTAM (eds), The ISOLDE Isotope Separator On-Line Facility at CERN, report CERN 70-3 (1970).

40. H. L. RAVN et al., Nucl. Instr. and Meth. 139, 267 (1976).

41. W. H. SCHMIDT-OTT et al., Nucl. Instr. and Meth. 124, 83 (1975).

42. R. L. MLEKODAJ et al., Nucl. Instr. and Meth. 139, 299 (1976).

43. Y. YOSHIZAWA et al., Nucl. Instr. and Meth. 134, 93 (1976).

44. D. D. BOGDANOV et al., Nucl. Instr. and Meth. 136, 433 (1976).

45. V. A. KARNAUKOV et al., Nucl. Instr. and Meth. 120, 69 (1974).

46. J. C. PUTAUX et al., Nucl. Instr. and Meth. 121, 615 (1974).

47. P. PARIS et al., Nucl. Instr. and Meth. 139, 251 (1976).

48. R. COUSSEMENT et al., Ref. 3, p. 51.

49. J. ÄYSTÖ et al., Nucl. Instr. and Meth. 139, 325 (1976).

50. K. H. BURKARD et al., Nucl. Instr. and Meth. 139, 275 (1976).

51. R. KIRCHNER and E. ROECKL, Nucl. Instr. and Meth. 139, 291 (1976).

52. S. K. MARK, private communication (1977).

TABLE 1: CHARACTERISTICS OF EXISTING ISOL FACILITIES AT REACTORS

Name, location (tial operation)	Target and target conditions	Neutron flux at target (cm^{-2} sec^{-1})	Delay time from production to ionization	Type of ion source (temperature)	Elements extracted, with decay products excluded	Approximate overall efficiency
ISTAN, Ames (Nov. 1966)	^{235}U as UO_2 (0.2g at 600°C)	2×10^{13} th.	12 sec trans.	oscil. elect. (1700°C)	Kr, Xe	10^{-2}-10^{-1}
	^{235}U as stearate (2-4g at 20°C)	3×10^{9} th.	1.2 sec trans.	"	Br,Kr,I,Xe	10^{-3}-10^{-1}
	^{235}U as UO_2 + UC (2g at 1500°C)	"	1-10^{2} sec	oscil. elect. (1500°C)	Zn,Ga,Ge,As,Br,Kr,Rb,Sr, Ag,Cd,In,Sn,Sb,Te,I,Xe,Cs,Ba	10^{-4}-10^{-2}
ARIEL, Grenoble (June 1968)	$^{233,35,38}U$, ^{232}Th (4g UO_2 or stearate)	10^{8} 14-MeV	4-6 sec trans.	oscil. elect. (1700°C)	Kr,Xe	10^{-2}-10^{-1}
	^{235}U as UO_2 (10g at 20°C)	3×10^{8} th.	"	"	"	"
SOLIS, Soreq (July 1968)	^{235}U as stearate (2-4g at 20°C)	2×10^{9} th.	0.3 sec trans.	oscil. elect. (1700°C)	Kr,Xe	10^{-2}-10^{-1}
	^{235}U as UO_2 (1g at 1800°C)	"	0.1 sec	surface ion. (1800°C)	Rb,Cs;or,I	10^{-3}
OSIRIS, Studsvik (July 1968)	^{235}U as UO_2 + UC (0.2g at 1500°C)	4×10^{11} th.	1-10^{2} sec	oscil. elect. (1500°C)	Zn,Ga,Ge,As,Br,Kr,Rb,Sr, Ag,Cd,In,Sn,Sb,Te,I,Xe,Cs,Ba	10^{-4}-10^{-2}
	^{235}U as UO_2 + UC (2g at 1500°C)	"	"	"	"	"
IALE, Buenos Aires (March 1969)	^{235}U as stearate (14g at 20°C)	5×10^{8} th.	1 sec trans.	oscil. elect. (1700°C)	Br,Kr,I,Xe	10^{-3}-10^{-1}
JÖSEF, Jülich* (Nov. 1972)	^{235}U as UO_2 (40mg at 500°C)	1×10^{14} th.	μsec recoil	none - recoil in Torr gas	all fission products (there is no chemical selectivity)	10^{-5}-10^{-4}
SIRIUS, Strasbourg (June 1973)	^{235}U as UO_2 (10mg at 20°C)	5×10^{10} th.	8 sec trans.	hollow cath. (2200°C)	Sb,Sb,Te,I,Xe,Cs,Ba,Ce,Pr + others (survey incomplete)	10^{-4}
	"	"	2 sec trans.	"	"	10^{-5}-10^{-4}
	^{235}U as UO_2 (0.6g at 50°C)	5×10^{11} th	2 sec trans.	"	"	"
SOLAR, Pullman (Jan. 1974)	^{235}U as UO_2 (1g at 1600°C)	5×10^{9} th.	0.1 sec (Sr,Ba: 7 min.)	surface ion. (1600°C)	Rb,Cs;Br,I;Sr,Ba	10^{-5}-10^{-3}
LOHENGRIN, Grenoble* (March 1974)	^{235}U as UO_2 (3mg at 500°C)	5×10^{14} th.	μsec recoil	non - recoil in vacuum	all fission products (there is no chemical selectivity)	10^{-6}-10^{-5}
OSTIS, Grenoble (Oct. 1975)	^{235}U as UO_2 (2g at 1800°C)	3×10^{9} th.	0.1 sec	surface ion. (1800°C)	Rb,Cs	10^{-2}
"ISOL", Mainz (Dec. 1975)	^{235}U as UO_2 (1g at 1800°C)	3×10^{11} th.	0.1 sec	surface ion. (1800°C)	Rb,Cs	10^{-2}

*Facility is often classified as mass analyzer rather than ISOL.

TABLE 2: CHARACTERISTICS OF EXISTING ISOL FACILITIES AT ACCELERATORS

Name, location (initial operation)	General classification of target materials	Particle current and energy	Delay time from production to ionization	Type of ion source (temperature)	Elements extracted, with decay products excluded	Approximate overall efficiency
ISOLDE, Geneva (Oct. 1967)	hydrous oxides of Zr, Ce, Th (room temp.)	4 x 10^{11} p/sec (600 MeV)	10 - 10^2 sec	oscil. elect. (1100°C)	Kr,Xe,Rn	10^{-2}-1
	molten metals or alloys (600 - 1400°C)	"	10 - 10^3 sec	oscil. elect. or surface ion.	Zn,Kr,Rb,Cd,In,I,Xe,Cs,Ba, Sm,Eu,Hg,Tl,Pb,Bi,Rn,Fr,Ra	10^{-4}-10^{-1}
	ThF_4-LiF eutectic (600 - 700°C)	"	10 - 10^2 sec	oscil. elect. (1600°C)	I,Xe,Te,Po,At,Rn	10^{-4}-10^{-2}
	Ce, Th ceramic oxides (500 - 2100°C)	"	10 - 10^2 sec	hollow cath. (2000°C)	Sb,Te,I,Xe,Cs,Au,Hg, Tl,Pb,Bi,Po,At,Rn,Fr	10^{-4}-10^{-2}
	fine powders of Nb, Ta (2000 - 2200°C)	10^{12} p/sec (600 MeV)	1 - 10^2 sec	surface ion. (2800°C)	Rb,Yb	10^{-3}-10^{-2}
	$^{238}UO_2$ in graphite matrix (2000°C)	"	10^{-1} - 1 sec	surface ion. (2000°C)	Rb,Cs,Fr	---
	all targets above can be used with ISOLDE II	8 x 10^{12} p/sec (600 MeV)	---	any of the types above	all 24 elements above are possible with ISOLDE II	---
PINGIS, Stockholm (June 1959)	thin Pt foils (1600°C)	1 x 10^{13} α/sec (43 MeV)	10^{-1} - 10 sec	oscil. elect. (1600°C)	Hg	10^{-3}-10^{-2}
	$^{238}UO_2$ in graphite matrix (1500°C)	"	10^{-1} - 10^2 sec	"	As,Br,Kr,Rb,Sr, Ag,Cd,In,Sn,Sb,Te,I,Xe,Cs	10^{-4}-10^{-2}
UNISOR, Oak Ridge (Sept. 1972)	thin metal foils (200 - 1200°C)	10^{13}/sec C,N,O,Ne (60-90 Q^2/A MeV)	10^{-1} - 10^2 sec	oscil. elect. (1600°C)	Br,Kr,I,Xe,Hg,Tl,Pb,Bi	10^{-3}-10^{-2}
	thin metal foils with He jet flow system	"	10 - 30 sec (gas flow time)	hollow cath. (2000°C)	Ga,Ag,Sb,Te,Dy	10^{-4}-10^{-3}
"ISOL", Tokyo (Nov. 1972)	thin Cu foils (600 - 1000°C)	5 x 10^{12} p/sec (52 MeV)	10^2 - 10^3 sec	oscil. elect. (1500°C)	Zn	10^{-4}
	thin Cu foils (1400 - 1800°C)	"	10 - 10^2 sec	hollow cath. (2200°C)	"	10^{-3}
BEMS, Dubna (Nov. 1973)	thin metal foils (200 - 1000°C)	10^{12}-10^{13} HI/sec (4-8 MeV/A)	1 - 10^3 sec	surface ion. (2700°C)	Rb,Cs,Ba,La,Pr, Nd,Pm,Sm,Eu,Dy	10^{-3}-10^{-1}
ISOCELE, Orsay (Mar. 1974)	molten metals or alloys (700 - 1800°C)	1 x 10^{12} p/sec (155 MeV)	10 - 10^3 sec	oscil. elect. (1800°C)	Cd,In,Sb,Ho,Er,Tm,Yb, Au,Hg,Tl,Bi,Po,At,Fr	10^{-3}-10^{-2}
	"	3 x 10^{13} p/sec (200 MeV)	"	"	all 14 elements above are possible with ISOCELE II	---
LISOL, Heverlee (May 1975)	Mo (as filament of ion source)	3 x 10^{13}/sec ^{14}N (72 MeV)	10 - 10^2 sec	oscil. elect. (1800°C)	In	---
"ISOL", Jyväskylä (Sept. 1975)	thin metal foils (He jet at 80°K)	10^{13}/sec p,d,^{3}He,α (20 Q^2/A MeV)	0.5 - 1 sec (gas flow time)	oscil. elect. (1300°C)	Cu,Zn,In,Sn,Sb,Cs,Ba,Bi	10^{-4}-10^{-3}
	thin metal foils (He jet with NaCl)	"	"	hollow cath. (2000°C)	"	10^{-3}-10^{-2}
"ISOL", Darmstadt (Jan. 1976)	thin metal foils (500 - 1000°C)	10^{11}-10^{13} HI/sec (2-8 MeV/A)	1 - 10 sec	direct dis. (2000°C)	Br,Kr,Pd,Ag,Cd,In,Sn, Sb,Te,I,Xe,At,Rn	10^{-3}-10^{-1}
	"	"	10^{-1} - 1 sec	surface ion. (2000°C)	Rb,Cs,Fr	10^{-1}
"ISOL", McGill (Jan. 1976)	^{238}U and ^{232}Th (1500°C)	10^{12}/sec p,d,^{3}He,α (100 Q^2/A MeV)	10^{-1} sec	surface ion. (2000°C)	Ga,Rb,In,Cs,Ba	10^{-2}-

TABLE 3: Source References for Existing ISOL Facilities

TRISTAN	Ref. 4 (Also Ref 24-27)
ARIEL	Ref. 28 (Also Ref. 24)
SOLIS	Ref. 29,30 (Also Ref. 24-26)
OSIRIS	Ref. 6,7,10 (Also Ref. 24,25,31)
IALE	Ref. 32 (Also Ref. 24)
JOSEF	Ref. 22,33 (Also Ref. 24,25,31)
SIRIUS	Ref. 34 (Also Ref. 25)
SOLAR	Ref. 35,36
LOHENGRIN	Ref. 23 (Also Ref. 24,25,31)
OSTIS	Ref. 37
"ISOL" Mainz	Ref. 38
ISOLDE	Ref. 39,40 (Also Ref. 24-26,31)
PINGIS	Ref. 11 (Also Ref. 24,25,27)
UNISOR	Ref. 41,42 (Also Ref. 25,26)
"ISOL" Tokyo	Ref. 43
BEMS	Ref. 44,45 (Also Ref. 31)
ISOCELE	Ref. 46,47 (Also Ref. 25,26)
LISOL	Ref. 48 (Also Ref. 26)
"ISOL" Jyväskylä	Ref. 49 (Also Ref. 26)
"ISOL" Darmstadt	Ref. 50,51 (Also Ref. 25,26)
"ISOL" McGill	Ref. 52

TABLE 4: Overall efficiencies for various elements obtained with old and new target arrangements at OSIRIS.

Element	Mass number measured	Half-life in sec	Overall efficiency in % Old system[a]	New system[b]
Zn	76	5.7	-	2.5
Ga	76	30	-	2.7
Ge	79	19	-	0.29
As	81	28	-	0.016
Br	87	56	0.02	0.040
Kr	91	9.1	-	0.025
Rb	91	58	0.3	0.25
Sr	94	72	-	0.0080
Ag	117	73	1.6	1.5
Cd	119	200	2.4	2.6
In	124	3.2	3.0	2.7
Sn	127	247	0.34	0.30
Sb	133	148	0.45	0.40
Te	135	19	0.06	0.060
I	137	24	0.04	0.090
Xe	139	39	0.008	0.035
Cs	141	25	0.04	0.045
Ba	143	12	0.0014	0.0020

[a] Old system (0.3g) refers to the original UO_2 loading technique.

[b] New system (1.5g) refers to the improved UO_2 impregnating technique; see Ref. 6 or Ref. 7 for details.

TABLE 5: Summary of Possible Studies at ISOL Facilities

Nuclear Masses

- Direct mass measurements
- Q-values of α decay*
- Q-values of β decay

Delayed-particle Emission

- Neutron or proton* emission probabilities
- Energy spectra of neutrons or protons*
- γ-n or γ-p* coincidences

Nuclear Spectroscopy

- Half-lives of β-decaying isomers
- γ singles and β-gated γ spectra
- e^- singles and β-gated e^- spectra
- γ-γ and e^--γ coincidences
- γ-γ angular correlations
- α spectra*
- α-γ coincidences*
- β spectra
- Absolute decay rates (β and γ)
- Half-lives of nuclear excited states
- Magnetic moments of nuclear excited states
- Search for new nuclides

Atomic Spectroscopy (Dye-Laser or rf studies)

- Nuclear spins
- Nuclear magnetic multipole moments
- Nuclear electric multipole moments
- Hyperfine anomalies
- Isotope shifts
- Isomer shifts

Reaction Yields

- Mass distributions or yields
- Nuclear charge distributions or yields
- Ionic charge distributions

Isotope Production

- Radioisotopes for medical uses
- Exotic radioactive targets for reaction studies

Solid-State Studies

- Measurements of atomic magnetic fields
- Ion implanatation studies
- Low-temperature nuclear orientation studies

*Indicates study not possible for ISOL facilities at reactors.

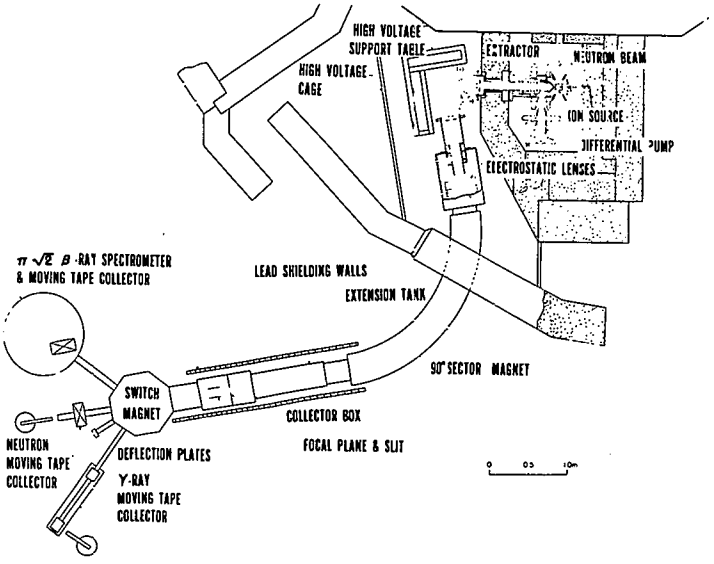

Figure 1. Schematic diagram of TRISTAN II at the ALRR in Ames.

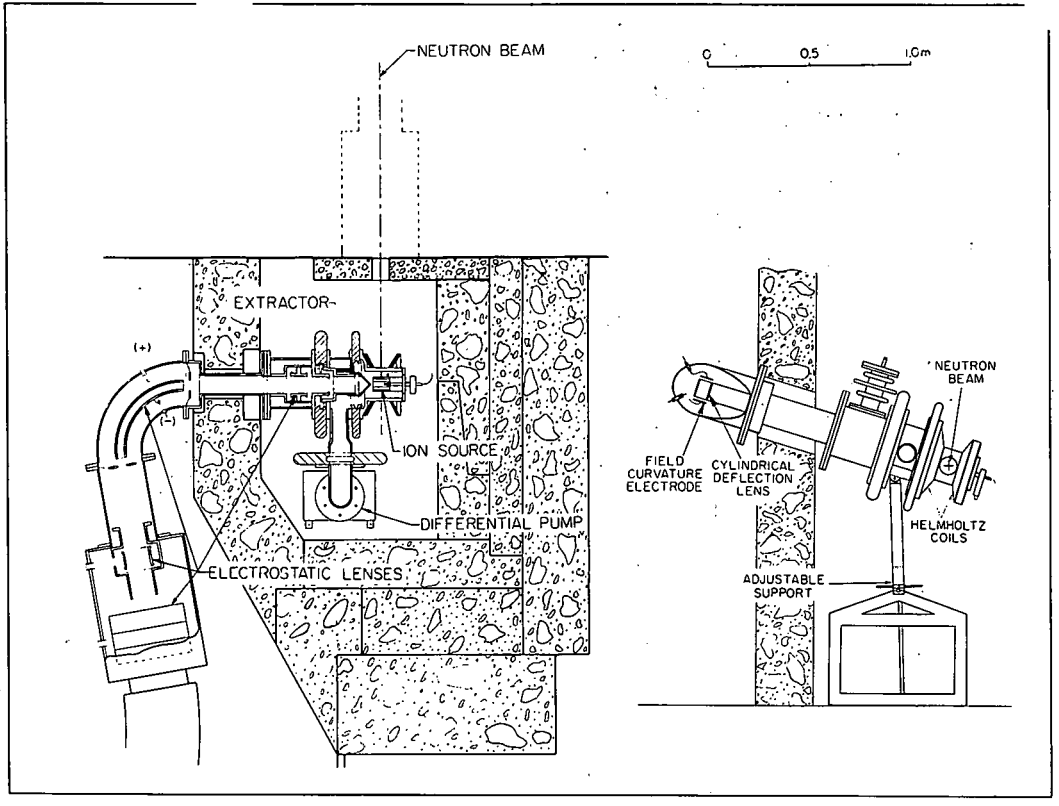

Figure 2. Close-up and vertical views of TRISTAN II at the ALRR.

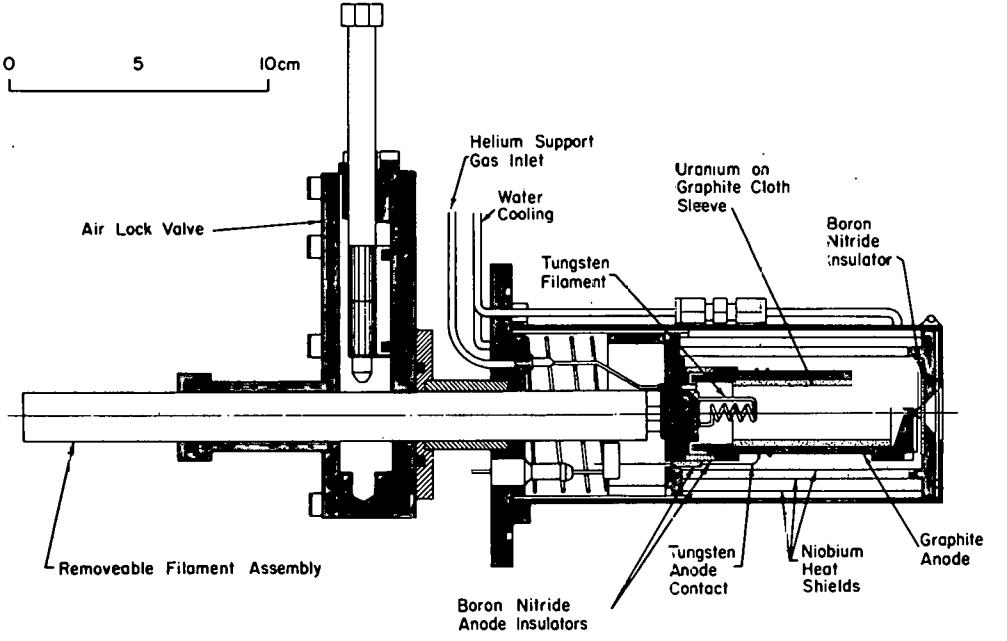

Figure 3. Details of the in-beam ion source used with TRISTAN II at the ALRR in Ames.

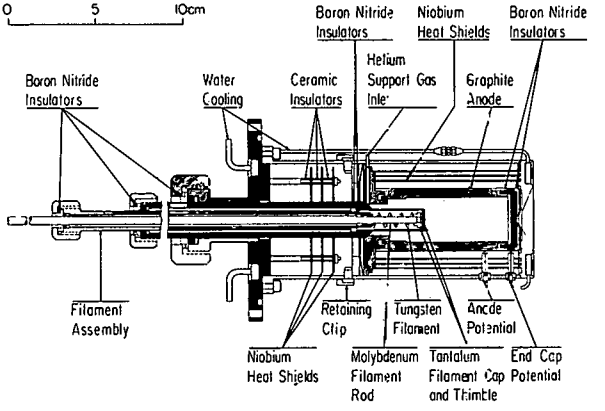

Figure 4. Details of the modified-FEBIAD in-beam ion source to be used with TRISTAN II.

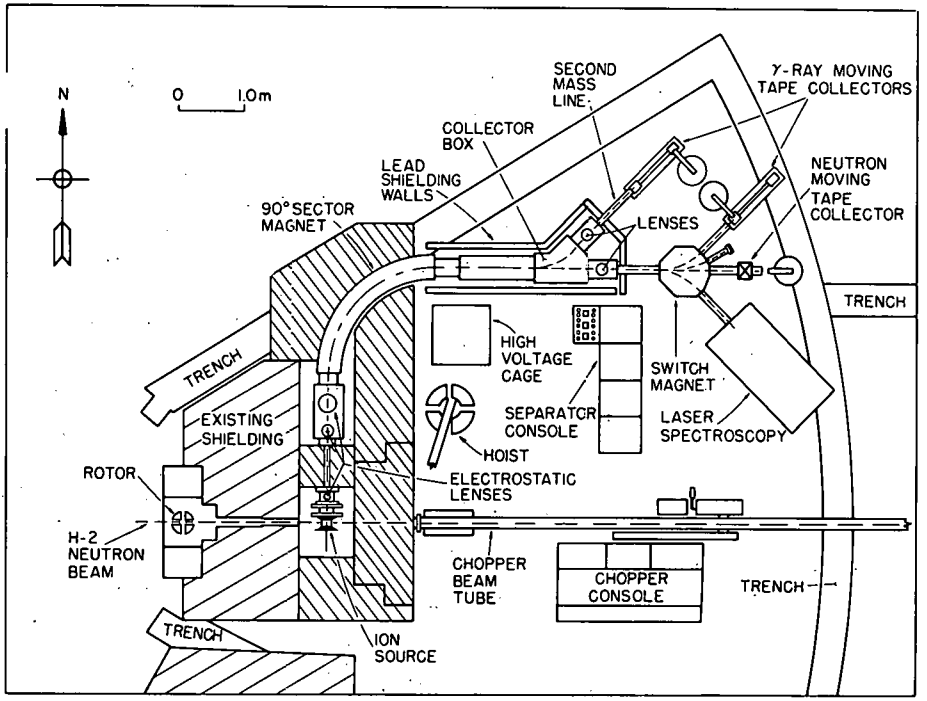

Figure 5. Schematic diagram of TRISTAN II at the HFBR in Brookhaven.

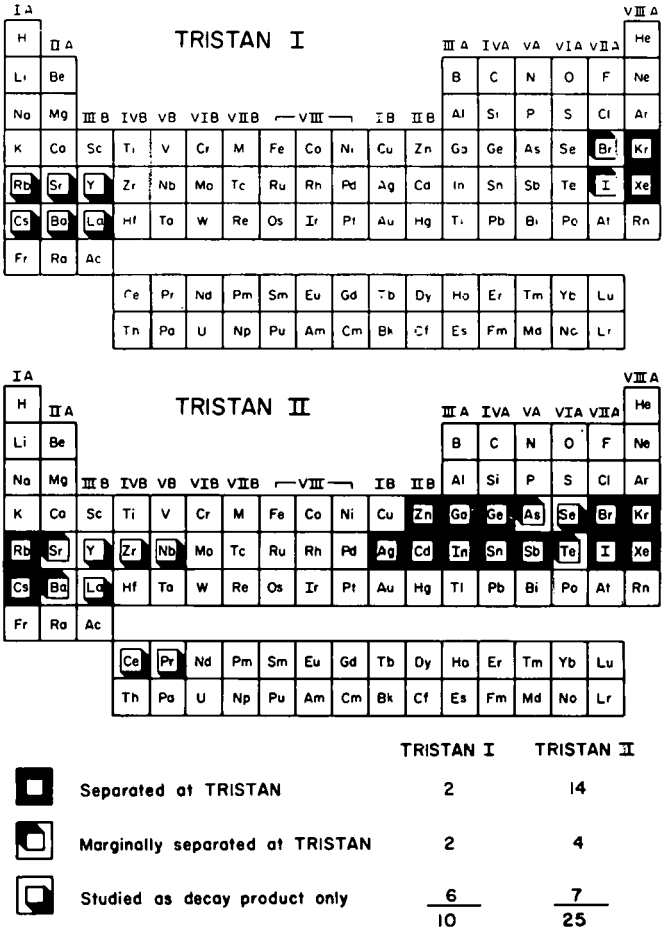

Figure 6. Periodic table of the elements, showing elements available with TRISTAN I and TRISTAN II.

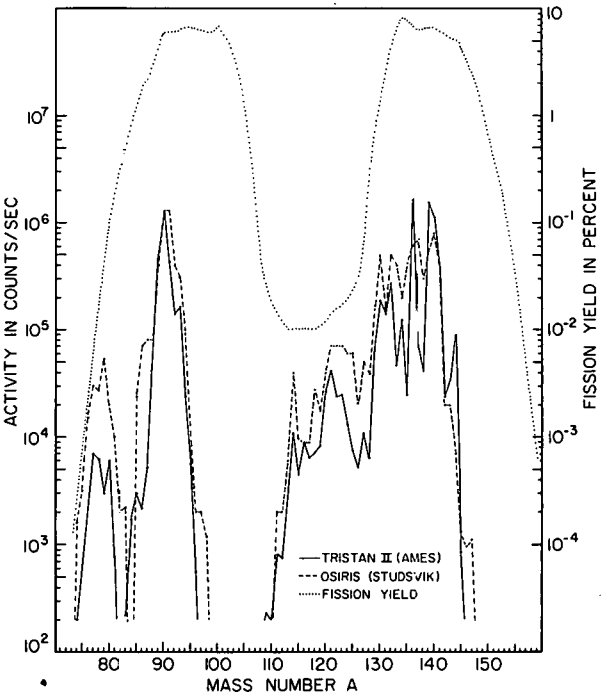

Figure 7. Mass scans of fission-product activities obtained with 4π β counting at OSIRIS and TRISTAN II in Ames; the mass distribution for thermal neutron fission of ^{235}U is included for reference.

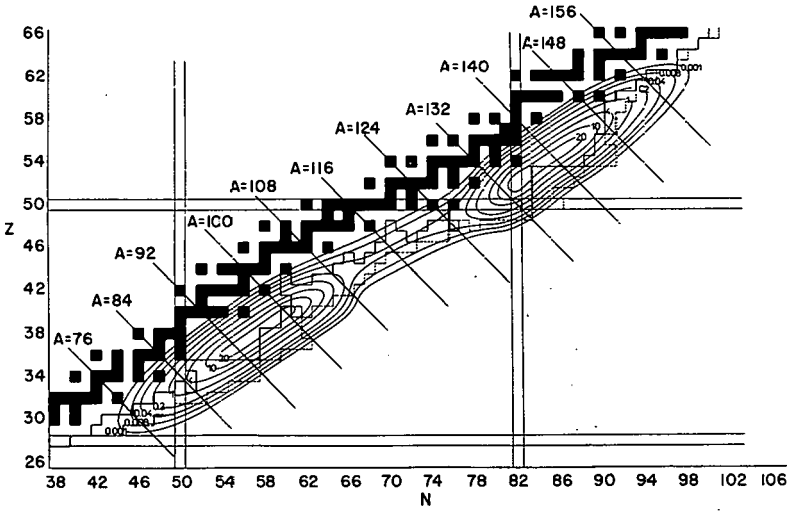

Figure 8. Contours of independent fission cross-sections in barns for $^{235}U(n_{th},fission)$.

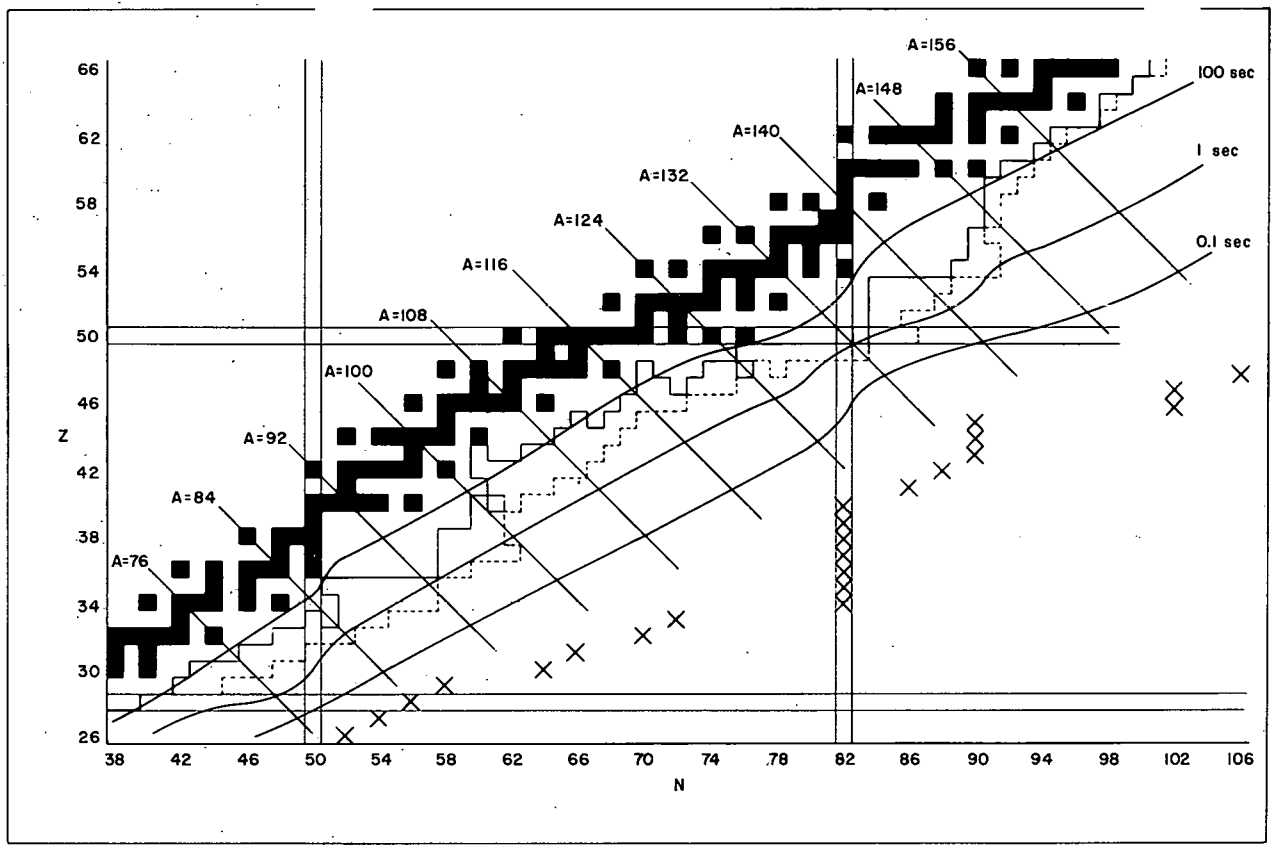

Figure 9. Contours of half-life predictions and neutron drip-line predictions for neutron-rich nuclei in the fission-product region of the chart of the nuclides.

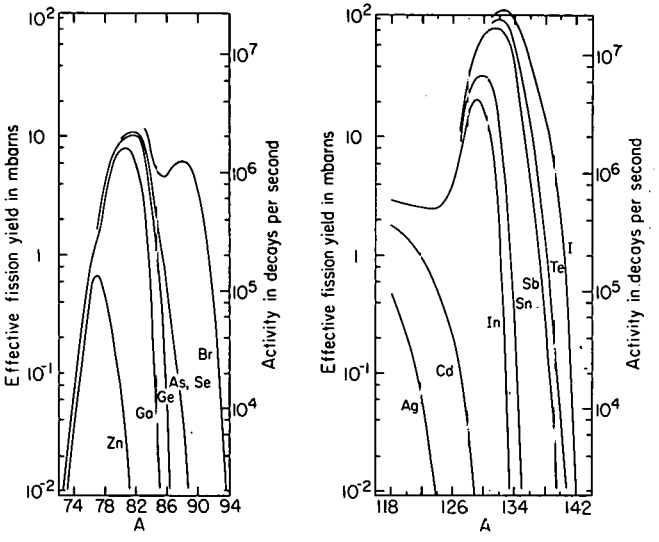

Figure 10. Effective fission yields calculated with the OSIRIS overall efficiencies (left-hand scales) and saturation activities expected with TRISTAN II at the HFBR (right-hand scales).

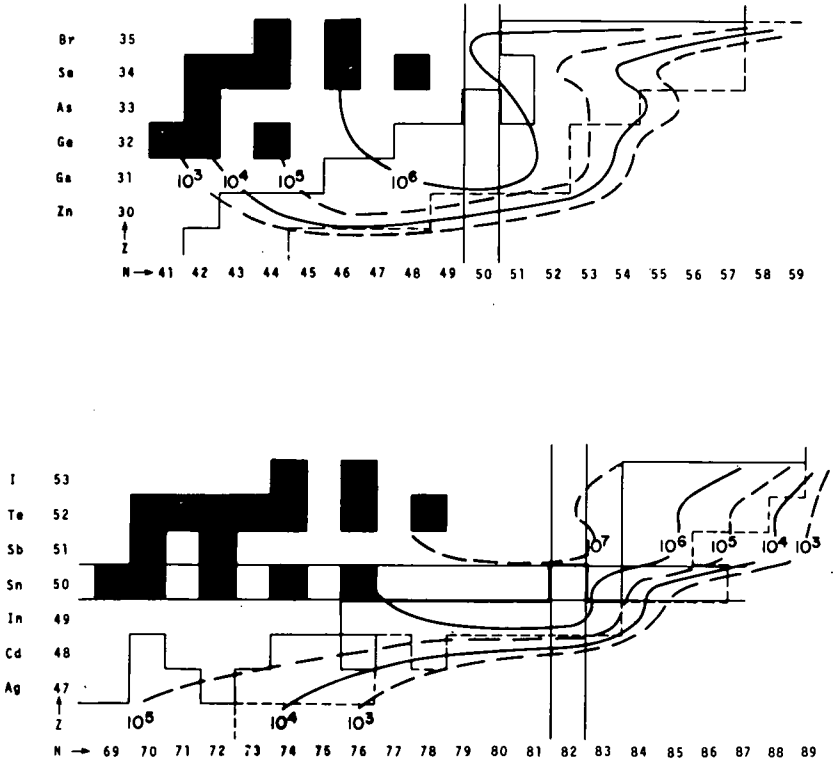

Figure 11. Contours of saturation activities in disintegrations/sec expected with TRISTAN II at the HFBR, calculated with the OSIRIS overall efficiencies.

INITIAL RESULTS WITH THE BERKELEY ON-LINE MASS SEPARATOR - RAMA*

Joseph Cerny, D. M. Moltz, H. C. Evans†, D. J. Vieira,
R. F. Parry, J. M. Wouters, R. A. Gough, and M. S. Zisman

Department of Chemistry and
Lawrence Berkeley Laboratory
University of California
Berkeley, California 94720

Introduction

We have for some time been interested in developing a reasonably fast and universal (having little or no chemical selectivity) on-line mass analysis system to expand our capabilities in studying nuclei far from stability. The system selected was originally proposed by Nitschke[1] and is termed RAMA, an acronym for Recoil Atom Mass Analyzer. Basically, this system utilizes the helium-jet method to transport activity to a Sidenius hollow-cathode ion source which is coupled to a mass spectrometer. A comprehensive discussion of RAMA will appear elsewhere.[2]

Present System

A schematic diagram of the overall RAMA system is given in Figure 1. The RAMA helium-jet employs chemical additives in the helium (presently ethylene glycol) which, in the presence of sufficient ionizing radiation, builds up aerosols.[3] Attachment of the radioactive nuclides to these high molecular weight aerosols is necessary to insure good transport efficiency and a small opening angle for the activity as it exits the 1 mm ID, 5.8 m long stainless steel capillary tube. Transport efficiencies of between 10 and 60% have routinely been achieved, though the latter is much more typical when conditions are optimized.

The capillary exit is aligned with a skimmer (1mm orifice) at a distance of approximately 7 mm. This skimming removes most of the helium while allowing a majority of the activity to pass through the skimmer undeflected. One series of tests with ^{20}Na activity demonstrated an opening angle of 2.8° for 55% of the activity. (Many tests of the RAMA system have been performed with the β-delayed alpha-emitter ^{20}Na, produced via the $^{24}Mg(p,\alpha n)$ reaction at 38 MeV, due to its easily identifiable alpha groups and its short half-life of 445 msec.)

As seen in Figure 1, the skimmed activity then enters the RAMA hollow-cathode ion source. This ion source has been operated using both tantalum and tungsten filaments, with the former lasting on the average ∿ 50 hours at 1600 °C. Tungsten filaments have been tested for periods of up to 100 hours at temperatures exceeding 2000 °C. Under the arc conditions prevalent at these temperatures, the species of interest is ionized primarily to +1 (recent tests indicate $^{40}Ar^{+1}/^{40}Ar^{+2} \approx 100$ under normal arc conditions (Arc Current = 1.0 - 1.5A; V_{ARC} = 180-250V).

In our setup, good ion source efficiency as well as optimal mass resolution depend strongly upon the arc conditions. Different arc conditions can change the emittance of the source, so that it is no longer well matched to the acceptance of the spectrometer system. The arc conditions are governed by three independently adjustable parameters: electron density (filament temperature), electron temperature (arc voltage), and neutral gas density.

Internal beams of $^{40}Ar^{+1}$ and $^{20}Ne^{+1}$ ions from the RAMA ion source were used to determine the effects of various optical devices in the mass analysis system. The first device after the ion source is an Einzel lens; this electrostatic element is used to focus the beam into the Wien filter, a crude velocity selector used to separate the large component of He^{+1} (arc support gas) produced in the ion source from the nuclide of interest.

The beam then enters the main mass analysis system which consists of an electrostatic quadrupole triplet, a sextupole, a dipole, and a second sextupole. A quadrupole triplet is necessary to match the beam profile to the acceptance of the dipole analyzing magnet. The first (upstream) sextupole corrects for second-order aberrations while the second (downstream) sextupole rotates the focal plane by 60° so that it is normal to the analyzed beam. When all components are optimized, values of $m/\Delta m$ from 170 to 210 are obtained. This resolution was calculated from the equation $Res = \frac{D}{2w}$ where D is the measured dispersion of 164 cm and w is the measured width in cm at one-tenth maximum (FW.1M).

Figure 2 presents the mass spectrum of most of the tin isotopes after the optics parameters were optimized. This spectrum was obtained with a CEM (Channeltron Electron Multiplier) which permits calibrations to be done with very low intensity beams. Quick calibrations are routinely obtained during an experiment to monitor any small changes in operating conditions not easily detectable by external means.

Once the activity has been focused through a symmetrically opening slit system in the focal plane onto a collection foil, the decay products from the nuclides of interest are detected by a counter on the focal plane. Alternatively, the activity can be physically removed from the collection point by a 180° rotary-solenoid-operated flipper-wheel system. In order to characterize the decays of the various nuclei of interest, solid state detector telescopes, a plastic scintillator telescope for high energy β^- particle detection, and γ-ray detectors are being incorporated into the flipper-wheel system.

Initial Experiments

The initial tests involved checking various optics parameters with ^{20}Na activity as well as ^{211}At produced via the $^{209}Bi(\alpha,2n)$ reaction at E_α = 27 MeV. Efficiencies for various components of the RAMA system for Na and At as well as for Te and Dy, which will be discussed below, are given in Table I.

After these tests, one sequence of experiments was performed to confirm the mass assignments of a number of the short-lived, high-Z rare-earth alpha particle emitters produced by (HI,xn) reactions on various targets. The initial reaction studied was $^{142}Nd(^{12}C,xn)^{154-x}$ Dy with the intention of observing the alpha emitters ^{150}Dy and ^{151}Dy, which are made in high yield (> 500 mb). Further experiments confirmed the mass assignments of other N = 84, 85 rare-earth alpha particle emitters from terbium through ytterbium with half-lives ranging from 4.1 h to 400 msec. Figures 3 and 4 are examples of these alpha particle emitters while Table II summarizes our observations compared to the literature assignments.[4]

Some of the odd-Z rare-earth alpha emitters were also investigated. These nuclides exhibit substantial isomerism, with the excitation functions for the low-spin isomers shifted relative to the high-spin isomers by as much as 18 MeV, much more than is usually observed in excitation function shifts for isomer production in other mass regions. This is particularly noticeable for ^{151}Ho, when produced by the $^{141}Pr(^{16}O,6n)$ reaction, has a peak yield for the high-spin isomer at 123 MeV relative to 105 MeV for the low-spin isomer.[5] This situation was investigated with the RAMA system to clarify the mass assignments of these isomers because the excitation function for $^{151}Ho^{(LOW\ SPIN)}$ peaks very near that for $^{152}Ho^{(HIGH\ SPIN)}$, and thus could conceivably have been an isomer of ^{152}Ho. Our experiments did, however, confirm the earlier mass assignments.

A more recent experiment has verified the mass assignment of ^{111}Te through the observation of the beta-delayed protons associated with its decay. he mass of this neutron-deficient Te nuclide was originally controversial with Macfarlane and Siivola[6] assigning the 19 sec β- delayed proton activity to ^{110}Te and Bogdanov et al.[7,8] assigning it to ^{111}Te. Figure 5 shows that the known proton spectrum appears at the mass 111 position so that the observed protons can be attributed to the decay of ^{111}Te; this has been separately confirmed by recent work reported from UNILAC.[9] Further studies in this region have led to the observation of delayed protons from ^{109}Te and the recently[9] discovered ^{112}I produced by the ^{102}Pd(^{12}C,5n) and ^{102}Pd(^{14}N,4n) reactions, respectively.

Planned Improvements

Several instrumental changes are planned for the near future. First, the entire ion source-extractor region will be modified to improve the geometry (and hopefully the efficiency) and to permit easier ion source access for changes and maintenance. Increasing the high voltage extraction from its present value of 10.5 kV will be investigated to reduce the beam emittance and improve the transport efficiency of the ion optical system. In order to remove the activity from the focal plane further than is now allowed by the flipper wheels, a fast tape transport system is being designed and built. An X-ray detection capability s being added for continuing experiments in the A = 50 closed shell region. Future studies will also involve searching for light, neutron-deficient, beta-particle emitters, such as ^{27}P produced by the ^{28}Si(p,2n) reaction.

REFERENCES

1. J. M. Nitschke, in Proceedings of the International Conference on the Properties of Nuclei Far from the Region of Beta-Stability, Leysin, Switzerland, 1970 (CERN Report 70-30, Geneva, 1970), Vol. 1 p. 153.
2. D. M. Moltz, R. A. Gough, M. S. Zisman, D. J. Vieira, and Joseph Cerny, Nucl. Instrum. Methods, to be published.
3. H. Jungclas, R. D. Macfarlane, and Y. Fares, Phys. Rev. Lett. 27, 556 (1971).
4. H. Gauvin, Y. Le Beyec, J. Livet, and J. L. Reyss, Ann. Phys. 9, 241 (1975).
5. R. D. Macfarlane and R. D. Griffioen, Phys. Rev. 130, 149 (1963).
6. R. D. Macfarlane and A. T. Siivola, Phys. Rev. Lett. 14, 114 (1964).
7. D. D. Bogdanov, I. Bacho, V. A. Karnaukhov, and L. A. Petrov, Sov. J. Nuc. Phys. 6, 650 (1968).
8. Ibid., 807.
9. R. Kirchner, O. Klepper, G. Nyman, W. Reisdorf, E. Roeckl, D. Schardt, N. Kaffrell, P. Peuser, and K. Schneeweiss, Phys. Lett. 70B, 150 (1977), and E. Roeckl et al., contribution to this conference.

*Work supported by the U.S. Department of Energy.

†Permanent Address: Queen's University, Kingston, Ontario.

Table I. RAMA Efficiencies

	^{20}Na	^{111}Te	^{150}Dy	^{211}At
He-jet	20%[a]	60%	10%[a]	15%[a]
Skimmer	70%	60%	60%	70%
Ion Source	0.2$_3$%	0.1$_2$%	~0.2%	0.2%
Magnetic Analysis[b]	50%	50%	50%	50%
Overall	0.016%	0.02%	0.01%	0.01%

a) Not Optimized.
b) Calculated based on measured ion source emittance.

Table II. Rare-Earth Alpha-Particle Emitter Mass Confirmations.

Nuclide	Z	E_α Observed[a] (MeV)	E_α Literature[b] (MeV)	$t_{1/2}$ Observed	$t_{1/2}$ Literature[b]
$^{149}Tb^g$	65	3.95	3.95	4.07±.1 h	4.1 h
^{151}Dy	66	4.07	4.07	17.5±.5 m	17.7 m
^{150}Dy	66	4.23	4.23	7.1±.7 m	7.2 m
^{152}Ho(High Spin)	67	4.45	4.46	53±4 s	52 s
^{151}Ho(High Spin)	67	4.51	4.52	36±2 s	35.6 s
^{153}Er	68	4.68	4.67	35±4 s	36 s
^{152}Er	68	4.82	4.80	-	9.8 s
$^{154}Tm^m$	69	5.02	5.04	-	3 s
^{155}Yb	70	5.19	5.21	-	1.65 s
^{154}Yb	70	5.32	5.33	-	400 ms

a) Typical errors are ± 0.03 MeV.

b) Ref. 4.

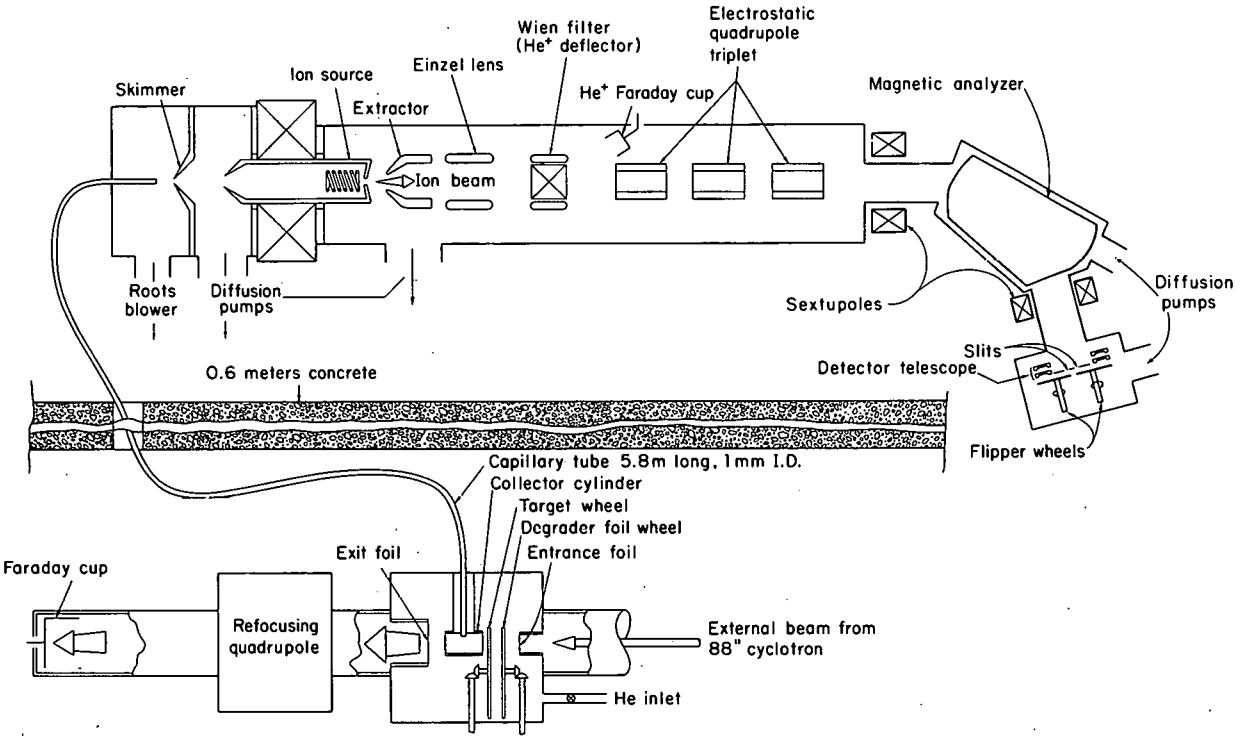

Figure 1. Overall schematic diagram of RAMA.

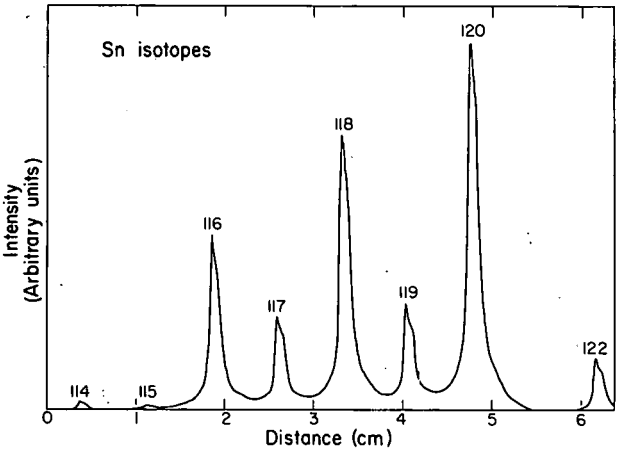

Figure 2. Channeltron electron multiplier scan of stable tin isotopes from 114 to 122. The valleys between adjacent masses do not go completely to zero because of response time in the CEM electronics and small amount of tailing.

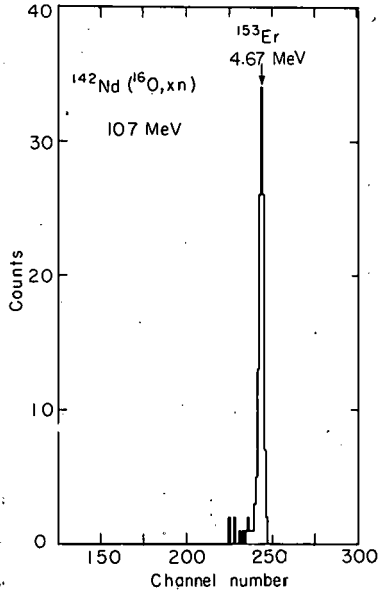

Figure 3. ^{153}Er alpha spectrum at the mass 153 focal plane position produced by the $^{142}Nd(^{16}O,5n)$ reaction.

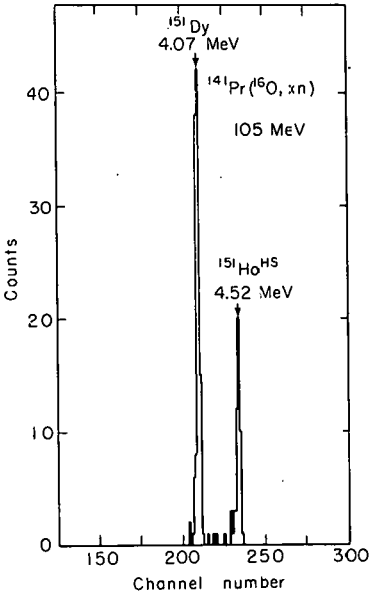

Figure 4. Mass 151 spectrum with ^{151}Dy and ^{151}Ho(High Spin) from ^{16}O reactions on ^{141}Pr.

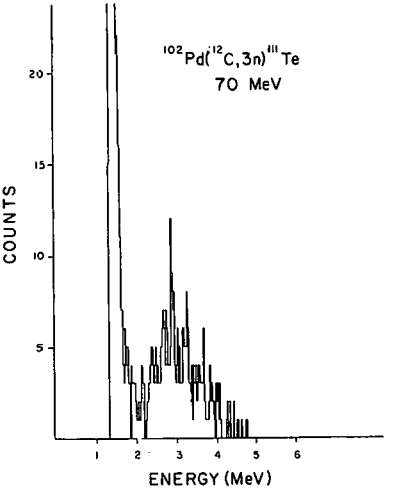

Figure 5. Proton spectrum at the mass 111 position from ^{111}Te produced by the $^{102}Pd(^{12}C,3n)$ reaction at 70 MeV.

STUDIES OF FISSION FRAGMENTS USING THE GAS FILLED RECOIL SEPARATOR JOSEF

T.A.Khan+ ,W.D.Lauppe and K.Sistemich

Institut fur Kernphysik, Der Kernforschungsanlage, Julich.

+ present address:Tandem Accelerator Laboratory,McMaster University, Hamilton, Ontario, Canada.

1. Introduction

I should like to begin this talk by a brief description of our separator itself and of the basic techniques used before I go on to discuss some of our recent electron and γ-ray experiments. Gas-filled separators have been successfully used for the investigations of recoils from fission or heavy ion reactions. One advantage of this type of separator is the high beam intensity which may be achieved since for suitable gas fillings the magnetic rigidity is approximately independent of the primary ionic charge and the kinetic energy and is essentially a function of the mass and nuclear charge of the ions. Another advantage is the short separation time which is of the order of a μsec and is determined by the time of flight of the recoils through the separator. The main disadvantage is that the mass resolution is limited by multiple scattering in the gas. A new gas-filled separator named JOSEF (Jülich On-line Separator for Fission Products) was installed at the reactor Dido of the Kernforschungsanlage, Jülich and has been in operation

since 1973. Compared with the smaller separator built in 1966, an improvement in beam intensity by a factor of 300 has been achieved and the mass resolution is 3 times better. With these improved conditions, many investigations such as the energy spectra of delayed neutrons emitted by fission products, and the spectroscopy of products with extremely small yields are possible.

In our present separator, the fission products are transferred from the U-235 source in the high flux region of the reactor, by an electrostatic particle guide, to the entrance slit of the magnet. After transmission through the magnet which contains a suitable gas filling (e.g., He at 4 torr for the light group or N_2 at 0.2 torr for the heavy group) the separated fission products are transferred by a second particle guide on to the tape of a moving tape transport system (MARIA) which may be moved either continuously or discontinuously. In general the discontinuous mode is used and after a preselected irradiation time, chosen to suit the lifetime of the nuclide, the tape is moved rapidly to the counting position 48 cm above. The separation of the irradiation and counting positions result in better geometry and much improved background conditions.

2. Calibration

Although the beam from JOSEF is not isotopically pure, the resolution is high enough to assign unambiguously the nuclide giving rise to a radiation. This is achieved in the following manner: The separator was calibrated by using a number of γ-ray lines whose assignment is well established and then measuring the intensity of the lines as a function of the magnetic field strength. The value of the

field strength B_{max} at maximum intensity is then characteristic of the nuclide. An example of the resulting calibration curves using He as the gas filling, is shown in ref. 1). It is seen that for a particular value of B_{max}, a number of mass-charge combinations are possible. Specific assignments may be made in several ways. The charge may be obtained independently, for example from x,γ coincidences. Once the origin of the main lines is known γ,γ coincidences establish the weaker transitions.

3. γ-ray and Conversion Electron Experiments

In our gamma and conversion electron work we have been concentrating on the Yr-Mo region with special emphasis on the Zr isotopes. This region is of particular interest because of the postulated region of deformation in neutron rich nuclei near mass 100, so that these nuclides are in a region of transition and show some very remarkable properties. For example, in moving from ^{98}Zr to ^{100}Zr the energy of the first 2^+ state appears to change from 1223 to 213 keV, a striking transition from apparently spherical to deformed behaviour (see fig. 1). Such properties have led Sheline, Ragnarsson and Nilsson to propose that there exists a second minimum in the nuclear potential (just as in the actinides) which moves down in energy to become the ground state minimum, for example, for the case of ^{100}Zr. Thus vibrational and rotational bands are presumed to coexist in these nuclei with 0^+ ground and excited states forming the respective bandheads. I shall skip over the Zr isotopes from 96 to 99 that we have studied and discuss the isotope Zr-100 where most of the interesting physics lies.

4. Zr-100: The 0_2^+ State

One of the puzzling questions with regard to this nucleus was whether a second excited 0^+ state existed in it and if so in what position? As may be seen in fig. 2, we had conjectured that the first excited state of ^{100}Zr was 0^+ and expected this fact to remove the drastic change in the level energies between 98 and 100 Zirconium. It was, therefore, decided to search for a 0^+ state in 100 Zirconium and to place it in the decay scheme. Our basic experimental arrangement had a retractable Si(Li) electron detector of resolution 3 keV on one side of the tape transport system, Ge(Li) or High purity germanium detector on the other side. The first experiment had the electron detector facing a high purity germanium detector and electrons in coincidence with the K-Xrays and low energy γ-rays were recorded. Fig. 3 shows the results of the X-ray, electron coincidences. Three strong peaks are seen in the Zirconium gate. Apart from the 836 keV peak in ^{98}Zr, the other two lines are at 313 and 194 keV. The 194 keV electrons are complimentary to the 213 keV γ-ray from ^{100}Zr as seen in fig. 4, which is a simultaneous singles measurement of the electrons and γ-rays. But there is no γ-ray at 331 keV which would be complimentary to the 313 keV electron line, thus establishing that line as due to an E0 transition. Its unambiguous assignment to ^{100}Zr may be seen in fig. 5 which shows the intensity versus magnetic rigidity distributions of the relevant lines. The maximum of the 313 keV electron line is located directly above that of the 213 keV γ-ray which is known to belong to ^{100}Zr. It is also situated the required distance away from the maximum of the 836 keV electrons from ^{98}Zr.

As far as the placement of the transition in the decay scheme was concerned, the X-ray, electron spectrum rules out the scheme suggested by our early speculation. This follows from the nearly equal magnitude of the 194 and 313 keV peaks whereas the 0_2^+ level populated by such a 213 keV γ-ray would be about 17 times larger than the 313 keV electron line. In our γ,γ coincidence results, the 213 keV line was strongly in coincidence with the 118.6, 352 and 666 keV γ-rays, the last three lines not being in coincidence with each other. In the γ,ce coincidences, we find the 313 keV electron line is not coincident with any of the above γ-rays whereas the 194 keV line is coincident with the 118.6 keV γ-rays. This pattern suggests the placement shown in fig. 6. According to this scheme the 213 and 352 keV cascade is still based on the ground state so that the drastic change in energy of the 2_1^+ states between ^{98}Zr and ^{100}Zr remains. A second remarkable feature is that one is confronted with a 0_2^+ state which is the lowest lying 0_2^+ state discovered so far. As a result of a series of measurements the decay scheme of ^{100}Y has been prepared. Among other features it was also found that ^{100}Y has two β-decaying isomers. The first with higher spin populates the 4^+ and 2^+ levels whereas the lower spin one populates only the 0^+ states. The decay of ^{100}Y which emerged is also shown in fig. 6.

5. The Decay Scheme of ^{100}Y: Nature of the 0_2^+ State

This extremely low lying 0_2^+ state in ^{100}Zr is perhaps the most remarkable feature in this level scheme and an understanding of its nature should shed considerable light on the many puzzling features of this nucleus. A number of explanations for the occurance of low lying

0^+ states in the Zr and Mo isotopes have been proposed. Of these, the two most worth exploring are that they are bandheads of β-vibrational bands and that they are due to a co-existence of nuclear shapes. If the present 0_2^+ state is indeed the bandhead of a β band then these are by far the lowest lying β vibrations. Since in that case even the approximate fulfilment of the adiabatic condition would be questionable, one would have to term them "quasi β vibrations". There are also a number of other difficulties with this explanation. Thus, despite a careful search, no other member of a β-band could be found, although at least the 2^+ member should be populated in β-decay. Secondly, if the Davydov and Chaban model is used to predict the 6^+ member of the ground state band and the 0^+ member of the β-band, one sees that the value of the 6^+ level is in good agreement with experiment but the predicted energy of the 0_2^+ level is very considerably higher.

Finally the coexistence of nuclear shapes giving rise to the two 0^+ states must be considered. According to the proposal of Sheline and co-workers there exists a second minimum in the potential surface in the even Zr isotopes, which comes down in energy to become the ground state minimum at ^{100}Zr. If this second minimum is presumed to be sharply defined and axially symmetric then certain problems arise with this explanation. Thus the transitions from the 0^+ level of the vibrational band, to the levels of the rotational band should be strongly hindered whereas, as we shall see, these transitions are relatively strong. Secondly the 2^+ level at 878 keV seems to have some of the characteristics of a γ-vibrational bandhead as far as its de-excitation pattern is concerned.

If this is indeed the case such a low lying γ-vibrational band would imply an axially asymmetric nucleus. Thus a sharply defined, axially symmetric second minimum is probably not consistent with our results. It is clear, however, that transition rates and level energies are sensitive to the depths of the minima and the height of the barrier in between them as well as the γ-degree of freedom. Moreover, dynamics are expected to play an important role.

Gneuss and Greiner have made a detailed investigation of various potential energy surfaces and have incorporated dynamics in their model. One of the potential energy surfaces generated by them, shown in fig. 7, seems to be remarkably compatible with the level scheme of ^{100}Zr. In the contour diagram of the β-γ plane one sees that the deformed minimum is axially asymmetric and located above the vibrational minimum. But due to the different zero point energies, the ground state is the deformed one and the higher lying 0^+ state the spherical one, for a value of 60 for their mass parameter B_2. As the value of B_2 increases, the spherical states are lowered much more rapidly so that the ground state becomes the spherical one at $B_2 = 200$. The situation in ^{100}Zr then appears to be the intermediate one where the ground state is still the deformed one, as substantiated by the measured value of 0.32 for the deformation parameter β_2 of ^{100}Zr.

6. The Lifetime of the 0_2^+ State

The lifetime of the excited 0^+ state has recently been measured. To do this a thin plastic (Ne 102) crystal of thickness 0.5 mm mounted on a photomultiplier was placed on one side of the tape transport and the Si(Li) detector was placed on the other side. A 1 mm thick

Aluminum absorber sheet was placed between the plastic detector and the tape transport to eliminate the low energy β-rays and conversion electrons from being detected by the plastic which was confined to having a high efficiency for the approximately 9 MeV end point energy β-particles which populate the 0_2^+ state. The Si(Li) detector detected the conversion electrons depopulating the level. Conventional constant fraction timing was used. In fig. 8 the timing distribution with the gate on the 313 keV electron peak is seen. From an anlysis of the two curves a half life of 3.37 ± 0.3 ns results for the 331 keV 0^+ state.

Now from the lifetime, and the branching ratio for the EO transitions to the ground state and the E2 transiticns to the 2_1^+ state, the nuclear monopole matrix element ρ may be obtained. Church and Weneser have defined ρ as

$$\rho^2 = \frac{1}{\tau\Omega_K(1+\frac{L+M}{K})(1+\frac{I(E2)}{I(EO)})}$$

where Ω_K is an electronic factor and τ is the mean life.

By inserting the appropriate values we get a value of

$\rho = 0.493 \pm 0.015$.

Now this is a surprisingly large value of ρ as may be seen in fig. 9 which shows the parameter ρ plotted against the quadrupole deformation β_2. It is seen that for all nuclei ρ has a value less than or equal to 0.9 β_2 except the present 0_2^+ state, suggesting that some factor is accelerating these transitions. This factor is the mixing of the two 0^+ states. For example, if the Variable Moment of Inertia model is used to predict the energy of the 6_1^+ state in ^{100}Zr using the E_4+/E_2+ ratio, the predicted value turns out to be 44 keV too low, suggesting that the 0^+ ground

state has been shifted downwards. Toki and I have applied the asymmetric VMI model of Toki and Faessler to ^{100}Zr to analyse this shift. As input in Toki's model we gave the position of 2_1^+, 4_1^+ and 2_2^+ and allowed the position of the 0^+ ground state to vary. For a perfect fit to the 6^+ state we got as output $\gamma = 17^o$ and $\Delta E_o = 60$ keV. Thus the two 0^+ states had shifted by 60 keV each from their unperturbed position. From the extent of the shifting we obtained the interaction matrix element and hence the values of 'a' and 'b' in the wave functions

$$|0_1> = a\ |0^+_{rot}> + b\ |0^+_{vib}>$$

$$|0_2> = -b\ |0^+_{rot}> + a\ |0^+_{vib}>$$

Thus the 0^+ states are regarded as linear combinations of the unmixed rotational and vibrational 0^+ states. The resulting $a^2 = 0.82$ and $b^2 = 0.18$.

To test these ideas with experiment, one can obtain the

$$\frac{B(E2)_{2_1^+ \rightarrow 0_2^+}}{B(E2)_{SP}} = 16 \text{ s.p.u. from the measured lifetime of the } 0_2^+$$

level. Now Jared and co-workers have measured the lifetime of the 2_1^+ level and hence obtained the value of

$$\frac{B(E2)_{2_1^+ \rightarrow 0_1^+}}{B(E2)_{SP}} \text{ as } 62 \text{ s.p.u.}$$

Then $\dfrac{B(E2);\ 2_1^+ \rightarrow 0_1^+}{B(E2);\ 2_1^+ \rightarrow 0_2^+} = \dfrac{a^2}{b^2} = \dfrac{62}{16}$ and since $a^2 + b^2 = 1$ one obtains

$a^2 = 0.79$ and $b^2 = 0.21$.

In the above analysis it has been assumed that the transition $0_2^+ \rightarrow 2_1^+$ proceeds due to the mixing of the 0^+ states only with no

contribution from any other source. In actual fact we know that such transitions without the mixing do occur, although with a strong hinderance. Nevertheless, the agreement of the prediction with experiment is good. Thus it appears likely that ^{100}Zr in its ground state is a triaxial nucleus with $\gamma=17^{\circ}$, as conjectured earlier.

7. ^{132}Sn

Finally, I would like to say a few words on the nucleus ^{132}Sn. For quite some time people in the field of nuclei far from stability have had their eye on this goal. Previous information on the nucleus ^{132}Sn was a 4041 keV line possibly seen by Kerek et al. in β-decay. The reason why this nucleus is so exciting is, of course, the fact that ^{132}Sn is the only doubly magic nucleus as yet unstudied and that it is very neutron rich (about 8 neutrons away from the nearest stable isotope). The principle experimentor for ^{132}Sn was W.D. Lauppe.

The reasons we could observe its level scheme are firstly that microsecond spin isomers exist in these nuclei which are populated through fission and secondly because of the 1 μs separation time of our separator.

The technique used for observation was as follows: The separated fragments were made to pass a pair of very thin muga detectors and then stopped on a catcher foil, all within the main beam (no tape transport was used for this experiment). The muga detectors provided the start signal and the detected γ-rays the stop signal. Intensity versus B_{ρ} and γ-γ coincidence runs were also carried out. The results are shown in figs. 10, 11, 12, 13. A 1.7 μs isomer was seen in ^{132}Sn and the 4041 keV γ-rays was found to be coincident with 374.3, 299.2 and 132.3 keV lines to form a stretched cascade. A 4415 keV line was seen as a cross over,

resulting in the level scheme shown. Particle-hole calculations carried out in our institute show the level sequence as 0^+, 2^+, 3^-, 4^+, 5^- and 6^+ for this nucleus. The calculated transition rates and level energies suggest that we are missing the 2^+ level but seeing all the others.

In conclusion one can say that the spectroscopy of nuclei far from stability on the neutron rich side is at least as fruitful as on the proton rich side. We have no means to populate very high spins on the neutron rich side as yet but the information resulting from the study of the low to medium spin members is yielding a wealth of new facts and ideas on the structure of the nucleus in this region.

REFERENCES

1. K. Sistemich, et. al., Nucl. Inst. and Math. 130, 491 (1975).

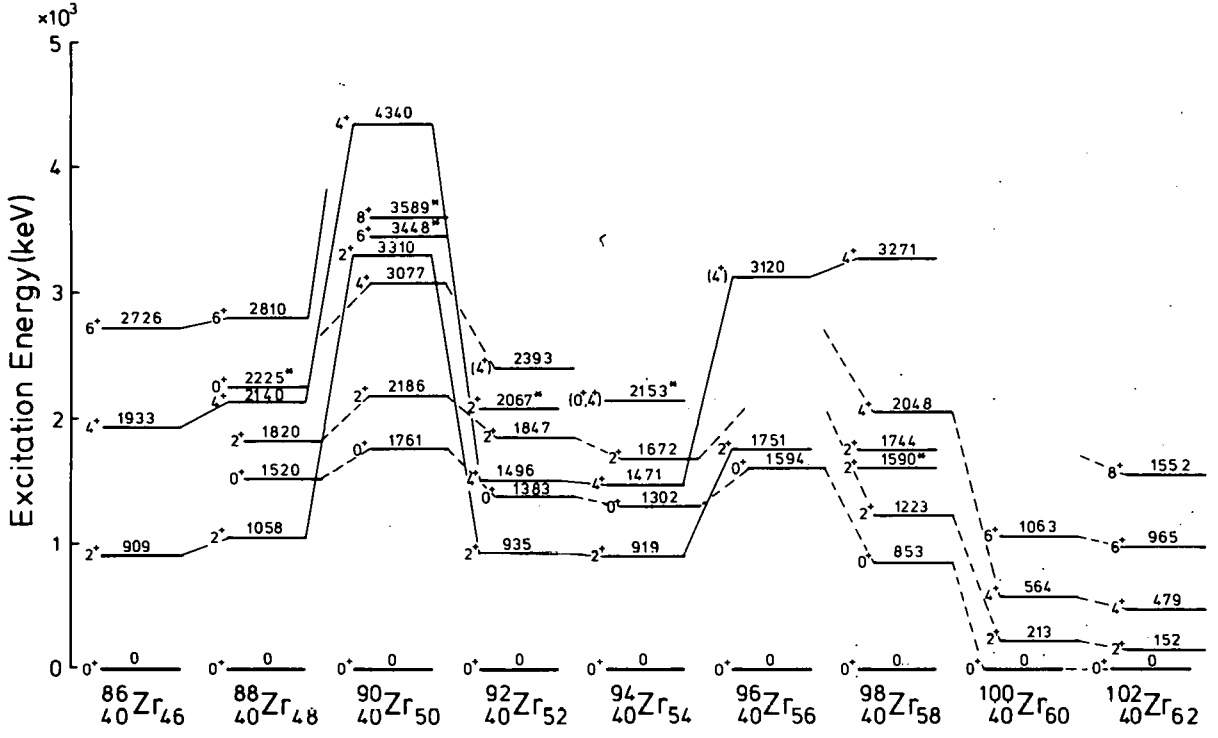
×10³
Excitation Energy(keV)
5
4
3
2
1
0
6⁺ 2726
4⁺ 1933
2⁺ 909
0⁺ 0
6⁺ 2810
0⁺ 2225*
4⁺ 2140
2⁺ 1820
0⁺ 1520
2⁺ 1058
0⁺ 0
4⁺ 4340
8⁺ 3589*
6⁺ 3448*
2⁺ 3310
4⁺ 3077
2⁺ 2186
0⁺ 1761
2⁺ 935
0⁺ 0
(4⁺) 2393
2⁺ 2067*
2⁺ 1847
4⁺ 1496
0⁺ 1383
(0⁺,4) 2153*
2⁺ 1672
4⁺ 1471
0⁺ 1302
2⁺ 919
0⁺ 0
(4⁺) 3120
2⁺ 1751
0⁺ 1594
4⁺ 3271
4⁺ 2048
2⁺ 1744
2⁺ 1590*
2⁺ 1223
0⁺ 853
0⁺ 0
6⁺ 1063
4⁺ 564
2⁺ 213
0⁺ 0
8⁺ 1552
6⁺ 965
4⁺ 479
2⁺ 152
0⁺ 0
86 40 Zr 46
88 40 Zr 48
90 40 Zr 50
92 40 Zr 52
94 40 Zr 54
96 40 Zr 56
98 40 Zr 58
100 40 Zr 60
102 40 Zr 62

Figure 1.

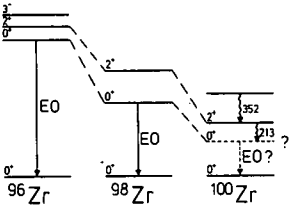

Figure 2.

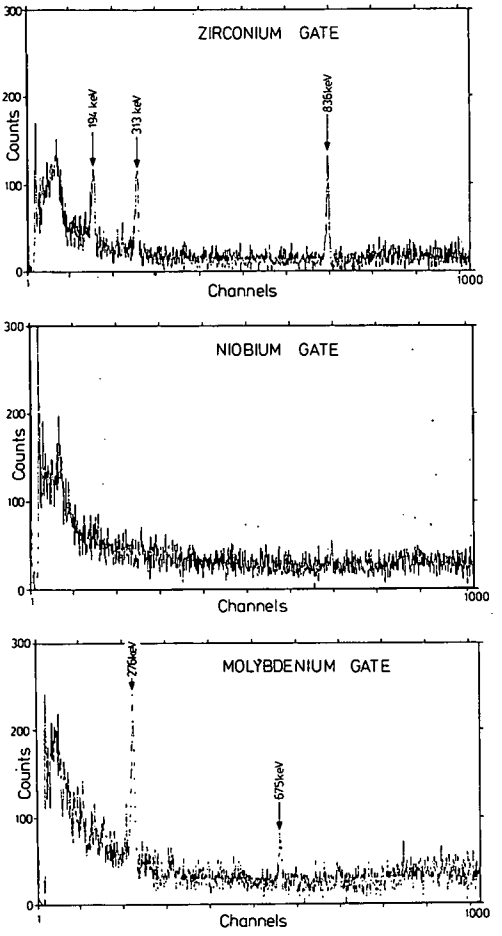

Figure 3.

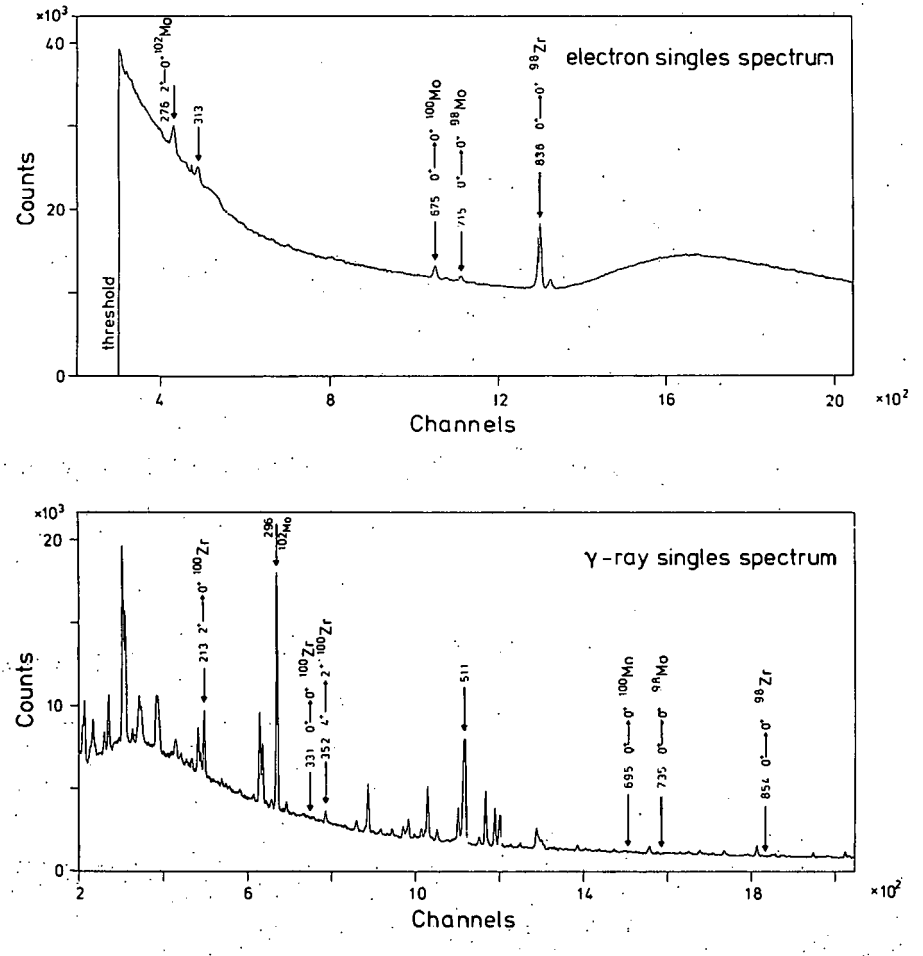
electron singles spectrum
Counts
Channels
threshold
γ-ray singles spectrum
Counts
Channels

Figure 4.

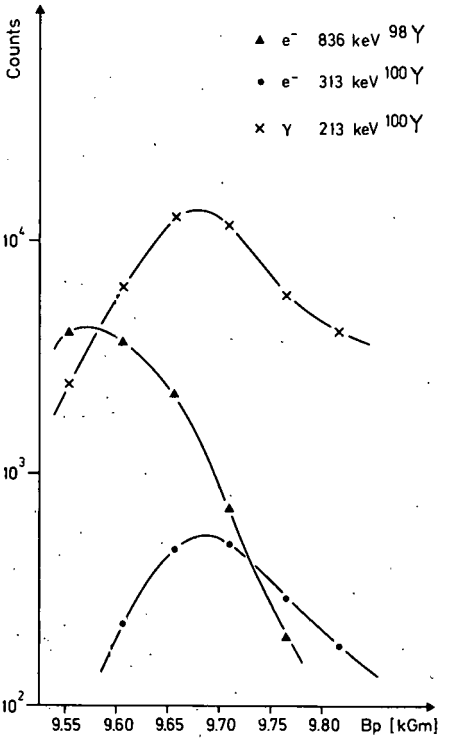
Counts
▲ e⁻ 836 keV 98Y
• e⁻ 313 keV 100Y
× γ 213 keV 100Y
10⁴
10³
10²
9.55
9.60
9.65
9.70
9.75
9.80
Bp [kGm]

Figure 5.

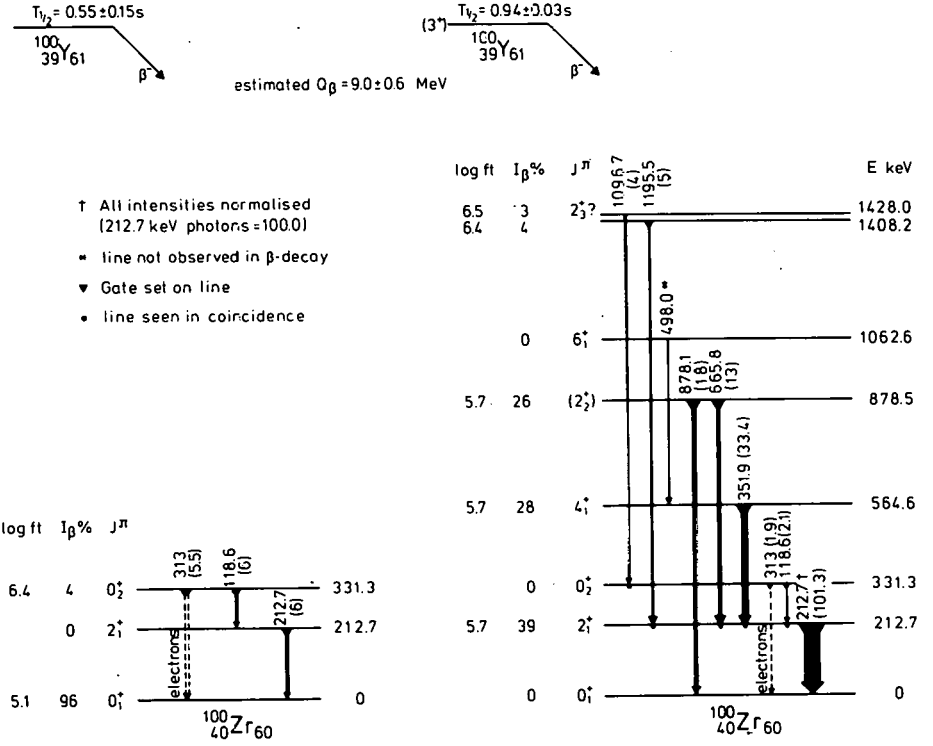
$T_{1/2}$ = 0.55±0.15s
$^{100}_{39}Y_{61}$
β⁻
$T_{1/2}$ = 0.94±0.03s
(3⁻)
$^{100}_{39}Y_{61}$
β⁻
estimated Q_β = 9.0±0.6 MeV
† All intensities normalised (212.7 keV photons = 100.0)
* line not observed in β-decay
▼ Gate set on line
• line seen in coincidence
log ft
I_β%
J^π
E keV
6.5
6.4
2_3^+?
3
4
1428.0
1408.2
1096.7 (4)
1195.5 (5)
498.0*
0
6_1^+
1062.6
878.1 (18)
665.8 (13)
5.7
26
(2_2^+)
878.5
351.9 (33.4)
5.7
28
4_1^+
564.6
313 (1.9)
118.6 (2.1)
212.7† (101.3)
0
0_2^+
331.3
5.7
39
2_1^+
212.7
electrons
0
0
0_1^+
0
$^{100}_{40}Zr_{60}$
log ft
I_β%
J^π
313 (5.5)
118.6 (6)
212.7 (6)
6.4
4
0_2^+
331.3
0
2_1^+
212.7
electrons
5.1
96
0_1^+
0
$^{100}_{40}Zr_{60}$

Figure 6.

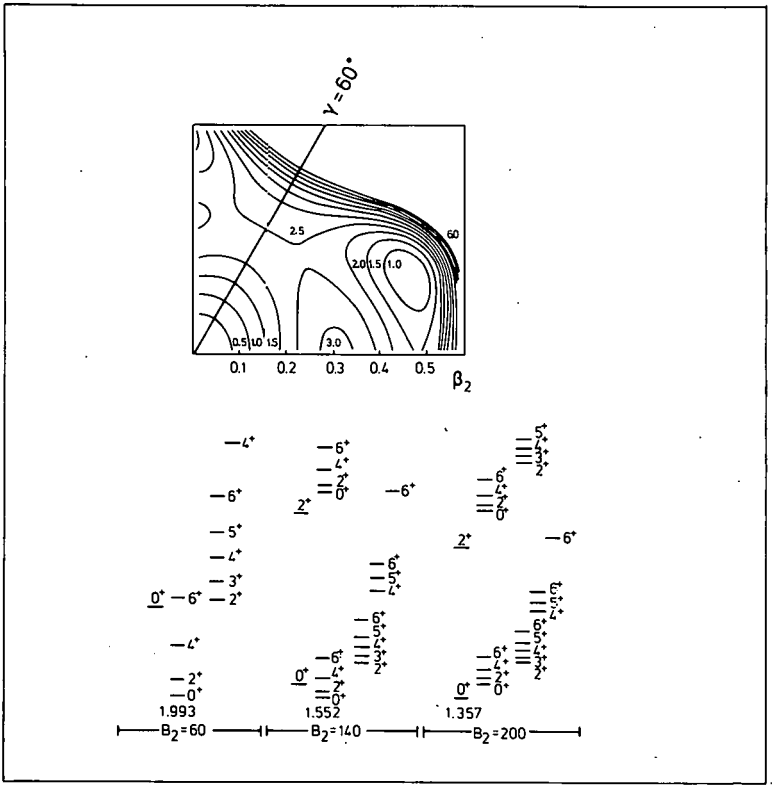
γ=60°
2.5
60
2.0
1.5
1.0
0.5
1.0
1.5
3.0
0.1
0.2
0.3
0.4
0.5
β2
1.993
1.552
1.357
B2=60
B2=140
B2=200

Figure 7.

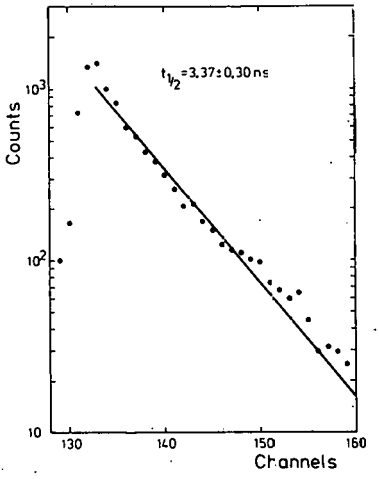

Figure 8.

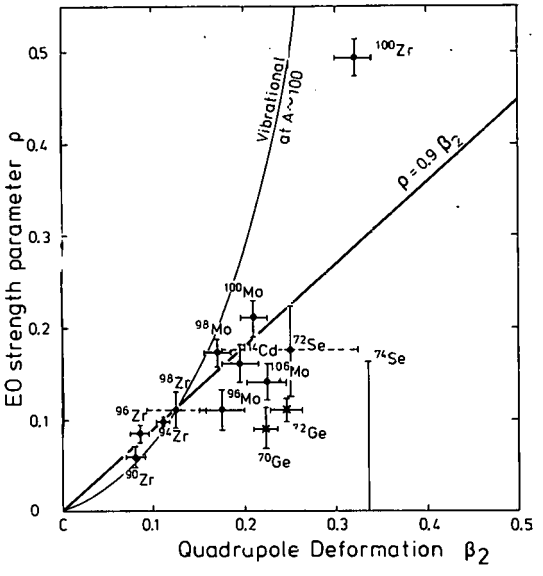

Figure 9.

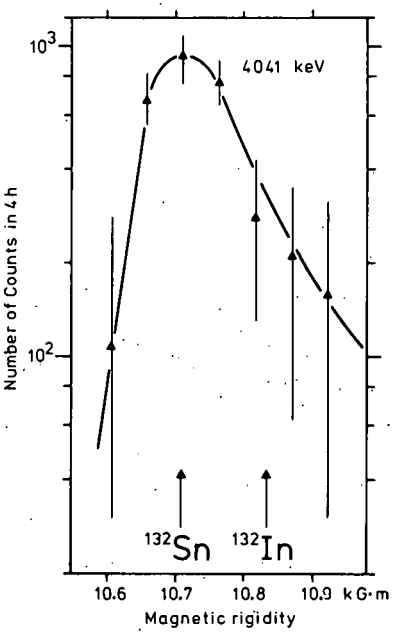

Figure 10.

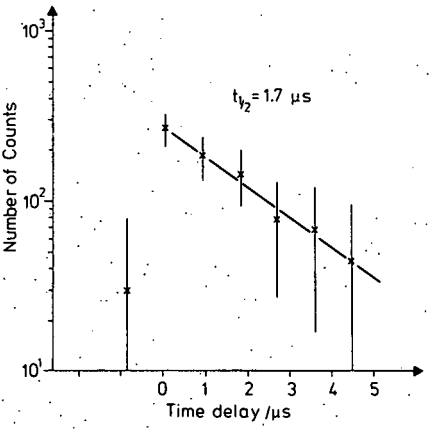

Figure 11.

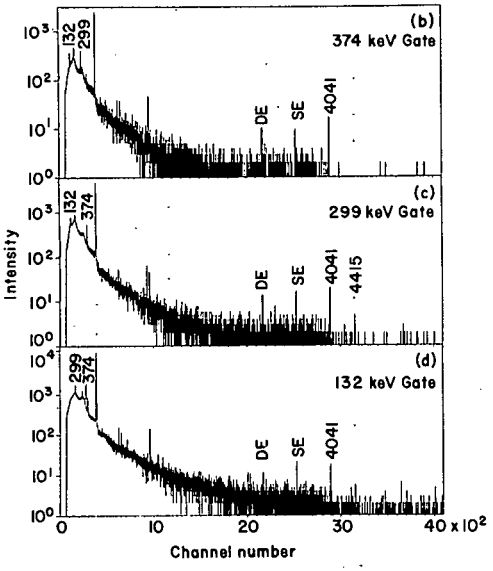

Figure 12.

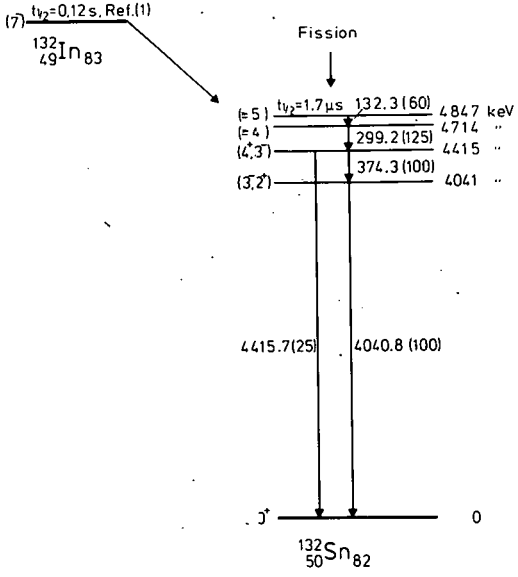

Figure 13.

Current Research on Delayed Neutron Emission at the SOLAR Facility

Paul L. Reeder
Battelle-Pacific Northwest Laboratories

Talk presented at

Ames-BNL Workshop on ISOL Systems

October 31, 1977

I. Introduction

The SOLAR facility is an on-line mass spectrometer operated by Battelle-Pacific Northwest Laboratories at a 1 MW TRIGA reactor located at Washington State University. The acronym SOLAR stands for Spectrometer for On-Line Analysis of Radionuclides and has nothing to do with a high intensity light source. The SOLAR facility was originally established to measure thermal neutron fission yields, but recently the effort has been devoted almost exclusively to study of the radioactive decay of delayed-neutron precursors.

Recent collaborators on the SOLAR project are listed in Table I. It should be mentioned that the mass spectrometer was designed and built by James Stoffels of Battelle[1] and that Bob Anderl, now at Idaho Falls, designed the shielding and participated in the first fission yield experiments.[2]

II. Description of SOLAR Facility

The floor plan of the SOLAR facility is shown in Fig. 1. The 1 MW TRIGA reactor is in a tank of water and can be moved next to the thermal column when needed. The neutron flux at the target position in the thermal column is 5×10^{10} n/cm^2 sec. The target consists of 1 g of 93.7% enriched ^{235}U in the form of UO_2 powder mixed with 1 g of graphite powder and pressed into thin wafers. Fission products diffuse out of this target matrix and are ionized on the hot surface of the oven. Intense beams of Rb^+ and Cs^+ fission products (> 10^6 ions/sec for high yield nuclides) are routinely obtained from a Ta oven. Molecular ions of BaF^+ and SrF^+ have been observed at 10-100 times lower intensities.[3] When Re is used for the hot surface, In^+ fission products are observed at intersities of

several thousand ions/sec. Negative ions of Br^- and I^- fission products have been obtained by ionization from a thoriated W surface.

Outside the thermal column shielding, the ion beams are bent 90 deg. by an electrostatic mirror into a 60 deg. magnetic sector. An electron multiplier is located at the focal point of the magnet and individual ions are detected by pulse counting techniques. A 60 deg. electrostatic deflector is located just in front of the electron multiplier. This device allows the ion beam of a single mass to be sent through a 2.4 m pipe to a collection station. A moving tape collection system is presently installed at this location which permits long-lived daughter activities to be removed while studying short-lived parent activities. The tape can be lifted out of the path of the ion beam to permit detection of the ion beam by a chevron channel electron multiplier. For our current experiments to measure delayed-neutron energy spectra, we have installed a vibration-isolation table under the collection point. The ^3He ionization chamber, proton recoil detector, and Ge(Li) gamma ray monitor can all be mounted on this table.

III. Gamma Spectroscopy

The gamma ray spectra from delayed-neutron precursors and their daughters provide several kinds of useful information. First of all one obtains the gamma spectra of the precursor and from the energies and intensities of the gamma peaks one can attempt to construct level schemes for the daughter nuclide. In the second place, one can use the relative intensities of some of the daughter or granddaughter gamma rays in the direct line of beta decay compared to the intensities of gamma rays of daughter nuclides from the delayed neutron branch to obtain delayed-neutron emission probabilities (P_n). Thirdly, one can observe those gamma rays

which follow neutron emission to excited states in the final nucleus in the so called $\beta n\gamma$ process. Fourthly, one can use the intensities of the gammas in the $\beta n\gamma$ process to determine what fraction of the delayed neutrons populate excited states. All these concepts are illustrated in Fig. 2 which shows a schematic representation of the precursor ^{94}Rb and its daughter nuclides.

The gamma spectra of Rb and Cs delayed neutron precursors were measured with a large Ge(Li) detector (14.2% of NaI eff., 2.13 keV resolution for ^{60}Co) mounted directly under the deposition point on the moving tape collector. Multi-spectral scaling techniques were used to determine which gammas were associated with a particular nuclide as illustrated in Fig. 3 for ^{143}Cs. The tape was moved periodically to remove long-lived background activity. Gamma spectra were stored in a PDP 8 computer operated as 4096 channel pulse height analyzer. Intensities of peaks were determined by the computer programs GASPAN or SKEWGAUS. Since only singles gamma ray spectra were obtained, we have attempted to construct decay schemes only for those cases where extensive studies in the literature are lacking. As an example, we show in Fig. 4 the levels of ^{145}Ba populated in decay of ^{145}Cs as determined from our data. Comparison of our energies and intensities of gamma rays with literature values generally gives good agreement.

To obtain P_n values from the relative intensities of daughter gamma rays, gamma ray spectra were recorded under conditions such that the daughter activities were in equilibrium with the parent activity. The relative intensities of particular gamma rays must be corrected by the absolute intensity of that gamma ray in its decay scheme. We have used literature values for these absolute intensities whenever possible. In some cases several gamma rays in the same nuclide could be used so multiple determinations

of P_n could be made. In Table II are given the resulting P_n values for the Rb precursors. These values are compared to our direct measurements published previously[4] and to values determined by Kratz et al.[5] Table III gives similar values for the Cs precursors. In general our results by the gamma method agree with our results by the direct counting method, but both methods disagree with the values determined by Kratz.

Gamma-rays from the $\beta n\gamma$ process have the same energies as gammas seen following beta decay of the precursor of one less mass. The relative intensities differ since the states are populated by different decay processes. The half-life of a particular gamma depends on whether it is a result of direct beta decay or whether it is a result of neutron emission from the next higher mass. If several gammas from neutron population of excited states are observed, they can be arranged into a level scheme. Intensity balance calculations can be used to obtain the relative population of various levels by neutron emission from the precursor. The $\beta n\gamma$ decay scheme for ^{96}Rb is shown in Fig. 5. as an illustration. Table IV summarizes the percentage of the neutron emissions going to particular states in the final nucleus for the case of ^{95}Rb and for ^{96}Rb. For many years it was thought that neutron emission would preferentially populate the ground state of the final nuclide. It is therefore of interest to see what fraction do go to excited states. Cur data for Rb are shown in Table V and our Cs data are shown in Table VI. The comparison of our data with that of Kratz, et al., shows quite good agreement.

IV. Neutron Spectroscopy

We have recently begun measurements of delayed-neutron spectra of mass separated precursors. At Battelle we have a ^{3}He ionization chamber of the Shalev type which gives a resolution (FWHM) of 18 keV (2.4%) for thermal neutrons. We have also collaborated with Prof. Woodruff of the University of Washington who has several proton recoil neutron spectrometers. In experiments performed this past summer, the ^{3}He spectrometer was located under the ion deposition point, a hydrogen filled proton recoil spectrometer was placed above the deposition point, and the Ge(Li) detector was located off to one side to monitor the ion beam during long runs. The proton recoil spectrometer has limited dynamic range, but has excellent resolution at low energies. The ^{3}He spectrometer was surrounded by a 1/8 in. thick Pb shield and a 3/8 in. thick B_4C shield. A temporary Cd shield was used before the B_4C shield was obtained. The neutron spectrum of ^{93}Rb obtained with and without the B_4C shield is shown in Fig. 6. The thermal peak is reduced by about a factor of 80 when the B_4C shield is used. The "raw" data shown in Fig.6. must be corrected by subtracting the thermal peak and by making an efficiency correction in order to obtain the spectrum of neutrons emitted by the precursor.

The efficiency curve for our ^{3}He spectrometer was obtained by using monoenergetic neutrons from the $^{7}Li\ (p,n)^{7}Be$ reaction. This calibration work was performed at the Van de Graaff accelerator located in the Safeguards Division of Los Alamos Scientific Laboratory. The spectrometer is operated in a two parameter mode with pulses sorted in a 4096 channel pulse height analyzer according to energy and risetime. A 512 channel energy by 8 channel risetime array was used. This method allows us to select various risetime

ranges to optimize the resolution of the spectrometer. Risetime analysis is particularly useful in discriminating against pulses due to elastic scattering of neutrons on ^{3}He. Spectra of risetime pulses obtained for two different neutron energies are shown in Fig. 7. The shortest risetime events are due to elastic scattering, a small peak is seen for thermal neutron induced pulses, and the longest risetime events are due to the desired $^{3}He\ (n,p)^{3}H$ reaction. However, all three types of events overlap each other in risetime.

The energy spectra of 0.5 Mev neutrons are shown in Fig. 8. for the first four risetime slices. At this energy the pulses due to elastic scattering fall below the thermal peak and can be ignored. However, the energy spectra for 1.5 MeV neutrons shown in Fig. 9. show that the elastic scattering pulses interfere strongly with the low energy fast neutron region. For most delayed neutron spectra the number of neutrons above 1.0 MeV is quite small so that the correction for elastic scattering is minimal. For the energy spectra given below we have used only the data in the first three risetime slices, i.e., risetimes ranging from 0 to 2.7 μsec. The relative efficiency of each risetime slice was determined at each neutron energy by integrating the area under the fast neutron peak and dividing by the number of counts in a monitor counter which has a flat response to neutrons of various energies. The resulting efficiency curves for two different risetime ranges are shown in Fig. 10. The cause of the structure in the curve at about 0.5 MeV is uncertain, but similar structure was observed by Krick and Evans[6] for a similar spectrometer.

In Fig. 11-14 are shown delayed-neutron spectra obtained at the SOLAR facility for the precursors ^{93}Rb, ^{94}Rb, ^{95}Rb, and ^{143}Cs. These spectra are the result of summing three risetime slices, subtracting the thermal peak, and dividing by the relative efficiency curve shown in Fig. 10.

The proton recoil spectrometer was operated simultaneously with the ^{3}He spectrometer, but was restricted to the lower neutron energy ranges. The statistical accuracy of the data was not as good as hoped for. In Fig. 15. and 16. are shown the neutron spectra of ^{93}Rb and ^{94}Rb at low energies. The spectra from the proton recoil data are compared to the ^{3}He spectrometer data of Kratz, et al. It appears that the proton recoil detector is showing even greater structure in the delayed-neutron spectrum thar can be seen with the ^{3}He spectrometer. However, there are some serious discrepancies as to the relative magnitudes of various peaks. It is clear that higher counting rates with high resolution spectrometers will be extremely valuable for understanding delayed-neutron spectra.

REFERENCES

1. J.J.Stoffels, Nucl. Instrum. Methods 119, 251 (1974).
2. P.L.Reeder, J.F.Wright, and R. A.Anderl, Conf. on Nuclear Cross Sections and Technology - March 1975, Ed. by R.A.Schrack and C.D.Bowman, NBS SP 425, p.401.
3. P.L.Reeder, L.J.Alquist, J.Lin, and J.F.Wright, Nucl. Instrum. Methods 133, 501 (1976).
4. P.L.Reeder, J.F.Wright, and L.J.Alquist, Phys. Rev. C 15, 2098 (1977).
5. K.-L.Kratz, Jahresbericht 1976, Institut fur Kernchemie der Universitat Mainz, Juni 1977.
6. A.E.Evans and M.S.Krick, Nucl. Sci. Eng. 62, 652 (1977).

Table I

SOLAR COLLABORATORS

BATTELLE - PACIFIC NORTHWEST LABORATORIES

PAUL L. REEDER
LARRY J. ALQUIST

WASHINGTON STATE UNIVERSITY

FRANK H. RUDDY

UNIVERSITY OF WASHINGTON

GENE L. WOODRUFF
GEORGE W. ECCLESTON
PAT GRANT

COLLEGE OF WILLIAM AND MARY

RICHARD KIEFER

LOS ALAMOS SCIENTIFIC LABORATORY

JAMES F. WRIGHT

Table II

DELAYED NEUTRON EMISSION PROBABILITY (%)

PRECURSOR	n, β	γ
^{93}Rb	1.86 ± 0.13 (1.24 ± 0.14)	2.22 ± 0.16 (1.32 ± 0.03)
^{94}Rb	13.7 ± 1.0 (9.7 ± 0.5)	8.77 ± 0.72 (10.1 ± 1.3)
^{95}Rb	11.0 ± 0.8 (8.4 ± 0.5)	11.4 ± 0.9 (8.6 ± 0.4)
^{96}Rb	17.0 ± 1.2 (12.5 ± 0.9)	? (13.4 ± 2.6)
^{97}Rb	35.9 ± 2.6 (25.2 ± 1.8)	>42 ± 10 (25.3 ± 4.8)

Table III

DELAYED NEUTRON EMISSION PROBABILITY (%)

PRECURSOR	n, β	γ
^{143}Cs	1.95 ± 0.14 (1.74 ± 0.12)	2.5 ± .3
^{144}Cs	4.3 ± 0.3 (2.95 ± 0.25)	4.6 ± 1.1
^{145}Cs	21.8 ± 1.5 (12.2 ± 0.9	19.7 ± .9

Table IV

NEUTRON EMISSION TO EXCITED STATES

PRECURSOR	LEVEL IN FINAL NUCLIDE	% OF P_n
^{95}Rb	0	51.5 ± 4.7
	837	33.1 ± 3.0
	1,308	5.7 ± 1.2
	2,395	9.7 ± 3.4
^{96}Rb	0	39.0 ± 21.3
	353	3.4 ± 16.0
	557	0.0 ± 2.4
	681	7.2 ± 11.9
	1,121	(12.6)
	1,259	37.8 ± 7.0

Table V

SUMMATION OF NEUTRON EMISSION TO EXCITED STATES (%)

PRECURSOR	SOLAR	KRATZ, et al.
^{93}Rb		9.0 ± 1.0
^{94}Rb		59.9 ± 9.3
^{95}Rb	48.5 ± 4.7	46.0 ± 3.5
^{96}Rb	61 ± 21	58.6 ± 4.6
^{97}Rb		91 $^{+9}_{-25}$

Table VI

NEUTRON EMISSION TO EXCITED STATES

PRECURSOR	LEVEL IN FINAL NUCLEUS	% OF P_n
^{143}Cs	359.5	12 ± 2
^{144}Cs	820.6	46 ± 12
^{145}Cs	198.9	100 ± 14

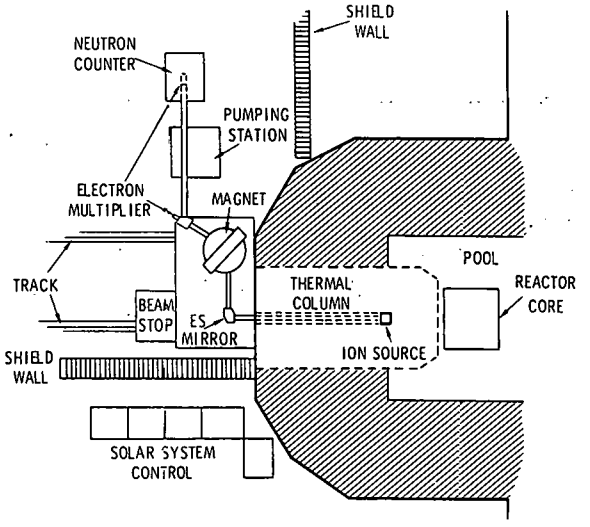

Figure 1. Floor plan of SOLAR facility.

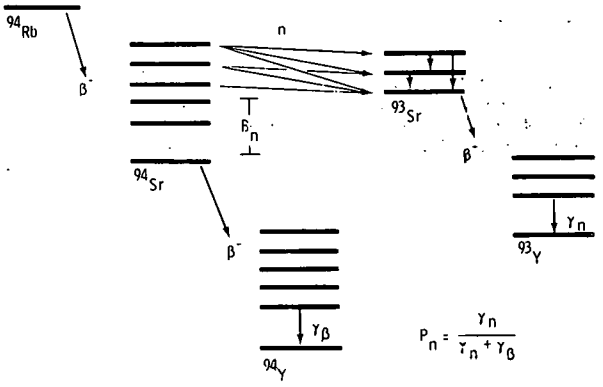

Figure 2. Schematic representation of ^{94}Rb and its daughters showing gamma transitions useful for determining the P_n value.

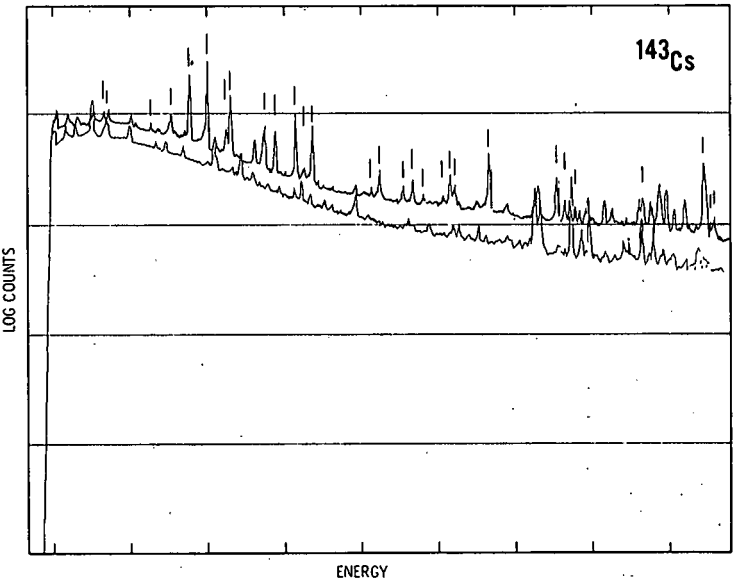

Figure 3. Upper curve - gamma spectrum of ^{143}Cs. Lower curve - background spectrum taken about two half-lives later. Lines above certain peaks indicate where short-lived peaks are disappearing.

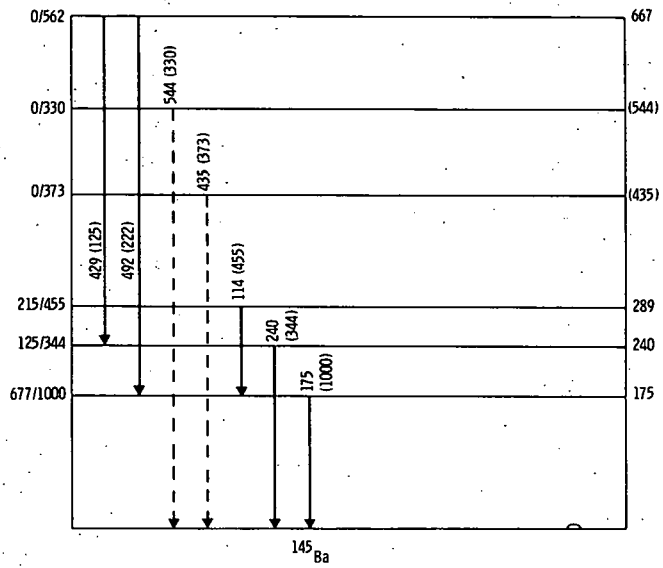

Figure 4. Decay scheme of ^{145}Cs based on singles gamma ray data only.

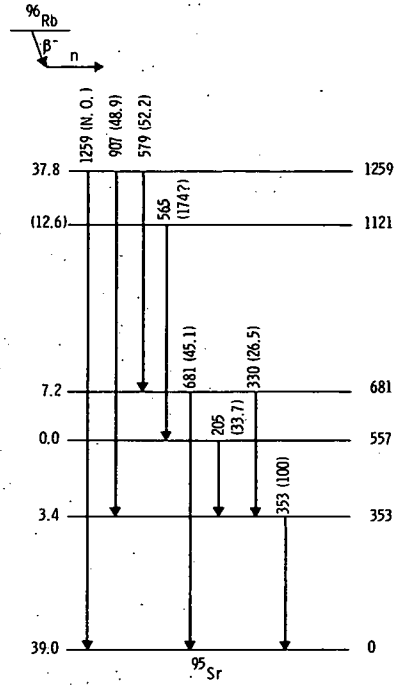

Figure 5. Neutron emission to excited states of ^{95}Sr from decay of the precursor ^{96}Rb.

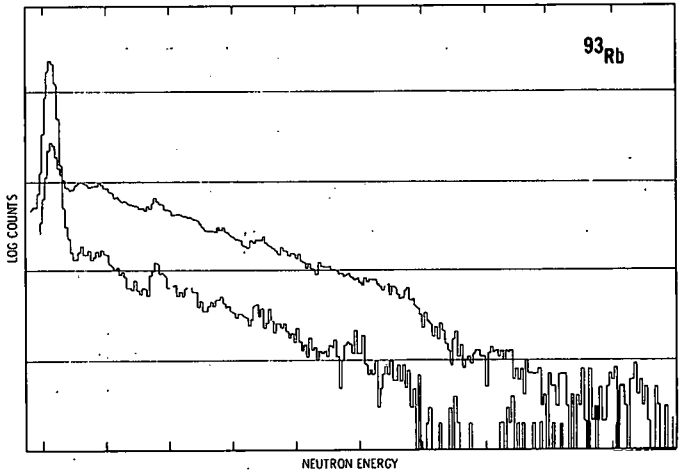

Figure 6. Delayed-neutron spectrum of ^{93}Rb with and without the B_4C shield.

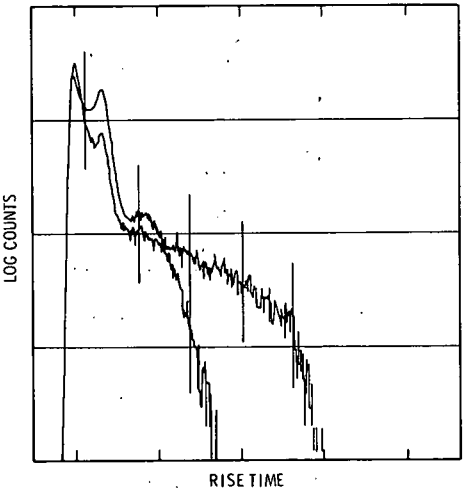

Figure 7. Risetime spectra taken at neutron energies of 0.2 and 1.25 MeV.

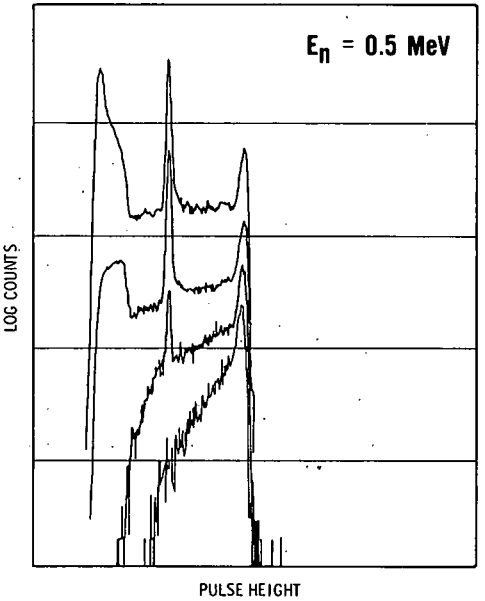

Figure 8. Pulse height spectra of 0.5 MeV neutrons for four risetime slices; 0-0.6, 0.6-1.6, 1.6-2.7, and 2.7-3.7 μsec.

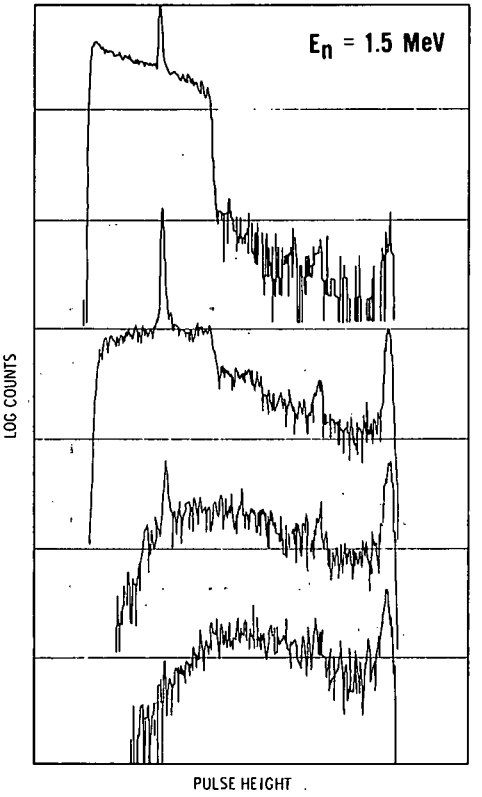

Figure 9. Pulse height spectra of 1.5 MeV neutrons for the same risetime slices as in Figure 8.

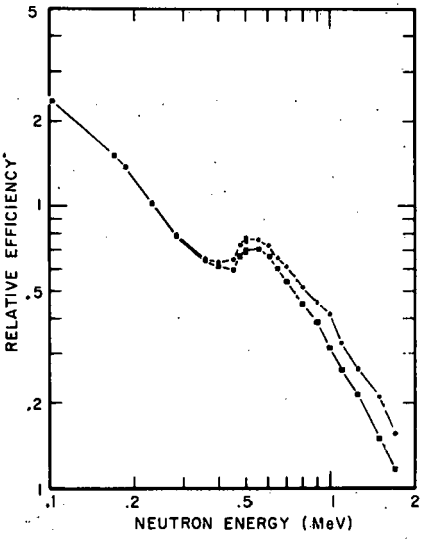

Figure 10. Relative efficiency curve of ^{3}He neutron spectrometer for full energy peak. Upper curve - risetime range 0-4.7 μsec, lower curve - risetime range 0-2.7 μsec.

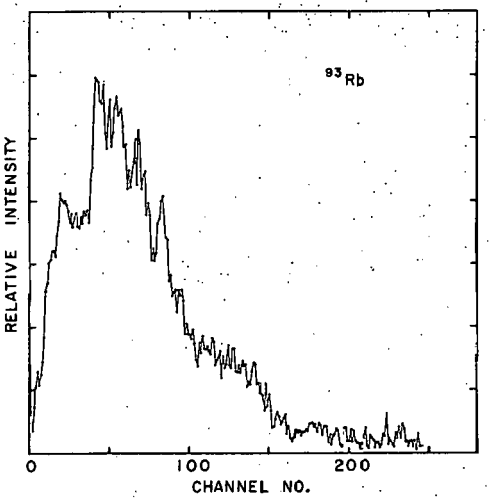

Figure 11. Delayed neutron spectrum for ^{93}Rb, 5.56 keV/ch.

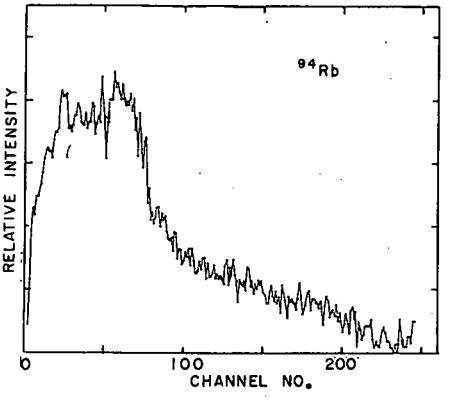

Figure 12. Delayed neutron spectrum for ^{94}Rb, 5.56 keV/ch.

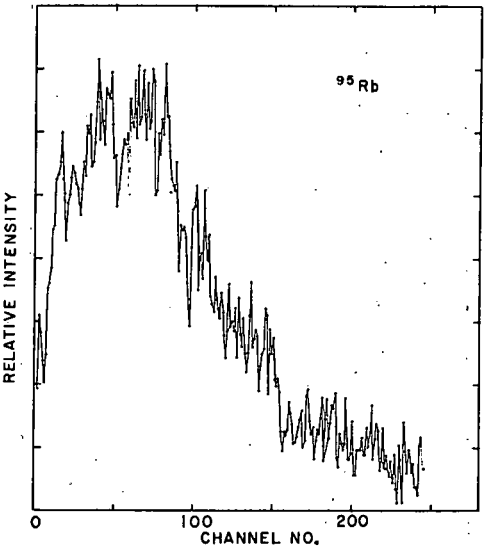

Figure 13. Delayed neutron spectrum for ^{95}Rb, 5.56 keV/ch.

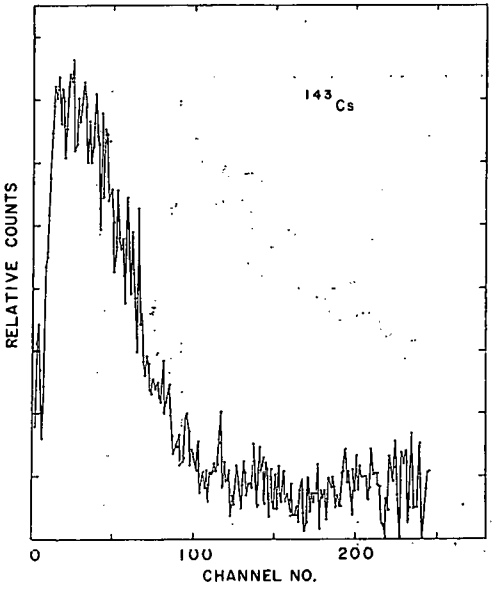

Figure 14. Delayed neutron spectrum for ^{143}Cs, 5.56 keV/ch.

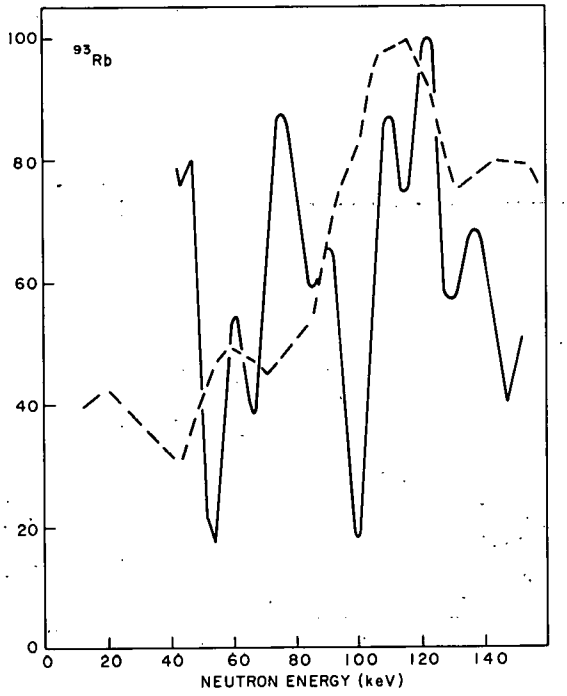

Figure 15. Low energy neutron spectra of ^{93}Rb, solid curve - from proton recoil detector, dashed curve - from Kratz, et al.

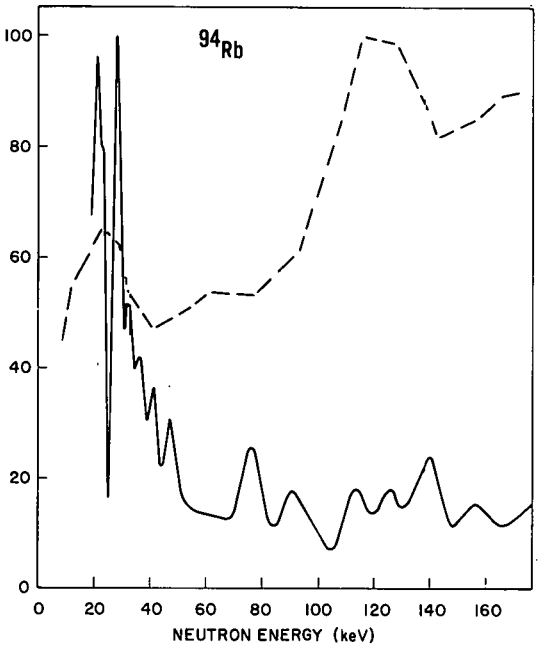

Figure 16. Low energy neutron spectra of ^{94}Rb, solid curve - from proton recoil detector, dashed curve - from Kratz, et al.

APPLICATIONS OF FISSION-PRODUCT DECAY DATA[†]

C. W. Reich
Idaho National Engineering Laboratory
EG&G Idaho, Inc.
Idaho Falls, Idaho

ABSTRACT

The relevance of fission-product decay data to a number of currently important activities is discussed. Specific reactor-related areas treated include fission-product decay heat, monitoring of nuclear power plants, fast-reactor dosimetry and the measurement of fission-product cross sections using activation techniques. The organization and content of the decay data included in the Evaluated Nuclear Data File (ENDF/B), an important user-oriented data evaluation, is given. A discussion of β-strength function measurements on short-lived fission products is presented and a possible application of data from these studies to the decay-heat problem is pointed out.

I. INTRODUCTION

At the present time, the most active and exciting phase of nuclear spectroscopy is the study of nuclides far off the line of beta stability. Evidence of the vitality and productivity of this area of research is provided by, among other things, the information presented at a number of international conferences[1,2,3] dedicated solely to this subject. Indeed, much of the content of this workshop deals with the information which can be and has been gained through study of a selected subgroup of such nuclei, namely, beta-unstable nuclides resulting from fission.

Because of the manner of their production, however, fission-product nuclides have always occupied a somewhat special position among the

[†]Work performed under the auspices of the U. S. Department of Energy.

radioactive nuclides. For ~40 years now, it has been recognized that the vast amount of energy released through neutron-inducec fission has the potential for supplying a significant portion of society's future energy needs. Because of the present scope and importance of this one activity alone, the practical impact of fission-product data is great. Research programs involving the study of fission-product activities thus have the potential for generating data of interest not only to basic nuclear physics but also to the solution of a wide range of important practical problems related to fission reactor systems. It should be emphasized that a measurement program to provide such data represents a valuable activity, even if no specific application were readily identifiable at the time. It often occurs that important needs are recognized only rather suddenly, as in the case of the decay-heat problem; and an appropriate and timely response to such situations requires the prior existence of an evaluated base of relevant data.

In this paper, we discuss certain applications of fission-product decay data that are of current interest. In Sect. II, specific applications are presented. In Sect. III we discuss the structure and content of a file of evaluated decay-scheme data which was set up several years ago to provide a base of such data for use in the reactor research and development program. We conclude in Sect. IV with a discussion of recent measurements of β-strength functions for a number of short-lived fission products and show how it may be possible that data from these studies can be applied to the currently important problem of the fission-product decay-heat source term in operating nuclear reactors.

II. EXAMPLES OF APPLICATIONS OF FISSION-PRODUCT DECAY DATA

In Table I, we summarize several general categories of decay data and some areas for which they have application. As illustrated below, many applications of decay data involve knowledge of the absolute emission rate of the various radiations, particularly gamma radiation. Consequently, half-life and absolute gamma-ray intensity (branching-ratio) data assume a position of special importance in these areas. However, knowledge of these latter quantities (particularly with the high precision required for many applications) is not generally of too great an importance for basic nuclear physics, and to measure them requires rather specialized techniques. Consequently, we often encounter situations in which a particular decay scheme is rather well studied but, because of the lack of a precise knowledge of the absolute gamma-ray intensities, the information is of little, if any, use for a specific practical application.

II.1. The Fission-Product Decay-Heat Source Term

The problem of the fission-product decay-heat source term provides an excellent example of the application of fission-product decay data to the solution of an important problem. Several years ago, questions regarding the adequacy of Emergency Core Cooling Systems (ECCS) in hypothetical Loss-of-Coolant Accidents (LOCA) focused attention on the problem of the decay heat produced by the fission-product inventory in power reactors. A decay-heat curve for "infinite" irradiation of uranium had been recommended by K. Shure[4] in 1961 and formed the basis of a proposed ANS Standard. Although this standard had not been formally adopted, it nonetheless formed the basis of AEC/NRC regulatory actions. Since it was

estimated that this curve could be low by ~20% or high by ~40% for cooling times up to ~1000 sec, the regulatory criteria required that, in the evaluation of ECCS performance in a hypothetical LOCA situation, it be assumed that the heat production rate by the decay of fission products was 20% greater than that predicted using this curve. Although this procedure was thought to be quite conservative, it was nonetheless important to better quantify the decay-heat source term and its uncertainty, particularly at short decay times.

A number of measurement programs, using a variety of experimental techniques, were funded both by NRC and by EPRI to provide experimental data on the decay-heat function. These experiments were designed to provide "benchmark" data, measured for a few selected and carefully specified irradiation conditions. They would thus provide important information on the decay-heat function for these conditions; and more importantly they would provide a stringent test of the analytical models and underlying nuclear data base used to calculate decay heat. With these models and the data base thus subjected to careful testing and evaluation, they could be applied with increased confidence to the quite wide range of different irradiation conditions existing in operating fission reactors.

In addition, a Decay-Heat Task Force was set up under the auspices of the Cross-Sections Evaluation Working Group (CSEWG) to provide a reliable calculational base for decay heat. The Task Force produced a comprehensive library of fission-product nuclear data (issued in 1974 as the Fission-Product File for Version-IV of the Evaluated Nuclear Data File, ENDF/B)

to serve as the data base for "summation" calculations of decay heat. Essentially all present decay heat calculations use the summation method, which involves predicting the fission-product inventory in an operating reactor system and then obtaining the decay heat by summing the contributions of the individual nuclides. The nuclear data required for this include direct fission yields, capture cross section, half-lives, decay modes and the average β- and γ-ray energies per decay.

Some of the "statistics" of the Version-IV Fission-Product File are as follows. There are 824 fission-product nuclides (including isomeric states) included, 113 of which are stable. Detailed decay data (as discussed in Sect. III below) are given for 180 radioactive nuclides of primary importance for decay heat. For the remaining nuclides, much less detailed data sets (half-life, average β- and γ-energy values) are given; for most (~380) of them, no detailed decay data exist. The average-energy values appearing in these less-detailed sets were calculated using theoretical considerations. In all, the file contains over 300,000 data entries.

Since its issue, the file has provided a common data base for the various summation codes. One of the early benefits of having this common data base was the demonstration that the three such codes - RIBD,[5] ORIGEN[6] and CINDER[7] - primarily used in the U. S. at that time gave essentially the same predictions of decay heat, even though they utilized different mathematical procedures.

Considerable effort, both calculational and experimental has been expended on the decay-heat problem for the past 3 to 4 years within the U. S.

A summary of the current status of this activity, including work carried out by other nations, is given in a review paper[8] presented at the recent Petten conference on fission-product nuclear data. Figure 1, taken from Ref. 8, gives a comparison between calculation and experiment for "infinite" irradiation on ^{235}U. The 'nominal' curve has been derived[8] from the different recent experimental studies. The agreement between calculation and experiment for this "infinite" irradiation condition is believed[8] to be within ~2% (1σ level) over this time interval. For the so-called "burst" irradiation condition, however, (where the short-lived fission products are relatively more important) the agreement is not as good (e.g., ~8% at 20 sec).

It seems reasonable to conclude at the present time that the summation method is quite useful in calculating decay heat, even for the short (<1000 sec) cooling times important for the assessment of loss of coolant situations. Considerable effort continues to be applied to the decay heat problem. Particular attention is being focused on the important problem of estimating the uncertainties in the calculated values of the decay heat. At present, these investigations are essentially sensitivity analyses, which consider the influence of uncertainties in the basic nuclear data on the calculated values. They indicate that the calculations are relatively insensitive to errors in the half-lives and fission yields but are much more sensitive to uncertainties in the average-energy values. A measurement program to isolate specific short-lived fission products important for decay heat and produce these data, either through detailed decay-scheme studies or other means such as, e.g., that described in Sect. IV

below, would have an important impact here. The BNL-TRISTAN facility would be ideally suited for such a program.

It needs to be emphasized that, in applications such as decay heat, the nuclear data have rather considerable economic implications. Inspection of Fig. 1 reveals that the "ANS + 20%" curve, the present basis for regulatory matters, is extremely conservative. This is reflected in both the design and the operating parameters in nuclear reactors. It has been estimated that for every 1% reduction in decay heat, a savings of ~$500,000 can be effected in the capital cost of the equipment needed to eliminate that extra decay heat. And as regards the economic impact of this, and of nuclear data in general, in the nuclear power industry, the following is appropriate[9]:

> "Validated analysis capability has been and is being developed with the recognition that user- and problem-oriented validated computation packages have a significant potential payoff to the consumer. The lifting of an operating restriction that permits increasing a plant's power output level from a derated condition by 1% results in a saving of several hundred thousand dollars per plant year. Similarly, the confident prediction of the course of a low-probability event can result in savings of tens of millions of dollars for a confirmatory test program for each event, and there could be more than a few of those. Finally, if such open-ended issues cause plant shutdown for only a few days, additional costs of hundreds of thousands of dollars per plant day would be incurred."

II.2. Radioactivity Monitoring of Nuclear Power Plants

The operation of nuclear power plants involves significant inventories of radioactive materials, and the effective monitoring of operational and effluent streams is an important component of the safe operation of

such facilities. Federal regulations require that the releases of radioactivity to the environment from a nuclear plant be "as low as is reasonably achievable." In order to show that this requirement will be satisfied, an applicant for a license must submit plant design information in the Safety Analysis Report for the proposed facility. This information is used by the NRC to calculate the releases of radioactive material in both gaseous and liquid effluents from the reactor. These calculations are carried out using large computer programs. To provide a data base for these programs, an in-plant measurement activity has been established at INEL. This effort identifies and provides quantitative information on the sources of radioactivity in, and pathways for release from, the reactor system. Specific objectives[10] are to provide the following:

(1) source-term information to permit the parameters of the calculational models to be upgraded;

(2) data concerning the inventory (i.e., locations, concentrations, etc.) of the radioactive isotopes present in the operating reactor systems; and

(3) operational data on the performance of radioactive-waste equipment for use in evaluations of radioactive-waste treatment systems.

To acquire the data necessary to achieve these objectives, extensive sampling is done in all parts of the reactor system. Analysis of these samples using Ge(Li)-based gamma-ray spectroscopy is performed to determine not only which radionuclides are present but also their absolute concentrations. The gamma-ray spectra obtained are generally quite complex.

An example is given in Fig. 2, which shows the gamma-ray spectrum of a sample of water in the primary coolant of a Boiling Water Reactor. Such samples are counted a number of times over a suitable time interval so that half-life data can supplement the gamma-ray energy and relative-intensity information to aid in the isotopic identification. To determine the absolute concentrations of radionuclides, absolute gamma-ray intensity data are required. To carry out the quantitative analyses of these samples to provide the desired input "source-term" data, extensive computer-based decay-data libraries are required.

In a separate, but related, matter, a request was received from the Office of Nuclear Regulatory Research of the NRC to prepare a specialized set of evaluated decay data for radionuclides that are important in the monitoring of nuclear power reactors. The purpose of this was to provide a common basis for reporting the results of effluent-monitoring programs at operating power plants. The data to be included in this data library consisted of half-life, gamma-ray energies and absolute intensities and average beta- and gamma-ray energies per disintegration. From these data, tables of recommended gamma-ray lines are provided for use in computer programs designed for isotopic assay of complex gamma-ray spectra. These data will serve to improve the accuracy in radioactivity-assay techniques used in the nuclear industry. A listing of nuclides included is given in Table II. These data are scheduled for publication in the near future.

II.3. Fast-Reactor Dosimetry: The ILRR Program

The importance of fast-neutron dosimetry for fast-reactor fuels and materials has been summarized in Ref. 11. The development of economically

feasible fast-reactor materials and components requires improvements in fuel, duct, cladding, structural and control materials which will enable them to withstand neutron exposures of up to ~2.5 X 10^{23} n/cm^2 (E_n > 0.1 MeV) Uncertainties in such parameters as swelling, irradiation creep, strength and ductility and corrosion resistance each contribute to conservatisms in design relating to cladding integrity, fuel pin interactions, coolant channel restriction, duct bowing and dilution, response to power transients and radionuclide transport through the coolant systems. These design conservatisms have a direct impact on fast reactor performance and economics. Consequently, dosimetry and damage analysis have and will continue to play a vital role in reducing fuels and materials performance uncertainties in fast-reactor development programs. Accuracies in the range of 1 to 3% (1σ level) are requested for the determination of fission rates, burnups and neutron fluxes and fluences for fast reactors.

To develop and demonstrate the capability of accurately measuring neutron-induced reaction rates in a variety of well-established and permanent neutron fields, the Interlaboratory LMFBR Reaction Rate (ILRR) program, involving groups at 8 laboratories, was set up in 1971. The reaction rates obtained would provide calibrations for the subsequent determination of fission rates, burnup, and flux-fluence spectra in high-flux test reactors, basic information applicable to fast-reactor fuels and materials development programs. The initial goal of the ILRR program was an accuracy of $\pm$ 2-1/2% or better (1σ level) for the reaction-rate measurements of the principal fission products of ^{235}U, ^{238}U and ^{239}Pu. For the fission products of ^{237}Np and selected non-fission reactions, an

accuracy of ± 5% or better was desired. An excellent overview of the program and its status is given in Ref. 12. Relevant to the present discussion is the fact that an essential ingredient of the reaction-rate determinations was the measurement of absolute disintegration rates of the various radioactive reaction products in the irradiated foils using Ge(Li)-based gamma-ray spectroscopy. In addition to the development of experimental techniques, this required a base of carefully evaluated decay data (half-lives and absolute-intensity values for the prominent gamma rays) for the radioactive isotopes used. The results of the first evaluation of these data were given in Ref. 13. At that time, the errors in the absolute intensities of the prominent gamma rays from ^{103}Ru, ^{132}Te and ^{144}Ce-^{144}Pr were not well enough known to meet the ILRR goal of 2-1/2% for fission reaction rates. Subsequently additional data have appeared; and a recent re-evaluation of this situation has indicated[14] that, of these three, only ^{132}Te is presently not well enough characterized to meet the ILRR goals. A summary of the recently re-evaluated[14] decay data relevant to the ILRR program is given in Table III.

II.4. Fission-Product Capture Cross Sections

The build-up of fission products during the operation of a nuclear reactor has a number of important consequences. From the point of view of core performance, the most important aspect of this is that the fission products absorb neutrons and thus represent an absolute loss of efficiency in the neutron cycle. The presence of fission products in reactor fuel reduces the reactivity cycle length for fuel of a given enrichment or, alternatively, requires an increase in enrichment in order to maintain

a given cycle length. The economic implications, as well as other facets, of this problem are treated in a number of reviews (see, e.g., Ref. 15).

Various techniques have been developed for measuring fission-product capture cross sections. An important one, valid when the capture product is radioactive, involves determination of the number of capture-product nuclides formed during irradiation of the fission-product nuclide under "known" conditions. This involves an absolute determination of the induced activity and a knowledge of the half-life and (when gamma-ray spectroscopy is employed) gamma-ray branching ratios. The accuracy of the resultant cross-section values is limited principally by uncertainties in the neutron flux characteristics and in the half-life and gamma-ray branching ratios. [These former uncertainties can in some cases be reduced by irradiation of "standards" whose values are accurately known.]

Several years ago, a number of fission products which act as important neutron absorbers (poisons) in fast-reactor systems were identified[16], and an effort to make measurements of their neutron-absorption cross sections in a documented "fast-reactor" neutron spectrum was undertaken. Some of the results of this program have recently been summarized[17]. A number of these fission-product nuclides have radioactive capture products and hence can be studied using activation techniques. A listing of these radioactive capture products, roughly in the order of the importance of their fission-product "parents" as fast-reactor poisons, is given in Table IV. The data on the absorption cross sections of these poisons are thus directly dependent on a knowledge of the values of these gamma-ray branching ratios.

III. THE FILE OF DECAY DATA FOR ENDF/B

As mentioned in Section. II.1 above, the scope of the Evaluated Nuclear Data File (ENDF/B) was expanded about four years ago to include detailed radioactive-nuclide decay data. It seems appropriate, within the context of this meeting, to present a discussion of the philosophy underlying the ENDF/B decay-data file and to describe its organization and the types of information it contains.

The initial motivation behind the expansion in scope of ENDF/B was the desire to provide a common base of fission-product decay data relevant to the decay-heat problem. However, from the outset of this effort it was recognized that, since ENDF/B represents the accepted base of nuclear data for the reactor research and development program in the U. S., such a file should have a data content sufficiently broad to be applicable to a wide variety of reactor-related activities (examples of which have been summarized above). Thus, the file has as its primary objective the provision of a commonly available, evaluated base of decay data for use in the U. S. nuclear-power program. As such, it was intended not to replace such broadly oriented data compilations as the Nuclear Data Sheets or the Table of Isotopes but rather to represent a carefully evaluated subset of such data, prepared with the needs of a certain group of users in mind and presented in a format readily usable by them. Basically, the data on the file provide, for each nuclide, a detailed description of the energy associated with the decay. It attempts to do this in a manner which lends itself to as broad a range of applications as possible, within the limits of a realistic content and size. In this context, it is encouraging to note

that, although the decay-data effort for ENDF/B represents a fairly recent one on the international nuclear-data scene, the revised format has recently been adopted as the one to be used in the exchange of decay data among the various data centers in Western Europe, Japan and the U. S.

The initial data content and format adopted has been described in detail elsewhere[18,19]; it formed the basis for the first collection of decay data, which was contained in Version-IV of ENDF/B, issued in 1974. Subsequently, the data content and format have been expanded and revised somewhat, principally to provide (1) a more detailed description of the radiation associated with internal conversion (important for the heavier nuclides, including the actinides); (2) a means of treating radiation (e.g., delayed neutrons) whose spectrum contains both a discrete and a continuous component; and (3) a means of identifying the source of the various radiations in situations where two or more nuclides are produced in the decay of a given isotope. This revised format forms the basis of the decay data to be included in Version-V of ENDF/B, scheduled for release early in 1978. At the present time, no further modifications of the decay-data content or format are planned. Although the focus of the present discussion is on fission products, it should be mentioned that a file of decay data for ~50 actinide isotopes has also been prepared for Version-V of ENDF/B and that plans are underway for a file of decay data for important reactor-related activation products.

III.1. Structure of the Decay-Data File

The file is most simply discussed by reference to actual examples of specific data sets. We have chosen two examples, ^{85m}Kr and ^{128}I, to serve

as vehicles for the discussion. Although no few actual cases can illustrate all facets of the file structure, these relatively simple cases provide a good orientation to it. The decay-data sets, in card-image format, as prepared for our laboratory, or "working," file for these two activities are shown in Tables V and VI. (The process by which they are transcribed into the final ENDF/B format will be mentioned below.)

The first card contains the following information: Z and A values (in the form 1000 Z + A) followed immediately by an isomer flag. A blank or zero in the latter column indicates the ground state of the nucleus, a 1, 2, ... indicates a first, second, ... isomeric state. (Isomers are arbitrarily restricted to nuclear states with half-lives > 0.1 sec and are listed as separate "nuclides" in the file.) Following this on the first card are the chemical symbol, the spin and parity of the state and a number indicating the number of "comment cards" to follow. The numbers (10, 20, ...) at the right on this and the other cards are used for file-editing and related computer-processing activities.

Next comes a group of cards which provide the documentation for and pertinent comments about the data set. These are followed by a card giving the half-life, its uncertainty, the units, the number of decay modes of the nuclide and the number of energy spectra to be listed.

This is followed by cards (equal in number to the indicated number of decay modes) giving the following information about each decay mode: the type of decay; whether or not an isomeric state in the daughter is fed; the Q-value in keV for the decay mode; its uncertainty; the branching ratio (in percent) of the decay mode; and its uncertainty. The decay

modes thus far treated are denoted as follows: β^-, 1; electron capture and/or β^+, 2; isomeric-transition, 3; α-particle, 4; neutron, 5; spontaneous fission, 6; and proton, 7. If one type of decay (e.g., β^-) feeds both the ground state and an isomeric state in the daughter nucleus, this is treated as two distinct decay modes. Any radiations (e.g., an isomeric transition) associated with the decay of the daughter-nucleus isomeric state are listed with the daughter-nucleus decay data.

The next card contains the average-energy information in keV/disintegration in the order: $\langle E_{electron} \rangle$; its uncertainty; $\langle E_{photon} \rangle$; its uncertainty; $\langle E_{heavy\ particle} \rangle$; and its uncertainty. These average energies contain the following contributions. $\langle E_{electron} \rangle$ includes the average energy from all processes involving electrons, such as β^-, β^+, conversion electrons and Auger electrons. The photon term includes not only γ rays, but also all other electromagnetic radiation (e.g., x rays and annihilation radiation) emitted in the decay process. The third energy includes contributions from α-particle emission, proton and neutrons. (It could also include spontaneous-fission-fragment contributions as well, if desired.)

Next comes the listing of the various radiation spectra. Each listing consists of two types of cards. The first of these contains the following information: a normalization factor (to convert relative intensities to absolute intensities); its uncertainty; the number of individual transitions listed; the radiation type; the average energy (in keV per decay) associated with the radiation type; and its uncertainty. The numbering of the radiation types is similar to that given above for

the decay modes with the additional conventions: 8 denotes discrete electrons (e.g., conversion electrons); 9 denotes photons not arising as transitions between nuclear states; and 0 denotes γ radiation. The second of these card types contains the specific spectral information, with one card for each individual transition. Except for the cases discussed below, the data given here are listed in the order: energy, its uncertainty, intensity and its uncertainty. For e.-c. and β^+ decay (radiation type 2, see Table VI) two sets of intensity information are given: namely that of the electron-capture component of the transition and that of the β^+ component. In this case the average energy listed is that of the β^+ component only. (That associated with the e.-c. decay appears in the form of x-radiation; and this is included in radiation type 9.) For β^+ and β^- transitions, provision is also made for including a "multipolarity flag," giving the spectrum shape of the particular transition. The symbol "1U" indicates a first-forbidden unique shape; and the computer program takes this into account in its calculation of $\langle E_\beta \rangle$ for that transition. In the absence of such a notation (which is the case of allowed or first-forbidden non-unique transitions) an allowed shape is assumed.

Shown next in Tables V and VI are the listings for γ radiation (radiation type 0). When available, the γ-ray data are always given last in the data set. Provision is made for the existence of two cards for each γ-ray transition. The first of these contains the following information: energy, its uncertainty; intensity, its uncertainty; multipolarity and a source flag, indicating with which decay process the

γ ray is associated. (Note that, in addition to pure multipoles, the alphanumeric information here can describe mixed multipoles and unsymmetric uncertainties in the contributions of these multipoles.) The second card contains internal-conversion-coefficient data, with uncertainties, for the K-, L-, and M-shells. Generally, however, as in the cases listed here, this information is not specifically entered. It is generated from the listed γ-ray data, using computer processing codes together with theoretical internal-conversion coefficients. Although adequate for most applications, this procedure can be in error in some cases (e.g., anomalous conversion coefficients); and it is always possible to enter measured values, if desired.

Before these data are entered into ENDF/B, two separate processings are carried out. The first of these consists of producing listings for the "discrete-electron" spectra (radiation type 8) and the x-ray and annihilation-radiation (radiation type 9), preparing the ICC values for the γ-ray transitions (where the multipolarities are given) and calculating the various average-energy values. For these two sets of spectra, the listings are given in the same format as for the others, viz., a normalization card, followed by an energy-intensity card for each of the individual transitions. These entries are generally calculated theoretically, using the known properties of the gamma-ray transitions and the various parameters of the atomic processes involved, although where measured values exist and are of particular importance, these can be entered directly.

After this processing, the data sets are converted into the ENDF/B format. This latter format is designed primarily for use in large

computer-based calculational codes and is not generally "people readable." Consequently, it is not treated here; a thorough discussion of it is given in Ref. 20.

More complicated decay processes can be treated within the structure of this data file. Delayed-neutron emission (β^- decay followed by neutron emission), for example, would be listed as decay mode "15" - 1 for β^- and 5 for neutron. And, a γ ray emitted from an excited state of the nucleus remaining after the neutron emission would carry a source flag "15." Spectra characterized by both a discrete and a continuous component, such as delayed neutron spectra, are listed in the following manner. The discrete components are listed as usual: energy, uncertainty; intensity, and uncertainty. For the continuous component, the energy values are chosen (and listed) at equally spaced intervals across the distribution, with a sufficient number of points chosen to permit a suitably accurate representation of the distribution. The intensity (and where appropriate, the uncertainty) values corresponding to these energy points are listed, not in the columns where the discrete data are given, but in the next two groups of columns (corresponding to positions of a fifth and a sixth entry). In this fashion, the discrete and the continuous components can be readily recognized.

IV. APPLICATIONS OF β-STRENGTH FUNCTION STUDIES

With the advent of on-line isotope separators in recent years, a considerable experimental and theoretical literature on β-strength functions of nuclides far off the line of beta stability has been generated. A summary of this field is provided by an excellent review article[21]. Although the majority of these studies have involved neutron-deficient nuclides, several papers dealing with β-strength functions of short-lived fission products have been published[22,23]. For most of these nuclides, detailed decay-scheme data do not presently exist. Consequently, for applications such as decay heat where β- and γ-ray related data are required, those data for these nuclides must be obtained from theoretical considerations. Because of their short half-lives, these nuclides make the bulk of their contribution to the decay-heat source term at relatively short times (~10^1-10^3 sec), which is the interval of importance for the assessment of the effects of loss-of-coolant accidents.

It has been pointed out[24] that the data generated from these β-strength-function studies may provide a means of deducing "experimental" $\langle E_\beta \rangle$ and $\langle E_\gamma \rangle$ values for these nuclides. This seems to us to represent an excellent illustration of the application of a rather exotic type of basic nuclear-structure data to the solution of an important practical problem; and we give a brief discussion of this application.

The experimental techniques and the methods of data analysis employed to obtain the β-strength functions for the decay of fission-product

nuclides has been described in detail elsewhere[22,23]. For purposes of this discussion, we will define only the pertinent quantities involved. A schematic decay scheme for a nuclide with relatively large Q value is shown in Fig. 3. The energy available for the decay is Q_β. The β-decay branching intensity to an energy interval, dE, centered at an excitation energy, E, in the daughter nucleus is defined as b(E)dE. At excitation energies of the order of a few MeV, this energy interval generally contains a relatively large number of discrete energy levels. The quantity of interest for nuclear structure, in this case, is the β-strength function, $S_\beta(E)$, which is defined by the relation[21-23]

$$S_\beta(E) = \frac{b(E)}{f(Z,Q-E) \cdot T_{\frac{1}{2}}} \quad ,$$

where $T_{\frac{1}{2}}$ is the parent-nucleus β-decay half-life and f(Z,Q-E) is the integrated rate function (or Fermi function). From the experiment, values are deduced for the quantity b(E)dE as a function of E. For experimental reasons, b(E)dE cannot be measured below a certain energy, E_o. For the experimental conditions of Ref. 23 (from which the data presented below were taken), E_o ~305 keV and dE ~142 keV. It should be noted that these measurements give absolute values for b(E)dE, not just relative ones. Our interest here centers on the β-feeding intensities, $b(E_i)dE$, since they can be used to infer $\langle E_\beta \rangle$ (and hence $\langle E_\gamma \rangle$) values. These β-decay branching data are not explicitly given in Ref. 23. However, they have been supplied to us by Dr. K. Aleklett.

By analogy with the more customary situation in which the energies and intensities of the discrete β-decay branches are known from decay-scheme studies, we can calculate an average β energy per decay, $\langle E_\beta \rangle_\alpha$, corresponding to the fraction, α, of the β intensity to levels above E_0, using the relation

$$\langle E_\beta \rangle_\alpha = \sum_i E_{\beta i} \, I_{\beta i} \, f_i(E_{\beta i}), \qquad (1)$$

where

$E_{\beta i} \equiv Q_\beta - E_i$ is the end-point energy of the $i^{\underline{th}}$ β-decay branch,

$I_{\beta i} \equiv b(E_i)dE$ is the intensity (expressed as a fraction per decay) of the $i^{\underline{th}}$ β-decay branch,

and $f_i(E_{\beta i})$ gives that fraction of the available energy $(Q_\beta - E_i)$ which is, on the average, carried by the β radiation. Similarly, the average (anti)neutrino energy, $\langle E_\nu \rangle_\alpha$, corresponding to these transitions is given by the expression

$$\langle E_\nu \rangle_\alpha = \sum_i E_{\beta i} \, I_{\beta i} \, [1 - f_i(E_{\beta i})]. \qquad (2)$$

The $f_i(E_{\beta i})$ values were calculated using a computer program described in Ref. 25.

To obtain values for $\langle E_\beta \rangle$, account must be taken of that fraction, 1-α, of the β-decay intensity which proceeds to daughter-nucleus levels below E_0. To do this, we have considered the following three situations, which cover the range of possible distributions of this remaining β intensity:

(1) the remaining fraction $(1-\alpha)$ goes directly to the ground state;

(2) this fraction goes to an assumed state halfway between the ground state and E_0;

(3) this fraction is split equally among four states (including the ground state) assumed equally spaced in the region below E_0.

The resulting average-energy values, $\langle E_\beta \rangle_{1-\alpha}$, can then be combined with the $\langle E_\beta \rangle_\alpha$ value to yield an overall $\langle E_\beta \rangle$ value consistent with each of these three cases. The $\langle E_\beta \rangle$ values calculated according to situation (3) above lie between those calculated according to situations (1) and (2). Consequently, in the absence of other information (such as, e.g., ground-state spins) regarding the distribution of this intensity, the $\langle E_\beta \rangle$ values given below have been calculated assuming the applicability of this third situation.

In Ref. 24, $\langle E_\beta \rangle$ values, calculated as described above, are given for the 68 fission-product activities studied by Aleklett, et al[23]. For purposes of discussion here, however, we list only those for the 11 nuclides for which $\langle E_\beta \rangle$ values, derived from conventional decay-schemes studies, are available. A comparison of our deduced $\langle E_\beta \rangle$ values for these nuclides with those obtained from the decay-scheme data given in the Fission-Product File currently being prepared for Version V of ENDF/B is given in Table VII. A comparison of the β-intensity distributions from these two sources is illustrated, for three typical cases, in Fig. 4.

It is difficult at present to provide a realistic assessment of the uncertainties to be associated with the $\langle E_\beta \rangle$ values listed in column 7 of Table VII. The uncertainties associated with these values have been estimated from a consideration of only two possible sources of error: (1) that associated with the distribution of the fraction $(1-\alpha)$ of the intensity; and (2) possible errors in the value of α itself. This first source has been treated by direct calculation; and its contribution reflects the spread in calculated values resulting from the three different assumptions listed above concerning the distribution of β intensity to levels below E_0. No estimate of the magnitude of possible errors in the α values is given in Ref. 23. In order to provide some estimate of the influence of errors in α on the derived $\langle E_\beta \rangle$ values, we have assigned, somewhat arbitrarily, an uncertainty of 10% to each of the listed α values. This seems to represent a reasonable estimate. Values of α greater than unity are, by definition, not possible. Of the α-values given in Ref. 23, only 5 (excluding those of some delayed neutron precursors) are greater than unity and, of these, only two (for which $\alpha \sim 1.2$) are significantly larger than 1.1. In calculating the overall uncertainty in $\langle E_\beta \rangle$, the error propagation took explicit account of the fact that $\langle E_\beta \rangle_\alpha$ and $\langle E_\beta \rangle_{1-\alpha}$ are constrained by the requirement that the total β-decay intensity is unity (or, for delayed-neutron emission, is $1-P_n$). No contribution from the uncertainty in the Q_β values is included in the $\langle E_\beta \rangle$ uncertainties in Table VII.

In general, as inspection of Table VII indicates, the agreement between the two sets of $\langle E_\beta \rangle$ values is quite good, particularly for those nuclides

situated in the heavy-mass peak of the fission-yield distribution. The nuclide, ^{140}Cs, appears to represent an exception, but here there is considerable uncertainty in the intensities of the β branches to the ground and first excited states of the daughter nuclide, ^{140}Ba. (In ENDF/B-V the sum of these two β-transition intensities is ~30%, while some data exist which indicate that this sum may be ≳ 40%. Use of this latter value would significantly reduce the difference in the two $\langle E_\beta \rangle$ values.) Consequently, ^{140}Cs may not represent a really good test case. The ^{76}Ga decay leads to doubly even ^{76}Ge. For this relatively light-mass daughter, the first excited-state energy is fairly high (~563 keV) and the level density up to excitation energies of ~5-6 MeV is low. Consequently, the assumptions underlying the data-analysis procedures of Ref. 23, namely that the γ decay of the levels excited following β decay can be treated statistically, may not be valid. Even in this case, however, the difference in the two $\langle E_\beta \rangle$ values is only about 240 keV (~14%).

The thrust of the discussion thus far has been only the evaluation of the $\langle E_\beta \rangle$ values, since our interest has centered on the validity of the idea that the β-strength function experiments can serve as a reliable source of average-energy data for otherwise unstudied short-lived fission products. The $\langle E_\beta \rangle$ values are the important ones from this point of view, since the $\langle E_\gamma \rangle$ values can then be inferred from the relation (see, e.g., Ref. 18)

$$\langle E_\gamma \rangle = Q_\beta - \langle E_\beta \rangle - \langle E_\nu \rangle ,$$

with the $\langle E_\nu \rangle$ values being determined from the same b(E)dE data as the $\langle E_\beta \rangle$ values (see Eqs. (1) and (2)) above.

It appears to us that the data of Ref. 23 can be usec to provide realistic $\langle E_{\beta^-} \rangle$ and $\langle E_{\gamma} \rangle$ values for a number of short-lived fission products for which at present only theoretically estimated values are available. As such, they can serve to extend the range of nuclides on the various fission-product libraries for which "experimental" average-energy values are available. Because these data have important practical applications as well as relevance to low-energy nuclear physics, a continuing research effort at on-line isotope-separator facilities such as BNL-TRISTAN to measure them for a wider range of nuclides would seem to be a highly worthwhile endeavor.

ACKNOWLEDGEMENTS

Helpful discussions with the following individuals during the preparation of this paper are gratefully acknowledged: R. A. Anderl, R. L. Bunting, N. C. Dyer, R. C. Greenwood, Y. D. Harker, J. W. Mandler and JW Rogers of INEL, and R. E. Schenter of HEDL. Special appreciation is expressed to R. C. Greenwood for helpful comments concerning the manuscript and to R. E. Schenter for one of the figures.

REFERENCES

1. Proceedings of the First International Conference on Why and How Should We Investigate Nuclides Far Off the Stability Line, Lysekil, 1967, Ark. Fys. 36, 1 (1967).

2. Proceedings of the Second International Conference on Properties of Nuclei Far from the Region of Beta Stability, Leysin, 1970; C.E.R.N. Report CERN 70-30 (1970).

3. Proceedings of the Third International Conference on Nuclear Far from Stability, Cargèse, 1976; C.E.R.N. Report 76-13 (1976).

4. K. Shure, "Fission Product Decay Energy," in U. S. AEC Report WAPD-BT-24, pp. 1-17 (Dec., 1961).

5. R. O. Gumprecht, "Mathematical Basis of Computer Code RIBD," DUN-4136, Douglas-United Nuclear, Inc. (1968).

6. M. J. Bell, "ORIGEN - The ORNL Isotope Generation and Depletion Code," ORNL-4628, Oak Ridge National Laboratory (May,1973).

7. T. R. England, "CINDER - A One-Point Depletion and Fission-Product Program," WAPD-TM-334 (Rev.), (1964).

8. R. E. Schenter, F. Schmittroth and T. R. England, "Integral Determination of Fission Product Inventory and Decay Power," Review Paper No. 15, presented at the Second IAEA Advisory Group Meeting on Fission-Product Nuclear Data, Petten, the Netherlands, Sept. 5-9, 1977.

9. W. B. Loewenstein and J. B. Moore, EPRI JOURNAL, No. 7, pp. 47-50 (September, 1977).

10. N. C. Dyer, E. B. Nieschmidt, J. H. Keller and B. G. Motes, "Procedures: Source Term Measurement Program," U. S. ERDA Report TREE-1178 (October, 1977).

11. W. N. McElroy, R. A. Bennett, D. L. Johnson and N. D. Dudey, Proceedings of the First ASTM-EURATOM Symposium on Reactor Dosimetry, Petten (Holland), Sept. 22-26, 1975; EUR 5667 e/f Part 1, pp. 1-26 (1977).

12. Nuclear Technology, Vol. 25, No. 2, pp. 169-422 (Feb., 1975).

13. R. G. Helmer and R. C. Greenwood, Nuclear Technology 25, No. 2, 258 (1975).

14. R. C. Greenwood, R. G. Helmer, JW Rogers, R. J. Popek, R. R. Heinrich, N. D. Dudey, L. S. Kellogg and W. H. Zimmer, "Radiometric Reaction Rate Measurements in CFRMF and BIG-10," invited paper, presented at Second ASTM-EURATOM Symposium on Reactor Dosimetry, Palo Alto, CA., Oct. 3-7, 1977.

15. J. G. Tyror, "The Importance of Fission Product Nuclear Data in the Physics Design of Power Reactor Cores," Review Paper No. 3, in Fission-Product Nuclear Data, IAEA Report IAEA-169 (Vienna, 1974).

16. The CSEWG Priority List, prepared under the auspices of the Cross Sections Evaluation Working Group, National Nuclear Data Center, BNL.

17. Y. D. Harker, D. A. Millsap and JW Rogers, "Fission-Product Studies at the Coupled Fast Reactivity Measurements Facility," contribution to the Second IAEA Advisory Group Meeting on Fission-Product Nuclear Data, Petten, the Netherlands, Sept. 5-9, 1977.

18. C. W. Reich, R. G. Helmer and M. H. Putnam, U. S. AEC Report ANCR-1157 (ENDF-210), August, 1974.

19. C. W. Reich and R. G. Helmer, Bull. Am. Phys. Soc., Ser. II, 20, 145 (1975), and Proc. Conf. on Nuclear Cross Sections and Technology, Washington, D. C., (1975), R. A. Schrack and C. D. Bowman, Eds., N.B.S. Special Publication 425, Vol. 1, 14 (Oct., 1975).

20. ENDF/B Summary Documentation, U. S. ERDA Report BNL 17541 (ENDF-201) (October, 1975). Revisions to this document for Version V of ENDF/B are currently being prepared.

21. P. G. Hansen, "The Beta Strength Function," Advances in Nuclear Physics, E. Vogt and M. Baranger, eds., (Academic Press, New York, 1974), Vol. 7, 159 (1974).

22. K. H. Johansen, K. Bonde Nielsen and G. Rudstam, Nucl. Phys. A203, 481 (1973).

23. K. Aleklett, G. Nyman and G. Rudstam, Nucl. Phys. A246, 425 (1975).

24. C. W. Reich and R. L. Bunting, "The Use of Data from β-Strength Function Experiments to Calculate Average β- and γ-Decay Energies," contributed paper to the Second IAEA Advisory Group Meeting on Fission-Product Nuclear Data, Petten, the Netherlands, Sept. 5-9, 1977.

25. W. B. Ewbank, "LOGFT - A Computer Program for Analyzing $\beta^{\pm}$, ε Decay," private communication (1976).

Table I

Several Categories of Decay Data and Areas of Their Application

Measured Quantity	End Use				
	Decay Heat	Nuclide Identification	Quantitative Nuclide Assay	Biomedical and Tracer	Basic Nuclear Physics
Half-life	X	X	X	X	X
γ-ray energy	X	X	X	X	X
γ-ray relative intensity		X	X	X	X
γ-ray branching ratio	X		X	X	
x-ray energy	X	X			
x-ray intensity	X			X	
electron energy	X			X	X
electron relative intensity				X	X
electron absolute intensity	X				
β-ray energy	X			X	X
β-ray relative intensity				X	X
β-ray branching ratio	X				
α-particle energy	X	X	X	X	X
α-particle relative intensity		X		X	X
α-particle branching ratio	X		X	X	
Q-value	X				X
level energy					X
level spin and parity					X

Table II

Important Radionuclides for
Nuclear Power Plant Monitoring

Activation Nuclides	Fission Nuclides		Background Nuclides	Transuranic Nuclides
^{3}H	^{82}Br	^{110m}Ag	^{40}K	^{235}U
^{7}Be	^{83}Br	^{122}Sb		^{238}U
^{14}C	^{84}Br	^{124}Sb		^{238}Pu
^{15}C	^{83m}Kr	^{126}Sb		^{239}Pu
^{16}N	^{85m}Kr	^{127}Sb		^{240}Pu
^{19}O	^{85}Kr	^{129m}Te		^{241}Pu
^{20}F	^{87}Kr	^{129}Te		^{241}Am
^{24}Na	^{88}Kr	^{131m}Te		
^{35}S	^{89}Kr	^{131}I		
^{32}P	^{90}Kr	^{132}I		
^{38}Cl	^{88}Rb	^{133}I		
^{41}Ar	^{89}Rb	^{134}I		
^{45}Ca	^{89}Sr	^{135}I		
^{46}Sc	^{90}Sr	^{131m}Xe		
^{51}Ti	^{91}Sr	^{133m}Xe		
^{51}Cr	^{92}Sr	^{133}Xe		
^{54}Mn	^{90}Y	^{135m}Xe		
^{56}Mn	^{91m}Y	^{135}Xe		
^{55}Fe	^{91}Y	^{137}Xe		
^{59}Fe	^{92}Y	^{138}Xe		
^{57}Co	^{93}Y	^{139}Xe		
^{58}Co	^{94}Y	^{134}Cs		
^{60}Co	^{95}Y	^{136}Cs		
^{63}Ni	^{95}Zr	^{137}Cs		
^{65}Zn	^{97}Zr	^{138}Cs		
^{72}Ga	^{95m}Nb	^{139}Cs		
^{75}Se	^{95}Nb	^{139}Ba		
^{187}W	^{98}Nb	^{140}Ba		
^{239}Np	^{99}Mo	^{141}Ba		
	^{101}Mo	^{142}Ba		
	^{99m}Tc	^{140}La		
	^{99}Tc	^{142}La		
	^{101}Tc	^{141}Ce		
	^{104}Tc	^{143}Ce		
	^{103}Ru	^{144}Ce		
	^{105}Ru	^{144}Pr		
	^{105}Rh	^{147}Pm		

Table III

Recommended Decay-Scheme Data
for the ILRR Program

	Half-life	Gamma Energy (keV)	Gamma Intensity (%)
^{24}Na	15.00(2) h	1368.599(29) 2753.965(56)	99.993(2) 99.873(6)
^{27}Mg	9.462(12) m	843.75(3) 1014.44(4)	71.7(5) 28.3(5)
^{46}Sc	83.9(3) d	889.253(16) 1120.521(19)	99.984(6) 99.987(6)
^{47}Sc	3.40(3) d	159.381(15)	69.0(25)
^{48}Sc	43.8(1) h	983.4(2) 1037.4(2) 1311.8 (4)	99.987(2) 97.5(3) 99.992(2)
^{51}Cr	27.700(10) d	320.076(5)	9.83(14)
^{54}Mn	312.5(5) d	834.827(21)	99.97(2)
^{58}Co	70.85(15) d	810.753(20)	99.44(1)
^{59}Fe	44.6(1) d	1099.228(19) 1291.568(23)	56.1(10) 43.6(10)
^{60}Co	5.27(2) yr	1173.208(20) 1332.464(28)	99.86(2) 99.980(3)
^{64}Cu	12.702(4) h	511.00 [a]	38.(2)
^{95}Zr	64.1(3) d	724.179(13) 756.710(18)	44.1(5) 54.6(5)
^{97}Zr	16.88(6) h	743.3(1)	92.9(3)
^{103}Ru	39.43(10) d	497.08(1)	89.(1)
^{106}Ru	368.2(12) d	-	-
^{106}Rh	30.0(2) s [e]	511.8(2)	20.5(2) [b]
^{115m}In	4.486(4) h	336.23(5)	45.9(1)
^{116m}In	54.2(1) m	1293.54(15)	84.8(5)
^{132}Te	77.9(5) h	228.16(6)	89.(5)
^{137}Cs	30.03(15) yr	661.647(12)	85.3(4)

Table III (Continued)

	Half-life	Gamma Energy (keV)	Gamma Intensity (%)
^{140}Ba	12.789(6) d	537.35(5)	24.4(3)
^{140}La	40.26(2) h[c,e]	1596.18(5)	95.40(8)
^{141}Ce	32.50(7) d	145.440(3)	48.(2)
^{143}Ce	33.0(2) h	293.26(2)	47.(4)
^{144}Ce	284.4(4) d	133.53(8)	11.0(2)
^{144}Pr	17.28(5) m[e]	696.49(2) 1489.15(5) 2185.70(6)	1.342(13) 0.279(3) 0.700(10)
^{196}Au	6.1(1) d	355.73(5)	87.7(20)
^{198}Au	2.6956(10) d	411.794(7)	95.52(5)
^{239}Np	2.355(4) d	277.60(3)	14.3(2)

[a]This is the value of the electron rest mass, m_0c^2. The observed annihilation photon energy may be lower.

[b]There may be some experimental problems in the use of this gamma ray due to the presence of 511.0 -keV photons from positron annihilation.

[c]In equilibrium, the ratio of the ^{140}La to ^{140}Ba activities is

$$T_{\frac{1}{2}}(Ba)/[T_{\frac{1}{2}}(Ba) - T_{\frac{1}{2}}(La)] = 1.15097(12).$$

[e]These isotopes will normally occur with the parent half-life.

Table IV

Radioactive Capture Products Whose Parents are Important Fast-Reactor Poisons

^{100}Tc	^{160}Tb	^{147}Nd
^{104}Rh	^{122}Sb	^{97}Zr
^{134}Cs	^{116}In	^{86}Rb
^{148}Pm	^{124}Sb	^{111}Pd
^{103}Ru	^{159}Gd	^{95}Zr
$^{110}Ag^{m}$	^{90}Y	^{137}Xe
^{105}Ru	^{88}Rb	^{136}Cs
^{99}Mo	^{161}Gd	^{107}Ru
^{142}Pr	^{153}Sm	^{130}I
^{149}Nd	^{155}Sm	^{156}Eu
^{151}Nd	^{133}Xe	^{138}Cs
^{128}I	^{135}Xe	^{96}Nb
^{143}Ce	^{101}Mo	^{95}Nb
^{141}Ce	^{109}Pd	^{92}Y

Table V

Sample Listing of Decay Data for ^{85m}Kr
Decay Prepared in the INEL Format

Z	A	IS		I^{π}	No. of Comment Cards	
36	851	KR	NPR-ENTRY	1/2-	4	10

Comments and Documentation

FILE ENTRY 1/ /75 CWR (INEL) 20
REFERENCES: C- 1973 REVISION OF WAPSTRA-GOVE MASS TABLES. 20
OTHER- F.K. WOHN,W.L. TALBERT, JR. AND J.K. HALBIG, 20
NUCL. PHYS. A152, 561 (1970). 20

$T_{\frac{1}{2}}$	σ	Units	No. of Decay Modes	No. of Spectra	
4.480	0.008	H	2	4	30

Decay Mode	Final-State Isomer	Q	σ	Branching	σ	
1	0	991.7	2.0	78.8	1.3	40
3	0	304.47	0.05	21.2	1.3	40

$\langle E_{elect.} \rangle$	σ	$\langle E_{phot.} \rangle$	σ	$\langle E_{h.p.} \rangle$	σ	
251.6		157.1		0.0		50

Normalization	σ	No. of Transitions	Radiation type	$\langle E_{\beta^-} \rangle$	σ	
0.788	0.013	1	1	226.1	2.0	61

E_{β^-}	σ	I_{β^-}	σ		
840.7	2.0	100.0			71

Normalization	σ	No. of Transitions	Radiation type	$\langle E_{\gamma} \rangle$	σ	
1.40		2	0	156.4		80

E_{γ}	σ	I_{γ}	σ	Multipolarity	Source Flag
150.99	0.05	53.8	1.0	M1	190
304.47	0.05	100.0	0.4	M4	390

Table VI

Sample Listing of Decay Data for ^{128}I
Decay Prepared in the INEL Format

Z	A	IS		I^{π}	No. of Comment Cards	
53128	1	NPB-ENTRY		1+	3	10

Comments and Documentation

```
FILE ENTRY:          1/  /75              CWR (INEL)                          20
REFERENCES: Q- 1973 REVISION OF WAPSTRA-GOVE MASS TABLES.                    20
            OTHER- SEE R.L. AUBLE, NUCL. DATA SHEETS 9, 157(1973)            20
```

$T_{1/2}$	σ	Units	No. of Decay Modes	No. of Spectra	
24.99	0.02	M	2	5	30

Decay Mode	Final-State Isomer	Q	σ	Branching	σ	
1	0	2127.	5.	93.9		40
2	0	1258.	5.	6.1		40

$\langle E_{elect.} \rangle$	σ	$\langle E_{phot.} \rangle$	σ	$\langle E_{h.p.} \rangle$	σ	
751.1		85.2		0.0		50

Normalization	σ	No. of Transitions	Radiation type	$\langle E_{\beta-} \rangle$	σ	
1.0		4	1	751.1		61

$E_{\beta-}$	σ	$I_{\beta-}$	σ	
544.	5.	0.012		71
1158.	5.	1.9		71
1684.	5.	15.		71
2127.	5.	77.		71

Normalization	σ	No. of Transitions	Radiation type	$\langle E_{\beta+} \rangle$	σ	
1.0		2	2	0.0013		62

E	σ	$I_{e.c.}$	σ	$I_{\beta+}$	σ	
510.		0.14		0.0		72
1258.		6.		0.002		72

Normalization	σ	No. of Transitions	Radiation type	$\langle E_{\gamma} \rangle$	σ	
0.16		7	0	83.9		80

E_{γ}	σ	I_{γ}	σ		Multipolarity		Source Flag	
442.91	0.07	100.		E2				190
526.62	0.10	9.6		E2	+2.3 +1.5 -0.8		M1	190
613.12	0.50	0.015	0.004					190
743.52	0.20	0.9	0.1	E2				290
969.42	0.40	2.4	0.3	E2				190
1139.72	0.20	0.060	0.008					190
1434.52	0.50	0.0033	0.0007					190

Table VII

Comparison of our calculated average β-energy values with those obtained from decay scheme studies. The Q_β-value adjustments necessary to complete the comparison are also listed. The quantities in parentheses represent the uncertainties in the least significant figure (or figures) of the associated value. For further discussion, see the text.

Nuclide	$T_{1/2}$(sec)	α	ΔJ^π	Reference	Q(keV)	$\langle E_\beta \rangle$
^{76}Ga	27.6	0.78	$(3^-)\rightarrow 0^+$	THIS WORK	6100	1837(61)
				ENDF	6100	1601(10)
^{86}Br	55.7	0.87	$(2^-)\rightarrow 0^+$	THIS WORK	8000	2227(102)
				ENDF	8000(438)	2090
^{89}Kr	281.0	0.96	$(5/2^+)\rightarrow(3/2, 5/2^-)$	THIS WORK	4930	1414(48)
				ENDF	4930(60)	1346(16)
^{90}Kr	32.2	0.68	$0^+\rightarrow(1^-)$	THIS WORK	4390	1517(26)
				ENDF	4390(30)	1316(4)
^{91}Kr	8.70	0.76		THIS WORK	6120	1742(69)
				ENDF	6120(70)	1941(15)
^{91}Rb	58.2	0.76	$?\rightarrow(5/2^+)$	THIS WORK	5680	1567(66)
				ENDF	5680(40)	1462(26)
^{92}Rb	4.50	0.15		THIS WORK	7580	3215(12)
				ENDF	7700(250)	3446
^{137}Xe	230.0	0.46	$7/2^-\rightarrow 7/2^+$	THIS WORK	4348	1718(7)
				ENDF	4347(24)	1722
^{139}Xe	40.4	0.91		THIS WORK	4880	1671(28)
				ENDF	4880(60)	1715(9)
^{139}Cs	562.0	0.18	$(7/2, 9/2)\rightarrow(7/2)^-$	THIS WORK	4290	1660(9)
				ENDF	4290(70)	1696(16)
^{140}Cs	64.0	0.56	$?\rightarrow 0^+$	THIS WORK	6050	2106(35)
				ENDF	6050(250)	1696(17)

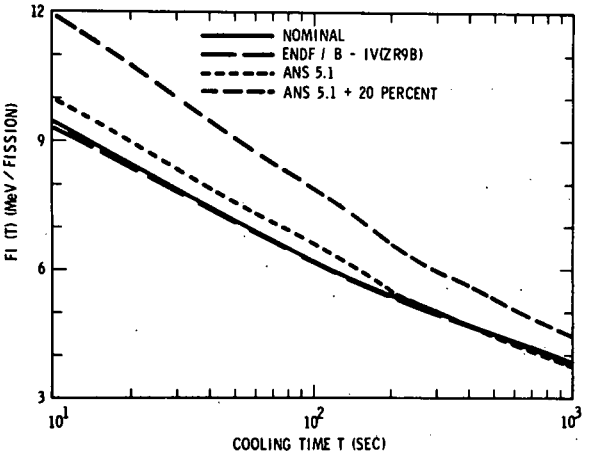

Figure 1. Comparison of decay-heat functions for ^{235}U fission with the "ANS Standard." This figure is taken from Ref. 8.

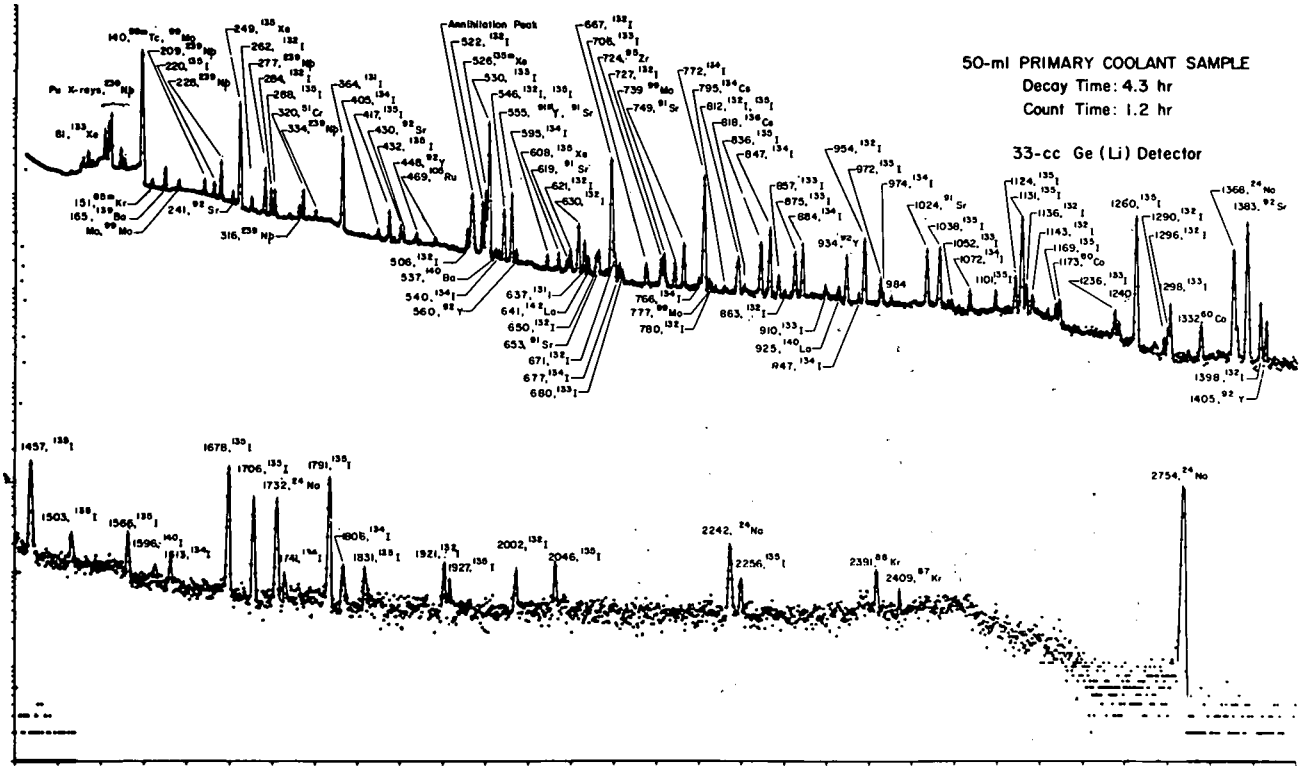

Figure 2. Gamma-ray spectrum of a sample of primary-coolant water in a boiling water reactor.

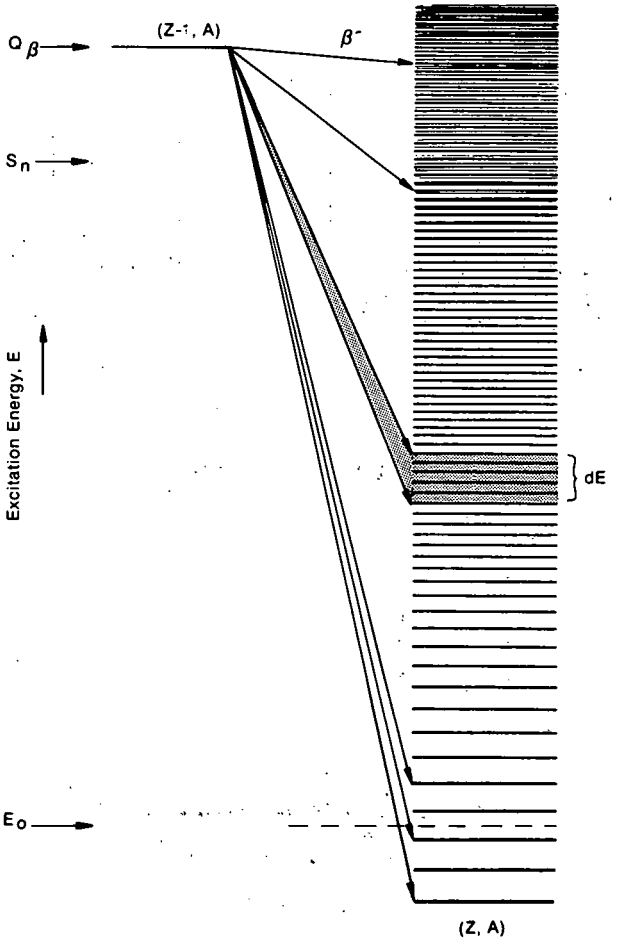

Figure 3. Schematic decay scheme illustrating the quantities discussed in the text.

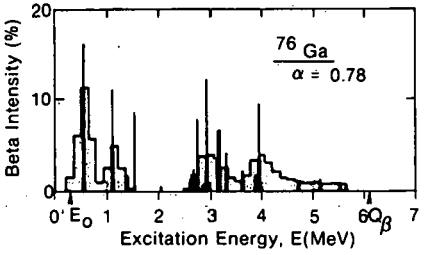

Fig. 4a) ^{76}Ga

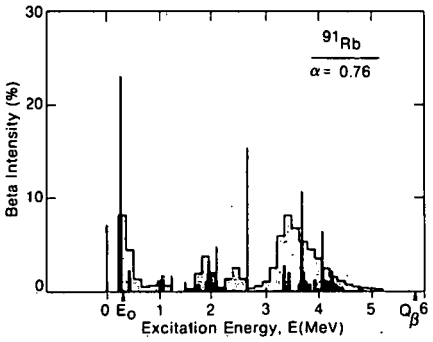

Fig. 4b) ^{91}Rb

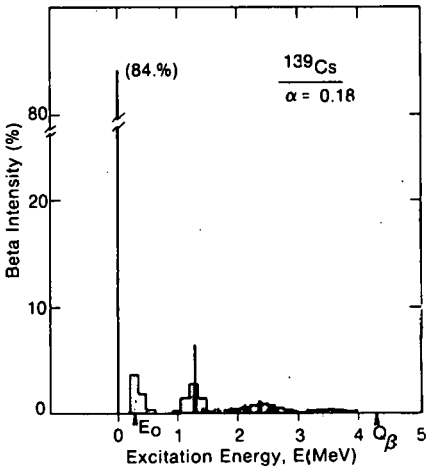

Fig. 4c) ^{139}Cs

Figure 4. Comparison of the β-intensity distributions deduced from the experimental β-strength function measurements (23) with those from decay-scheme studies for the decay of a) ^{76}Ga, b) ^{91}Rb and c) ^{139}Cs.

The UNISOR Project: Techniques and Results

E. H. Spejewski
UNISOR*, Oak Ridge Associated Universities, Oak Ridge, TN 37830

I. Introduction

The UNISOR (Universities Isotope Separator at Oak Ridge) consortium was formed in 1970 for the primary purpose of nuclear structure studies in the region far from the line of beta stability. By installing an isotope separator on-line with the Oak Ridge Isochronous Cyclotron (ORIC) it was planned to take advantage of the relatively greater specificity and higher angular-momentum transfer of heavy-ion reactions for the production of short-lived nuclei. Initial planning, proposal writing, etc., were carried out by representatives from the member institutions with the support of Oak Ridge Associated Universities, within which UNISOR is formally organized.

The project officially began in FY 1972 (July 1971) with joint funding from the (then) Atomic Energy Commission and the member universities. This joint, financial support of the project by a number of universities is, I believe, unique and is a strong indication of their commitment to the project

*UNISOR is a consortium of the University of Alabama in Birmingham, Georgia Institute of Technology, Emory University, Furman University, the University of Kentucky, Louisiana State University, the University of Massachusetts, Oak Ridge Associated Universities, Oak Ridge National Laboratory, the University of South Carolina, the University of Tennessee, Tennessee Technological University, Vanderbilt University, and Virginia Polytechnic Institute and State University. It is supported by these institutions and by the U. S. Department of Energy.

and of its cooperative nature. The universities initially agreed to provide funding for the project for a five-year period, and have now extended these agreements for an additional five years. In addition, the initial capital equipment, including the isotope separator, was obtained through the universities.

With funding having been obtained, construction of a building to house the facility was begun in July 1971, and completed the following January. The isotope separator was delivered in March, the installation and final acceptance tests being completed in late May. Following some additional internal construction, the initial tests of the on-line system were successfully completed in early September 1972, with the observation of Ag isotopes on the separator focal plane.[1] Initial scientific results[2] were presented at the Bloomington meeting of the Division of Nuclear Physics in 1973.[3]

II. The UNISOR Facility

The UNISOR facility is housed in an addition to the ORIC building, Fig. 1. This addition also houses several other facilities, with UNISOR presently occupying approximately half the total space, as shown. Although not originally so planned, the UNISOR beam line is very strategically placed because it is the only line which is capable of transporting a beam directly from ORIC and directly from the 25-MV tandem accelerator now under construction.

The isotope separator is installed with two ion-source/lens combinations. One is in the target room and is used for on-line studies. The other is at the normal ion-source position and can be used for conventional separations. The drift tube, which connects the two through the shielding wall, has a "quick-disconnect" coupling to the off-line ion-source housing permitting

fast and convenient switching between the two modes.

The output end of the separator is labelled "beam switch" in Fig. 1 with three beam lines indicated. The separator control console is located adjacent to the "normal" collection chamber within this experimental area. Also within this area are source-transport systems and data-acquisition systems, not shown in Fig. 1.

A. Isotope Separator Ion Sources

The isotope separator is a commercial[4] version of the Scandinavian type. It is a 90°, 150-cm radius-of-curvature device having a resolution $\Delta m/m < 1/2000$. It is capable of providing well-focussed beams at the focal plane in the mass range of approximately ±8% of the central beam, providing either a line or a spot focus.

The ion source and associated targeting, *i.e.* the ability to introduce the reaction products into an ion source, to ionize and extract them are the most crucial aspects of an ISOL system. They are, furthermore, the most technologically difficult problems to be faced. Several conceptually different ion sources, with many different modifications of each, have been and are being investigated at UNISOR. All take advantage of the large recoil linear-momentum imparted to the reaction products by the heavy-ion beams and, therefore, relatively thin targets (2-3 mg/cm^2) are required.

The most used ion source has been the Integrated-Target Ion Source,[5] the latest version of which is shown in Fig. 2. This is essentially a standard Nielsen oscillating-electron ion source,[6,4] with holes cut through the anode cylinder and heat shield to allow the mounting of a target and a catcher. In operation, reaction products from the heavy-ion beam recoil out of the target and are stopped in a porous graphite-

felt catcher ($\sim$ 30 mg/cm^2). The catcher being at a temperature of approximately 1000°C, the reaction products diffuse into the ion source. The graphite felt was originally installed to prevent deposition of tungsten emitted from the filament onto the back of the target. It has had the further serendipitous effect of increasing the ion-source efficiency and of shielding the target from ion-source thermal radiation.

This ion source has been used for experiments on Xe, I, Bi, Pb, Tl, and Hg isotopes, as well as initial tests with Ag isotopes. Efficiencies have been determined, on line, for isotopes of Xe, I, and Tl. The values fall within 2-5% and account for all losses including possible transmission losses as well as decay losses because the products spend a finite amount of time within the source. The delay-time characteristics of this ion source were investigated for 2.9-sec ^{116}I.[7] The collection rate for the activity was a decreasing exponential with a time constant ("half-life") of 4 ± 1 sec.

Recently developed was a High Temperature Ion Source, Fig. 3. It was designed to operate at a temperature of $\sim$ 2000°C in order to increase the vapor pressure of the reaction products within the ion source and, thereby, increase the ionization efficiency. Because this source is so new, there has not yet been time to determine its efficiencies and delay behavior, although it has been used for several experiments. In operation, it appears to have an efficiency for Hg comparable to the ITIS, and higher efficiencies for Tl, Pb and Bi. In addition, 20-sec ^{182}Au has been observed with this ion source at an apparently comparable efficiency.

The coupling of a helium-jet transport system[8] to a modified hollow-cathode ion source[4] has also been investigated.[9] The primary purpose of

this investigation was to develop a system for the rare-earth elements. In its best form, this combination produced an efficiency of approximately 1% for Sb and Te, and approximately 0.1% for Dy. With the available cyclotron-beam intensities and the necessarily thin targets this latter efficiency is too low for practical use at the UNISOR facility, except in some special cases.

In an additional attempt to produce rare-earth isotopes, a Surface-Ionization ion source, Fig. 4, is currently under development. This consists of a tantalum chamber with a thin ($\sim$ 1 mg/cm^2) tungsten window, and a tungsten ionizer. The ion source is heated to temperatures > 2000 C by means of electron bombardment from a multiturn tungsten filament. Because of the high thermal radiation from the ion source, it is necessary to mount the target at some distance from the ion source.

This ion source has shown the capability, in off-line tests, to ionize all the rare-earth elements, although it is very difficult to control. A graphite version has been used successfully for Rb experiments, with an apparently high ($\sim$ 10%) efficiency. The metal version was very recently tested on-line with a Pr target. Holmium and Dy isotopes were observed, but it was impossible to estimate the efficiency.

B. Beam and Source Handling

The back-end of the separator collection chamber is equipped with a beam port on the separator axis, and two additional ports at ± 30°. Recently the 30° ports were each equipped with an externally adjustable deflection electrode. The electrode is a channel forming a 30° circular arc. The exit end of the channel moves along the axis of the port, so that the entrance end can intercept any mass-beam within 6% of the central beam and steer it along the axis of a 30° port.

The central beam port is presently attached to a 2-meter-long beam line containing two focussing lenses. A second, 1-meter-long beam line is available for one of the 30° legs and a third beam line is under construction. When this is completed, the facility will be capable of three simultaneous, fully on-line experiments.

In addition, the collection chamber is equipped with a pair of tape vacuum seal devices.[10] Each consists of a small reel of aluminum-coated mylar tape mounted onto a small plate which forms a sliding seal on the vacuum chamber wall. Mounted on the other side of the plate is a small chamber, Fig. 4, through which the tape passes. The chamber contains two rubber sheets with a slot cut in each through which the tape passes and which isolate the vacuum chamber from the room pressure.

These tape-seal devices are externally adjustable to intercept any mass beam along the focal plane. A source collected on the tape can be pulled out of the vacuum chamber and put in front of a detector within a few seconds. Thus, two additional "semi-on-line" experiments can be simultaneously performed.

Attached to the downstream side of the central beam line is a transport system,[11] Fig. 6, which collects the mass-separated isotopes and transports them to the place where the measurements are performed. This system, which also uses aluminum-coated mylar tape, is modular in design. It consists of a collection station, takeup- and feed-reel chambers and several experiment stations. The modular concept is used so that special experiment stations, when needed, can be constructed and easily integrated into the basic system. The collection, transport, and measurement cycles can be sequenced in several different ways and are ultimately controlled by a small computer, which

forms the basis of a data acquisition system. The transport time between adjacent stations is approximately 0.2 sec.

A simpler transport system was constructed for use on the second beam line. This consists of one or two chambers which are identical to the standard experiment stations on the original system. The tape-feed reel and driving mechanism are outside of the vacuum system, the collection tape passing into and out of the vacuum chamber through a pair of tape-seal devices mounted on the end of the chamber. The air-leakage rate through the tape-seals is small enough to permit this system to be used successfully with a cooled Si(Li) detector.

A third transport is now under consideration. This will probably contain a single continuous loop of tape, and may be driven by a capstan magnetically coupled to a drive motor, eliminating the necessity for a rotating seal through the vacuum wall.

C. Data Acquisition

A number of detectors are available to UNISOR experimenters. These include several large Ge(Li) detectors, Si(Li) electron detectors, a Ge(Li) and a Si(Li) detector, NaI(Tl) positron detectors, and Si surface barrier detectors. A Gerholm lens and a mini-orange spectrometer are also available for on-line use.

Under construction is a positron spectrometer which will allow the setting of a triple gate: two annihilation photons plus a gamma-ray. Also under development is an on-line angular correlation station. The station itself has been constructed, but the electronic hardware and system software have not yet been obtained.

The primary UNISOR data-acquisition system[11] is a TP-5C00[12] system based on a PDP-11 computer interfaced to a Tennelec PACE analog-to-digital converter. Peripherals which are interfaced to the computer include two magnetic-tape drives, a 1.2-million-word disk, an oscilloscope and light pen, a teletype, a line printer, and a control panel. An additional 48 thousand words of extended memory has been added to the standard 28-thousand-word core.

The present system permits the simultaneous acquisition of data from four detectors in a spectrum multiscaling mode. These spectra are acquired in core, stored on disk, and recalled into core during the next cycle. At the same time, data from two 3-parameter experiments can be acquired in list mode on magnetic tape.

The data-acquisition sequence is set by means of a program written in a simple language, TIL.[13] In addition, TIL can access input and output signals at the control panel, so that external devices (e.g., separator beam switch, tape transport control, cyclotron beam stop) can be controlled by means of the same program.

A second data-acquisition system has just been obtained. It is very similar to the above system, lacking only the extended memory and line printer. It, however, uses Wilkinson-type ADC's rather than the PACE system.

Two other, smaller "analyzers", one of which can be programmed, are at the UNISOR facility. In addition, four systems at ORIC are usually available for a run. These include another TP-5000 system, two larger computers with interfaced PACE ADC's and a small pulse-height analyzer.

III. Some Results

In this section, some of the scientific results obtained at the UNISOR facility are presented as examples of the kind of information that can be obtained at an ISOL facility. In many cases, it is the systematic behavior of nuclear properties over the range of several nuclei which can lead to the development of new insights or to the choice of a particular model as the most appropriate one to describe the region. An ISOL system is nearly ideal in that several species can be studied simultaneously and virtually free of contamination. Furthermore, levels are often populated in radioactive decay which are not contained in the yrast band seen in in-beam spectroscopy, and which can be crucial to the interpretation of the nuclear structure effects.

In the even-mass, neutron-deficient Hg isotopes, in-beam studies[14-16] revealed an apparent sudden shift in the yrast states from spherical or nearly-spherical levels to ones having a large deformation. UNISOR investigations[17,18] have revealed several additional levels in ^{184,186,188}Hg, Fig. 7. These levels and their relative transition probabilities clearly demonstrate the existence of two well-defined bands, one built on the nearly-spherical, the other on an excited 0^+ state. These results confirm, to some extent, the prediction[19] that the potential-energy surface for these Hg isotopes should have a double well, the lower lying one yielding a slightly oblate shape and the other minimum corresponding to a well-defined prolate shape. Also confirmed was the prediction that the second (prolate) minimum should become deeper for the lighter isotopes, *i.e.* that the 0^+ deformed bandhead should drop in energy.

Another case in which radioactive-decay data has been important in the interpretation of nuclear structure is in the case of the odd-mass Au

isotopes. Two well-defined bands,[20] Figs. 8 and 9, based on the $d_{3/2}$ and $h_{11/2}$ proton orbitals persist through $^{189-195}$Au. The members of the positive parity band are nearly independent of neutron-number and suggest, even though their spacings do not follow the J(J+1) rule, a very stable collective mode of excitation. The spin sequence in the $h_{11/2}$ band of ^{195}Au has been interpreted[21] as arising from a rotation-aligned coupling of the odd proton to an oblate core. Furthermore, the ordering of the $9/2^-$ and $13/2^-$ members required the incorporation of a triaxial degree of freedom.[22] The states, particularly the low-spin ones, observed at UNISOR from the decay of both high- and low-spin Hg isomers has significantly extended the information on the $h_{11/2}$ rotation-aligned band structure and adds support to the existence of triaxial nuclear shapes in this region. Furthermore, bands based on the $h_{9/2}$ orbital have also been observed. The systematic behavior of these two negative-parity bands suggests that their structure is largely determined by the even-even cores corresponding to an $h_{11/2}$ hole and an $h_{9/2}$ particle. For ^{189}Au in particular, it is concluded[23] that the $h_{11/2}$ band is very well described as an $h_{11/2}$ hole coupled to an asymmetric prolate ^{190}Hg core, and the $h_{9/2}$ band is an $h_{9/2}$ particle coupled to an asymmetric oblate ^{188}Pt core.

The above two cases are examples of how UNISOR data was able to extend or to demonstrate conclusively the applicability of particular concepts of nuclear structure in that region. The major point is that these data could almost certainly not have been obtained by the use of any other experimental technique. Several other examples should be mentioned: the discovery of isomers in ^{185,187}Tl, yielding evidence that the $h_{9/2}$ intruder state is

departing the Z = 82 shell;[24] the first observation of α-decay in Tl isotopes;[25] and nuclear mass differences from positron-decay Q-values.[26] In some of these latter examples, other techniques had been tried, but the use of an ISOL system was essential.

Acknowledgments

The work reported here is the result of efforts by a rather large number of people whom I will not attempt to list. The scientific results, in particular, contain contributions from faculty, students, and staff from each of the member institutions, working in the spirit of cooperation envisioned in the formation of UNISOR. I would, however, like to acknowledge personnally Ron Mlekodaj and Ken Carter of the UNISOR staff, who have been major contributors to the development of the facility.

References

1. E. H. Spejewski and J. H. Hamilton, Nucl. Instr. Meth. 107 (1973) 203.
2. J. H. Hamilton *et al.*, Bull. Am. Phys. Soc. 18 (1973) 1379; A. C. Xenoulis *et al.*, *ibid*, p. 1424; R. S. Lee *et al.*, *ibid*, p. 1425; K. S. R. Sastry *et al.*, *ibid*, p. 1425.
3. For a more detailed version of the UNISOR planning, organization, and early history, see J. H. Hamilton, Science 185 (1974) 819.
4. Danfysik A/S, Jyllinge, Denmark.
5. R. L. Mlekodaj *et al.*, Nucl. Instr. Meth. 139 (1976) 299.
6. O. Almen and K. O. Nielsen, Nucl. Instr. Meth. 1 (1957) 302.
7. G. M. Gowdy *et al.*, Phys. Rev. C 13 (1976) 1601.
8. R. D. Macfarlane and R. D. Griffioen, Nucl. Instr. Meth. 24 (1963) 461.
9. W.-D. Schmidt-Ott *et al.*, Nucl. Instr. Meth. 124 (1975) 83.

10. H. K. Carter and R. L. Mlekodaj, Nucl. Instr. Meth. 128 (1975) 611; U.S. Patent 4,008,899.

11. H. K. Carter *et al.*, Nucl. Instr. Meth. 139 (1976) 349.

12. Tennecomp Systems, Inc., Oak Ridge, TN.

13. Tennecomp Interpretative Language, trademark of Tennecomp Systems, Inc.

14. D. Proetel *et al.*, Phys. Rev. Lett. 31 (1973) 896.

15. N. Rud *et al.*, Phys. Rev. Lett. 31 (1973) 1421.

16. D. Proetel, R. M. Diamond, and F. S. Stephens, Phys. Lett. 48B (1974) 102.

17. J. H. Hamilton *et al.*, Phys. Rev. Lett. 35 (1975) 562.

18. J. D. Cole *et al.*, Phys. Rev. Lett. 37 (1976) 1185.

19. S. Frauendorf and V. V. Pashkevich, Phys. Lett. 55B (1975) 365.

20. E. F. Zganjar *et al.*, Phys. Lett. 58B (1975) 159.

21. F. S. Stephens *et al.*, Phys. Rev. C7 (1973) 2163.

22. J. Meyer ter Vehn, F. S. Stephens and R. M. Diamond, Phys. Rev. Lett. 32 (1974) 1383.

23. J. L. Wood *et al.*, Phys. Rev. C14 (1976) 682.

24. A. G. Schmidt *et al.* Phys. Lett. 66B (1977) 133.

25. K. S. Toth *et al.*, Phys. Lett. 63B (1976) 150.

26. B. D. Kern *et al.*, *Atomic Masses and Fundamental Constants*, Vol. 5, edited by J. H. Sanders and A. H. Wapstra, Plenum Publishing Corp., New York (1976) p. 81.

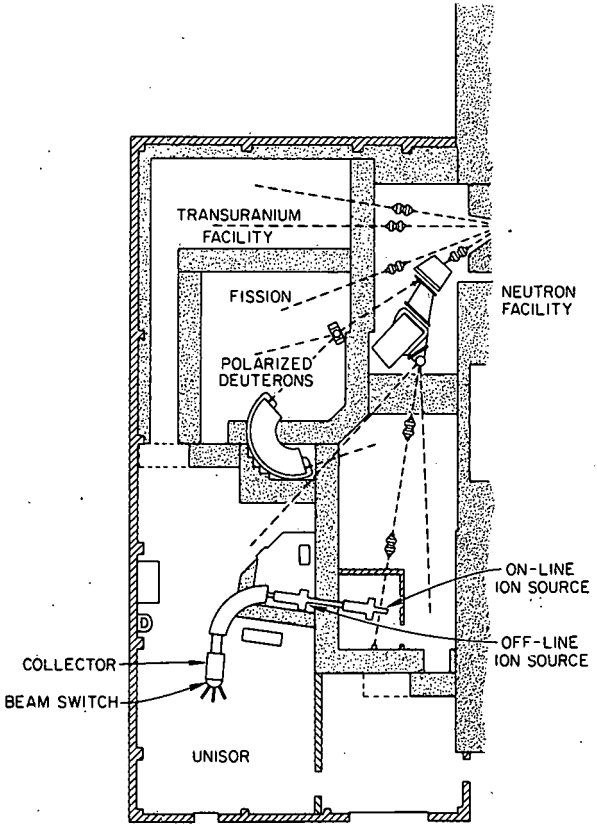

Figure 1. The south annex to the ORIC building

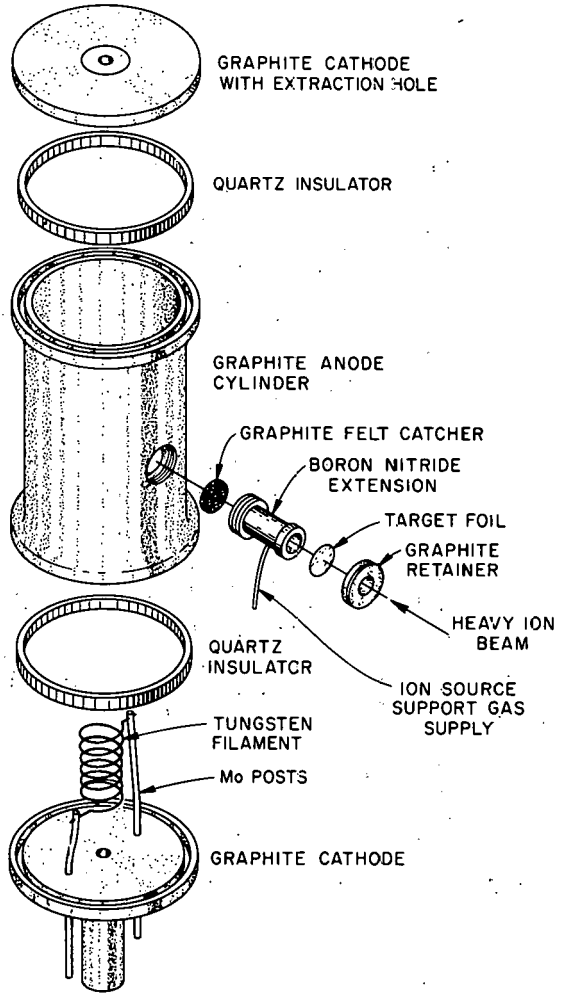

Figure 2. The UNISOR integrated-target ion source

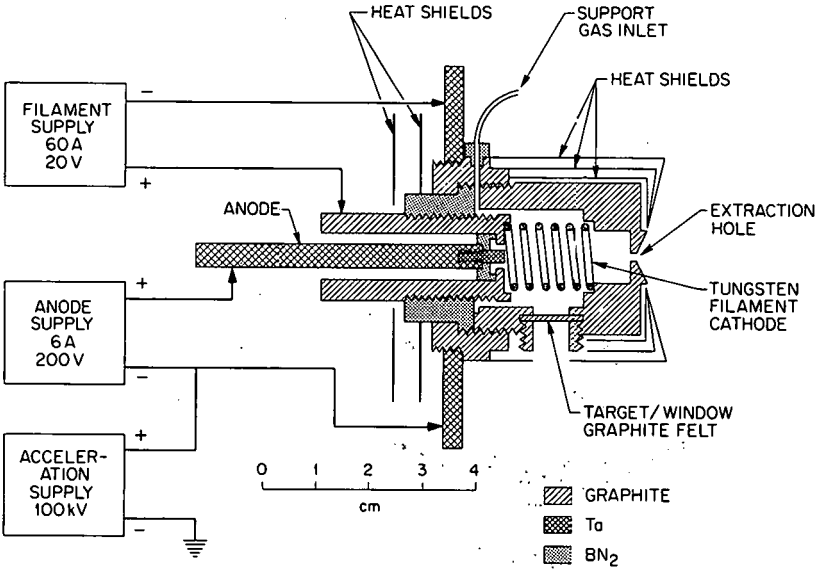

Figure 3. The UNISOR high-temperature ion source

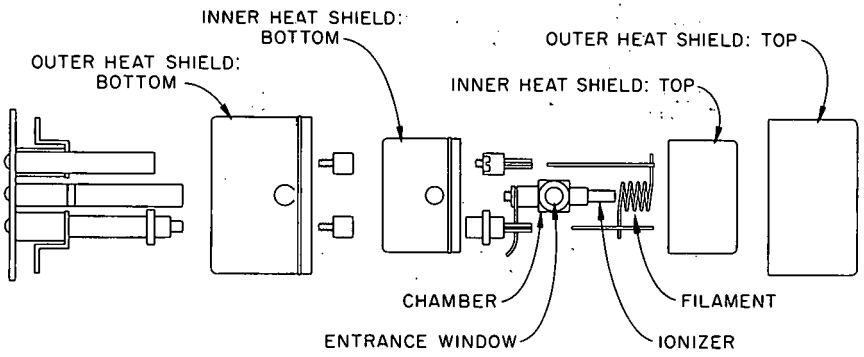

Figure 4. An on-line surface-ionization source under development

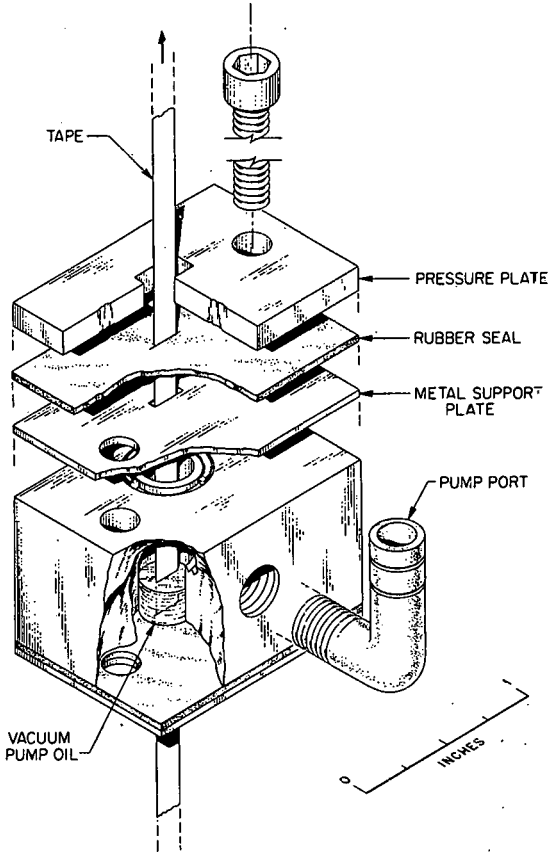

Figure 5. Tape vacuum seal used for quickly removing samples from the collection chamber

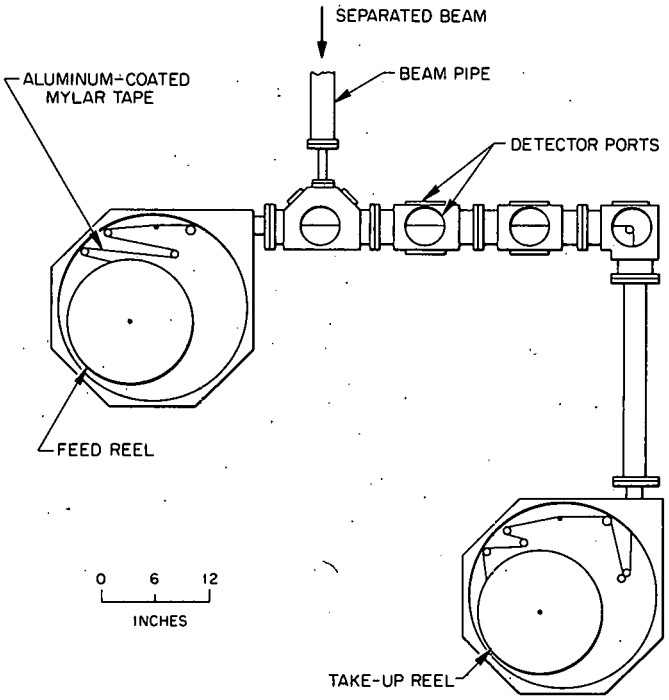

Figure 6. The original UNISOR tape transport system

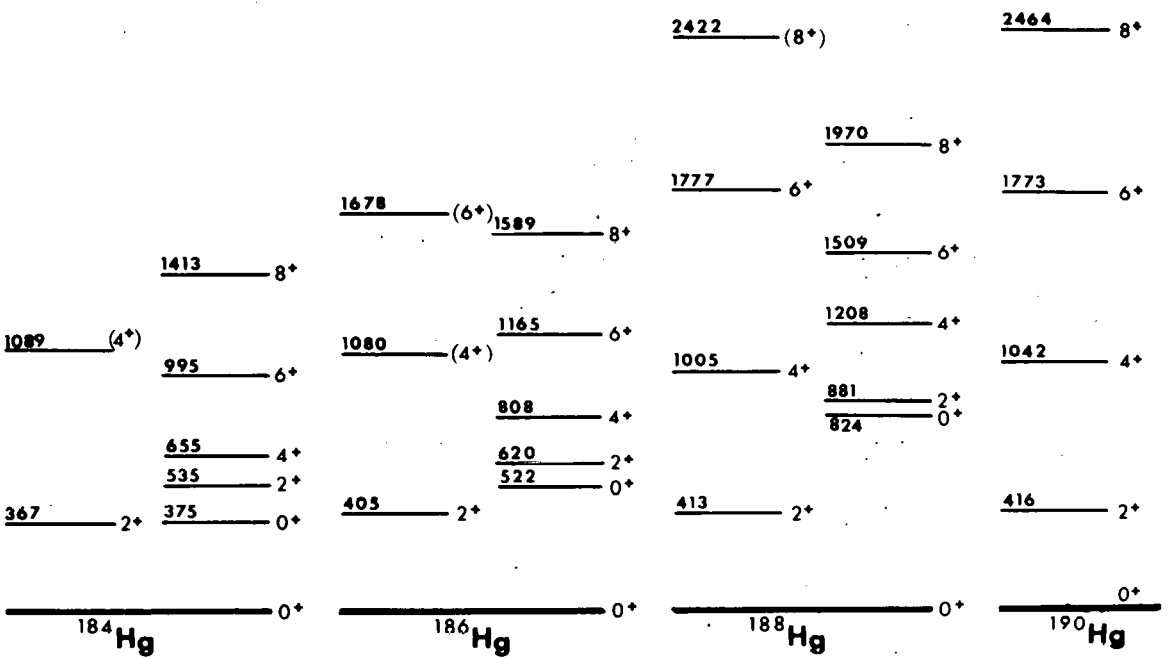

Figure 7. Systematics of the deformed and near-spherical bands in light-mass mercury isotopes

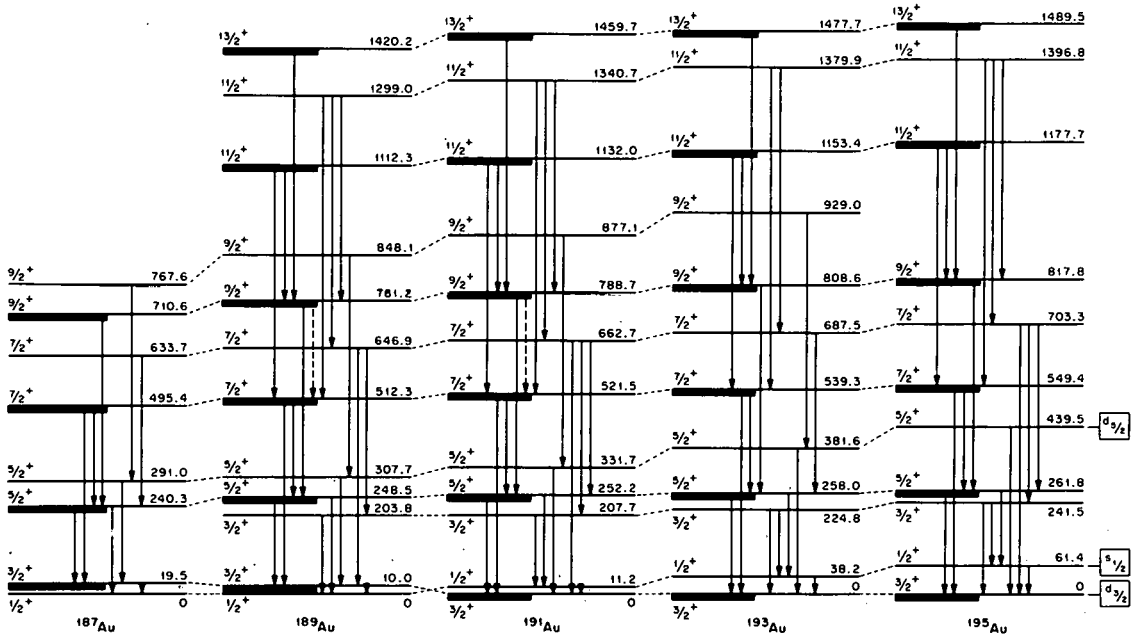

Figure 8. Positive-parity states in odd-A gold nuclei. The states associated with the $d_{3/2}$ orbital are shown as levels with heavy bars.

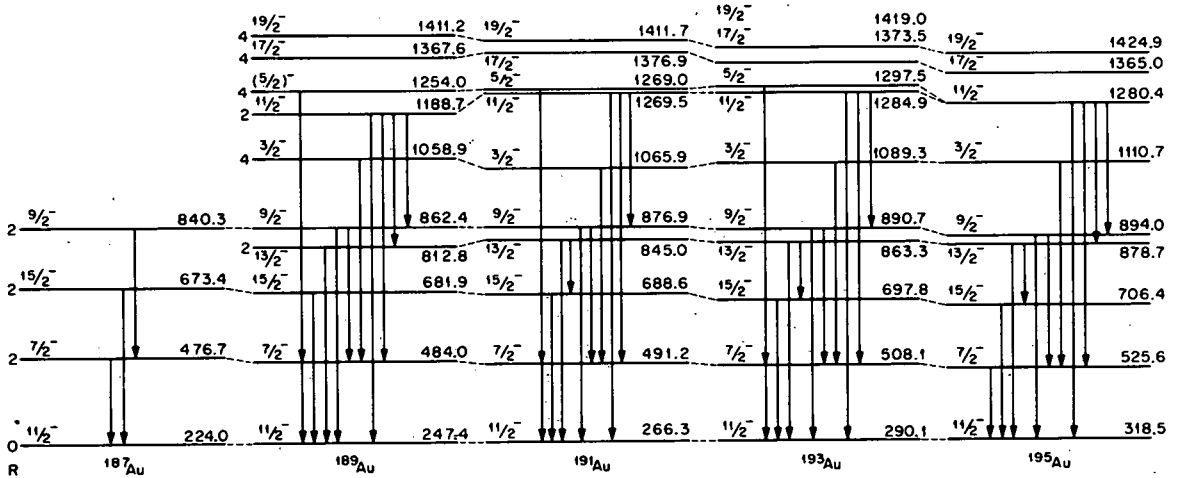

Figure 9. Negative-parity states in odd-A gold nuclei based on the $h_{11/2}$ orbital. The quantum number R is the dominant core spin contributing to the state.

Recent Results from Studies of Non-Gaseous Fission Products with TRISTAN II

JOHN C. HILL

Ames Laboratory-USDOE and Department of Physics,

Iowa State University, Ames, Iowa 50011

ABSTRACT: A new in-beam target ion-source combination has been installed at the TRISTAN isotope separator facility. Mass separated beams of non-gaseous fission products are now available for study. Studies of levels in even-even Cd and Sn nuclei populated through the decay of Ag and In fission products are described, and an evaluation of possibilities for future research is made.

1. Introduction

The TRISTAN isotope separator facility located at the Ames Laboratory Research Reactor has been used for many years to study the properties of the fission-product nuclei Kr and Xe and their daughters. A description of the capabilities and accomplishments of this facility has been given by Talbert[1] in these proceedings. Although a large number of comprehensive studies were carried out, the system was limited by the inability to study fission products other than the rare gases and their daughters.

The above situation changed in the Summer of 1976 due to the successful operation of a new in-beam target ion-source combination of the type used at the OSIRIS separator[2]. The new ion-source allowed us to ionize and mass separate beams of Zn, Ga, Br, Kr, Rb, Ag, Cd, In, Sn, Sb, Te, I, Xe, and Cs.

It will also probably be possible to separate Ge, As, Se, Sr and Ba. The new system was christened TRISTAN II and its capabilities are described in these proceedings by Wohn[3]. In sections 2, 3, and 4, results from the first year of operation of TRISTAN II are described, and in section 5 a discussion of the future possibilities for nuclear structure research is given.

2. Survey Results for Non-Gaseous Fission Products

Soon after the successful installation of the new ion-source a 4π survey of fission-product activity as a function of mass number was carried out. (The results of the survey are shown in Fig. 1.) The details of this measurement are described by Wohn[3] but it is useful here to discuss some of the principal features. The small peak near mass 78 represents production from our ion source of beams of Zn and Ga fission products. A γ ray survey run was made at mass 78 using a 15% efficient Ge(Li) detector. The A=78 beam was collected on the tape of the moving tape collector (MTC). The tape was moved every 3 sec. to enhance the short-lived $^{78}Zn(T_{1/2} = 1.5$ sec.) and $^{78}Ga(T_{1/2} = 5$ sec.) activities. A spectrum accumulated in a 15 min. run is shown in Fig. 2. It is evident from the figure that sufficient activity is available to carry out detailed spectroscopic studies on the above activities and that holdup times in the ion source for Zn and Ga are short.

A γ ray survey run was also made at A = 86 to determine the availability of Br activities from TRISTAN II. The A = 86 beam was collected on the tape of the MTC and counting was done in equilibrium since the ^{86}Kr daughter of $^{86}Br(T_{1/2} = 55$ sec.) is stable. A spectrum accumulated in a 20 min. run is shown in Fig. 3. Yields of Br isotopes appear to be sufficient for decay studies.

The peak in the 4π survey at about A = 90 results from the high yields out of our ion source of Kr and Rb. Studies of Kr and Xe fission products have been carried out in great detail at TRISTAN I and studies of Rb and Cs are being made at several different ISOL facilities using surface-ionization ion sources, therefore the emphasis in the TRISTAN II program should not be on these elements. Nevertheless a γ ray survey was made at A = 96. Large quantities of $^{96}Rb(T_{1/2}$ = 0.2 sec.) were observed indicating an extremely short holdup time for Rb in our ion source. The deep valley in our 4π yield curve running from A = 98 to A = 111 is caused by the onset in the periodic table of a series of refractory elements ranging from Y(Z=39) to Pd(Z=46). These elements are not volatized in our ion source but can be studied in systems[4] like LOHENGRIN and JOSEF where the fission fragments are directly mass analyzed.

A very important plateau in the 4π yield curve occurs between A = 114 and A = 129. This plateau results from high yields of Ag, Cd, and In fission products from our ion source. Spectroscopic studies at TRISTAN II in the first year have concentrated on decay characteristics of even A nuclei in this region. Representative γ spectra obtained during studies of the decay of ^{118}Ag and ^{122}Ag are presented in section 3. A γ spectrum obtained at A = 126 is shown in Fig. 4. The tape on the moving tape collector was moved every 5 sec. to enhance activities from $^{126}Cd(T_{1/2}$ = 0.5 sec) and $^{126}In(T_{1/2}$ = 1.6 sec). Yields of Ag, Cd, and In fission products are sufficient for detailed spectroscopic studies of nuclei even though these elements are in the valley of the fission mass-yield curve. Also successful studies of short-lived isotopes such as $^{120}Ag(T_{1/2}$ = 0.3 sec.), $^{126}Cd(T_{1/2}$ = 0.5 sec.),

and ^{128}In ($T_{1/2}$ = 0.8 sec.) indicates that the holdup time for these elements in the TRISTAN II ion source is quite short.

The second major peak in the 4π mass yield curve starts at about A = 130 and continues to about A = 144. The fission products I, Xe, and Cs are the major contributors to this peak but significant quantities of Sn, Sb, and Te are also produced. A 15 min. γ spectrum at A = 130 taken under equilibrium conditions at our MTC is shown in Fig. 5. Peaks from γ rays emitted in the decay of ^{130}Sn($T_{1/2}$ = 3.7 min.), ^{130}Sb($T_{1/2}$ = 37 min.), and $^{130}Sb^{*}$($T_{1/2}$ = 6.6 min.) are clearly evident. In Fig. 6 a 15 min. γ spectrum taken in equilibrium at A = 134 is presented. Most of the γ strength is from the decay of ^{134}I($T_{1/2}$ = 53 min.) but significant activity from ^{134}Te($T_{1/2}$ = 42 min.) is also observed. It is evident from Fig. 6 that large yields of I are produced from the TRISTAN II ion source. Although neutron-rich I isotopes have been observed up to ^{141}I, no structure information is available from I decays on mass numbers greater than 136 except for a recent study of ^{138}I decay[5]. This area is certainly appropriate for future studies. Fig. 5 and Fig. 6 illustrate the production of Sn, Sb, Te, and I at TRISTAN II but holdup times in our ion source for elements like Sn, Sb, and Te may be somewhat longer than for elements like Ag, Cd, and In. Future surveys will be needed to study this problem. If detailed decay studies of short-lived Sn, Sb, and Te can be carried out, much new information on the very interesting region near doubly-magic ^{132}Sn can be obtained.

3. Studies of Neutron-Rich Even-Even Cd Nuclei

Soon after the successful operation of the in-beam ion source a series of experiments was started with the object of studying the detailed level

structures of neutron-rich even-even Cd nuclei populated in the β decay of Ag fission products. Earlier in this paper, we pointed out that the yield of Ag from our ion source was high even though Ag is at the bottom of the valley of the fission mass-yield curve. Also the holdup time for Ag in our ion source was seen to be short as evidenced by observation in good yields of the short-lived isomer of $^{120}Ag(T_{1/2} = 0.3$ sec.), thus it was possible to observe Ag nuclei out to ^{122}Ag. Studies of the decays of ^{118}Ag and ^{120}Ag are in progress[6,7] and work on ^{122}Ag has been completed[8].

Cd nuclei contain 48 protons which is only two less than the Z = 50 closed shell. It was thus thought that the low-lying excitations of even-even Cd nuclei could be described in terms of simple collective vibrations. Models of this type were unable to describe levels in even-even Pd(Z=46) nuclei. Hsue et al.[9] developed a rotation-vibration collective model which correctly predicted level ordering and B(E2)'s for ^{106}Pd below 2.5 MeV. Hsu et al.[10] have extended this model to all even-even Pd nuclei from ^{102}Pd to ^{114}Pd.

It is of interest to determine if the above model can be extended to describe even-even Cd nuclei. We therefore undertook a series of detailed decay studies of Ag fission products in order to extend the systematics of even-even Cd nuclei out to A = 122. We report below on results of studies of the decay of $^{118}Ag(T_{1/2} = 3.8$ sec.), $^{118}Ag^{*}(T_{1/2} = 2.0$ sec.), and $^{122}Ag(T_{1/2} = 0.48$ sec.). Studies of $^{120}Ag(T_{1/2} = 1.2$ sec.) and $^{120}Ag^{*}(T_{1/2} = 0.3$ sec.) are also in progress. Elsewhere in these proceedings, Williams[11] discusses the results of his model calculations in relation to our level information on Cd nuclei.

3.1. Decay of ^{118}Ag to Levels in ^{118}Cd

The existence of ^{118}Ag was first confirmed by Fritze and Griffiths[12] during a search for new fission products from ^{235}U. A $T_{1/2}$ of 5 sec. was reported. No information on levels in ^{118}Cd was available until the work of Fogelberg et al.[13] who observed two isomers of ^{118}Ag with $T_{1/2}$'s of 2.8 ± 0.2 and 3.7 ± 0.2 sec. respectively. Eight γ transitions were placed in a level scheme consisting of seven excited levels.

In what follows we will describe in some detail the measurements and results obtained in the study of ^{118}Ag decay. This study is a good example of how the TRISTAN II facility can be used to obtain detailed spectroscopic information on short-lived non-gaseous fission products. Results from γ singles, γγ-coincidence, and γ multispectrum scaling are described below.

A 30 hour ^{118}Ag γ singles measurement was made using a 15% efficient Ge(Li) detector and a LEPS detector which accumulated spectra in the energy ranges of 0-4 MeV and 0-400 keV respectively. The activity was collected on the tape of the MTC system. The tape was moved every 6 sec. to minimize activity from the Cd and In daughters. A separate spectrum was taken to enhance Cd and In. The activity was accumulated for 120 sec. but before counting a 30 sec. delay was introduced to eliminate ^{118}Ag activity. The ^{118}Ag singles spectrum from 70 to 3400 keV is shown in Fig. 7 and the LEPS spectrum from 0 to 300 keV is shown in Fig. 8. A total of 53 ^{118}Ag γ rays were observed.

The $T_{1/2}$'s of both ^{118}Ag isomers were measured by γ multispectral scaling. A total of 16 time bins each containing 1024 channels of information were used. The resulting decay curves are shown in Fig. 9. The $T_{1/2}$ of the ^{118}Ag ground state was determined to be 3.76 ± 0.15 sec. from the decay of

the 488-keV γ ray and the $T_{1/2}$ of the ^{118}Ag isomeric state was determined to be 2.0 ± 0.2 sec. from the decay of the isomeric γ ray at 128 keV. The isomeric state $T_{1/2}$ is considerably less than the value of 2.8 ± 0.2 sec. obtained by Fogelberg et al.[13]

Two Ge(Li) detectors of about 15% efficiency were used in 180° geometry for a 17-hour γγ coincidence study. The data was stored event-by-event in a 4K by 4K array for later computer sorting. Typical γ spectra in coincidence with the 488- and 2778-keV γ rays are shown in Fig. 10.

The results of the singles and coincidence measurements were used to construct a level scheme for ^{118}Cd which is shown in Fig. 11. Of the 53 γ rays observed 38 were placed depopulating levels in ^{118}Cd up to 3382 keV. It is difficult to determine the β feedings from each of the two ^{118}Ag isomers due to the similarity of their $T_{1/2}$'s, but work on this is in progress. Until this is completed it is risky to assign spins to the higher lying levels in ^{118}Cd. It is clear though that levels like the one at 2788 keV which decays directly to the ground state is fed primarily by the low-spin ground-state isomer of ^{118}Ag while the level at 1936 keV which decays only to the 4^+ level at 1165 keV is fed primarily by the high-spin excited-state isomer of ^{118}Ag. Interpretation of the ^{118}Cd level scheme in terms of a rotation-vibration collective model is given elsewhere in these proceedings by Williams.[11] The preliminary results from this work are compared with those from the OSIRIS experiment[13] in Fig. 12.

3.2. Decay of ^{122}Ag to Levels in ^{122}Cd

^{122}Cd is the most neutron-rich nucleus of Cd about which level information exists. ^{122}Ag was first reported by Fogelberg et al.[13] on the basis of

measurements made at the OSIRIS separator at Studsvik. The ^{122}Ag $T_{1/2}$ was measured to be 1.5 ± 0.5 sec. and only two γ rays at 570 and 760 keV were observed. Their intensities were not given. The decay study of ^{122}Ag was the first one to be completed with the TRISTAN II facility and the results are discussed below.

A γ singles run was made in which activity was collected on the tape of our MTC system. The tape was moved every 3 sec. to minimize activity from the ^{122}Cd and ^{122}In daughters. The run time was 12 hours and both Ge(Li) and LEPS detectors were used. The spectrum from 70 to 1450 keV is shown in Fig. 13. Six γ rays were observed from ^{122}Ag decay. It is interesting to note that the intensity of the ^{122}Ag γ rays is weak compared to those from ^{118}Ag. This is due to a combination of the shorter $T_{1/2}$ and lower fission yield of ^{122}Ag.

The $T_{1/2}$ was determined as for ^{118}Ag by γ multispectral scaling. The decay curve for the 569-keV γ ray is shown in Fig. 14. The value obtained for the ^{122}Ag $T_{1/2}$ was 0.48 ± 0.08 sec. which is much smaller than the value[13] of 1.5 ± 0.5 sec. obtained at OSIRIS. A γγ-coincidence measurement was also made. Definite coincidences were observed in four γ ray gates. Representative coincidence spectra in coincidence with the 569- and 760-keV γ rays are shown in Fig. 15.

The above results were used to construct a decay scheme for ^{122}Ag which is shown in Fig. 16. The first excited state at 569 keV is probably 2^+ as is the case for all even-even Cd nuclei. The level at 1368 keV is also 2^+ since it decays to both the ground and first excited states. The 1329-keV level was assigned a J^π of 4^+ due to the strength of the 760-keV transition and the fact that the 4^+ is lower in energy than the 2^+ member of the vibrational

triplet for ^{118}Ag and ^{120}Ag. The log ft's of 5.3 and 5.8 for β feedings to the 569- and 1329-keV levels respectively limit the J^{π} for the ^{122}Ag ground state to 3^+. A survey of the available shell model orbitals indicates that the configuration for the ^{122}Ag ground state is probably $\pi(g_{9/2})\nu(d_{3/2})$. We favor a J^{π} of 3^+ or 4^+ for the 1979-keV level on the basis of its log ft of 5.3 and the absence of a γ transition to either of the 2^+ states.

Measurements on the decay of ^{120}Ag ($T_{1/2}$ = 1.2 sec.) and ^{120}Ag*($T_{1/2}$ = 0.3 sec.) to levels in ^{120}Cd have been completed at TRISTAN II and analysis of the data is in progress. Of a total of 65 γ rays observed, 37 have been placed in a preliminary level scheme consisting of levels up to 3559 keV. The details of this study will not be presented here, but our results for low-lying levels in ^{120}Cd will be used in the discussion of the systematics of even-even neutron-rich Cd nuclei that follows.

3.3 Systematics for Even-Even Cd Nuclei

The systematics for the low-lying levels in even-even Cd nuclei are given in Fig. 17. The level energies for ^{118}Cd, ^{120}Cd, and ^{122}Cd are those measured at TRISTAN II. Several features are of interest. The first excited 2^+ state (one phonon quadrupole state in the vibrational model) is fairly constant in energy but reaches a minimum at A = 118. The rise in energy is quite symmetric on each side of A = 118. One might expect the 2^+ state to have its lowest energy at A = 114 midway between the N = 50 and N = 82 closed shells where the nucleus might be expected to be the softest. The first excited 4^+ state (member of the two phonon vibrational triplet) is typically a little more than twice the energy of the one phonon 2^+ state. The behavior of the 4^+ state with neutron number is remarkably similiar to that of the one

phonon state with a energy minimum at A = 118. The behavior of the second excited 2^+ state (2^+ member of the two phonon vibrational triplet) is quite different. Its energy is about twice that of the one phonon state but its energy minimum is at A = 114 (mid-shell). In the rotational-vibrational model of Williams[11] the energy of this state is largely determined by the asymmetry parameter. The minimum at mid-shell is consistent with maximal collective motion near mid-shell.

Our preliminary results on levels in ^{118}Cd are in good agreement with the rotational-vibrational model[11] but this model is unable to account correctly for the energy and γ branching of the level in ^{122}Cd (see Fig. 16) at 1979 keV. This breakdown in the rotational-vibrational model may be due to the neglect of the single-particle character of the ^{122}Cd nucleus. This is not surprising since Cd (Z = 48) is only two protons away from the Z = 50 closed shell. Also as we add neutron pairs we are approaching the N = 82 closed shell.

4. Studies in the Tin Region at TRISTAN II

The Sn(Z = 50) nuclei have been subjected to intensive study for many years due to the fact that they contain a magic number of protons. In spite of this our knowledge of the structure of the neutron-rich Sn nuclei with A = 126 and above is very incomplete. Almost all of the knowledge that does exist comes from work done at the OSIRIS separator.[14] The structure of Sn nuclei between A = 126 and 132 is also of great interest in determining to what degree the magic numbers Z = 50 and N = 82 are still magic far to the neutron-rich side of stability (^{132}Sn region). We report below on decay studies[15-17] of ^{126}Cd, ^{126}In, and ^{128}In.

4.1. Structure of ^{126}Sn and ^{128}Sn from the Decay of In Fission Products

One of the principal objectives of the TRISTAN II program was to extend the systematics of even-even Sn nuclides toward doubly-magic neutron-rich ^{132}Sn. We therefore undertook a detailed decay study of ^{126}In and ^{128}In. Some information on the decay of ^{126}In and ^{128}In has been obtained at the OSIRIS separator.[14]

In the study of ^{126}In decay a $T_{1/2}$ of 1.6 ± 0.2 sec was obtained by γ multispectral scaling. Of 42 γ rays associated with the decay of ^{126}In, 35 were placed in a preliminary ^{126}Sn level scheme which is shown in Fig. 18. Levels also seen at OSIRIS are indicated by an asterisk. In the study of the A = 128 decay chain several different $T_{1/2}$'s were observed. Their relationship is not completely clear but an activity with a half-life of 7.1 sec. is associated with the decay of the 7^- isomeric state in ^{128}Sn at 2091 keV and an activity with a half-life of 0.83 sec. is associated with ^{128}In decay. A total of 50 γ rays have been placed in a preliminary ^{128}Sn level scheme which is shown in Fig. 19. In the work at OSIRIS only the excited states at 1169, 2001, 2092, and 2121 keV were observed.

Systematics for even-even neutron-rich Sn nuclides are given in Fig. 20. Although our results are more detailed than those from Ref. 14 our analysis is not complete and J^π's have not been assigned for the new levels. Several systematic features of the levels are worthy of note. First the first-excited 2^+ level rises slowly as N = 82 is approached. This is consistent with the idea that the nucleus becomes more tightly bound as the neutron number nears 82. In contrast to this the 4^+, 5^-, and 7^- levels decrease in energy as N = 82 is approached. This feature is not well understood, but a

similiar effect[5] has been noted for low-lying levels in the even-even N = 82 nuclides.

4.2. The Decay of ^{126}Cd

We report here the first decay scheme for ^{126}Cd. This very neutron-rich nucleus has been observed[2] at the OSIRIS separator but no decay scheme was given. In a survey of A = 126 activity at TRISTAN II several γ rays belonging to ^{126}Cd were observed. A γ multispectral scaling measurement was made and the $T_{1/2}$ of 0.51 ± 0.01 sec. for ^{126}Cd was obtained from the 260- and 428-keV γ rays. The ^{126}Cd decay curve is given in Fig. 21.

Singles spectra at A = 126 were taken in which the tape of the MTC was moved every 2 sec. in order to minimize activities from longer lived ^{126}In. The resulting spectrum was shown in Fig. 4. A total of 9 γ rays were placed in a preliminary ^{126}Cd decay scheme which is shown in Fig. 22. No discussion of odd-odd In systematics is possible since practically no information on levels in other In nuclei in this region is available. Such nuclei are interesting since their low-lying levels should be describable in terms of one proton hole in the Z = 50 closed shell coupling with an odd neutron between N = 50 and N = 82.

5. Possibilities for Future Studies at TRISTAN II

During the first year of operation spectroscopic studies at TRSITAN II have concentrated on even A nuclei in the region just below singly-magic Sn. There are several other regions of great interest which can be studied with our present system. A discussion of future possiblities follows.

5.1. The Region Near Doubly-Magic ^{78}Ni

It is of interest to determine if the magic numbers near stability remain magic far from stability. The doubly-magic nucleus ^{78}Ni is probably too far from stability to enable a study of its properties using a fission source. Nevertheless the region just above it in the nuclide chart is accessible to study at TRISTAN II. This is possible due to the good yields and short holdup times for Zn and Ga in our ion source as can be seen from the 4π fission product yield curve in Fig. 1 and the A = 78 γ spectrum in Fig. 2. In particular it should be possible to study a number of N = 50 nuclei just above ^{78}Ni.

The nuclide chart for N = 50 just above doubly-magic ^{78}Ni is shown in Fig. 23. It should be possible to determine the structure of the N = 50 nuclei starting from ^{81}Ga(^{78}Ni core + 3 protons) up to ^{85}Br(^{78}Ni core + 7 protons). Wohn[3] in these proceedings has shown that yields of ^{82}Ga, ^{83}Ge, ^{84}As and ^{85}Se should be large enough for decay studies. The yield of ^{81}Zn is quite low but with increased neutron fluxes it should be sufficient for decay studies if its $T_{1/2}$ is not too short. Identification of one-quasiparticle states in ^{81}Ga, ^{83}As, and ^{85}Br and location of the core breaking states in ^{82}Ge and ^{84}Se would be of great help in determining the degree to which ^{78}Ni is doubly-magic.

Preliminary studies of Ge nuclei in this region are in progress at TRISTAN II. Some data has been obtained[18] on the decay of ^{78}Ga($T_{1/2}$ = 5 sec.). Systematics for low-lying levels in even-even Ge nuclides is given in Fig. 24. The results shown for A = 78 are from our work. These nuclei are unusual in that the 0^+ level lies very low and is the first excited state in ^{72}Ge. One might expect that as the neutron number approaches the magic number 50 the

nucleus would become more tightly bound and the first excited 2^+ state would rise in energy. This is first noted in Ge in going from A = 76 to A = 78. Also one would expect the Ge nucleus to become more like a quadrupole vibrator as N = 50 is approached. Estimate of the yield[3] for Ga isotopes indicates that it should be possible to study the structure of Ge nuclides out to singly magic ^{82}Ge.

5.2 The Doubly-Magic ^{132}Sn Region

The region around neutron-rich ^{132}Sn is of great interest since it is the most accessible doubly-magic region that is far from stability. Most of our knowledge of nuclei very close to ^{132}Sn has come from experiments carried out at the OSIRIS separator. A good set of references on that work is given by Rudstam.[2] The status of our knowledge of nuclei consisting of a ^{132}Sn core plus one or two particles or holes is given in Fig. 25. We have indicated the level structure of these nuclei as determined by β decay experiments and also the $T_{1/2}$'s of their parents if known.

It is of great interest to determine to what degree the nucleus ^{132}Sn is doubly-magic. In particular the location and character of the core excited states in the nuclei in Fig. 25 would shed much light on this question. The only core states known from β decay are the two in ^{132}Sn. Due to the large Q_β's available it should be possible to excite core states in ^{132}Sn (core), ^{133}Sb (core + proton), and ^{131}Sn (core + neutron hole) if detailed decay studies with very good statistics are carried out. Most of the core states are probably above 3 MeV so their corresponding β feedings would be weak. Another indication of the degree to which a region is doubly-magic is the accuracy with which shell model calculations involving only extra-core

particles can describe levels up to several MeV. Two, three, and four valence nuclei such as ^{128}Sn, ^{129}Sn, ^{130}Sn, ^{134}Te, ^{135}I, and ^{136}Xe are good test nuclei[19] for this purpose. ^{136}Xe has been studied at TRISTAN I and preliminary results on ^{128}Sn are given above. With TRSITAN II it should be possible to study in some detail levels in ^{129}Sn, ^{130}Sn, ^{131}Sn, ^{132}Sn, ^{133}Sb, ^{134}Te, and ^{135}I. The decay of ^{132}Sn to levels in ^{132}Sb is well characterized. Study of levels in ^{134}Sb from the decay of ^{134}Sn should be possible if the holdup time for Sn in the ion source is not too long. Because of low yields studies of levels in ^{130}In, ^{131}In, ^{132}In and ^{130}Cd are probably not feasible with fission sources.

ACKNOWLEDGMENTS

This work was supported by the U. S. Department of Energy, Division of Basic Energy Sciences. The success of TRISTAN II was due to the efforts of many people. W. L. Talbert, Jr., F. K. Wohn, A. R. Landin, and R. G. Struss were responsible for the design of the in-beam ion source. A. R. Landin, R. L. Gill, D. R. Lekwa, and M. A. Cullison kept the system in running order and the data was taken and analyzed by M. L. Gartner, D. R. Margetan, R. L. Gill, T. K. Li, and L. L. Shih.

REFERENCES

1. W. L. TALBERT, JR., "TRISTAN I Techniques, Capabilities, and Accomplishments," in these proceedings, p.
2. G. RUDSTAM, Nucl. Instrum. Methods 139, 239 (1976).
3. F. K. WOHN, "TRISTAN II - Extension of Capabilities to Non-Gaseous Fission Products," in these proceedings, p.
4. P. ARMBRUSTER, Proc. 3rd Internat. Conf. on Nuclei Far from Stability, Cargese, 1976, p. 3.
   T. A. KHAN, "Nuclear Structure Studies at JOSEF," in these proceedings, p.
5. W. R. WESTERN, JOHN C. HILL, W. C. SCHICK, JR., and W. L. TALBERT, JR., Phys. Rev. C 14, 275 (1976).
6. D. R. MARGETAN, JOHN C. HILL, S. A. WILLIAMS, and W. L. TALBERT, JR., Bull. Amer. Phys. Soc. 22, 594 (1977).
7. J. C. WELLS, JR., JOHN C. HILL, R. L. GILL, S. A. WILLIAMS, and W. L. TALBERT, JR., Bull. Amer. Phys. Soc. 21, 995 (1976).
8. T. K. LI, L. L. SHIH, and JOHN C. HILL, Bull. Amer. Phys. Soc. 22, 1G25 (1977).
9. S. T. HSUE, H. H. HSU, F. K. WOHN, W. R. WESTERN, and S. A. WILLIAMS, Phys. Rev. C 12, 582 (1975).
10. H. H. HSU, S. A. WILLIAMS, F. K. WOHN, and F. J. MARGETAN, Phys. Rev. C 16, 1626 (1977).
11. S. A. WILLIAMS, "Collective Structure of Medium-Mass Nuclei," in these proceedings, p.
12. K. FRITZE and K. GRIFFITHS, Radiochim. Acta 7, 59 (1967).

13. B. FOGELBERG, A. BACKLIN, and T. NAGARAJAN, Phys. Lett. 36B, 334 (1971).

14. K. ALEKLETT, Thesis, Chalmers University of Technology, Göteborg, Sweden, 1977.

15. JOHN C. HILL, M. L. GARTNER, T. K. LI, and W. L. TALBERT, JR., Bull. Amer. Phys. Soc., 22, 595 (1977).

16. M. L. GARTNER, JOHN C. HILL, and T. K. LI, Bull. Amer. Phys. Soc., 22, 595 (1977).

17. R. L. GILL, JOHN C. HILL, and A. F. VOIGT, Bull. Amer. Phys. Soc., 22, 595 (1977).

18. M. L. GARTNER and JOHN C. HILL, Bull. Amer. Phys. Soc. 22, 1028 (1977).

19. W. J. BALDRIDGE, Phys. Rev. C, to be published.

J. P. VARY, "Nuclear-Shell Theory Near Doubly-Magic ^{132}Sn," in these proceedings, p.

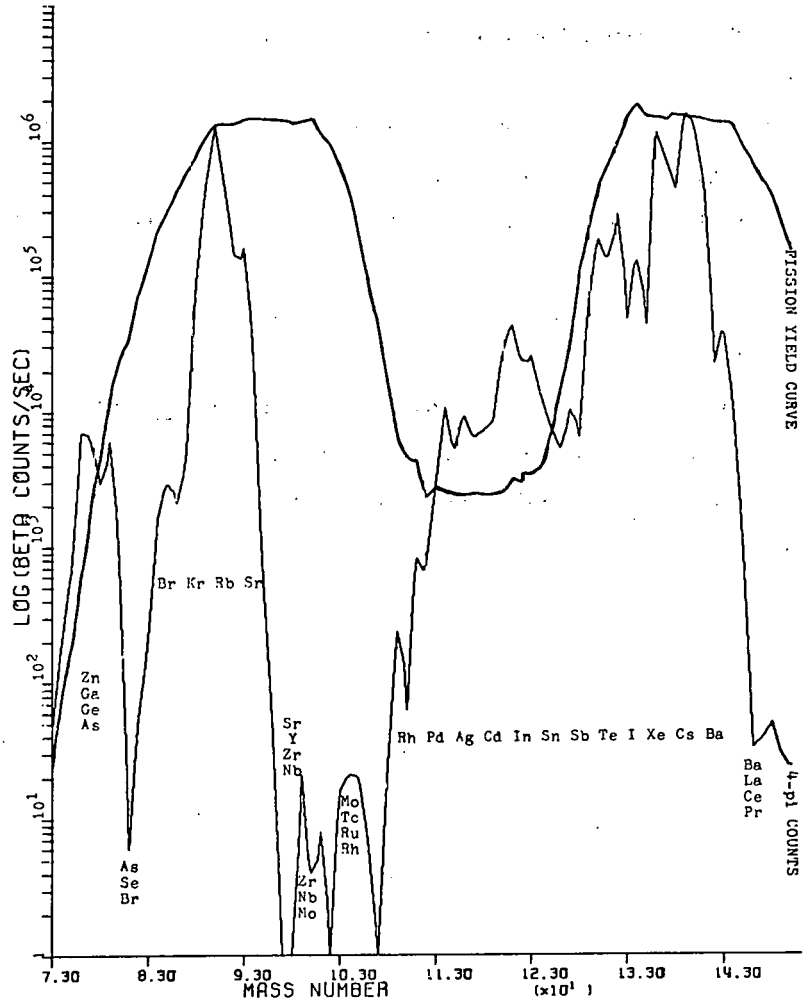

Figure 1. Mass scan of fission-product activity obtained with 4πβ counting at TRISTAN II. The mass distribution for thermal neutron fission of ^{235}U is included for reference.

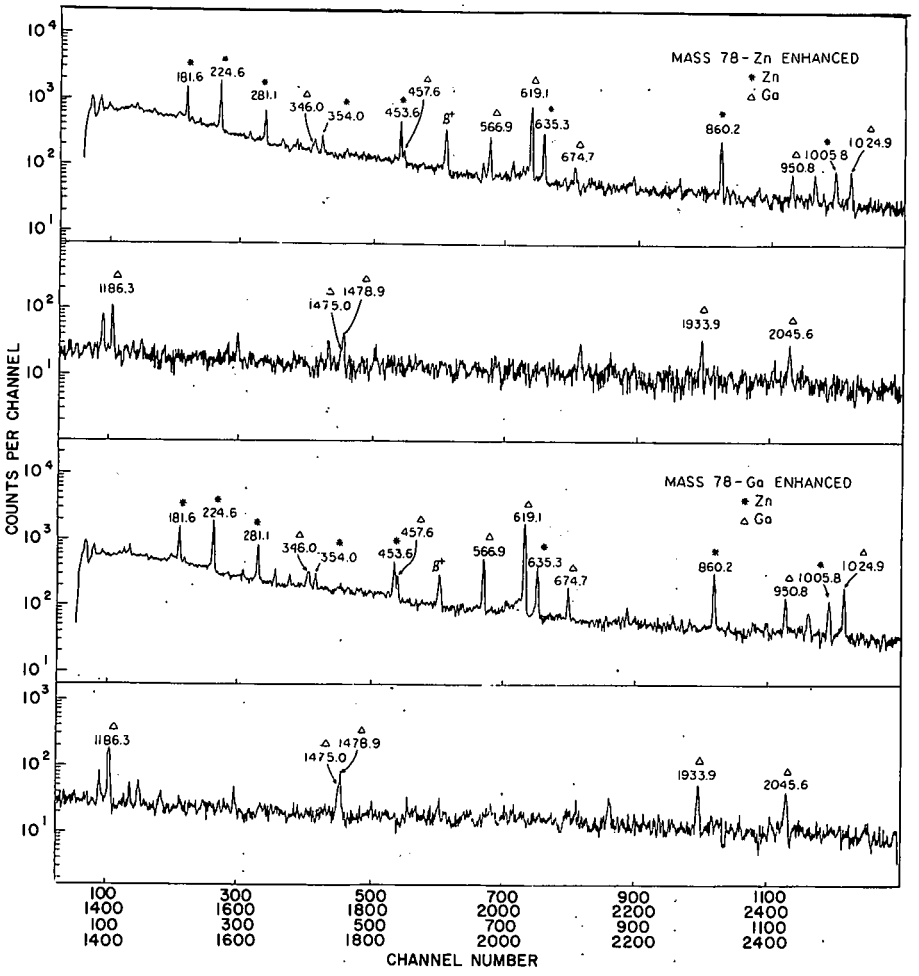

Figure 2. Gamma spectrum from survey run at A = 78. Run time was 15 min.

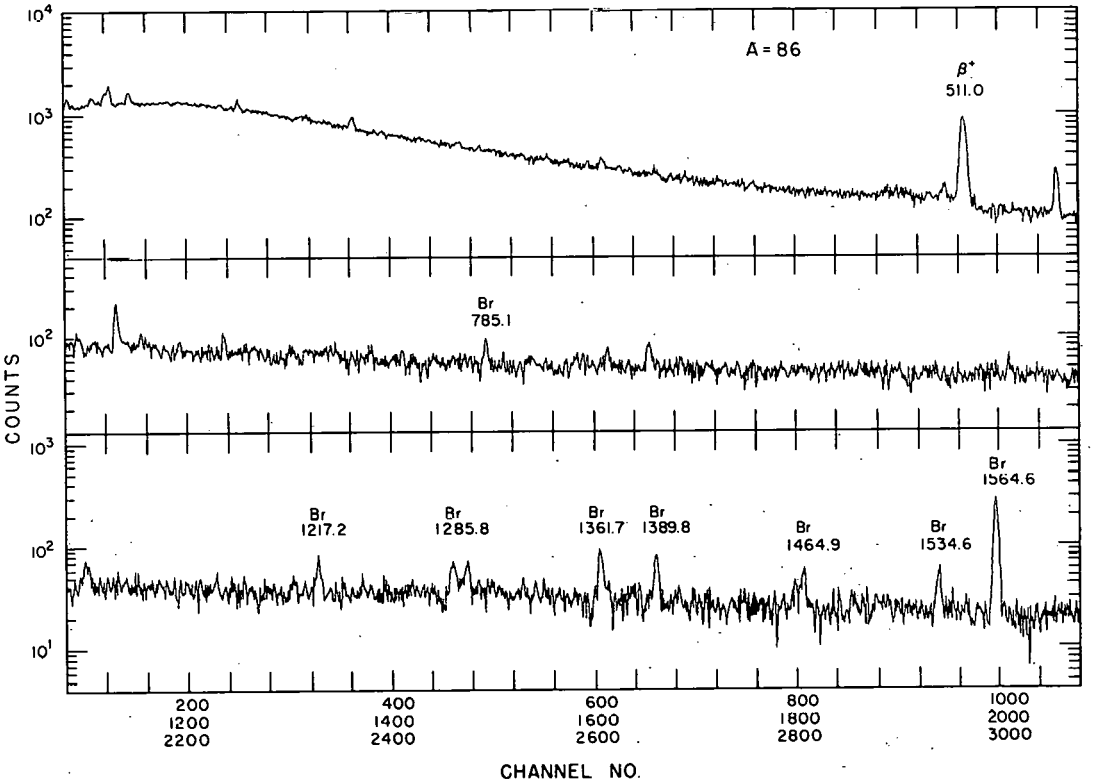

Figure 3. Gamma spectrum from survey run at A = 86. Run time was 20 min.

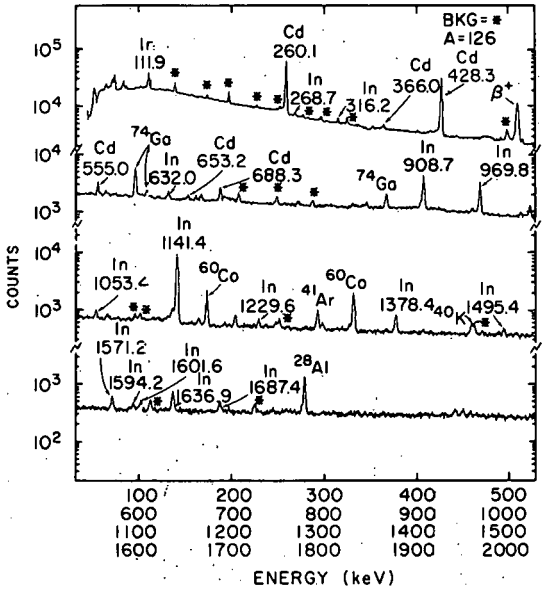

Figure 4. Gamma spectrum obtained in study of ^{126}Cd and ^{126}In decay. Run time was 20 hours.

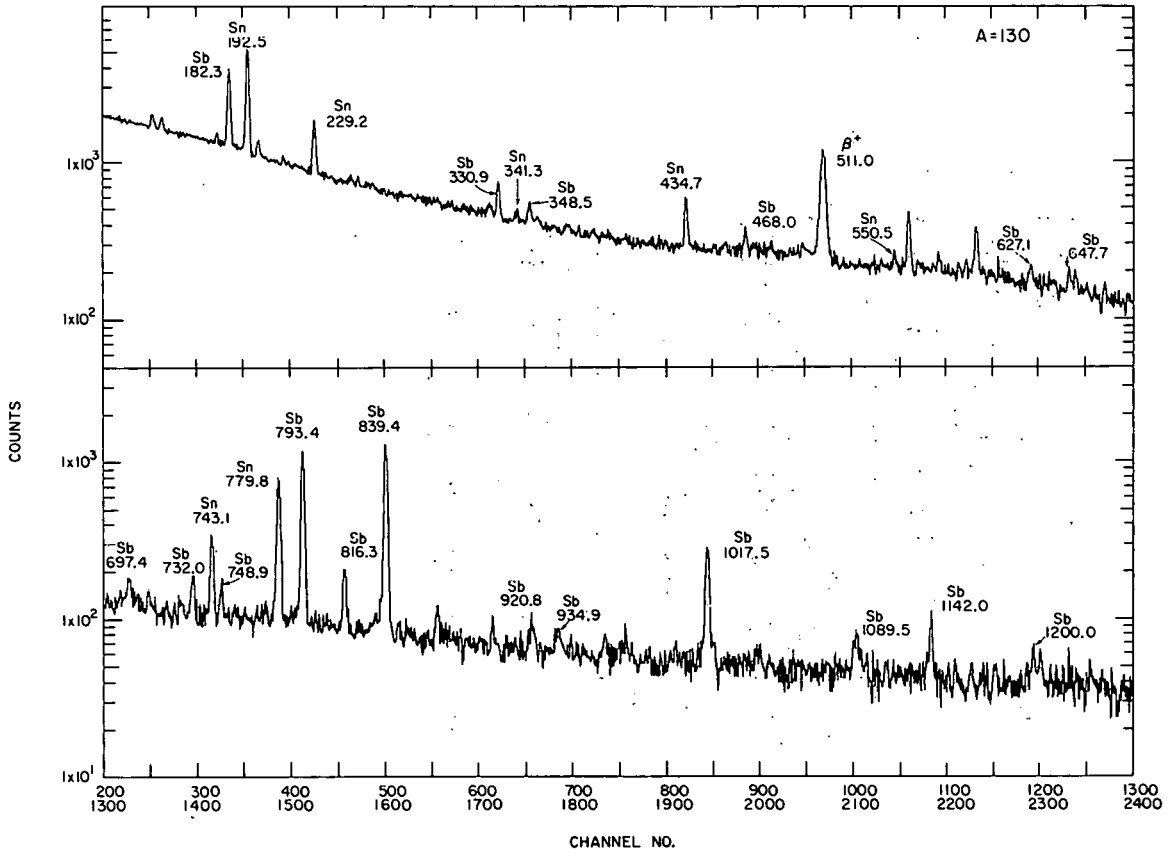

Figure 5. Gamma spectrum from survey run at A = 130. Run time was 15 min.

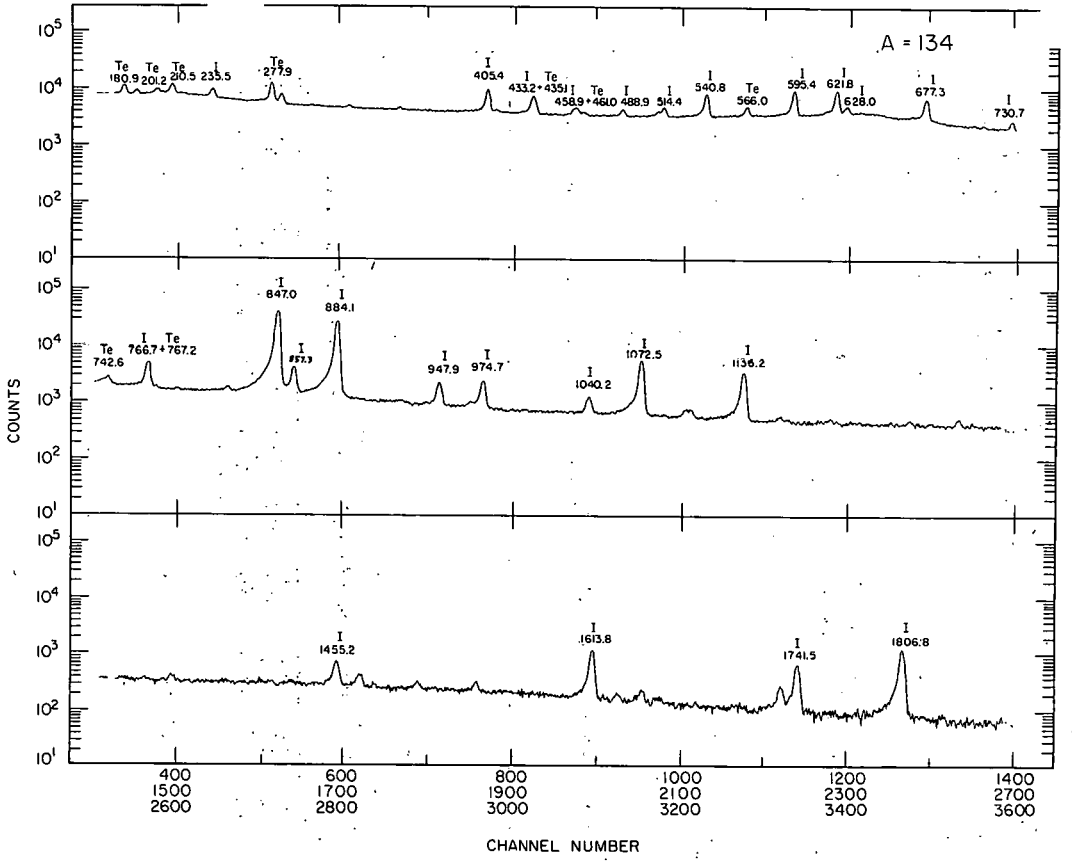

Figure 6. Gamma spectrum from survey run at A = 134. Run time was 15 min.

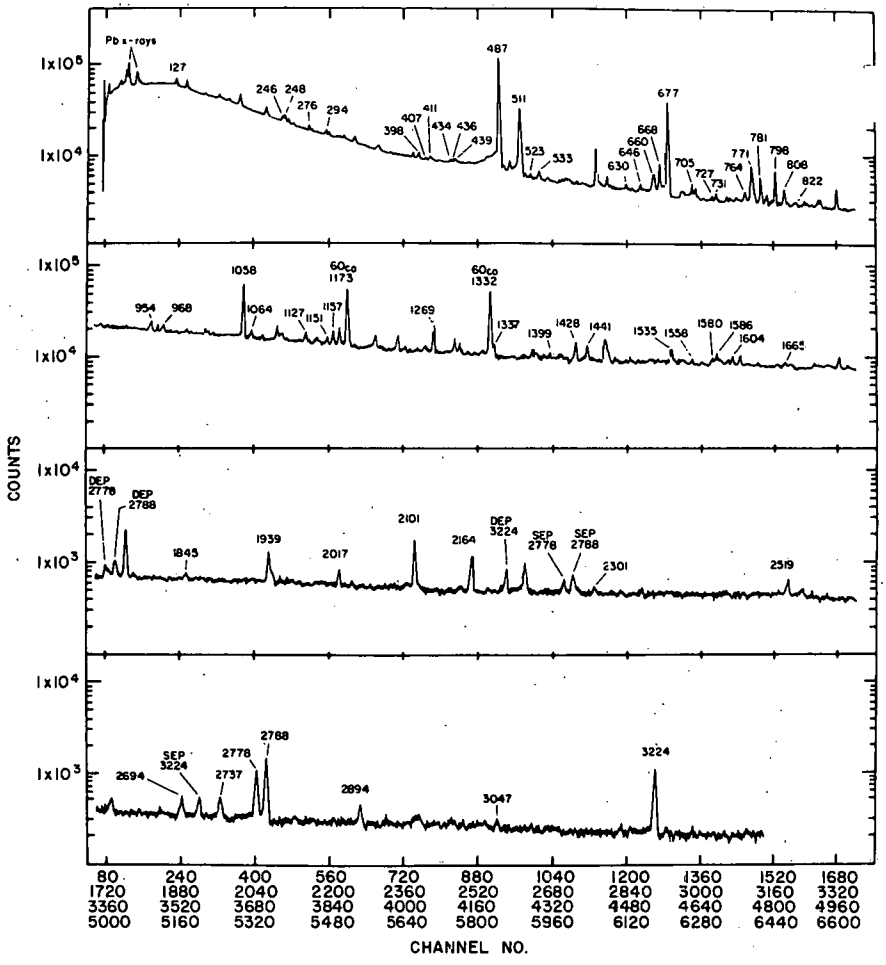

Figure 7. Gamma spectrum for ^{118}Ag decay between 70 and 3400 keV.

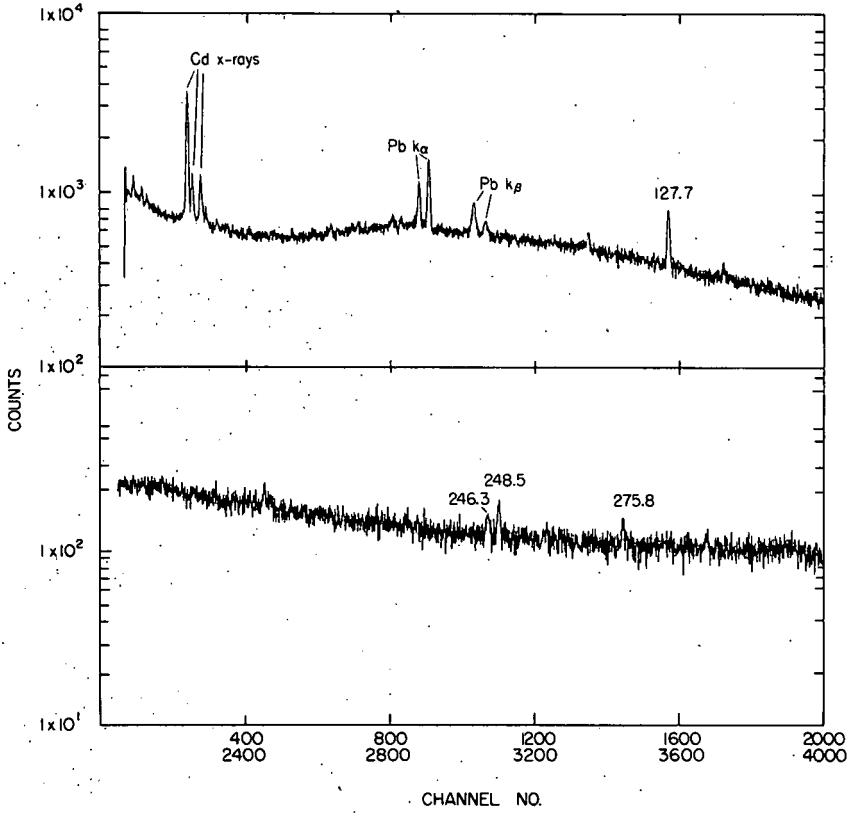

Figure 8. LEPS spectrum for ^{118}Ag decay between 0 and 300 keV.

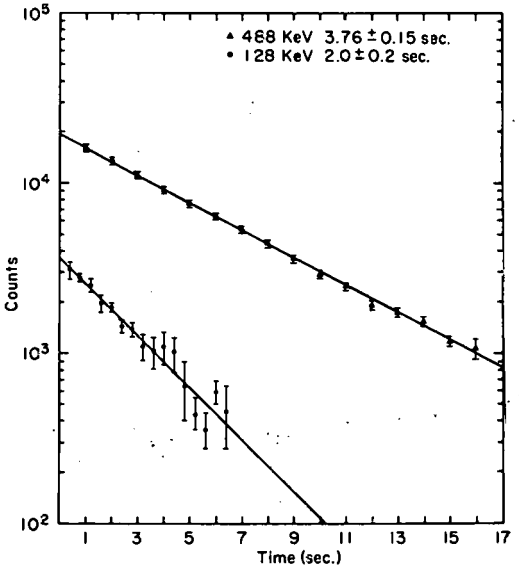

Figure 9. Decay curves for the decay of ^{118}Ag isomers.

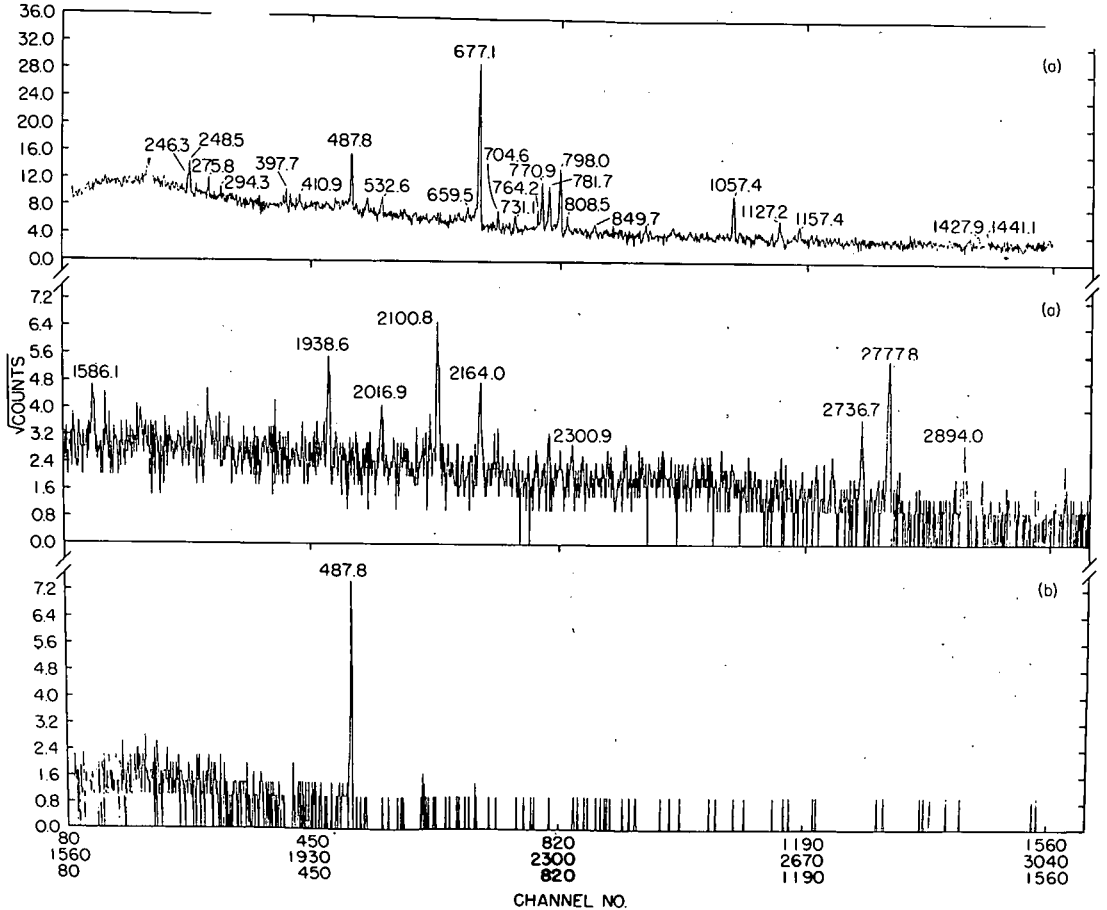

Figure 10. Gamma spectra in coincidence with the (a) 488- and (b) 2778-keV γ rays from ^{118}Ag decay.

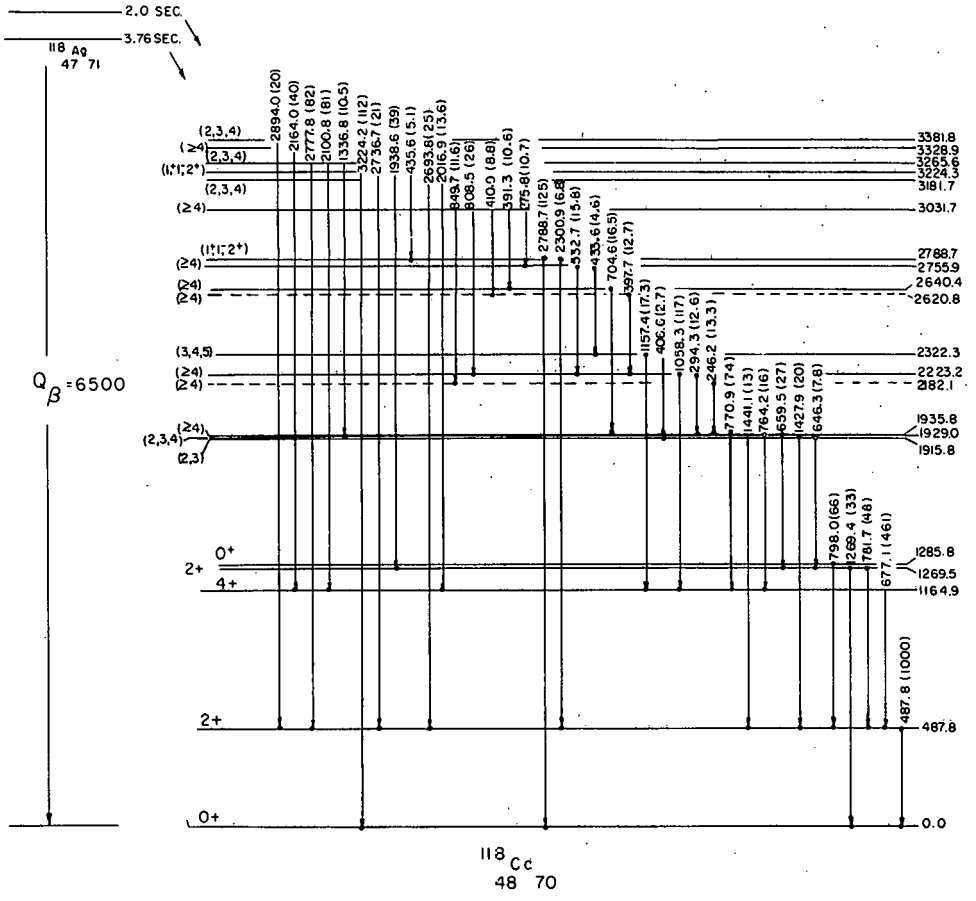

Figure 11. Decay scheme for ^{118}Ag.

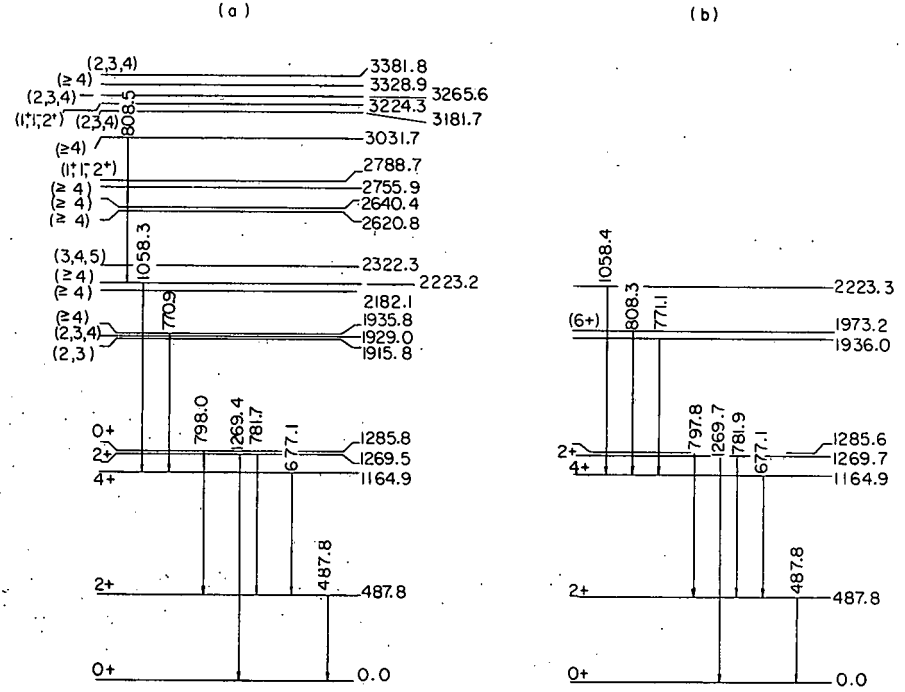

Figure 12. Comparison of the results from this work with those from Ref. 13.

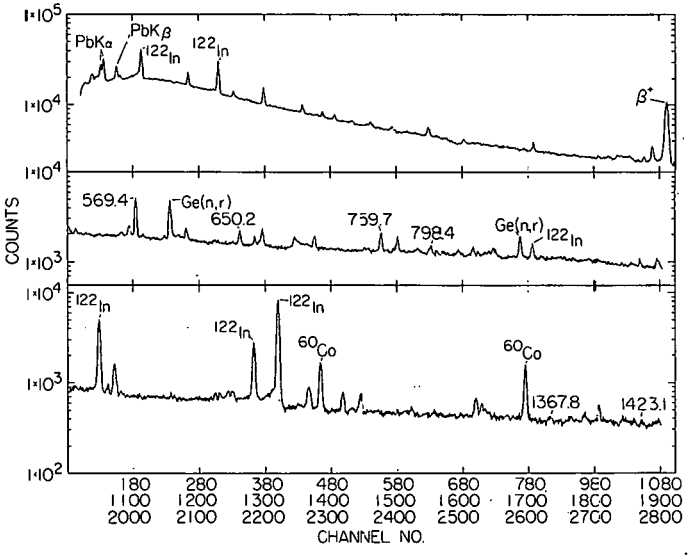

Figure 13. Gamma spectrum for ^{122}Ag decay between 70 and 1450 keV.

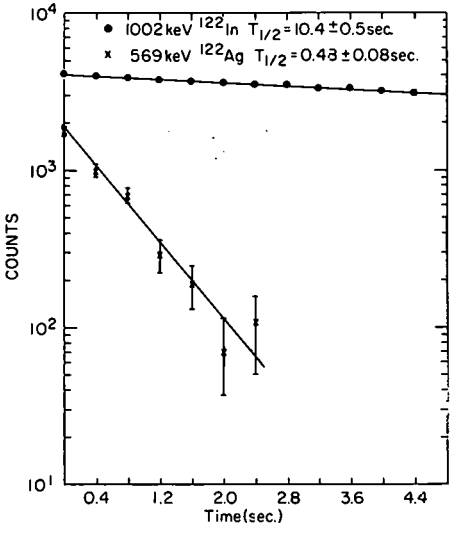

Figure 14. Decay curve for the decay of ^{122}Ag.

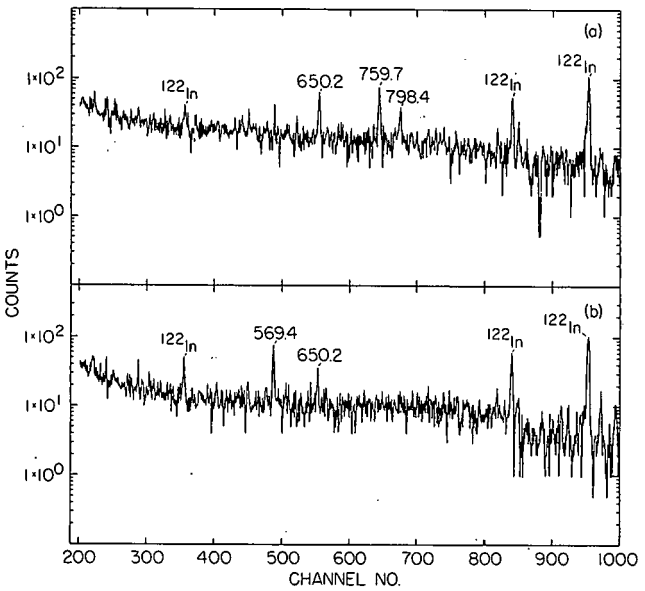

Figure 15. Gamma spectra in coincidence with the (a) 569- and (b) 760-keV γ rays from ^{122}Ag decay.

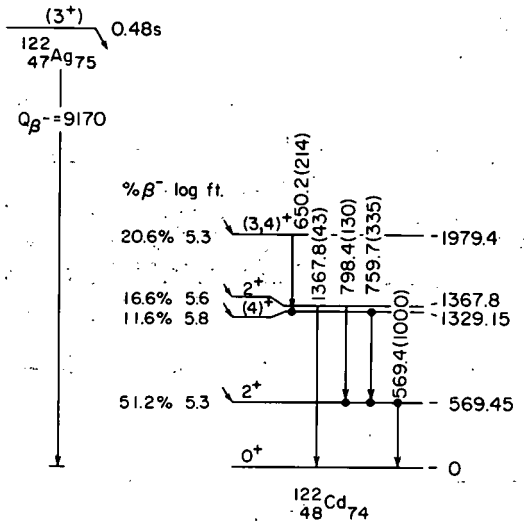

Figure 16. Decay scheme for ^{122}Ag.

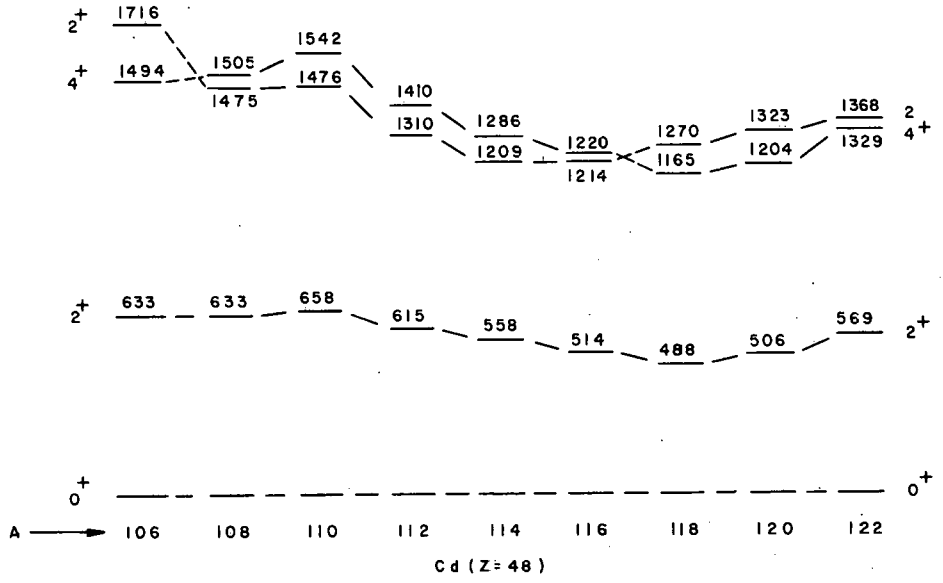

Figure 17. Systematics of low-lying levels in even-even Cd nuclei.

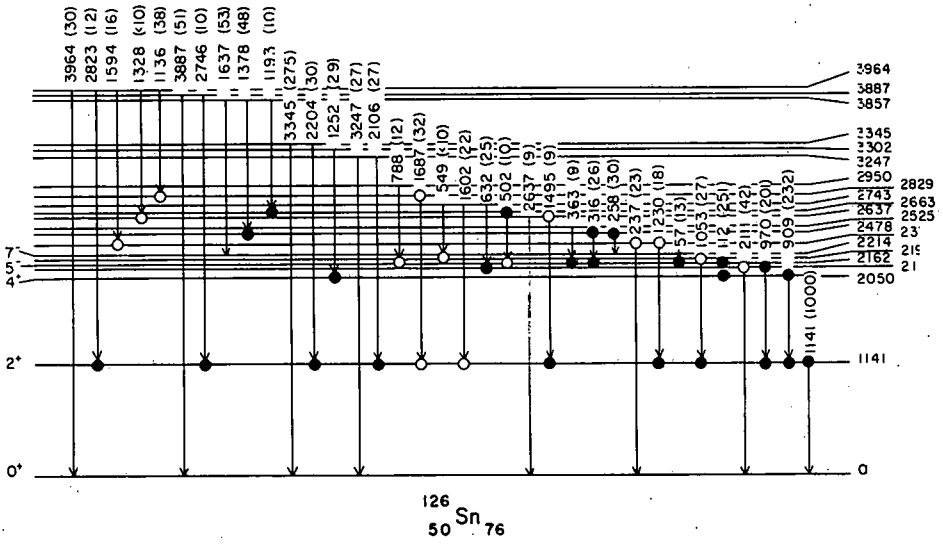

Figure 18. Level scheme for ^{126}Sn.

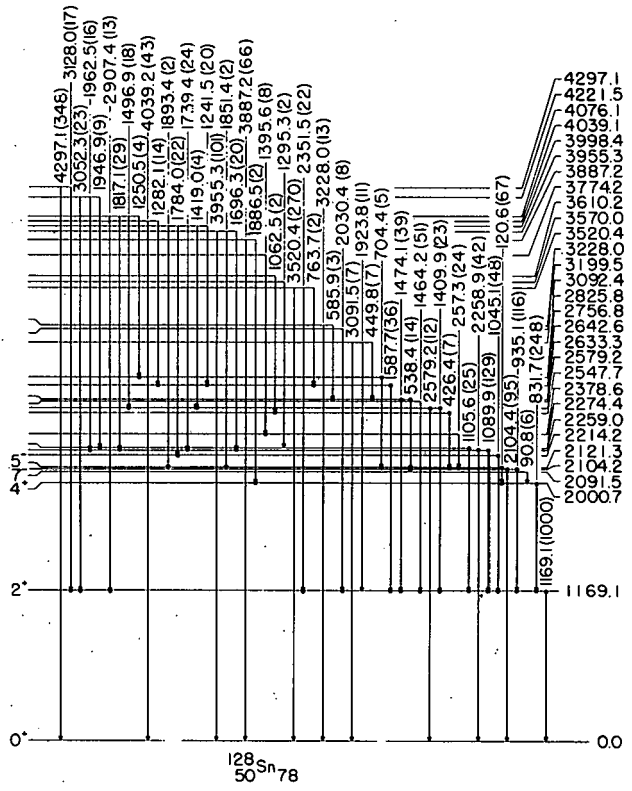

Figure 19. Level scheme for ^{128}Sn.

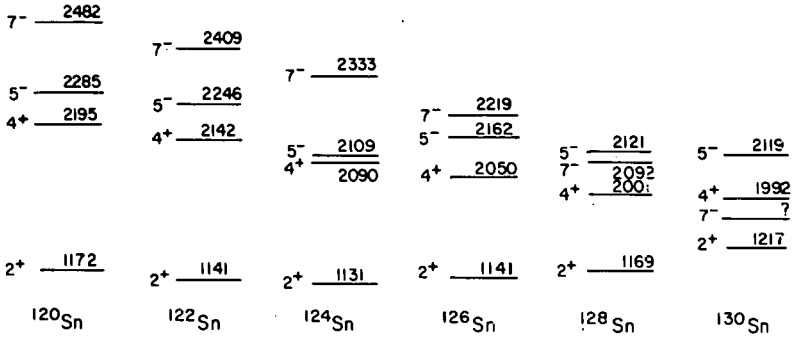

Figure 20. Systematics for neutron-rich even-even Sn nuclei. Levels from Ref. 14 except for A = 126 and 128 where our results are given.

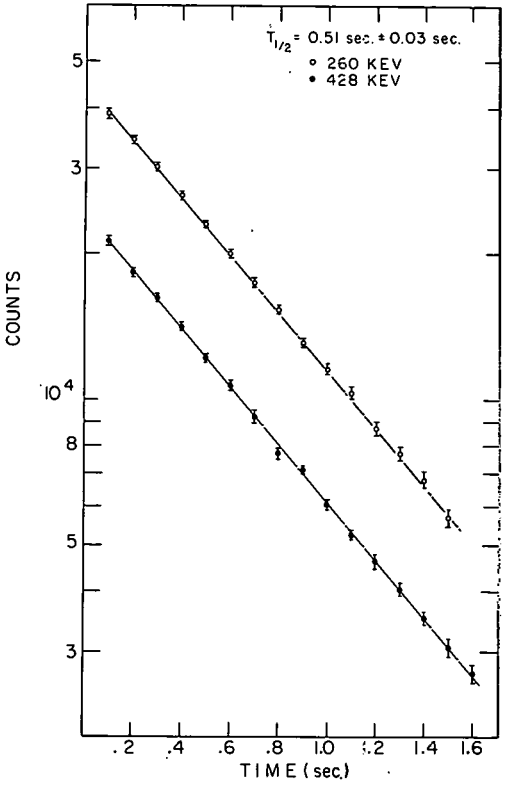

Figure 21. Decay curve for the decay of ^{126}Cd.

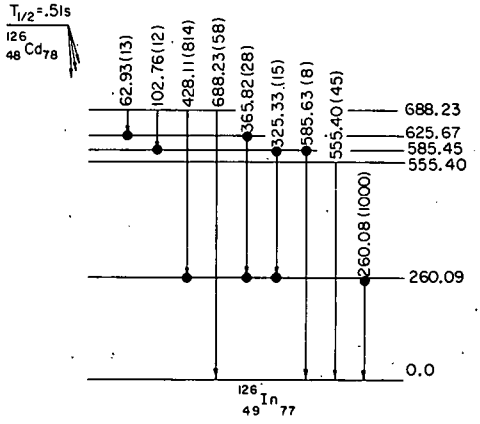

Figure 22. Decay scheme for ^{126}Cd.

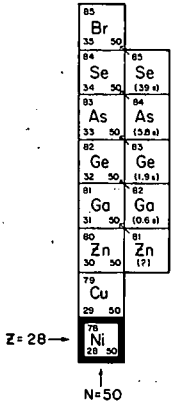

Figure 23. The N = 50 line on the nuclide chart above doubly-magic ^{78}Ni.

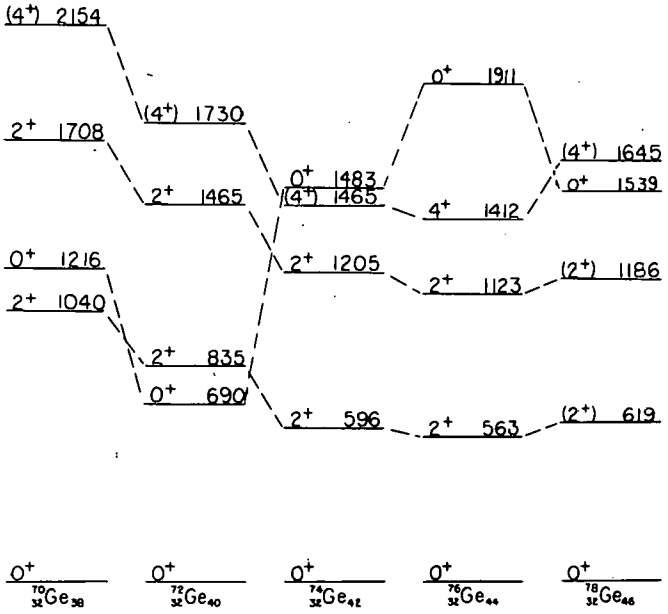

Figure 24. Systematics for even-even Ge nuclei.

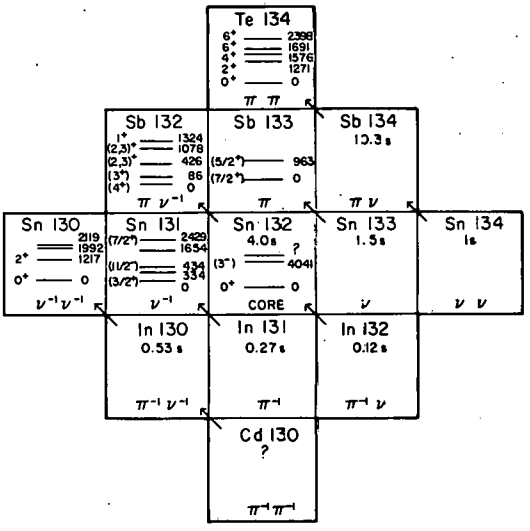

Figure 25. The nuclide chart near doubly-magic ^{132}Sn.

REALISTIC NUCLEAR SHELL THEORY AND THE DOUBLY-MAGIC ^{132}SN REGION

J. P. Vary

I. INTRODUCTION

As a prelude to a discussion of nuclear shell theory with a concentration on the ^{132}Sn region, I wish to outline a broader picture of the theoretical motivation and interest in results that are acquired with isotope separators. Several areas have already been discussed by other speakers at this workshop and I would just like to add a few more to that growing list.

Certainly one of the most exciting aspects of the results obtainable with isotope separators is their ability to open up entire new regions of the periodic table for theoretical study. Especially important are regions where one can possibly discover new collective phenomena. One could speculate, for example, the possibility of having strong proton-proton pairing and/or strong neutron-proton pairing. The latter is not realized in the conventional regions of the periodic table as far as I know.

We know also that the very unstable nuclei would provide a critical testing ground for our ability to make mass predictions.

Thirdly, one is very interested in the possibility of the results of isotope separators opening up other doubly-magic regions, specifically, that of ^{78}Ni, ^{100}Sn, as well as the one that will be described in this talk.

There is considerable theoretical interest in measurements of the moments of nuclear ground state and isomeric state density distributions as a function of neutron and proton number. Such measurements using tunable dye lasers were described in the talk by George Greenlees.[1]

Newest on my list is the topic of testing theories of statistical behavior or nuclear level densities. I learned in the talk given by Stan Prussin[2] of their very recent level density measurements through delayed

neutron spectra. I am particularly excited by the possibility of measuring level densities as a function of angular momentum, and I will relate this to some of our recent theoretical work later in this talk.

Let me now concentrate on my central theme, namely, realistic nuclear shell theory. A long standing goal of nuclear theory has been to derive the shell properties of nuclei from two fundamental inputs; nonrelativistic many-body quantum mechanics and a basic nucleon-nucleon interaction. We are willing to assume that only nucleon variables are necessary and that one can work with non-relativistic quantum mechanics to derive both a finite dynamical framework (many-body theory) and the proper associated Hamiltonian. This theoretical problem is of fundamental significance since it is based on what we would consider to be first principles.

II. REALISTIC NUCLEAR SHELL THEORY

I shall divide my remarks here into two sections. The first outlines the fundamental problem and the second presents a brief historical review.

A. The Fundamental Problem

In the interest of attempting to update the terminology of the realistic nuclear shell theory to incorporate language of wider understanding to many-body theorists, I would like to pose the shell model problem in the context of renormalization theory.

Basically nuclear shell theory encounters two infinites. The first is that of the infinite dimensional Hilbert space and the second is that of the singularity of realistic nucleon-nucleon interactions. Each may be treated by renormalization theory.

The solution to the first fundamental problem is given by renormalization theory in the form of the theory of effective operators. The early work of Bloch and Horowitz[3] and later updated by Brandow[4] gives the basic tools of this renormalization approach. We proceed in the following fashion. First we define a total Hamiltonian H

$$H = T + V = \sum_{\ell} t_{\ell} + \sum_{\ell<m} V_{\ell m} \qquad (1)$$

and we seek the full solutions

$$H \Psi_i = E_i \Psi_i \qquad i = 1, \ldots, \infty \qquad (2)$$

such that the E_i are the eigenenergies of the total Hamiltonian and the Ψ_i are the total nuclear wave functions.

The program of renormalization goes as follows: first we choose a suitable reference Hamiltonian H_0 whose solutions are known

$$H_0 = T + U = \sum_{\ell} t_{\ell} + \sum_{\ell} U_{\ell} \tag{3}$$

th

$$H_0 \Theta_i = \varepsilon_i \Theta_i \qquad i = 1, \ldots, \infty \tag{4}$$

then we choose a suitable d dimensional subspace such that, for the index $j = 1, \ldots, d$, we define a projector P onto that subspace,

$$P = \sum_{j=1}^{d} | \Theta_j \rangle \langle \Theta_j | \tag{5}$$

such that another projector Q is defined via

$$P + Q = 1 \tag{6}$$

We then solve for an effective Hamiltonian operating in the finite model space;

$$H_{eff} \Phi_j = E_j \Phi_j \qquad j = 1, \ldots, d \tag{7}$$

such that the finite wave function is the projection of the total wave function

$$\begin{aligned} \Phi_j &= P\Psi_i \qquad j = 1, \ldots, d \\ E_j &= E_i \qquad i \in 1, \ldots, \infty \end{aligned} \tag{8}$$

and the set of eigenvalues obtained are a subset of the infinite set of eigenvalues in the full problem. Note that it is not necessarily true that the nite model space problem obtain the d lowest eigenvalues of the full problem. The states which are actually obtained in the finite problem must correspond to d states in the total problem but these will, in general, be the d states whose overlap is greatest with the d model space states. In addition, note that the effective Hamiltonian is defined only to operate within the chosen d dimensional model space. That is,

$$H_{eff} \equiv P H_{eff} P \tag{9}$$

Furthermore it is convenient to write the total Hamiltonian now as comprised of our conveniently chosen H_0 and a residual piece call H_1;

$$H = (T + U) + (V - U)$$

$$= H_0 + H_1 \tag{10}$$

In the next stage of developing this problem it is worth noting that additional simplicity can be obtained by restricting the number of nucleon degrees of freedom that we have to consider. This is motivated by the knowledge that there is extra stability of certain configuration of nucleons. In particular we are referring to the stability of semi-magic and doubly-magic nuclei. This simplicity is achieved by formally partitioning the total number of nucleons into a set of core nucleons and a set of valence nucleons. Notationally:

$$\ell = \underbrace{1, \ldots, \ell_c}_{\ell_c \text{ core}} \quad \underbrace{\ell_c + 1, \ldots, A}_{\ell_v \text{ valence}} \tag{11}$$

where ℓ_c will represent the number of core nucleons and ℓ_v will represent the number of valence nucleons. We can then rewrite the formalism in terms of a "vacuum state" of ℓ_c core nucleons which we will call $|\Phi_0\rangle$ where:

$$|\Phi_0\rangle = a_1^\dagger \, a_2^\dagger \ldots a_{\ell_c}^\dagger \, |0\rangle \tag{12}$$

where we have invoked second quantized notation to relate our vacuum state to the absolute vacuum $|0\rangle$ by means of ℓ_c nucleon creation operators. Our vacuum state is the lowest unperturbed state of the system of ℓ_c nucleons and therefore satisfies:

$$H_0 \, |\Phi_0\rangle = \varepsilon_0 \, |\Phi_0\rangle \tag{13}$$

We divide the total projection operator Q into a series of components which are labelled by the number of particle-hole excitations of the core that are involved. That is,

$$Q = \sum_{\substack{m,n \\ (m-n=\ell_v)}} Q_{mp,nh} = Q_{\ell_v} + Q_{\ell_v+1,1} + Q_{\ell_v+2,2} + \ldots + Q_{A,\ell_c} \qquad (14)$$

where the double subscript indicates the number of nucleons outside the core and the number of holes in the core involved in the projection operation. By recasting the original problem into the particle-hole language we have provided a simpler representation for the possible model space states which are usually arranged in the order of their unperturbed energies ε_i. As a simple example, by an appropriate choice of the d states we could treat the situation of a single valence nucleon in one valence nucleon states, or we could expand the space to include two valence nucleon-one hole states along with one valence nucleon states, etc.

All of the above have been introduced to simply define the problem. The solution is given by the effective operator formalism of Bloch-Horowitz[3] and Brandow[4] and is called the linked cluster expansion (which, for completeness, is noted to contain folded diagrams - a technical feature of the series which will not be discussed further here):

$$H_{eff} = H_0 + \left\{ \sum_{k=0}^{\infty} H_1 \left(\frac{Q}{\varepsilon_0 - H_0} H_1 \right)^k \right\}_{\text{Linked, Folded}} \qquad (15)$$

where we can rewrite this simply as

$$H_{eff} \equiv H_0 + V_{eff} \qquad (16)$$

and V_{eff} is generally called the effective interaction and H_{eff} operates in a finite demensional subspace of the entire problem. We note we have obtained

a finite space operator by trading in the infinite dimensional Hilbert space for an infinite series which is hopefully well behaved and reasonably convergent. This formal mathematical problem itself deserves and has received considerable theoretical attention. It is of special utility for problems where the interaction V is reasonably weak. Such problems do occur, for example, in solid state and atomic physics. However, the nuclear situation is more complicated. There is another singularity as mentioned above: the infinite (or near-infinite) hard-core repulsion that is attributed to the realistic nucleon-nucleon interaction. (I should note that the terminology "realistic nuclear shell theory" is ascribed to those theoretical efforts that employ such singular nucleon-nucleon interactions. They are, for the most part, believed to be the ones that are realistic).

The solution of this problem is again handled by a renormalization approach called Brueckner-Bethe-Goldstone Theory.[4,5] The main goal is to imbed a renormalized interaction into the above formalism. This is accomplished as follows: First we divide the projection operator Q into two components, one having two valence nucleon coordinates and the other having all the remainder of the projection operator components. That is;

$$Q = Q_2 + \bar{Q} \tag{17}$$

from here one develops an effective two-particle interaction called the G matrix defined as follows

$$G = \sum_{k=0}^{\infty} H_1 \left(\frac{Q_2}{\epsilon_0 - H_0} H_1\right)^k \tag{18}$$

which is then imbedded in the first renormalization by means of the following linked folded diagram expansion.

$$V_{eff} = \left\{ \sum_{k=0}^{\infty} G \left(\frac{\bar{Q}}{\varepsilon_0 - H_0} G \right)^k \right\}_{\text{Linked, Folded}} \qquad (19)$$

This way the effective interaction operating in a finite model space has been expressed entirely in terms of the G matrix which is an interaction having well behaved two-particle matrix elements.

For the sake of drawing contact with conventional diagramatic pictures, we display the first and second order terms (neglecting exchange and self-energy diagrams) for the case where the effective interaction is operating between two-valence nucleons and where the wavey lines are used to represent the G-matrix.

$V_{eff} =$ 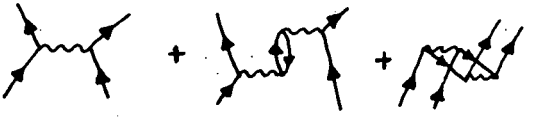 (20)

The second diagram is traditionally called the core-polarization diagram.

B. A Brief Historical Review of H_{eff}

I would like to briefly discuss some of the important developments that have occurred over the last 15 years in the derivation and application of this realistic nuclear shell theory. I shall not attempt to be exhaustive in this brief summary but the particular steps in the development chosen for emphasis those which will help understand the results described in the remainder of the talk as well as the concentration of the doubly-magic ^{132}Sn region.

During the period from 1962 to 1965 there were a number of initial efforts[6] to calculate the effective Hamiltonian to first order in the G-matrix. The primary characteristic of these results was the correct level ordering of the 0^+, 2^+ and 4^+ levels in even-even nuclei with two nucleons outside of a closed

core. Although there was qualitative agreement with experiment, the main deficiency of these earlier calculations was that failure to reproduce the amount of level spreading that had been observed experimentally.

Then during the period of 1966 to 1967 the work of Kuo and Brown[7] demonstrated that good agreement with the data could be obtained by including the second order diagrams as pictured above in Eq. 20. In addition, and perhaps of more fundamental significance was the fact that a convincing argument could be made for the importance of the core-polarization diagram in achieving a good physical picture of the valence-core interactions.

There followed a period of some euphoria within the nuclear community over the successes obtained in 1966 and 1967.

However, this era was brought to a dramatic end during the period from 1970 to 1972 when the efforts of Barrett and Kirson[8] demonstrated that using the same approximate techniques as those of Kuo and Brown, one finds that the third order terms of the effective Hamiltonian are of comparable magnitude to the second order terms. This was very disturbing to the theory community because this result demonstrated the possible nonconvergence of the effective Hamiltonian expansion which had been successful in describing data through second order. However, some theorists began to doubt the reliability of a number of approximations that were conventionally employed in all of these studies. So, at almost the same time, a number of efforts were in progress to examine the reliability of some of these individual approximations.

Then, in 1973, the strong intermediate-range components of the tensor force were shown[9] to cause the intermediate-state summations in higher order diagrams to be very slowly convergent. Thus, the previous calculations in second and third order which truncated at the lowest possible particle-hole

excitation energies were in error by substantial amounts. The conclusion reached at this stage was that all of the previous efforts through third order must be regarded with skepticism. It was now necessary to recalculate the effective Hamiltonian, avoiding as many of the approximations as possible, but especially, providing for a careful treatment of the effective tensor force. What I shall now describe are the more recent efforts that have followed this conclusion and have yielded encouraging results in both light and medium-mass nuclei.

During the period of 1975 and 1976, we were involved in extensive calculations of the effective Hamiltonian for nuclei from mass 110 to mass 238.[10] The central goal of these calculations, which were only performed through first order, was to put the effective Hamiltonian into a much larger dynamical framework including many valence nucleons in a very enlarged model space in order to treat, in a dynamical fashion, as many of the higher order diagrams as possible. Specifically, one invoked a large-scale mean-field approach which includes the possibility of treating strong pairing correlations as well as deformed field correlations in a fully self-consistent way. Both the calculation of the effective Hamiltonian and then the solutions of the mean-field equations were enormous undertakings and it was still necessary to make a couple convenience approximations which it would be desirable to remove in a future effort. A number of applications of this effective Hamiltonian to the nuclei in the rare-earth region[10] as well as those of the doubly-magic ^{132}Sn [11,12] and ^{208}Pb [13] regions have yielded encouraging results and will be described below. However, Since this approach had a couple of approximations and was only carried through first order, some results are inconclusive and will require additional effort in the future.

Within the last year, a complete first plus second order effective Hamiltonian has been obtained[14] for nuclei from mass 16 through mass 40. It now seems safe to say that this particular second order Hamiltonian will achieve nearly as much success in describing the properties of light nuclei as has been obtained with the Hamiltonian of Kuo and Brown. This is particularly satisfying since the new Hamiltonians have properly included all the effects of the tensor force through second order. In fact, there are some data which are better reproduced by the new Hamiltonians than by the previous Hamiltonians. Specifically, the binding energies of light nuclei are more accurately given with the new Hamiltonians.[15]

Finally, an initial effort to re-examine the third order part of the effective Hamiltonian has recently been completed[16] and shows that it is reasonable to conclude that, with the correct treatment of the tensor forces as well as the elimination of other approximations previously made, the third order diagrams will now be quite small compared to previous estimates.[8] Hence, there is solid encouragement now to believe that the program of realistic nuclear shell theory will eventually be successful in describing the properties of nuclei in that it will be a properly converging theory which accounts for experimental observations.

III. DOUBLY MAGIC ^{132}Sn REGION

Before proceeding to a description of this region we will discuss the vantages and limitations of doubly-magic regions of the periodic table.

The region around ^{16}O is characterized by the advantage of having a relatively small valence space which renders calculations considerably more comfortable, however, this region is plagued by the phenomena of "intruder states". These are states whose main parentage is outside the model space but which are positioned between or among states whose dominant configurations are in the model space. This leads to convergence difficulties in the order-by-order expansion of the effective Hamiltonian. The amount of these convergence difficulties depends on the degree of mixing between the intruder states and the model states. In the case of the ^{16}O region the degree of mixing is very high.

Another popular area for shell-model studies is in the region of ^{40}Ca. We now know that the ^{40}Ca core is very soft against deformations. This means that our core is not a very stable one and, in particular, it also will lead to intruder states which are, in this case, coherent superpositions of particle-hole states. Here again, we can expect difficulties in the order-by-order expansion of the effective Hamiltonian.

The ^{208}Pb region is known to be an excellent shell-model region for both ticle and hole systems. There is extensive experimental and phenomenological evidence that the systems are very simply characterized by a few valence degrees of freedom outside of a very rigid core. The main limitation here seems to be the very sizeable nature of the model spaces that are involved. Traditionally one attempts to include a whole major shell of particles

of the appropriate type being considered. Thus, if one studies systems of neutrons and protons outside of ^{208}Pb the model spaces are indeed very large. This, in itself, inhibits the theoretical efforts.

The main conclusion is that we need more than just one good vacuum region to test nuclear shell theory. This is motivation enough for extensive theoretical and experimental investigations of the region around ^{132}Sn.

There are two unique advantages to the ^{132}Sn region which I would like to describe.

The first unique advantage is its proximity to the neutron superfluid transition in the lighter Sn isotopes. This implies the possibility of addressing a major fundamental question of nuclear shell theory: to what extent can this unique Fermi-surface phenomenon (the superfluid transition) be accurately predicted by realistic microscopic theory? This question is of fundamental importance since we know by experience that phase transitions provide a most sensitive test of a microscopic theory.

The second unique advantage is that ^{132}Sn will provide the core for a large-scale microscopic approach to all nuclei up to ^{208}Pb. In this way, we will be able to address another fundamental question: can a single nuclear Hamiltonian, operating in the model space between these two nuclei, predict the dominant shell model behavior near shell closure as well as the strong collective phenomenon of the rare-earth region? We note that the initial results are very encouraging in this direction and we will outline some of those results below.

IV. RESULTS

The Ground State Properties of ^{132}Sn from the Density Dependent Hartree-Fock Approach.

We follow traditional discussions of doubly-magic nuclei by first describing the single-particle properties (single-particle level spacings and level orderings) and also the one-body density distributions. In fact, when such level arrangements are known, one can make statements about the validity of the doubly-magic characterization of a given nucleus. In the case of ^{132}Sn experimental information is nearly totally lacking in this aspect. Thus, one cannot display the level spacings of the particles and holes around ^{132}Sn and draw conclusions about shell closure on that basis. However, there is much indirect evidence that supports the contention that it is a very good doubly magic nucleus.

The best available way to predict the single-particle level orderings is to use the Skyrme Hamiltonian in the density-dependent Hartree-Fock approach.[17] Figure 1 displays the results of such a calculation for the neutron and proton single-particle levels. The main conclusion to be drawn is that all the parameterizations of the Skyrme Hamiltonian yield a pronounced prediction for large shell gaps at ^{132}Sn. In all cases, the spacing between the last occupied neutron orbital and the first unoccupied neutron orbital is of the order of MeV as is the spacing between the last occupied proton orbital and the first unoccupied proton orbital.

On the other hand from applications to other regions[17] and from the fluctuations in the results here one knows that the exact level orderings are not well predicted by this theoretical approach. There is a large uncertainty as to the detailed spacings between orbitals within the major

shells involved. This irresolution is unfortunate because such information is necessary in order to proceed with shell model studies in this region. Of course the Skyrme Hamiltonian is a phenomenological Hamiltonian whose parameters were adjusted to fit the properties of nuclear matter and certain doubly-magic nuclei whose properties were known. The fluctuations indicated in figure 1 are those that result from the imprecise pinning down of those parameters by the known doubly-magic nuclei and from the inadequacies of the phenomenological Hamiltonian. Thus, we can summarize Fig. 1 by saying that, based on the best phenomenological approach at hand, and the knowledge of other doubly-magic nuclei, this is the best we can predict for the properties of the single-particle spectra of ^{132}Sn. On this basis it is doubly magic but precise level orderings are unknown.

Within the same approach one obtains the single-particle density distributions for ^{132}Sn, and these are displayed in Figure 2. It is safe to say that these single-particle distributions will not be measured in the conventional sense by elastic electron scattering since such experiments have rather low cross sections and require stable targets. We present these theoretical results for the purpose of completeness.

B. A Single Theoretical Hamiltonian for All Nuclei for Doubly-Magic ^{132}Sn to Doubly-Magic ^{208}Pb.

The first attempt in this direction will be labelled "The Brookhaven Hamiltonian" since it was generated at Brookhaven. Insofar as it is a first approach it has a number of convenience approximations which we feel can be eliminated in the second generation which will be described below. The basic effective Hamiltonian is calculated to first order and is given by

$$V_{eff} = G = \sum_{k=0}^{\infty} V \left(\frac{Q_2}{\varepsilon_0 - H_0} V\right)^k \qquad (21)$$

:re V is chosen to be the Reid Soft Core porential,[19] and H_0 is the harmonic oscillator Hamiltonian. The valence space was chosen to comprise 52 proton orbitals ($2s_{1/2}$, $1d_{5/2}$, $1d_{3/2}$, $0g_{9/2}$, $0g_{7/2}$, $0h_{11/2}$, and $0h_{9/2}$) and 66 neutron orbitals ($2p_{3/2}$, $2p_{1/2}$, $1f_{7/2}$, $1f_{5/2}$, $0h_{11/2}$, $0h_{9/2}$, $1g_{9/2}$, $0i_{13/2}$). The model space was not entirely appropriate to a ^{132}Sn core since it was chosen to be sufficiently large for meaningful Hartree-Fock calculations in the rare-earth region.

The main tests and predictions of the Brookhaven Hamiltonian (described in references 10 through 13) range from treatment of ground state and high-spin properties of rare-earth nuclei, to shell-model properties near ^{132}Sn, and to shell-model properties of nuclei near ^{208}Pb.

In order to treat nuclei near shell closure it is necessary to remember that the effects of core polarization have not yet been calculated for this Hamiltonian. Therefore it is reasonable to adopt some intermediate way of handling these core-polarization effects and we chose to add phenomenological terms to the realistic microscopic Hamiltonian corresponding to a pairing force and a quadrupole force:

$$H'_{eff} = H_{eff} + \alpha P_0 + \beta P_2 \qquad (22)$$

: adjustable strength constants α and β are determined by fitting only one nucleus, the one which has two valence particles outside of the closed core. Then the Hamiltonian, H'_{eff}, is kept fixed for treatment of all other nuclei in the region of the doubly-magic core. In addition to handling core-polarization effects, the adjustable terms could handle, in principle, some truncation effects and corrections to the imprecisely known single-particle energies. It has

been found that the additive terms amount to less than 10% of the total Hamiltonian, giving reassurance of the validity of this semirealistic procedure.

One purpose for showing these results is to motivate a second generation Hamiltonian, "The Ames Hamiltonian" where the single-particle Hamiltonian is chosen to be a realistic, i.e., Woods-Saxon or Hartree-Fock single-particle potential.

We now describe the results[10] for the single-particle properties of nuclei from Sn through Pb in the mean-field approach where the unadjusted Brookhaven Hamiltonian is employed. These results are displayed in figures 3, 4 and 5.

The neutron single-particle energies with respect to neutron number near doubly-magic ^{132}Sn and ^{208}Pb, are shown in Fig. 3 as calculated in the spherical Hartree-Fock approximation. In the upper part of Fig. 3 one finds satisfying agreement in terms of level orderings and level spacings for neutron single-hole orbitals near ^{208}Pb. In addition, the Hamiltonian correctly predicts the shell closure at N = 126.

In the bottom portion of Fig. 3 the neutron magic gap at N = 82 is not quite so well reproduced. However, this is felt to be an indication of one of the inadequacies of this current first-order calculation and is expected to be improved in calculations with the Ames Hamiltonian.

The proton single-particle energies a function of neutron number are displayed in Fig. 4 for this spherical Hartree-Fock calculation. An interesting prediction emerges with the neutron hole dependence of the proton magic gap at Z = 82. One finds a disappearance of the gap at around mass 200 which is consistent with the onset of strong collective states in the low-lying spectra of nuclei in this vicinity. For the proton magic gap at Z = 50 (lower portion of Fig. 4) there seems to be a well-developed spacing in the prediction. The

detailed location of the crossing of the $d_{5/2}$ and the $g_{7/2}$ orbital in the Sn topes is not so well reproduced. However, this feature is very sensitive minute changes in the Hamiltonian.

In Fig. 5 one sees the neutron single-particle spacings as a function of the proton number for nuclei above the doubly-magic cores. There is not a great deal of mass dependence for these quantities.

The conclusion from the above spherical Hartree-Fock results with the Brookhaven Hamiltonian is that there is quite a bit of structure in both the theory and the experiment and that the first attempt, which does not include Hamiltonian adjustments to take care of core polarization, is rather encouraging.

I would now like to move on to discuss the applications of the Brookhaven Hamiltonian with the phenomenological pairing and quadrupole terms added. An initial effort[13] showed that this procedure could be quite successful to improve the detailed shell model predictions of nuclei in the vicinity of ^{208}Pb. In particular, the multi-neutron hole states in the ^{208}Pb core were satisfactorily treated with such a semirealistic approach.

More recently Baldridge and Dalton[11, 12] have studied nuclei consisting of 2 through 9 valence protons outside the doubly-magic ^{132}Sn core. A detailed analysis of the phenomenological adjustments shows that the corrections are ut 7% of the total Hamiltonian when a 2 orbital model space, consisting of ... $g_{7/2}$ and $d_{5/2}$ orbitals, is chosen and the corrections are reduced to about 3% of the total Hamiltonian when a model space of 5 single-particle orbitals is chosen. For nuclei consisting of 5 or more valence protons, it is necessary to employ the smaller model space in the shell model diagonalizations.

In order to obtain the energies of the single-particle valence orbitals, it is necessary to make some extrapolations from the data. These extrapolations

are depicted in Fig. 6 by the dashed lines. It is expected that the errors that might be incurred by these extrapolations could at least be partially accomodated by the two adjustable constant α and β in the modified effective Hamiltonian. As mentioned above, these two constants are fixed by the spectra of the two valence proton nucleus, ^{134}Te. With the Hamiltonian then fixed, the nuclei up to ^{141}Pr are calculated. An interesting study is made of the detailed behavior of the lowest $7/2^+$ and $5/2^+$ levels as a function of proton number throughout these nuclei. Figure 7 depicts the $5/2^+$ state (solid dots) with respect to the $7/2^+$ ground state and compares the $5/2^+$ state with the data (open circles). This can be considered to be a rather striking and spectacular agreement of the semirealistic approach with available data.

Although I have attempted to stress the broad range of results that can be obtained within the realistic nuclear shell theory, it is useful to examine one spectrum for the sake of an overview. The theoretical spectrum of ^{137}Cs shown in Fig. 8 is in satisfactory overall agreement with the available experimental information. The column labelled "Western et al., represents data taken about a year and a half ago at TRISTAN.

C. Level Densities of Theoretical Hamiltonians Through Spectral Distribution Methods.

In view of the discussion of the delayed neutron results presented by Stan Prussin,[2] I would like to expand the discussion of the results from these realistic Hamiltonians to include predictions of shell-model level-density distributions obtained with spectral distribution methods. I feel that we are moving into a new area where it may be possible to test some of the more global features of our Hamiltonians with this type of data which cannot be adequately tested through detailed comparisons of a few levels.

Spectral distribution methods have been advanced in the last three years to the point where many average properties of nuclei such as level densities, in-cutoff factors and average electromagnetic transition strengths can be calculated directly from the Hamiltonian. To perform such calculations a large configuration moment code has been jointly developed by the Ames Laboratory and Lawrence Livermore Laboratory. Using this configuration code one can calculate the level densities separately for both parties, all spins and all isobaric spins.

Fig. 9 shows the shell-model prediction[12] of the level densities for the J = 6 levels in ^{136}Xe with a large energy bin of 1.5 MeV. Fig. 9 also shows the Gaussian calculated by the spectral distribution methods directly from the Hamiltonian. This demonstrates good agreement between large energy bin shell-model results and spectral distribution methods using the lowest two moments.

A remarkable change occurs when one turns up the energy resolution on the shell-model results as shown in Fig. 10: there is a significant clustering of levels. Not only are spectral distribution methods now refined sufficiently[20] to calculate such complicated features but the experiments are yielding data[2] that show these features. This is particularly exciting since a spectrum with this much detail offers a more challenging test to the theory than a single Gaussian. Furthermore, for nuclei with many valence degrees of freedom the theoretical predictions can only be obtained with these recently developed methods. Since the delayed neutron spectra can be obtained with the TRISTAN separator, it would be of particular fundamental interest to mount experimental programs in this direction once TRISTAN is operational at Brookhaven.

The fundamental aspect of such results remains to be elluciated further. For example, to what extent do the locations and widths of these clusters shown in Fig. 10, change with changes in the microscopic Hamiltonian? Studies which should answer this question are in progress in Ames.

To conclude this section I would like to emphasize that the results shown for the ^{132}Sn region, taken in conjunction with the other regions, are very exciting and indicate some of the possibilities for fundamental progress in microscopic shell theory that can be made with additional data to fill out these pictures.

I am grateful to R. Belehrad of Iowa State University for performing a number of the calculations presented here. This work supported by the U. S. Department of Energy, Division of Basic Energy Sciences.

References

1. G. Greenlees, invited talk - this workshop.

2. S. Prussin, invited talk - this workshop.

3. C. Bloch and J. Horwitz, Nucl, Phys. 8, 91 (1958).

4. B. H. Brandow, Rev. Mod. Phys. 39, 771 (1967).

5. K. A. Brueckner, Phys. Rev. 97, 1353 (1955).

6. J. F. Dawson, I. Talmi and J. D. Walecka, Ann. Phys. (N.Y.) 18, 339 (1962); S. Kahana, Nucl. Phys. 31, 315 (1962); A. Kallio and K. Kolltveit, ibid. 53, 87 (1964); A. D. Mackellar and R. L. Becker, Phys. Lett. 18, 308 (1965); S. Kahana and E. Tomusiak, Nucl Phys. 71, 402 (1965); T. T. S. Kuo and G. E. Brown, Phys. Lett. 18, 54 (1965).

7. T. T. S. Kuo and G. E. Brown, Nucl. Phys. 85, 40 (1966); T. T. S. Kuo, Nucl. Phys. A103, 71 (1967).

8. B. R. Barrett and M. W. Kirson, Nucl. Phys. A148, 145 (1970); A196, 638 (1972); M. W. Kirson, Ann. Phys. (N.Y.) 66, 624 (1971).

9. J. P. Vary, P. U. Sauer, and C. W. Wong, Phys. Rev. C 7, 1776 (1973).

10. A. L. Goodman, J. P. Vary and R. A. Sorensen, Phys. Rev. C 13, 1674 (1976); A. L. Goodman and J. P. Vary, Phys. Rev. Lett. 35, 504 (1975).

11. W. J. Baldridge, Iowa State University preprint, to be published.

12. W. J. Baldridge and B. J. Dalton, Iowa State University preprint, to be published.

13. W. J. Baldridge and J. P. Vary, Phys. Rev. C 14, 2246 (1976).

14. J. P. Vary and S. N. Yang, Phys. Rev. C 15, 1545 (1977).

15. B. J. Dalton, J. P. Vary and W. J. Baldridge, Phys. Rev. Lett. 38, 1348 (1977).

16. M. S. Sandel, R. J. McCarthy, B. R. Barrett and J. P. Vary, to be published.

17. D. Vautherin and D. M. Brink, Phys. Rev. C 5, 626 (1972).

18. R. H. Belehrad and J. P. Vary, to be published.

19. R. V. Reid, Ann. Phys. (N.Y.) 50, 411 (1968).

20. B. J. Dalton, private communication.

21. J. W. Negele and D. Vautherin, Phys. Rev. C 11, 1031 (1975).

22. R. L. Bunting, Nucl. Data Sheets 15, 335 (1975).

23. W. R. Western, John C. Hill, W. L. Talbert, Jr., and W. C. Schick, Jr., Phys. Rev. C 15, 1024 (1977).

24. B. H. Wildenthal, private communication to K. Heyde and M. Waroquier, Nucl. Phys. A 167, 545 (1971).

25. N. Freed and W. Miles, Nucl. Phys. A 158, 230 (1970).

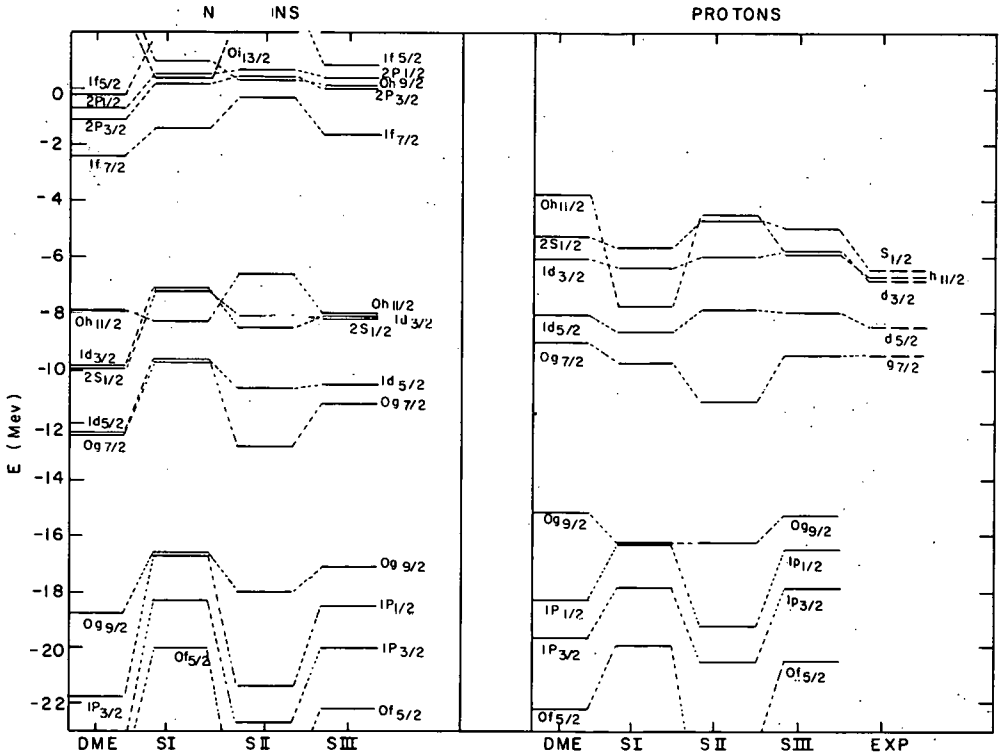

Figure 1. Neutron and proton single-particle orbitals for ^{132}Sn calculated in the density-dependent Hartree-Fock approximation.[17] The columns SI, SII and SIII refer to different parameter sets for the Skyrme Hamiltonian while the column labeled DME refers to Density Matrix Expansion techniques of Negele and Vautherin.[21]

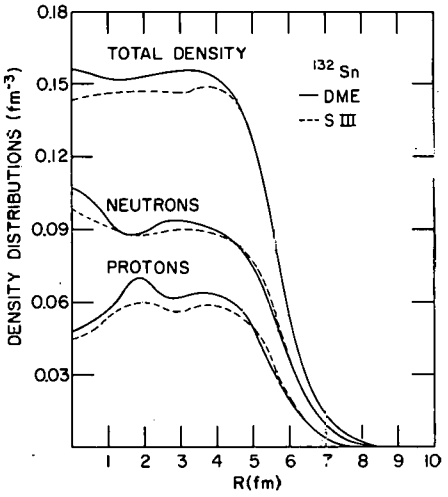

Figure 2. Coordinate space density distributions of ^{132}Sn as calculated in the density-dependent Hartree-Fock approximation with the Density Matrix Expansion[21] (DME) and Skyrme-III[17] (SIII) parametrizations of the Hamiltonian.

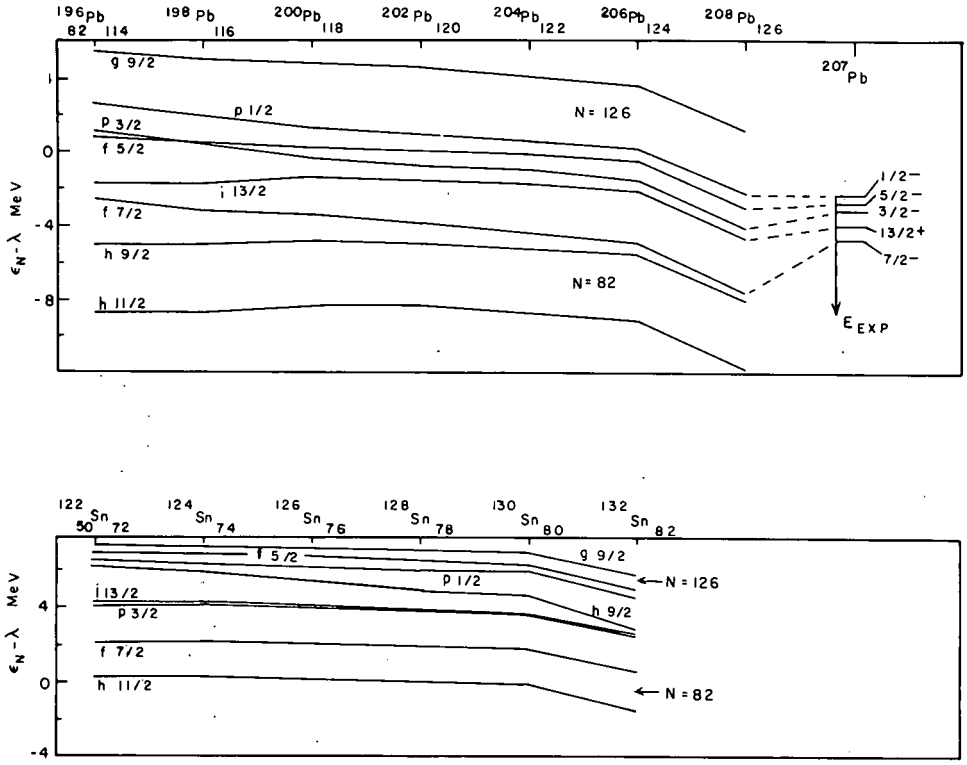

Figure 3. Hartree-Fock-Bogoliubov (HFB) neutron single-particle energies $\epsilon_n-\lambda$ relative to the Fermi energy. The upper part of the figure is for N and Z values for Pb nuclei while the lower part is for Sn. The experimental ^{207}Pb levels are also shown (inverted since this is a one neutron hole nucleus) for comparison.

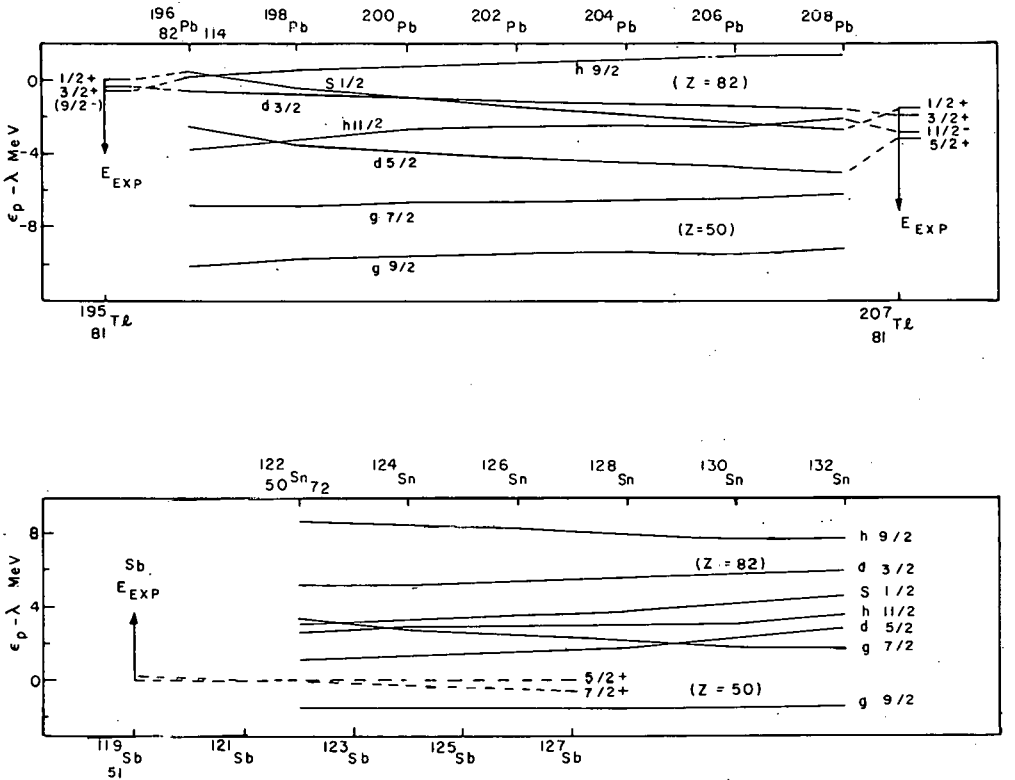

Figure 4. HFB proton single-particle energies for Pb and Sn nuclei. Also shown are the experimental spectra for $^{195}_{81}Tl$ and $^{207}_{81}Tl$ (inverted) and for a sequence of odd mass $^{}_{51}Sb$ nuclei.

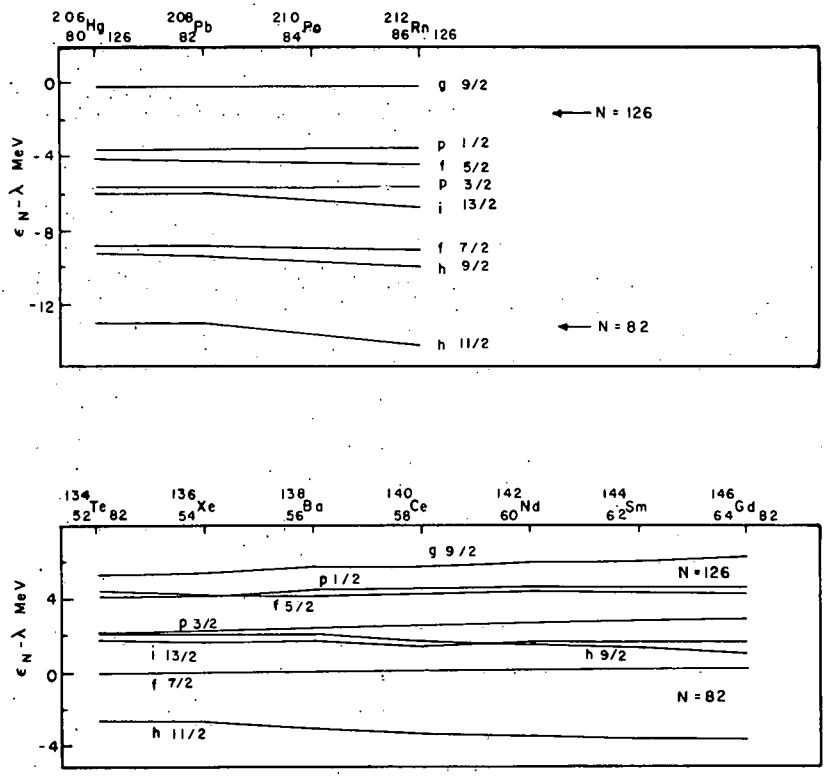

Figure 5. HFB neutron single-particle energies for N = 126 nuclei in the top figure and N = 82 nuclei below.

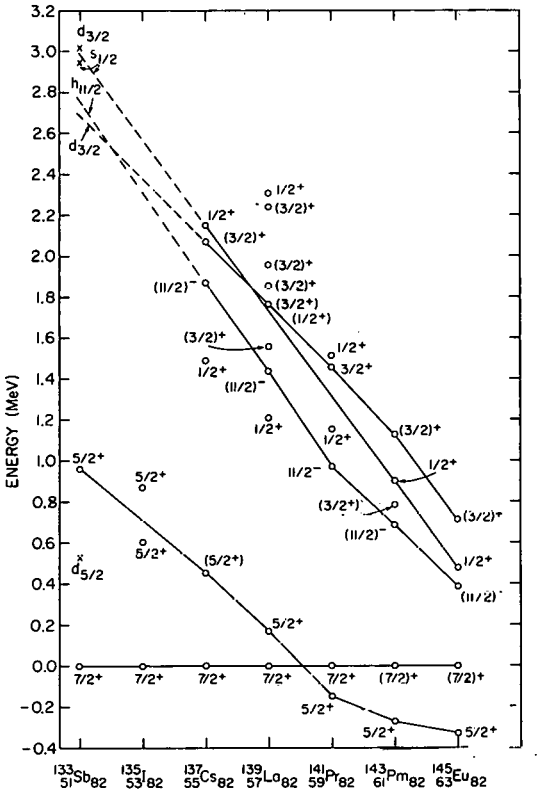

Figure 6. Extrapolation (dashed line) of experimental (circles) single proton energies. Low-lying levels of nuclei having N = 82 and odd Z from 51 to 63 are used to estimate the higher single proton energies.

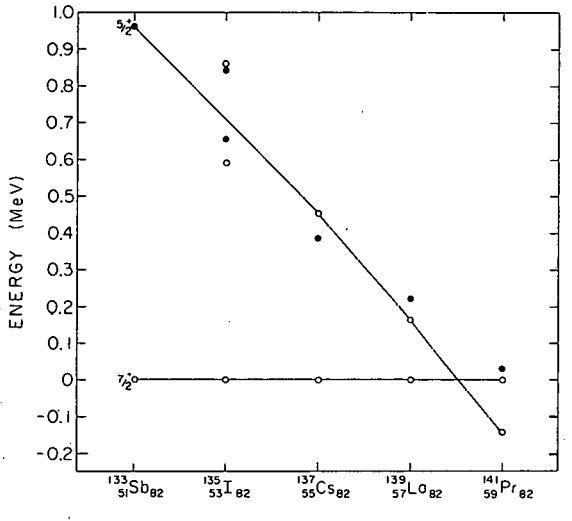

Figure 7. Systematics of positions of $5/2^+$ levels with respect to lowest $7/2^+$ levels. The open and solid circles show, respectively, the experimental and shell model excitations of lowest $5/2^+$ levels with respect to the lowest $7/2^+$ level. Experimentally observed systematics are well reproduced by the shell mo although inversion at nine protons is not quite icted.

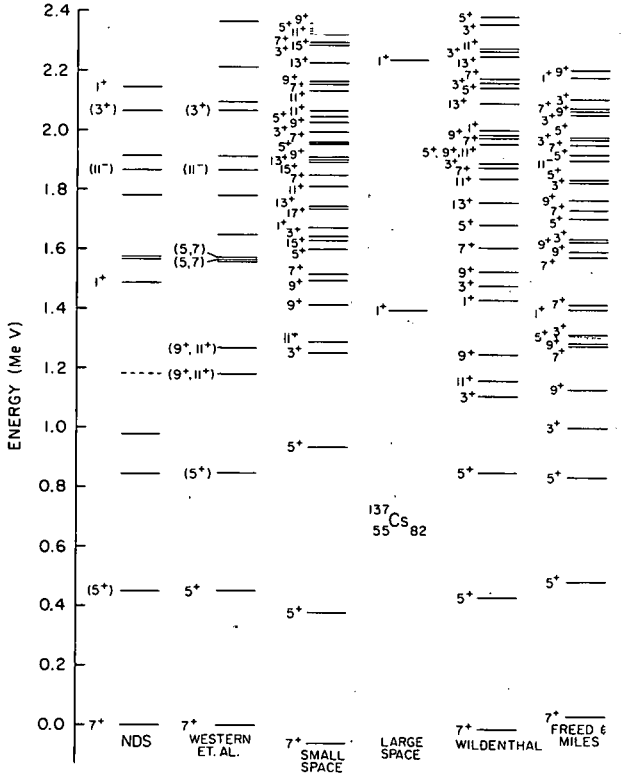

Figure 8. Experimental and theoretical spectra for ^{137}Cs. NDS[22] and Western et al.[23] are experiment. Small and large space columns are results of this study. Wildenthal[24] is a shell model study using the Surface Delta Interaction. Freed and Miles[25] is a quasiparticle Tamm-Dancoff approximation calculation. All levels are labelled by 2J.

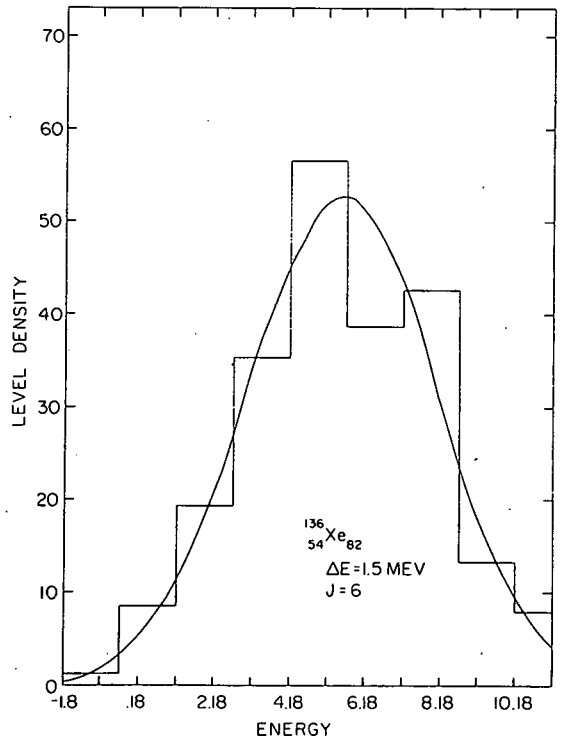

Figure 9. Comparison of Gaussian level density calculated via moment methods with histogram (interval 1.5MeV) from exact shell-model diagonalization for ^{136}Xe, J = 6 levels. Both calculations were made in the ($0g_{7/2}$, $1d_{5/2}$, $0h_{11/2}$, $1d_{3/2}$, $2s_{1/2}$) space.

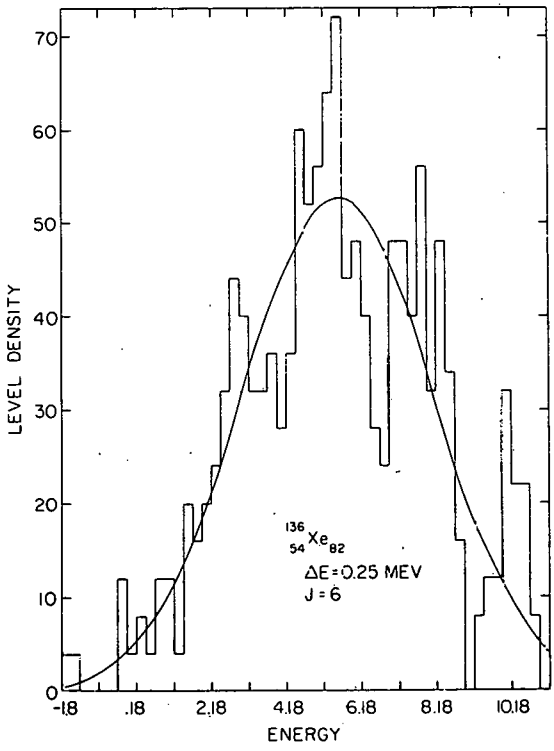

Figure 10. Comparison of statistical level density with histogram from exact shell model spectrum for ^{136}De J = 6. The histogram interval is .25MeV. Both calculations were made in the ($0g_{7/2}$, $1d_{5/2}$, $0h_{11/2}$, $1d_{3/2}$, $2s_{1/2}$) space.

Talk to be Presented to BNL - ISOL Workshop

October 31, 1977

Thermochromatographic Separations On-Line

John M. D'Auria
Department of Chemistry
Simon Fraser University
Burnaby, B.C. V5A 1S6
Canada

On-line mass separators are quite useful and valuable scientific systems. However they do have certain disadvantages or limitations; namely,

1. relatively high installation and maintenance costs,
2. a high degree of complexity in their operation,
3. at present only about 25 elements are available,
4. at reactors, only provide A identification.

There are alternate methods for providing A and/or Z selectivity and identification which can complement the above systems; these include,

1. fast wet chemical separations,[1,2]
2. gas jet recoil transport system with A selectivity, e.g., RAMA,[3] Maggie,[4]
3. gas jet recoil transport system with Z selectivity,
   i. fast "wet" chemistry, e.g., SISAK,[5]
   ii. on-line gas phase thermochromatographic separation systems.

The purpose of this paper is to discuss this latter

technique, namely fast chemical separations with a gas phase thermochromatographic system. Recent studies performed elsewhere will be reviewed and experiences gained at SFU in recent initial attempts to operate similar systems will be mentioned.

The application of gas phase thermochromatographic systems to separation of radioactive reaction products is relatively recent and references (2, 6-17) in reasonably available journals are indicated for your information. The general usefulness of this technique for the study of short-lived radioactive species is well demonstrated by the recent studies of Trautmann (ref. 15), Trautmann and Herrmann (ref. 2), Bächmann, et al. (ref. 6), and Matschoss and Bächmann (ref. 14), and I will discuss these in more detail.

A pressure-driven (or without pump) gas jet recoil transport system can be used to bring radioactive nuclides to a chemical reaction chamber (see, for example, figure 1 taken from ref. 2). These activities can be fission products from ^{252}Cf, products from neutron-induced fission of uranium in a reactor, or indeed products from any accelerator beam reaction. The carrier gases used by Trautmann and co-workers for fission product transport were ethylene mixed with nitrogen, or just ethane At SFU a similar cell utilized only ethylene but not without difficulty.[16] The chemical reaction cell is heated to about 400°C (at SFU using Nichrome wire wrapping) to break up the clusters which carry the activities over long distances. Glass frits are positioned on both sides of this chamber to contain

the clusters and prolong the reaction time. In general for most in-stream gas thermochromatographic separations, halides are formed and Trautmann fed a Br_2/N_2 gas mixture into the reaction chamber to form metallic bromides of the fission products. The outlet of the reaction chamber is connected to a quartz condenser tube in which a negative thermal gradient is established. An oven can be used to heat air entering the outer jacket of the condenser tube for maintaining this thermal gradient. The exit of the condenser is connected to a charcoal trap, a liquid nitrogen cold trap and then into a small pump, e.g., water aspirator pumping system, for gas exhaust. The distribution of fission products along the condenser and in the traps reported by Trautmann and Herrmann[2] from thermal neutron induced fission of uranium are presented in figure 1. The bromides of the alkali, alkaline and lanthanide elements as well as those of Y, Pd and Ag are non-volatile and stay in the cell. Other bromides are distributed along the tube as indicated while some of the very volatile substances go into the trap. Broad separation bands were observed but these apparently can be reduced in width by using glass beads in the inner tube. A delay time between production and deposition is reported to be about 4 sec while activities with half-lives as short as 1.7 sec were studied.

A cell, similar to the one shown in figure 1 was constructed at relatively low cost and tested at Simon Fraser University.[16] Fission products from a thinly covered (50 $\mu g/cm^2$

Au foil) ^{252}Cf source (5 μC) were transported through a 4 mm diameter tube over a one meter distance into the chemical reaction cell. Use of pure ethylene as the carrier gas while successfully transporting radioactivity, did introduce complications as the combination of ethylene, Br_2 gas, trace amounts of air and high temperatures lead to unwanted chemical compounds and a high degree of carbonation. The use of the ethylene/N_2 gas mixture or ethane only, now seems a more appropriate choice for successful operation. Nevertheless activities were deposited as a function of the thermal gradient in the condenser tube, although at levels too low for positive Z identification due to inefficient transport and insufficient source strength.

The advantages and drawbacks of such Z separators can be summarized as follows:

Advantages

1. can provide fast (~ seconds), continuous, on-line chemical separation of specific elements in a nuclear reaction produced mixture of many radioactive nuclides;
2. has been used after a gas jet system or (as will be mentioned later) an electromagnetic mass separator to provide Z identification.

Drawbacks

1. single step separation scheme yields broad, overlapping elemental deposition zones;
2. slow, but noticeable drift in deposition occurs towards lower temperatures with time (~ hours);

3. gas phase inorganic chemistry especially when dealing with microscopic amounts not well understood.

Bächmann and co-workers[6,10,11,14] have reported a different approach and have had some success in overcoming these drawbacks. They have used chlorides and oxychlorides, rather than bromides along with, as needed, a second reactive gas. More importantly, they recommend coating of the inner tube of the condenser with different chemical compounds (see figure 2 taken from ref. 6). The different metallic chlorides react at different temperatures with the different inner surface coatings. Improved elemental separation is obtained. They also recommend that the drift problem can be overcome by substituting a sharp-step decrease to lower temperatures rather than a gradually decreasing thermal gradient.

A further modification is the use of a sample changer (see fig. 3 of ref. 6) which allows standard spectroscopy studies. A combined multi-step separation scheme optimizing various parameters as reaction cell temperature (up to 900°C), wall coatings, additional reactive gases, along with this sample changer can produce clean, elemental separation within seconds. Activities with half-lives of the order of 3 seconds were studied in this manner.[14]

Finally such thermochromatographic separation systems have been adopted to work with the mass separator at Osiris.[13] The separated ion beam is deposited onto a heated filament of a thermo-separator. Pure samples of such elements as Zn, Ge, Br,

Kr, Cd, I, and Xe in appropriate chemical form can be collected on a catcher in front of a detector by correct adjustment of the thermal gradient along a heated quartz tube. In this manner A and Z selectivity can be achieved and results are reported for new, neutron-rich Zn and Cd activities.[13)]

In summary, this short review has been intended to demonstrate the general usefulness and applicability along with some of the drawbacks of this relatively new technique of performing fast chemical separations. With further understanding of the gas phase chemistry involved especially when dealing with microscopic quantities, it could become a very useful, inexpensive tool for performing nuclear spectroscopy studies of nuclides far from beta stability.

References

1. G. Herrmann and H.O. Denschlag, Ann. Rev. Nucl. Sci. 19 (1969) 1-32.
2. N. Trautmann and G. Herrmann, Jour. Radioanal. Chem. 32 (1976) 533-548.
3. J.M. Nitschke, Proc. 2nd Int. Conf. on Nuclides Far From Stability, Leysin, Switzerland, 1970, CERN Report 70-30, pp. 153-162.
4. H. Jungclas, R.D. Macfarlane, and Y. Fares, Radiochim. Acta 16 (1971) 141.
5. P.O. Aronsson, G. Skarnemark and M. Skarestad, J. Inorg. Nucl. Chem. 36 (1974) 1689.
6. K. Bächmann, V. Matschoss, J. Rudolph, A. Steffen and S. Tsalmas, Nucl. Instr. Meth. 139 (1976) 343-348.
7. I. Zvara, O.L. Keller, Jr., R.J. Silva and J.R. Tarrant, Jour. of Chromatography 103 (1975) 77-83.
8. B. Grapengiesser and G. Rudstam, Radiochim. Acta 20 (1973) 85-96.
9. G. Rudstam and B. Grapengiesser, Radiochim. Acta 20 (1973) 97-107.
10. W. Bogl, K. Bächmann, and K. Buttner, Radiochim. Acta 21 (1974) 33-40.
11. K. Bächmann and J. Rudolph, Jour. Radioanal. Chem. 32 (1976) 243-263.
12. I. Zvara, V.Z. Eelov, L. Chelnokov, V.P. Domanov, M. Hussonois, Yu. S. Korotkin, V.A. Schegolev, and M.R.

Shalaevski, Inorg. Nuc. Chem. Letts. 7 (1971) 1109-1116.

13. G. Rudstam, Nucl. Instr. Meth. 139 (1976) 239-249.

14. V. Matschoss and K. Bächmann, 3rd Int. Conf. on Nuclides Far From Stability, Consica, France, May 1976. CERN Report 76-13, pp. 59-62.

15. N. Trautmann, ibid., pp. 30-38.

16. B. Palmer, Undergraduate Summer Research Project, Dept. of Chemistry, Simon Fraser University, 1977.

17. B. Eichler, Jour. Inorg. Nucl. Chem. 35 (1973) 4001.

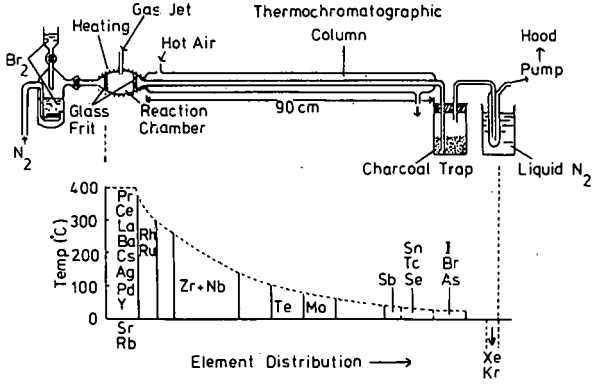

Figure 1. Schematic diagram of the thermochromatographic apparatus for continuous separation of the fission product bromides with a gas-jet as the transport method for the reaction products (taken from ref. 2).

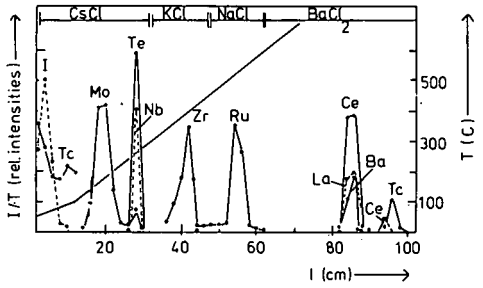

Figure 2. Separation of ^{235}U fission products using different wall coatings and temperatures; carrier and reactive gas N_2 (13% CCl_4) (taken from ref. 6).

Study of Neutron-Rich Rb and Cs Isotopes at OSTIS

K.D. Wünsch and H. Wollnik

II. Physikalisches Institut der J.-Liebig-Universität, 63 Giessen, Germany

and Institute Laue Langevin, 38042 Grenoble, France

ABSTRACT

An on-line mass separator for thermally ionized fission products (OSTIS) has been installed at a neutron guide tube of the High Flux Reactor of the Institute Laue Langevin in Grenoble. This aparatus provides pure Rb and Cs isotope beams with intensities of up to a few 10^6 atoms per second focussed to an area of less than 5 mm diameter. The contamination by neighbouring masses or by other elements is lower than 10^{-5}. Several arrangements are used for beta, gamma and delayed-neutron spectroscopy as well as for the measurements of yields and half-lives. Some of the results are discussed.

Introduction

ISOL systems are now commonly in use to produce pure samples of nuclei far away from stability. The major requirements are short transport time, high separation power and high efficiency. These conditions are easily fulfilled by the technique Bernas and Klapisch[1]) first used at the Orsay synchrocyclotron. The OSTIS ion-source is of the same type but slightly modified to fit the needs of an installation at a neutron guide tube. This demands a high concentration of target atoms into a small volume. Also stability over a long time is necessary to compensate for the low absolute intensity available by long measuring times.

1. A short technical description of the mass separator OSTIS

The name originates from: "On-line Massen-Separator für thermisch ionisierbare Spaltprodukte". A more general description of the apparatus is given in refs[2,3]). A schematic drawing of OSTIS is shown in Fig. 1

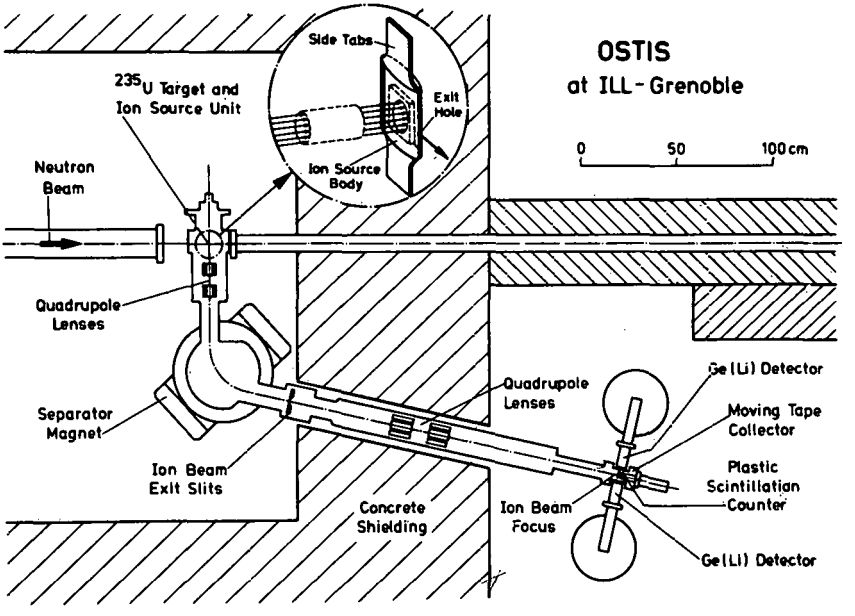

Figure 1. Schematic diagram of the OSTIS separator facility as it is installed at a neutron guide of the High Flux Reactor of the Institute Laue-Langevin.

as it is installed at a neutron guide tube of the ILL high flux reactor in Grenoble with an intensity of $10^9 n_{th}/sec \cdot cm^2$. The ion source and the magnet of the separator are located behind a shielding of 1 m of concrete and additional plastic material to ensure that the surrounding experiments are not disturbed by the fast neutrons originating from fission. The ion source consists of up to six slabs of porous grahite (dimensions:20x20x0.7 mm^3) containing about 2 grams of enriched ^{235}uranium as target material. The uranium oxide is distributed in clusters of a few µm size over the whole volume by a special technique[2,3]) to assure that the fission fragments can penetrate these clusters and reach the graphite where they diffuse by orders of magnitude faster. These loaded graphite slabs are placed in a rhenium container and heated up to 1900°C by passing a current through it. Fig.2 shows such a mounted source.

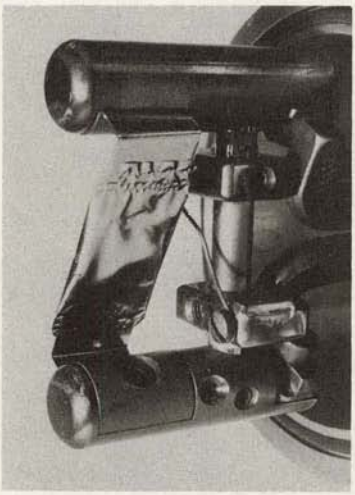

Figure 2. OSTIS ion source mounted on a source holder.

The alkali elements diffuse very fast out of the graphite and after being ionized on the hot surface leave the oven by a channel of 1,5x0,4 mm^2 acting as an entrance slit to the separator. The ions are accelerated by 20 keV, pass through a quadrupole doublet, to shape the beam properly, and are then bent by 77.5 degrees in a magnet of 21.5 mm radius before they pass through the exit slit. A second quadrupole doublet focusses the ions on a spot of less than 5 mm diameter located 1 meter outside the shielding where different detection techniques can be applied.

2. Performance

The cross contamination of neighbouring masses is lower than 10^{-5}. Due to differential punping with 4 stages, the contamination by rare gases is also lower than 10^{-5}. No independent production of the alkali earth elements is observed so that a very pure beam of rubidium or cesium isotopes is produced.

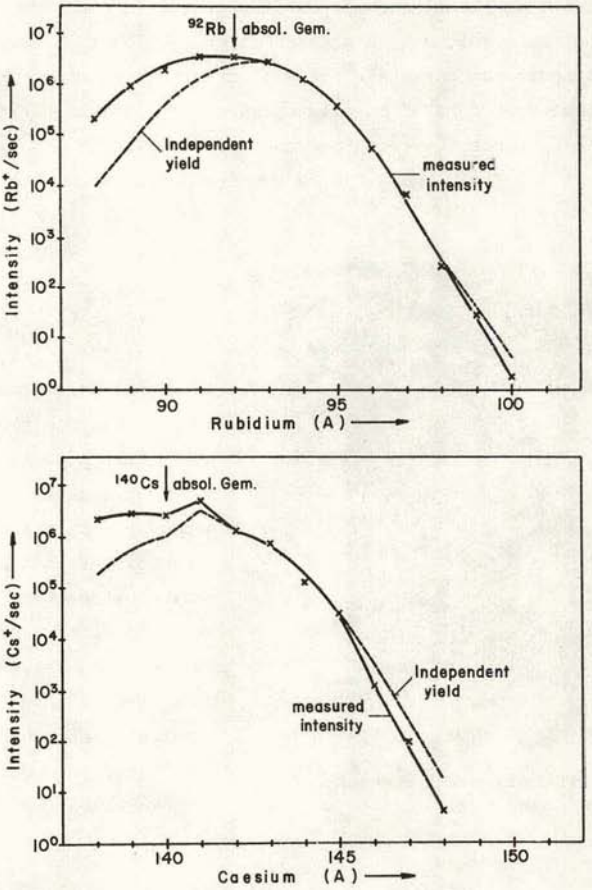

Figure 3. The measured β intensities at the exit of OSTIS are shown as black curves and as dotted curves the independent yields determined with the known half lives of the Rb and Cs isotopes. The absolute intensity was determined for ^{92}Rb and ^{140}Cs by absolutely calibrated γ-ray measurements.

Fig.3 shows the intensity available at the detector region measured with a beta counter and with a current probe absolutely calibrated by gamma-ray measurements of well-known nuclei. In the most abundant cases more than 10^6 atoms per second are available. The overall efficiency is about 3%. The apparatus was built and tested at the reactor of the Technical University of Munich and then brought to the High Flux Reactor in Grenoble. After one month of installation work, it became operational in November 1975. Since early 1976 the duty cycle was about 80% of the reactor time, that is to say measurements were made on about 200 days of 24 hours in one year. The whole system is designed for automatic stand alone-measurements over-night. The best ion source withstood eight months of continuous operation, while the longest measurements lasted 20 consecutive days. The organisation and the structure of the scientific work at the ILL and the special features of OSTIS made it possible for more than 28 experiments based on proposals to be carried out. Each experiments ran for an average beam time of about two weaks.

3. Experiments performed during the last two years at OSTIS

Tabe 1 shows all experimental activities and first results listed versus the mass of the isotope ranging from mass 88 to 99 for the rubidium and from 138 to 148 for the cesium isotopes. The different experiments will be discussed below in more detail together with their corresponding results. The first column of table I gives the actual intensity available at the detector. Up to ^{92}Rb and ^{141}Cs roughly the cumulative yields of the corresponding mass chain is obtained because the biggest part of the rare gas atoms stays within the source until they decay to the alkaline elements and diffuse out quickly. For higher masses this contribution can be neglected. This measured intensity represents almost the independent yields. From the masses 98 and 145 onward the delay in the ion source reduces the intensity further[4]).

3.1 The independent fission yields of Rb and Cs Isotopes

(This work was mainly carried out by S. Balestrini, LRL Los Alamos, and E. Koglin, G. Siegert ILL Grenoble)

The second column of table I represents the independent yields of the rubidium and cesium isotopes. These yields are preliminary results since the data evaluation is not yet completed because of the involved corrections

which have to be made for precursors and the diffusion delay in the ion source. The diffusion delay was measured by a fast neutron chopper monitoring its efficiency by a ^{3}He neutron counter which records the fission neutrons originating from the source.

In parallel the fission yields were measured with a small ion source of only 2 mg of ^{235}U. The overall diffusion time in this source was about 5 msec, much shorter than the shortest half-life of a nucleus concerned. Thus no explicit correction had to be applied to these measurements.

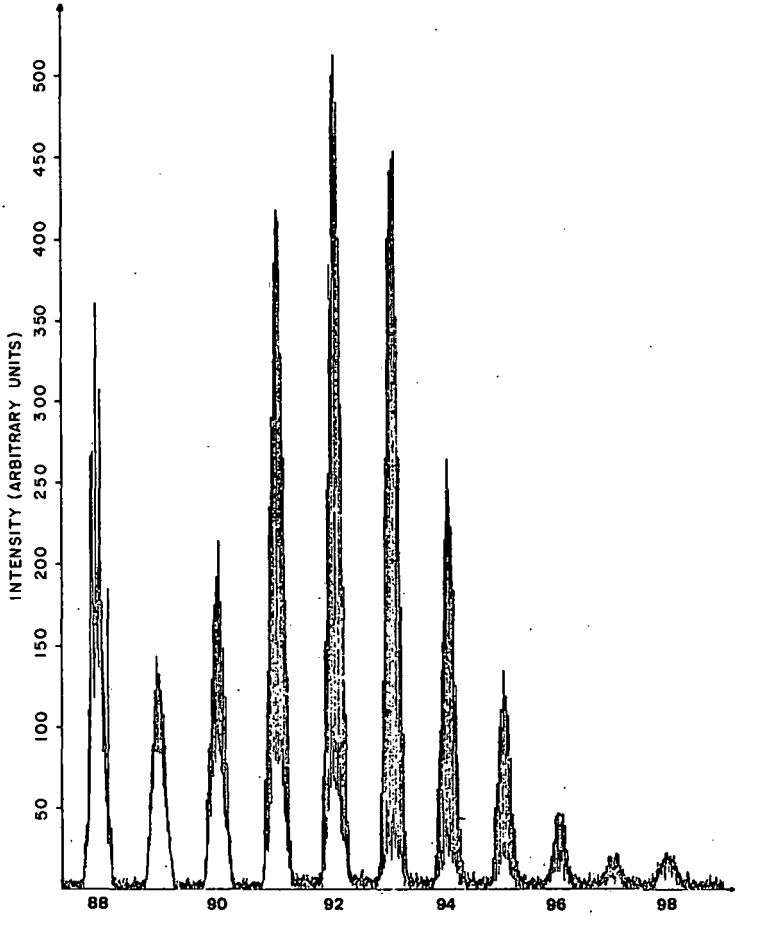

Figure 4. Yields of Rb-isotopes obtained as explained in the text.

Fig.4 shows the ion intensity versus magnetic field strength (i.e. isotope mass) in the light mass region with a chopped neutron beam. The difference f the two envelopes thus represents the independent yields of the rubidium isotopes. Both measurements are in good agreement proving that the corrections applied to the measurements with the big source were done correctly[5]).

3.2 Half-life

(This work was mainly carried out by K. Wünsch Uni Giessen, G. Jung, G. Siegert ILL Grenoble and F. Wohn Uni Ames)

The measured half-lives are indicated in column three of table I. The half-lives were measured by two methods. First the integral beta counting rate of a thin plastic counter placed after the collection point was recorded and unfolded by an involved computer code for the different daughters of one specific Rb or Cs isotope. The ion beam was periodically switched on and off, the timing adjusted to the particular beta chain under investigation. In addition a Ge-Li detector of 25% efficiency monitored 8 or 16 consecutive γ-spectra, starting when the ion beam was cut off. Several measurements were made for each isotope investigated. This resulted in low root mean square values for the errors.

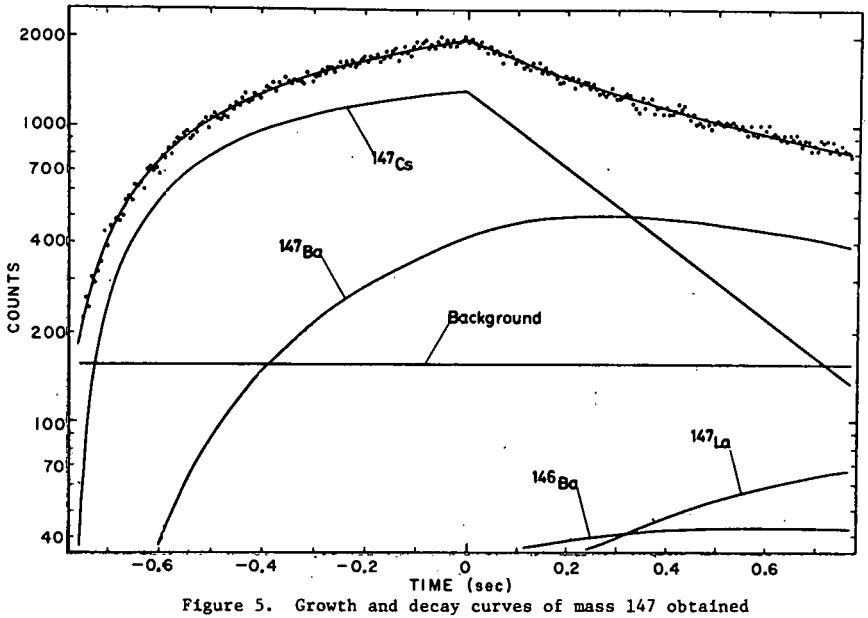

Figure 5. Growth and decay curves of mass 147 obtained from β-multiscaling.

Fig.5 shows the ß-countrate for the increase and decay of the new isotope ^{147}Cs. Included in the analysis is not only the 147 decay chain but also the 146 decay chain fed by delayed-neutron decay. All values obtained by ß or γ measurements are in good agreement also with the literature[6]) and with the values independently determined by neutron counting[7]).

3.3 Beta-end point energies and $Q_ß$-values

(This work was mainly carried out by K. Wünsch, R. Decker, H. Wollnik Uni Giessen, G. Siegert, G. Jung and E. Koglin ILL Grenoble)

In column four of table I all obtained $Q_ß$-values are shown. For determining the ß-endpoint energy, we used an intrinsic Ge-detector which has several advantages over a conventional plastic detector[8]). The resolution and the linearity are better than $2 \cdot 10^{-4}$. This and the response function to monoenergetic electrons (see Fig.6) was measured at the conversion electron spectrometer BILL at the ILL.

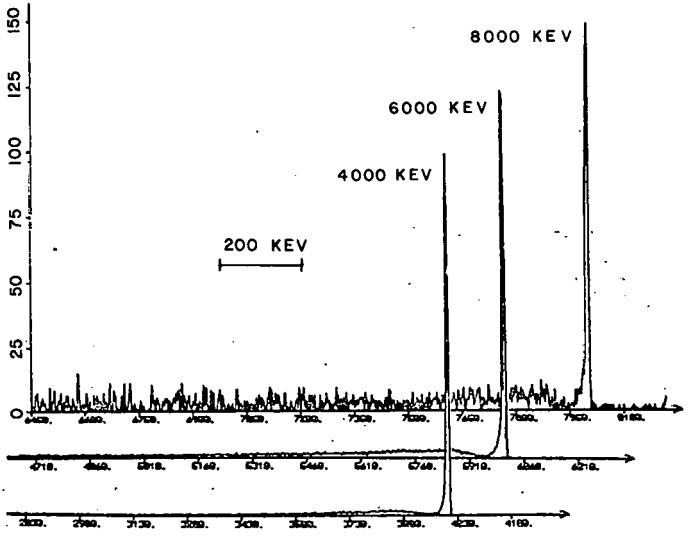

Figure 6. The last 1 MeV portion of the response function of our intrinsic Ge-detector to monoenergetic electrons of 4, 6 and 8 MeV is shown. The width of the main response peak is about 10 keV. Since the available electron intensity decreased rapidly with electron energy the signal to noise ratio in the three response curves decreased considerable with increasing electron energy.

To our knowledge this is the only device which can deliver a beam of electrons up to 11 MeV with an accuracy and energy spread of less than 10^{-4}. To assure daily calibration we used the γ-sensitivity of our ß-detector in combination with a calibration source of 90-Rb (produced on-line) for which the γ-lines are known up to 5.3 MeV[9]). Drift during a 20 hours measurement was controlled by measuring that no unnormal peak broadening of the γ-rays was observed for γ-lines present in the lower part of a beta-spectrum. A pile-up rejection logic extends the acceptable counting rate at the detector to about 2000 beta counts per second without any noticable ß pile-up. All energy endpoint determinations were based on at least two measurements with different counting rates. In parallel to the ß-singles spectra we measured up to 8 beta-spectra coincident with the most interesting gamma lines, each of them with its corresponding background. The small width of the detector response peak and its high resolution as well as the high intensity available for the Rb and Cs sources result in a high accuracy of the $Q_{ß}$-values.

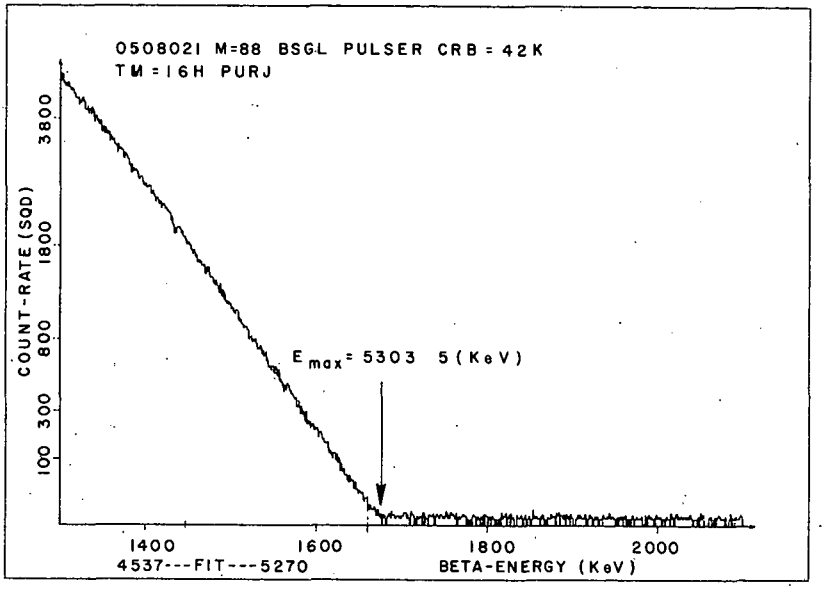

Figure 7. Endpoint region of the ^{88}Rb beta-spectrum.

Fig.7 shows the endpoint region of the ß-spectrum of 88 Rb resulting in a $Q_{ß}$-value of 5312±7 keV which is in very good agreement with known values. For cases far away from beta stability, however, where beta-decay normally feeds levels high above the ground state one should point out that the decay-scheme has to be known very well for an unambiguous $Q_{ß}$-determination. Otherwise one can easily miss a γ-line and deduce a too low $Q_{ß}$-value. In all such cases the $Q_{ß}$-values should be regarded as lower limits[10]).

3.4 Delayed Neutron emission

(This work was mainly carried out by J. Craçon, C. Ristori CEN Grenoble K.L. Kratz, H. Ohm, Uni Mainz, K. Wünsch Uni Giessen and G. Jung ILL Grenoble)

The delayed neutron emission (Pn) of Rb and Cs precursors has received extensive studies. At OSTIS these Pn values were determined using for the neutrons a conventional long counter of 12% efficiency and for the electrons a 2 π beta-counter. The Pn values for ^{147}Cs was measured here for the first time[7]). In parallel, measurements were made taking γ-spectra where the delayed neutron branch feeds an adjacent beta chain. The relative strength of γ-rays from well known daughters from each decay chain were then used to determine the Pn value. This was done for ^{94}Rb[11]) and showed good agreement, thereby establishing the reliability of this technique.

3.5 Gamma-spectroscopy

(This work was mainly carried out by G. Jung ILL Grenoble, F. Wohn Uni Ames, H. Wollnik Uni Giessen, F. Schussler and E. Monnand CEN Grenoble)

Gamma-spectroscopy work on the decay of $^{143-147}Cs$, started at the Lohengrin fission fragment separator by a group of the CENG, was continued with the much higher intensities at OSTIS. The work on Rb isotopes[12]) was continued from earlier work in Munich where first the delayed neutron emission to excited states of the final Sr nuclei were found. In particular the gamma-spectrum of ^{98}Rb was determined with γ-γ coincidences and the low energy level scheme of ^{98}Sr was deduced showing that the 2^+ level of ^{98}Sr is at 140 keV[13]). While all other neutron rich even-even Sr isotopes have their 2^+ levels in the vicinity of 800 keV (see fig.8).

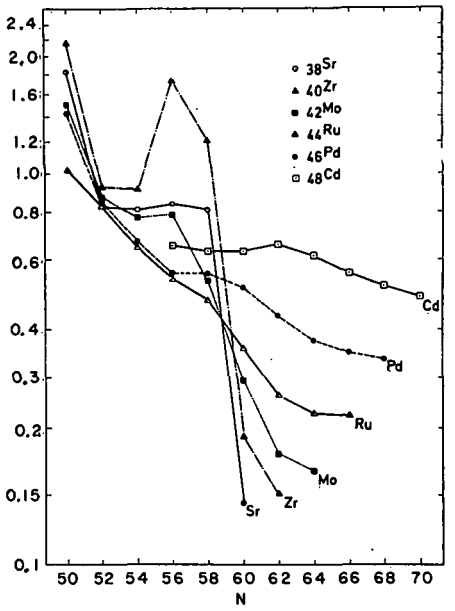

Besides other observed facts this is a strong indication that ^{98}Sr is a deformed nucleus and that the predicted area of deformed nuclei near mass 100 begins here.

Figure 8. The energy of the 2^+ levels of even-even nuclei drop sharply in going from ^{96}Sr to ^{98}Sr. This indicates an onset of nuclear deformation.

3.6 Delayed neutron spectroscopy

(This work was mainly carried out by K.L. Kratz, H. Ohm Uni Mainz, J. Crançon, C. Ristori CEN Grenoble)

Up to three higher resolution ^3He-counters were used to measure the energy spectra of beta delayed neutrons. Despite the low efficiency of some 10^{-4} and the strange timing behaviour (output-pulse up to 10 µsec after the event) even coincidences with a 25% Ge-Li detector were made succesfully to investigate the ß-neutron-gamma decay. The singles spectra (an example is given in fig.9) show the good energy resolution of about 13 keV as well as the discrete neutron energy peaks. This discrete neutron peaks are found in all spectra[15]). They are most significant in the case of odd rubidium precursors leading to even-even strontium final nuclei where the Q-values are high and the low energy level density is low. An initial coincidence measurement between neutrons and γ-rays of the final nucleus yielded a very poor but significant spectrum[16]) mainly due to the low overall efficiency of 10^{-6} for the arragement. This measurement was repeated in August of this

year, increasing the intensity delivered from OSTIS by a factor of four and using three instead of one ^{3}He-counters as well as counting for 3 weeks instead of 5 days. This increased the counting statistics by nearly two orders of magnitude.

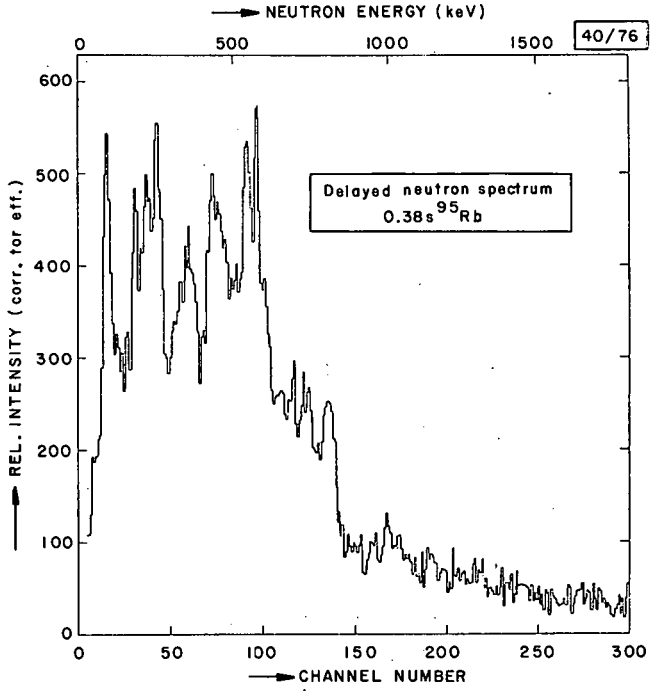

Figure 9. Energy spectrum of the delayed neutrons emitted after the beta decay of ^{95}Rb.

3.7 Conversion electrons

(This work was mainly carried out by J.v. Klinken, J. Feenstra Uni Groningen, F. Schussler, E. Monnand CEN Grenoble)

A mini orange conversion electron spectrometer[10]) consisting of permanent magnets and a Si-detector was mounted for the first time. Due to experimental difficulties only a few short measurements were possible.
Fig. 10 shows the conversion electron spectrum of ^{144}Ba measured in one hour[18]).

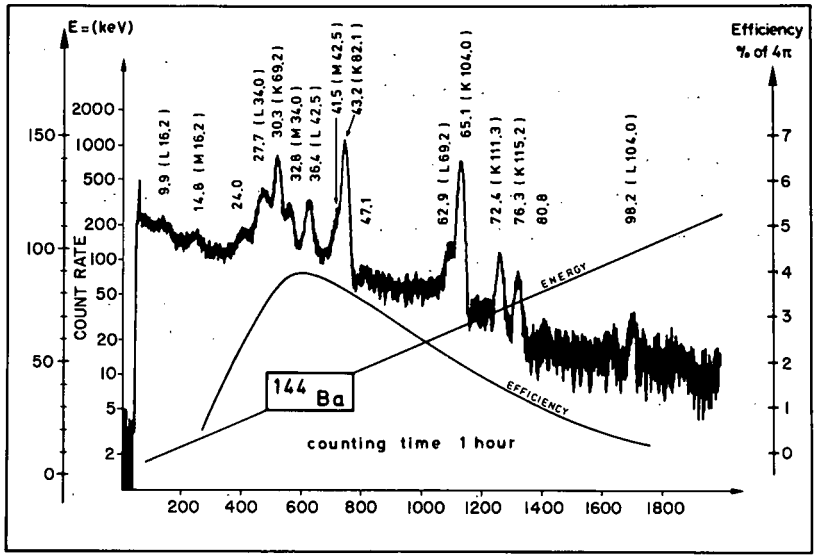

Figure 10. Conversion electron spectrum of ^{144}Ba obtained by using a mini orange energy filter and a Si(Li) detector.

Outlook

We plan to continue and complete all the measurements mentioned above and perform also γ-γ angular correlations. In the near future we will install an off-line measuring position which allows also to work on the beta daughters. Changing the ion source to indirect heating in the next year should permit higher temperatures and therefore allow studies of alkaline earth and perhaps rare-earth isotopes.

Acknowledgement

The complexity of modern nuclear research reduced the possibility of individual projects and led more to teamwork. The performance and the reliability of the OSTIS separator would not have been possible without the help of many collaborators who formed a very homogeneous group. We are indebted to Dr. G. Siegert for his continuous advice and help. We also acknowledge much help from G. Jung, R. Decker, E. Koglin, S. Balestrini, W. Jung, J. Münzel, J. Crançon and C. Ristori at the various stages of construction, installation, improvement and running of OSTIS. The support from the II. Physikalisches Institut of the University of Giessen, from the ILL and the CENG-DRF Grenoble is very much appreciated. For financial support we finally are grateful to the Bundesministerium für Forschung und Technologie.

References

[1]) I. Amarel, R. Bernas, J. Chaumont, R. Faucher, J. Jastrzebski, A. Johnson, R. Klapisch and J. Teillac, Arkiv för Fysik 36, 77 (1966).

[2]) K. D. Wünsch, Doctoral Thesis Technical University of Munich (1974) unpublished.

[3]) K. D. Wünsch (1977) in preparation.

[4]) K. D. Wünsch, H. Gunther, G. Siegert and H, Wollnik, J. Phys. A6, L93 (1973).

[5]) K. D. Wünsch, H. Wollnik and G. Siegert, Phys. Rev. C10, 2523 (1974)

[6]) H. Gunther, G. Siegert, K. D. Wünsch and H. Wollnik, Nucl. Phys. A242, 56 (1975).

[7]) Annex to the annual report of the Institut Laue-Langevin, Grenoble. ILL experimental report, No. 03-03-029 (1977) in print.

[8]) Annex to the annual report of the Institut Laue-Langevin, Grenoble, ILL experimental report Nr. 03-03-063 (1977) in print.

[9]) F. Wohn, K. D. Wünsch, R. Decker, H. Wollnik, G. Siegert, G. Jung and E. Koglin, to be submitted to Physical Rev. C.

[10]) Annex to the annual report of the Institut Laue-Langevin, Grenoble, ILL experimental report No. 03-01-018, p. 29 (1976) and (1977) in print.

[11]) Annex to the annual report of the Institut Laue-Langevin, Grenoble, ILL experimental report No. 03-01-030, p. 33 (1976) and ILL experimental report 03-03-043 (1977) in print.

[12]) Nucl. Data Sheets 16, 55 (1975).

[13]) Annex to the annual report of the Institut Laue-Langevin, Grenoble, ILL experimental report No. 03-03-023, (1977) in print.

[14]) H. Wollnik, F. K. Wohn, K. D. Wünsch and G. Jung, Nucl. Phys. A in print.

[15]) Annex to the annual report of the Institut Laue-Langevin, Grenoble, ILL experimental report No. 03-01-027, p. 32 (1976).

[16]) Annex to the annual report of the Institut Laue-Langevin, Grenoble, ILL experimental report Nr. 03-01-027 (1977) in print.

[17]) J. van Klinken, S. J. Feenstra, K. Wisshak and H. Faust, Nucl. Instr. Meth. 130, 427 (1975).

[18]) Annex to the annual report of the Institut Laue-Langevin, Grenoble, ILL experimental report No. 03-03-045 (1977) in print.

Table 1

Experimental activity and first results received with OSTIS listed versus the mass of the nuclei (October 1977).

Nucleus	Intensity Atoms/sec	Yield† Y (%)	$T_{1/2}$ (msec)	Q_β (keV)†	Neutron emission P_n (%)	Spektroscopy Gamma	Beta	Neutron	Convers. elec.
^{86}Rb	$0,15\times10^{6}$	0,033±0,01	(17,8m)	5313±7	-	-	γ-γ	-	-
^{89}Rb	$0,7\times10^{6}$	0,17±0,04	(15,2m)	4499±10	-	-	x-γ	-	-
^{90}Rb	$1,4\times10^{6}$	0,78±0,08	(2,6m)	6550±40	-	-	x-γ	-	-
^{91}Rb	$2,2\times10^{6}$	1,88±0,22	(58s)	5820±50	-	-	x-γ	-	-
^{92}Rb	$2,3\times10^{6}$	3,01±0,16	(4,5s)	8055±40	(0,012±0,004)	-	x-γ	-	-
^{93}Rb	$2,0\times10^{6}$	3,09±0,24	(5,8s)	7443±40	1,32±0,03	-	x-γ	x-γ	-
^{94}Rb	$1,0\times10^{6}$	1,68±0,12	2,73±0,02s	10270±40	9,7±0,5	x-γ	x-γ	x-γ	o
^{95}Rb	$0,26\times10^{6}$	0,76±0,08	377±6	x	8,5±0,5	x-γ	x-γ	xx-γ	o
^{96}Rb	43×10^{3}	0,21±0,03	203±4	x	12,5±0,9	x-γ	x-γ	x-γ	o
^{97}Rb	9×10^{3}	0,05±0,01	170±2	x	25,2±1,8	x-γ	x-γ	x	x
^{98}Rb	$0,2\times10^{3}$	$(4\pm1)\times10^{-3}$	108±5	o	18,4±2,9	xx-γ	o	o	o
^{99}Rb	$0,03\times10^{3}$	o	(76±5)	o	o	o	-	-	-
^{138}Cs	$2,2\times10^{6}$	1,0±0,6	(32m)	5334±40	-	-	x-γ	-	-
^{139}Cs	$2,7\times10^{6}$	1,8±0,5	(9,3m)	4206±8	-	-	x-γ	-	-
^{140}Cs	$2,6\times10^{6}$	2,3±0,35	(64s)	6177±35	-	-	x-γ	-	-
^{141}Cs	$5,0\times10^{6}$	3,92±0,36	(25s)	5187^{+75}_{-25}	(0,07±0,1)	-	x-γ	o	-
^{142}Cs	$1,2\times10^{5}$	1,75±0,22	(1,68s)	7287±30	(0,27±0,07)	-	x-γ	o	o
^{143}Cs	$0,7\times10^{6}$	0,98±0,15	1765±30	6010±40	1,74±0,12	xx-γ	x-γ	o	x
^{144}Cs	$0,13\times10^{6}$	0,34±0,02	1000±10	8150±100	2,95±0,25	xx-γ	x-γ	o	x
^{145}Cs	28×10^{3}	0,09±0,01	603±20	x	12,2±0,9	xx-γ	x-γ	o	x
^{146}Cs	$1,3\times10^{3}$	$(11\pm3)\times10^{-3}$	315±10	x	13,2±0,8	x-γ	x-γ	o	x
^{147}Cs	$0,1\times10^{3}$	$(1\pm1)\times10^{-3}$	218±9	o	25,4±3,2	x-γ	o	-	x
^{148}Cs		$\leq10^{-4}$	o	o	o	o	o	-	-

( ) from literature, o planned, x under evaluation, xx first results, † preliminary results, -γ coincidence with gamma-rays

Collective Structure of Medium-Mass Nuclei

S. A. Williams

Physics Department and Ames Laboratory, USDOE
Iowa State University, Ames, Iowa

Presented at BNL Workshop on ISOL Systems
1 November 1977

Which Nuclei

I want to discuss our efforts to understand the level structure and electromagnetic transitions for the even-even Palladium and Cadmium isotopes. In particular, we have studied all the even-even Palladium isotopes from A=102 to A=114 and all the even-even Cadmium isotopes from A=100 to A=122. The data for the last three Cd isotopes (^{118}Cd, ^{120}Cd and ^{122}Cd) were taken only very recently at TRISTAN II and their experimental analysis is preliminary. Accordingly, our theoretical results for these nuclei must be considered tentative; the parameter values used for these nuclei fit the pattern of the values for the other Cd nuclei, however.

These two isotope strings are of interest for at least two reasons. First of all, they comprise the Z=46 (Pd) and Z=48 (Cd) chains which are four and two protons respectively from the presumed shell closure at Z=50, yet the nuclei of both chains exhibit strong collective features. Secondly, because they occur as fission decay products, the chains may be extended experimentally quite far to the neutron-rich side of stability. It is of strong theoretical interest to ascertain the effect of increasing neutron number on the collective features of these nuclei.

Our interest in these isotope chains began with ^{106}Pd about three years ago when we discovered that the level structure of that nucleus could not be accounted for by anharmonic surface vibrations about spherical equilibrium as was previously thought to be the case. Yet, BE2 ratios clearly indicated a strong collective nature for this nucleus. Furthermore, the energy spectrum was clearly not that of a pure rotor. This really left only the possibility of some sort of rotation-vibration model and we found that a modification of the Davydov-Chaban[1] model could be applied with great success. Let me review that model very briefly.

The Model

The model presupposes a permanently deformed nucleus which undergoes both rotation and breathing-mode vibrations. The essential features of this model are shown in Figure 1. The variable β describes the nuclear deformation and these breathing-mode (non-angular momentum carrying) are

presumed to occur in harmonic approximation about an equilibrium value β_0. In addition, there exist rotations of the asymmetric nucleus whose asymmetry is given by the parameter γ. The Euler angles of orientation of the principal axes of inertia relative to the laboratory frame are denoted by θ_i. One sees that these rotations enter the vibrational Hamiltonian in a manner analgous to the centrifugal barrier in a three-dimensional oscillator. The rotor energies, $E_{IN}(\gamma)$ are labeled by the angular momentum I and an ordinal number N. The assumed A-type symmetry for this rotor results in one I=0 state (which will become the ground state), two I=2 states, one I=3 state, three I=4 states, two 5 states, etc.

For a given rotor state (IN) the vibrational potential energy is the sum of the parabolic potential about β_0 and the centrifugal barrier term. A parabolic approximation for this complete potential is made with the result that vibrations occur about an equilibrium β_{IN} which depends upon the rotation energy. The strength of this coupling between rotations and vibrations is measured by the model parameter μ. For small μ (near 0) the rotations and vibrations are essentially uncoupled while for large μ (nearer 1) there is considerable mixing; the nucleus is said to be quite soft. The dependence of the dynamic equilibrium β_{IN} on the rotor energy results in a dependence of the vibrational quantum number ν_n on the rotor energy. Thus the ν_n are not integers and we use instead an ordinal number n to label the particular β-vibration band: n=1 is the ground-state (lowest) β-vibrations, n=2 is the first excited β-band, etc. The rotation-vibration energies are as indicated and depend upon three model parameters only. These are the stiffness μ, the asymmetry γ and the scale energy $\hbar\omega_0$. These are adjusted to fit the spectrum of a nucleus to which the model is applied.

We have found it necessary to assume, in addition, the existence of another degree of freedom. This additional degree of freedom is not to interact strongly with the rotations and vibrations, but rather to reproduce complete rotation-vibration bands similar in structure to that which contains the ground state. These additional sequences begin at some excitation energy with a 0^+ state. Later, I shall indicate what we now believe this additional degree of freedom to be. We label each sequence by an ordinal number S. The sequence of rotation-vibration bands which contains the ground state is labeled S=1. A typical spectrum is shown in Figure 2.

The Pd Isotopes

Figure 3 shows both the experimental and theoretical energy levels for ^{106}Pd. In this and subsequent figures, levels with a star were not used in the fitting procedure which determines the model parameters. One sees in ^{106}Pd three very well developed rotation-vibration sequences. Including the sequence heads there are 9 effective parameters used since γ and $\hbar\omega_c$, but not μ, were allowed to vary from sequence to sequence.

There are 34 known levels below about 3500 keV and of the 23 model levels shown, 20 may be correlated with experimental levels of the correct spin. The remaining three higher spin levels are not yet known experimentaly. The agreement between theory and experiment is really very good. The uncorrelated experimental values are all thought to be low spin and in many cases their spin is extremely poorly known. The yrast states (the 6111, 8111 and 10111) were not known experimentally at the time this calculation was done, yet apart from the 10^+ located experimentally at 3532 keV but predicted at 4419 keV, the agreement with these states is reasonably good. The model prediction of the high-spin yrast states as too high persists throughout the Pd nuclei where such high spins are known. This clearly indicates that the present model does not have a sufficient amount of effective back-bending.

Figure 4 shows the case of ^{108}Pd where a great deal less is known experimentally. The agreement between theory and experiment is again quite good and one sees a second well-developed sequence and the presumed sequence head of the third. Figure 5 shows a quite similar situation for ^{110}Pd. Figure 6 shows the cases of ^{112}Pd and ^{114}Pd where there is very little known experimentally. There is real need for further experimental study of these nuclei particularly ^{114}Pd for which only the yrast states are known.

Figure 7 shows the case of ^{104}Pd which displays two sequences. As with ^{106}Pd, the agreement between theory and experiment is excellent. There are, as with ^{106}Pd, some experimental levels which cannot be correlated with the theoretical predictions. In ^{104}Pd these include some presumed spin 2 and spin 3 levels. I shall comment more about these later. We also show the variable moment of inertia (VMI) model predictions of the yrast states as reported by Cochari *et al.*[2] Using root-mean-square error as a criterion, the present model apparently does a better job of predicting the location of these states than does the VMI model.

In Figure 8 we show the two experimental spectra proposed for ^{102}Pd. The theoretical agreement is sometimes with one scheme and sometimes with the other. I understand that the experimental dichotomy has been resolved but the results are not yet published. Again we show the VMI result and again the current model has better overall agreement with the yrast states than does the VMI model. There is no known second sequence in this nucleus and I shall comment further on that later.

Figure 9 shows the trends in the model parameters. This illustrates that all the Pd isotopes except for A=102 are relatively stiff, but ^{102}Pd is quite soft. The asymmetry of the ground state sequence (denoted by circles) increases modestly from A=102 to A=114. The energy of the first 2^+ state (the 2111) largely dictates the value of $\hbar\omega_0$ and the upper part of the figure shows that this parameter slowly decreases with increasing A. In a sense, the smaller the value of $\hbar\omega_0$, the "more collective" is the nuclear behavior. Figure 10 displays essentially the

same information by states except that relative energy has been used; the 2111 state has been assigned the energy value 1. Perhaps the most interesting thing about this graph is the movement of the β-band head, the 0121 level. The location of this level is dictated largely by the value of μ and to a lesser extent the value of $\hbar\omega_0$ relative to the 2111 actual energy. What this graph shows then is that relatively small changes in μ (when μ is considerably less than 1) result in large changes in the relative position of the 0121 level. This shows that there is very little tolerance in this parameter for good agreement between theory and experiment. The fact that we have good success in fitting the levels of all these nuclei would seem, therefore, to indicate that this model represents a great deal of the truth concerning the collective description of these nuclei. Presuming that such exists, whatever the ultimate model description is for these nuclei, said model will have to have many of the features of this relatively simple collective model.

As a test of the model wavefunctions we have also computed BE2 ratios and compared them with experiment where such information is available. The results are shown in Figure 11. There are only a few apparent descrepancies. For both ^{108}Pd and ^{110}Pd the 2211-2111 transition seems badly described. But, it is noted in the literature[3] that the M1-E2 mixing ratio for the transition in ^{108}Pd can only be determined experimentally to be either -5.2 or -0.73. The quoted experimental BE2 ratio presumes the former value, but theory favors the latter value. There is no indication in the literature of a similar situation for ^{110}Pd, but the theory certainly suggests that such might be the case. In any case, the existence of <u>any</u> M1 component is a thorn in the side of any purely collective theory since <u>all</u> such theories must of necessity predict no M1 transitions. This gives a clue as to what the remaining degree of freedom ought to be. The 0112 → 2111/2111 → 0111 ratio was calculated as if there were no sequence change, so disagreement between theory and experiment here displays our ignorance as to the role played by this extra degree of freedom. Before I discuss that extra degree of freedom let me briefly summarize the situation for the Cd isotopes.

The Cd Isotopes

We have fitted the spectra of all the Cd isotopes from A=100 to A=122 with a fair degree of success. The experimental information for the Cd isotopes is in much worse shape than for the Pd isotopes; in many cases very little is known. Accordingly, I shall only show a few cases to i) indicate the general quality of the agreement, ii) show the similarity between the Cd nuclei and the Pd nuclei, and iii) to point out some differences between the spectra of these two chains which we feel are important clues to the behavior of both.

We begin with ^{106}Cd shown in Figure 12. The agreement between theory and experiment is really very good including that for the presumed 8^+ yrast-state at 3406 keV. Next, in Figure 13 we show the case for ^{112}Cd where as with ^{110}Cd and ^{114}Cd there appears to be a second sequence head near 1200 keV. There is so little known experimentally that we cannot go much further with this nucleus at present. The preliminary data for ^{118}Cd taken by the TRISTAN II group at Iowa State is shown in Figure 14. The model can account for most of the tentative levels shown and appears to agree reasonably well with experiment. This apparent agreement may be a little misleading in that it suggests that one of the triplet near 1920 keV ought to be a 4^+. Very preliminary beta decay feeding analysis suggests that one of this triplet is probably a 0^+ in contradiction to the theoretical prediction. Presumably the 4^+ which would correspond with the 4211 level is unseen and if ^{122}Cd is a guide, would be expected below the triplet near 1920 keV. The case for ^{122}Cd is shown in Figure 15. Again the experimental data is from ISU and for this isotope the experimental analysis is essentially complete. The experimental spins have been assigned largely on the basis of beta decay information, but the 1979 keV-level is almost certainly either a 3^+ or 4^+ with the latter favored a bit. The theory would agree, but would place this level higher by an error which is much worse than any seen in the Pd isotopes. Furthermore, the relative branching ratios for transition among these levels of ^{122}Cd are not very well described. This is rather curious since for other Cd isotopes the BE2 ratios are rather well predicted as shown in Figure 16.

It seems safe to conclude from these Cd studies that the extra degree of freedom (responsible for the multiple sequences in the Pd isotopes) interacts more strongly with the collective degrees of freedom than in the Pd isotopes. But, this extra degree of freedom apparently does not alter much the E2 transition probabilities from those predicted only on the basis of rotations and β-vibrations. We suppose then that the poor description of the branching ratios in ^{122}Cd must be due to large (unaccounted for) M1 components. So, let us turn to this extra degree of freedom.

The Extra Degree of Freedom

Before I tell you what I think the extra degree of freedom is, let me tell you what it is not. Prior to our undertaking the Cd studies we attempted to describe this extra degree of freedom as γ vibrations. That is, instead of treating the asymmetry as a parameter we allowed it to be a variable oscillating about some equilibrium value γ_0. The γ-part of the potential had the form $C_\gamma(\gamma-\gamma_0)^2$ and we refer to this as the quadratic model. There is then one additional parameter, but our hope was to fix all the levels with just $\hbar\omega_0$, μ, γ_0 and C_γ. The results for ^{106}Pd are shown in Figure 17. The ground state rotational band is somewhat better predicted than before as is the excited β-vibration band associated with it. But, the first excited-sequence head seen

experimentally at 1134 keV is predicted to lie at 6033 keV. The position of this γ-band head is dictated largely by the value of C_γ, and any attempt to lower this γ-band head below the first β-band head (of the ground state sequence) destroys agreement with the ground state sequence. The reason for this is that a fairly large value of γ_0 is required in order that γ stabilize about γ_0 which is the approximation of the Davydov-Chaban model. But as one sees in Figure 18 the γ-band head rises rapidly with increasing C_γ. In that figure ℓ labels the seniority which is a good quantum number at C_γ=0. The γ-band head is a seniority 3 state which is degenerate with the ground state 3,4 and 6 levels when C_γ=0. As C_γ is increased to bring about onset of the validity of the Davydov-Chaban approximation to the original quadrupole surface oscillation problem (and thereby agreement with the ground state sequence) the γ-band head rises rapidly. It becomes painfully clear that the extra degree of freedom is not γ vibrations; all we got for our effort was a vindication of using the Davydov-Chaban model in the first place.

So, that leaves only the possibility of particle motion. From our experience in the Pd isotopes it seems clear that the predominant mode of motion of these extra-core particles will be as zero-coupled pairs. These are sometimes referred to as pairing-vibrations, but to avoid confusion with the collective vibrations, I shall call them zero-coupled pairs or quasi-bosons. We have not as yet done a full and proper calculation to incorporate these into the collective motion. We have done some rather simple calculations to determine whether or not this idea is qualitatively correct. These I shall discuss.

First of all, one might regard the ground state of ^{108}Pd as the action of a zero-coupled neutron pair creation operator acting on the ground state of ^{106}Pd. Similarly, the ground state of ^{104}Pd would be a (different) zero-coupled two neutron destruction operator acting on the ground state of ^{106}Pd. This is indicated symbolically at the top of Figure 19. Then, there should be an excited state in ^{106}Pd which is the result of the pair creation operater acting as the ground state of ^{104}Pd. Its excitation energy would then follow from binding energy differences. For ^{106}Pd this yields 867 keV. This is to be compared with the experimental energy of 1134 keV. One can repeat this process for ^{104}Pd, ^{108}Pd and ^{110}Pd. The results are shown. If we do simple scaling to the 1333 keV level in ^{104}Pd then this approach would predict a first excited 0^+ level in ^{106}Pd at 1163 keV which compares favorably with the 1134 keV experimental value. Indeed, the trends are correct up to ^{110}Pd. This seemed encouraging, so we preceeded to a somewhat more complicated scheme along the same lines. The lower part of Figure 19 shows the idea. For each of ^{98}Pd to ^{112}Pd we list the shell configuration based upon i) the shell ordering thought to be correct near the beginning of the major shell at N=50 and ii) use of only that configuration in which the shells are filled in order. This is, of course, a great over-simplification but is useful. Also shown are the binding energy differences. Then we consider the 0^+ states of ^{106}Pd. The ground state would be $(d_{5/2})^6(s_{1/2})^2(d_{3/2})^2$ and the first excited state

would be $(d_{5/2})^6(s_{1/2})^2(d_{3/2})^0(g_{7/2})^2$. To determine the energy of this state we start with the ground state of ^{110}Pd. If all other things were left unchanged the destruction of the $(d_{3/2})^4$ (or two "$(d_{3/2})^2$-0^+ pairs") would cost 32401 keV. The ground state of ^{110}Pd is 30,718 keV below that of ^{106}Pd so this state is at 1683 keV excitation.

Similarly, the $(d_{5/2})^6(s_{1/2})^0(d_{3/2})^4$ is at 1861 keV excitation and there are two more simple configurations as indicated at 2676 keV and 3109 keV. To simplify further, we consider these only in pairs and presume that whatever the interaction that mixes them is, it has a diagonal contribution Δ and an off diagonal part δ. We then force the diagonal 2x2 matrix to have eigenvalues at 1134 and 1706 keV. These are the first two sequence heads in ^{106}Pd. This yields Δ=352 keV and δ=272 keV. Then, using these same values we consider the next two 0^+ states and find that the next sequence head should be at 2190 keV. There is a 0^+ state in ^{106}Pd at 2001 keV which we presume starts the fourth sequence so this again looks promising.

Finally let me turn to a somewhat more detailed, but still overly simplified, calculation. We have treated all the neutrons beyond N=50 in a quasi-boson approximation. If there are N_p zero-coupled-pairs we use as a basis the set of all possible ways of placing these N_p zero-coupled-pairs in the orbitals $d_{5/2}$, $s_{1/2}$, $d_{3/2}$ and $g_{7/2}$ consistent with not more than three pairs in the $d_{5/2}$ state, etc. This is the only way in which the Pauli principle enters; no attempt is made at antisymmetrization among single particles making up the quasi-bosons. The excitation energy associated with each configuration is determined by using the experimentally-determined shell spacings (determined near the N=50 nuclei and possibly not entirely correct here). We have used as a residual interaction a quadrupole-quadrupole plus pairing interaction between the two neutrons which make up a quasi-boson. This interaction is denoted by V_{ij} in Figure 20. This interaction involves two parameters: C, the strength of the quadrupole-quadrupole term and G, the pairing strength. We then did a χ-squared fit to these two parameters to obtain the best values for predicting the first two sequence heads in ^{106}Pd, ^{108}Pd and ^{110}Pd. G has the usual form of a constant divided by the number of nucleons from which we could obtain the values for ^{102}Pd, ^{104}Pd, ^{112}Pd and ^{114}Pd by extrapolation. The values for C obtained by χ-squared fit were fitted to a parabolic interpolation and thus we could extrapolate the values for the indicated Pd isotopes. This is more dangerous than the extrapolation for G. In the end then, we have but one data point to compare: the excited sequence head in ^{104}Pd. This simple calculation predicts 1340 keV and experimentally the state is seen at 1333 keV. The extreme accuracy of the prediction is without a doubt fortuitous, but we note that the first excited sequence head in ^{102}Pd is predicted to lie near 3200 keV. Such a high-energy 0^+ might be difficult to see and if cross sequence transition probabilities are small, one might have difficulty detecting the other states of this excited sequence. This theory also predicts sequence heads at quite low energies for ^{112}Pd and ^{114}Pd. The experimental data for these nuclei is

sparse and they will no doubt be studied in more detail in the future. We look forward to seeing whether or not our predictions prove true.

The qualitative and quantitative success of these simple calculations are encouraging and suggest that this line of approach to the understanding of the Pd and Cd isotopes be pursued. Several improvements will be required. It would, of course, be essentially impossible to deal properly with all the neutrons (and protons) outside whatever really constitutes the collective core and in any case, this quasi-boson approximation looks quite promising. To have any chance to explain the cross-sequence transitions in the Pd nuclei and the apparently stronger interaction (between particle and collective motion) in the Cd nuclei one must i) consider an explicit interaction between the quasi-bosons and the core, ii) allow for explicit interaction among the quasi-bosons, and iii) expand the basis to include other than 0^+ quasi-boson states. The latter is particularly important since one might expect the explicit core-boson interaction to be predominently the coupling to 0 of a core surface coordinate (an angular momentum 2 quantity) to a second rank tensor in the boson space. This interaction will only have non-zero matrix elements for boson states of angular momentum greater than 0. Further, the large number of low spin states seen at moderate energies in ^{106}Pd and ^{104}Pd could likely be the coupling of a single core phonon (2^+) to a 2^+ quasi-boson state. The stretched case, coupled to 4^+, would be expected to mix strongly with the 4^+ collective states and hence alter their positions and branching ratios. One expects the BE2 transition (except for cross-sequence ones) to be dominated by collective effects because of the collective enhancement of the E2 operator. But, the coupling of quasi-boson to collective core states will allow M1 transitions. The total angular momentum operator will be the sum of that due to the core and that due to the bosons. The magnetic dipole operator will be the sum of collective and boson operators with presumably different gyromagnetic ratios. Hence the M1 operator will not be proportional to the total angular momentum operator and M1 transitions can occur. It would appear that a collective core-quasi-boson model has all the necessary ingredients for success; whether this promise is realized or not must await future research.

References:

1. A. S. Davydov and A. A. Chaban, Nucl. Phys. 20, 499 (1960). S. A. Williams and J. P. Davidson, Can. J. Phys. 40, 1423 (1962).
2. S. Cochari, O. Kistner, M. McKeown and G. Scharff-Goldhober, in proceedings of the European Conference on Nuclear Physics, Aix-en-Provence, France, 1972 [J. Phys. (Paris) Suppl. 33, 102 (1972)].
3. R. L. Robinson, F. K. McGowan, P. H. Stelson, W. T. Milner and R. O. Sayer, Nucl. Phys. A124, 553 (1969).

$$H = T_\beta + \frac{\hbar^2}{4B\beta^2} H_{rot}(\gamma, \theta_i) + \frac{C}{2}(\beta - \beta_0)^2$$

$$H_{rot}\, \Psi_{IN}(\theta_i;\gamma) = E_{IN}(\gamma)\, \Psi_{IN}(\theta_i;\gamma)$$

$$H_{rot} = \sum_{k=1}^{3} \frac{I_k^2}{\mathcal{I}_k(\gamma)}$$

$$U_{IN}(\beta) = \frac{\hbar^2}{4B\beta^2} E_{IN}(\gamma) + \frac{C}{2}(\beta - \beta_0)^2$$

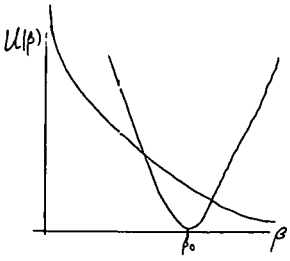

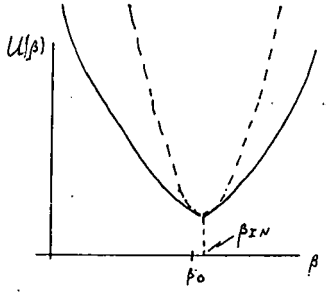

$$U_{IN}(\beta) \simeq U_{IN}(\beta_0) + \frac{C_{IN}}{2}(\beta - \beta_{IN})^2 \qquad U'_{IN}(\beta_{IN}) = 0$$

$$\beta_{IN}^4 - \beta_0 \beta_{IN}^3 - \beta_0^4 \frac{\mu^4}{2}\left(E_{IN} + \frac{3}{2}\right) = 0 \qquad \mu = \frac{1}{\beta_0}\sqrt{\frac{\hbar\omega_0}{C}}, \quad \omega_0 = \sqrt{\frac{C}{B}}$$

$$z \equiv \beta_{IN}/\beta_0\mu$$

$$z^4 - \frac{1}{\mu} z^3 - \frac{1}{2}\left(E_{IN} + \frac{3}{2}\right) = 0 \qquad z_1 \equiv \left[z^4 + \frac{3}{2}\left(E_{IN} + \frac{3}{2}\right)\right]^{1/4}$$

$$D_{\nu_n}\left(\sqrt{2}\, z_1, \frac{\beta - \beta_{IN}}{\beta_{IN}}\right)$$

$$D_{\nu_n}\Big|_{\beta=0} = 0$$

$$E_{IN\,n} = \hbar\omega_0 \left\{ \left(\nu_n + \frac{1}{2}\right)\left(\frac{z_1}{z}\right)^2 + \frac{\left(E_{IN} + \frac{3}{2}\right)}{4z^2}\left[1 + \frac{E_{IN} + \frac{3}{2}}{2z^4}\right]\right\}$$

Parameters: $\hbar\omega_0$, γ, μ

Figure 1. Summary of the Davydov-Chaban model.

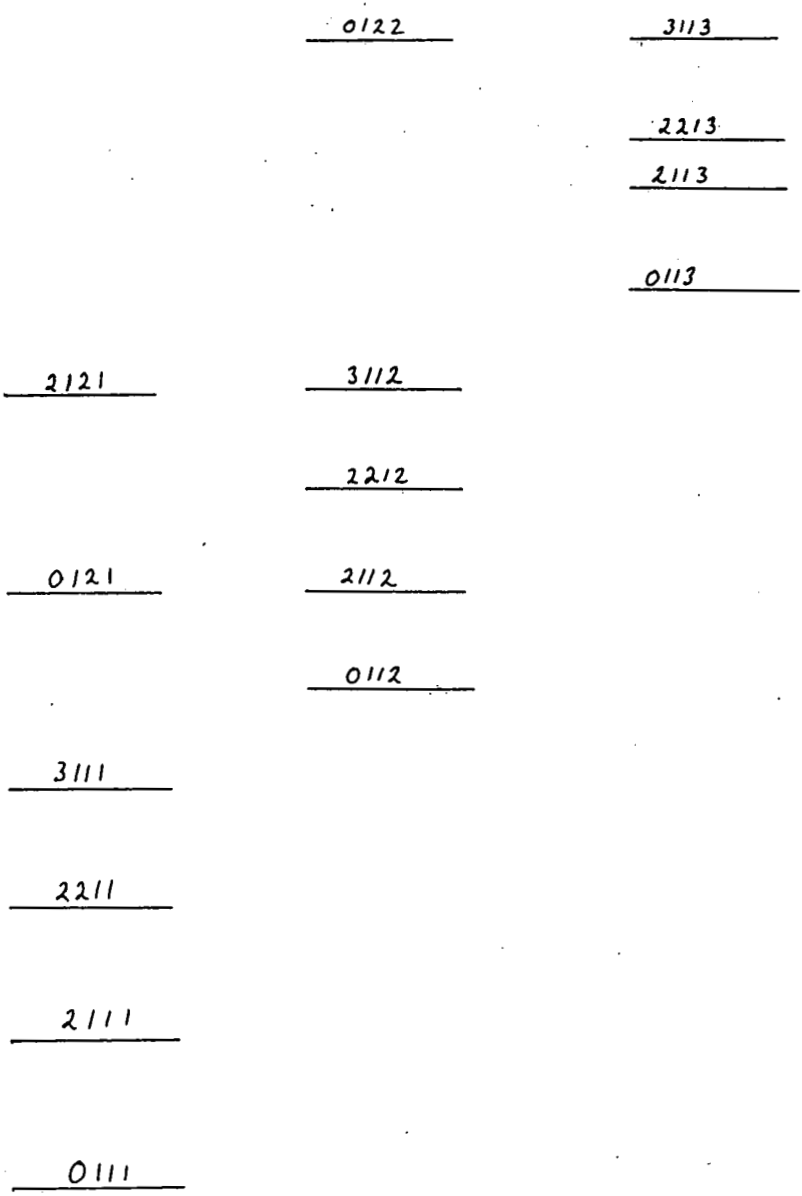

Figure 2. Typical rotation-vibration sequences.

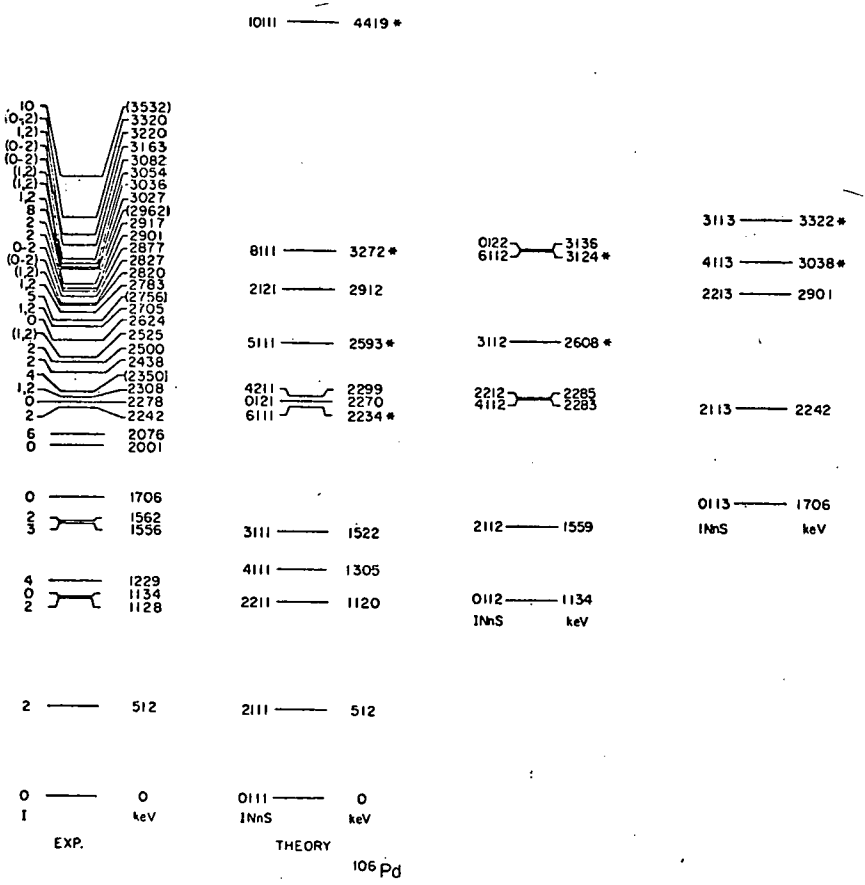

Figure 3. Comparison between theoretical and experimental spectra for ^{106}Pd. New experimental levels are enclosed in parentheses to facilitate their location; starred theoretical levels are not used in determining the model parameters. The theoretical states are labeled by INnS as explained in text. The model parameters are: μ = 0.392; 1st sequence: $\gamma = 25.2^{o}$, $\hbar\omega$ = 2174 keV; 2nd sequence: $\gamma = 22.2^{o}$, $\hbar\omega$ = 1927 keV; 3rd sequence: $\gamma = 24.9^{o}$, $\hbar\omega$ = 2302 keV.

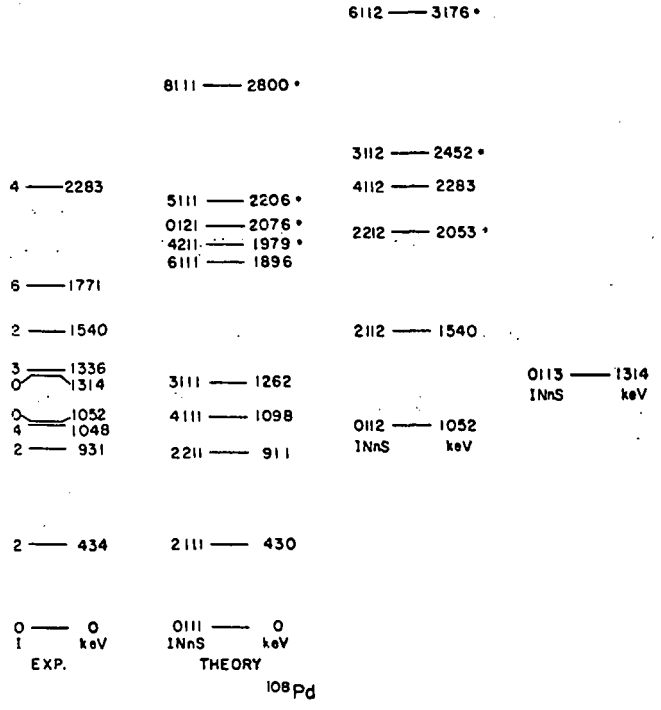

Figure 4. Comparison between theory and experiment for ^{108}Pd. The labels INnS are explained in text and starred levels were not used to determine the model parameters. These parameters were: $\mu = 0.370$; $S = 1$: $\gamma = 26.1^{o}$, $\hbar\omega = 2019$ keV; $S = 2$: $\gamma = 26.7^{o}$, $\hbar\omega = 2264$ keV.

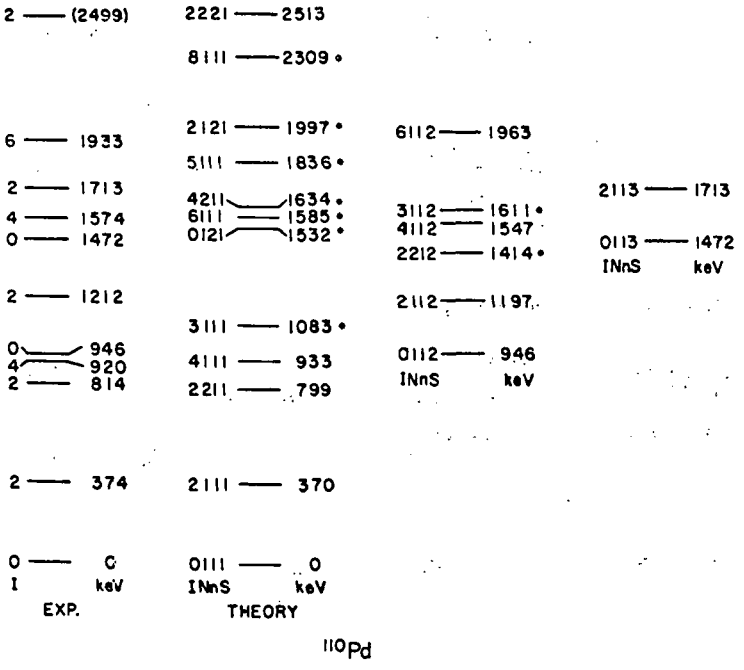

^{110}Pd

Figure 5. Theoretical and experimental spectra for ^{110}Pd. The labels INnS are explained in text. Starred levels were not used in fitting. The model parameters were: $\mu = 0.41$; S = 1: $\gamma = 25.34^{o}$, $\hbar\omega = 1458$ keV; S = 2: $\gamma = 30^{o}$, $\hbar\omega = 941$ keV.

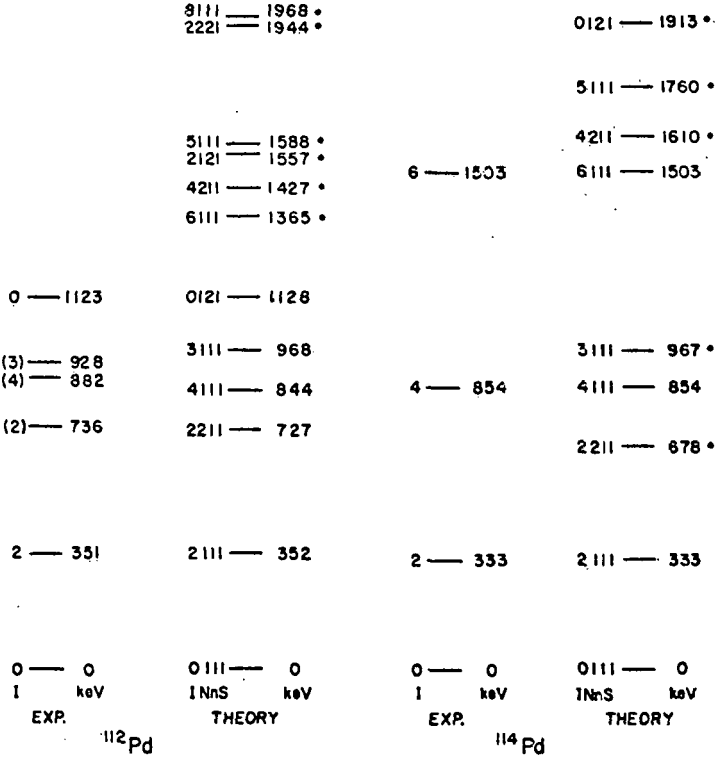

Figure 6. The experimental and theoretical spectra for ^{112}Pd and ^{114}Pd. The parameters for ^{112}Pd are: $\mu = \mp 0.51$, $\gamma = 25.4^{o}$, $\hbar\omega = 994$ keV. For ^{114}Pd the model parameters are: $\mu = 0.33$, $\gamma = 27.3^{o}$, $\hbar\omega = 1925$ keV.

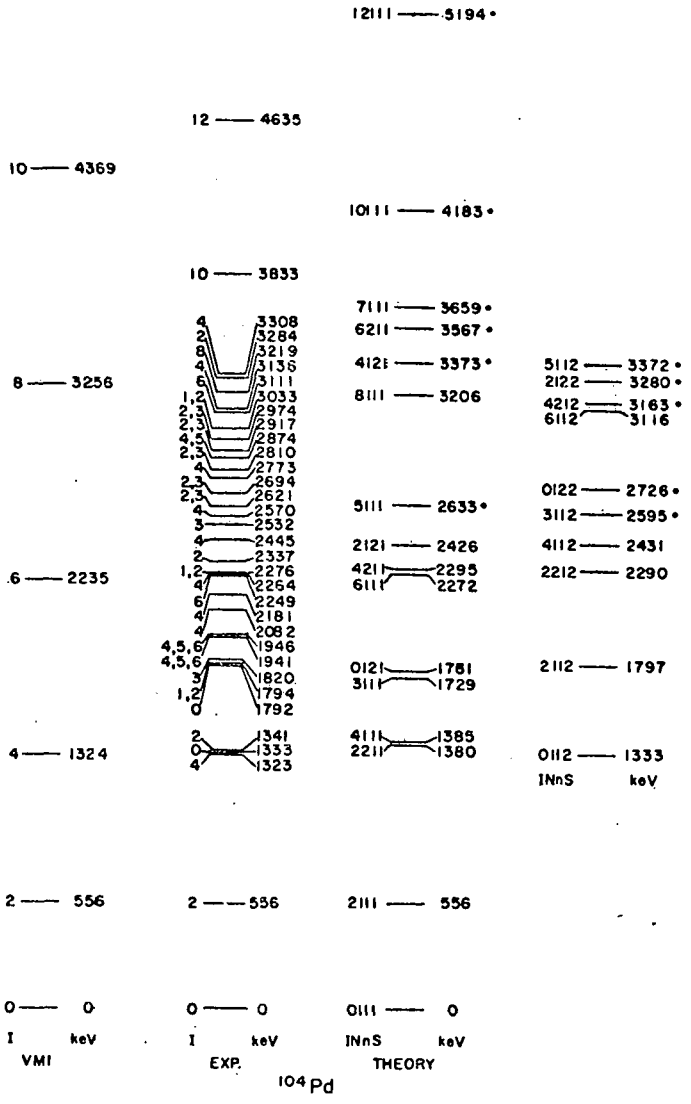

Figure 7. Comparison between theory and experiment for ^{104}Pd. The model parameters are: $\mu = 0.553$; S = 1: $\gamma = 22.3^{o}$, $\hbar\omega = 1487$ keV; S = 2: $\gamma = 25.2^{o}$, $\hbar\omega = 1176$ keV. The spectrum labeled VMI is on the basis of the variable moment of inertia model.

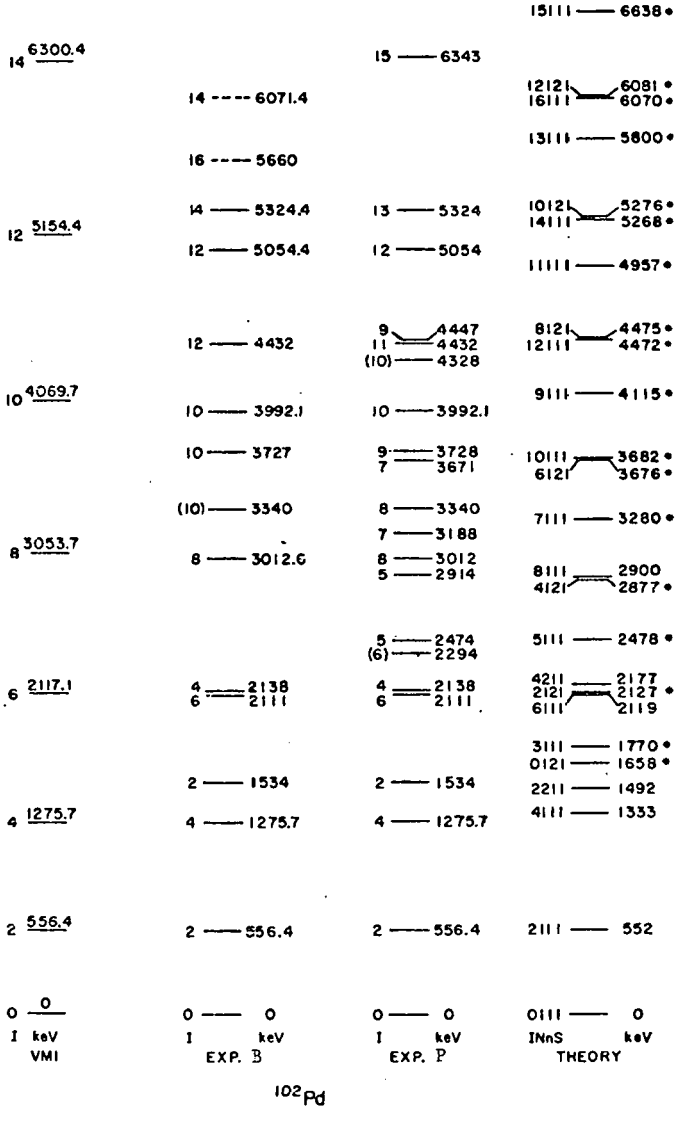

Figure 8. The level structure of ^{102}Pd. The experimental scheme labeled B is that due to the Brookhaven group and that labeled P is proposed by the Purdue group. The starred theoretical levels were not used in fitting the model parameters $\mu = 1.3$, $\gamma = 20.3^{o}$, $\hbar\omega = 1089$ keV.

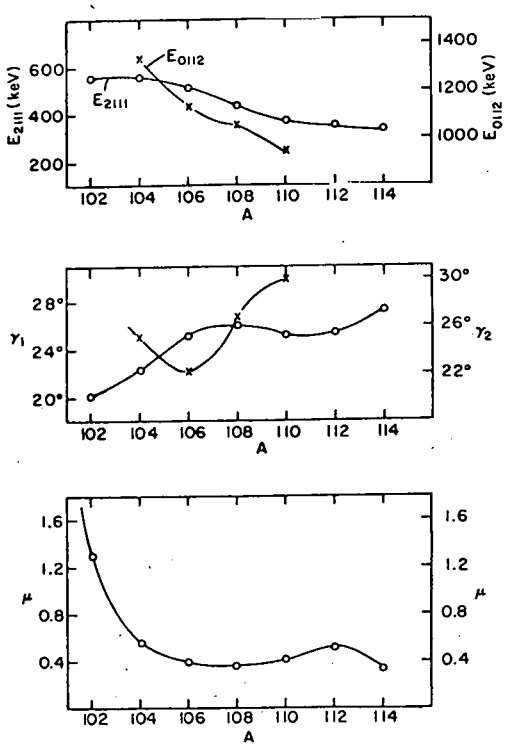

Figure 9. Trends in the model parameters.

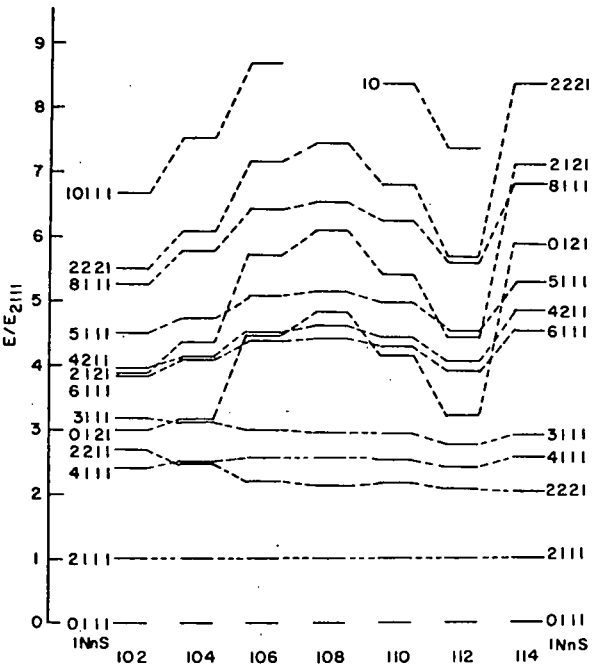

Figure 10. Experimental energies of the low lying states of the even mass Pd isotopes as identified by the model. The ratio with respect to the first 2^+ state (2111) is graphed with E_{2111} set equal to 1 unit.

B(E2) RATIOS

$\frac{I_1N_1n_1S_1 \rightarrow I_2N_2n_2S_2}{I_3N_3n_3S_3 \rightarrow I_4N_4n_4S_4}$	104	Theoretical Value / Experimental Value 106	108	110
$\frac{2211 \rightarrow 2111}{2111 \rightarrow 0111}$	0.70	$\frac{1.04}{0.96 \pm 0.14}$	$\frac{1.10}{1.8 \pm 0.4}$	$\frac{1.08}{0.99 \pm 0.19}$
$\frac{4111 \rightarrow 2111}{2111 \rightarrow 0111}$	1.76	$\frac{1.58}{1.55 \pm 0.23}$	$\frac{1.57}{1.84 \pm 0.18}$	$\frac{1.57}{1.68 \pm 0.17}$
$\frac{2211 \rightarrow 2111}{2211 \rightarrow 0111}$	10	$\frac{24.3}{38 \pm 6}$	$\frac{29}{79 \pm 19}$ [a]	$\frac{27}{70 \pm 13}$
$\frac{4111 \rightarrow 2111}{2211 \rightarrow 2111}$	2.5	$\frac{1.52}{1.62 \pm 0.31}$	$\frac{1.43}{1.04 \pm 0.27}$ [a]	$\frac{1.45}{1.72 \pm 0.36}$
$\frac{0112 \rightarrow 2111}{2111 \rightarrow 0111}$	4.93	$\frac{5.05}{0.63 \pm 0.14}$	$\frac{5.0}{0.89 \pm 0.17}$	$\frac{4.9}{0.63 \pm 0.10}$

[a] If the mixing ratio is -0.73 ± 0.10 the experimental values become 28 ± 8 and 2.95 ± 0.91 respectively.

Figure 11. Comparison between the theoretical and experimental B(E2) ratios for transitions between the indicated states.

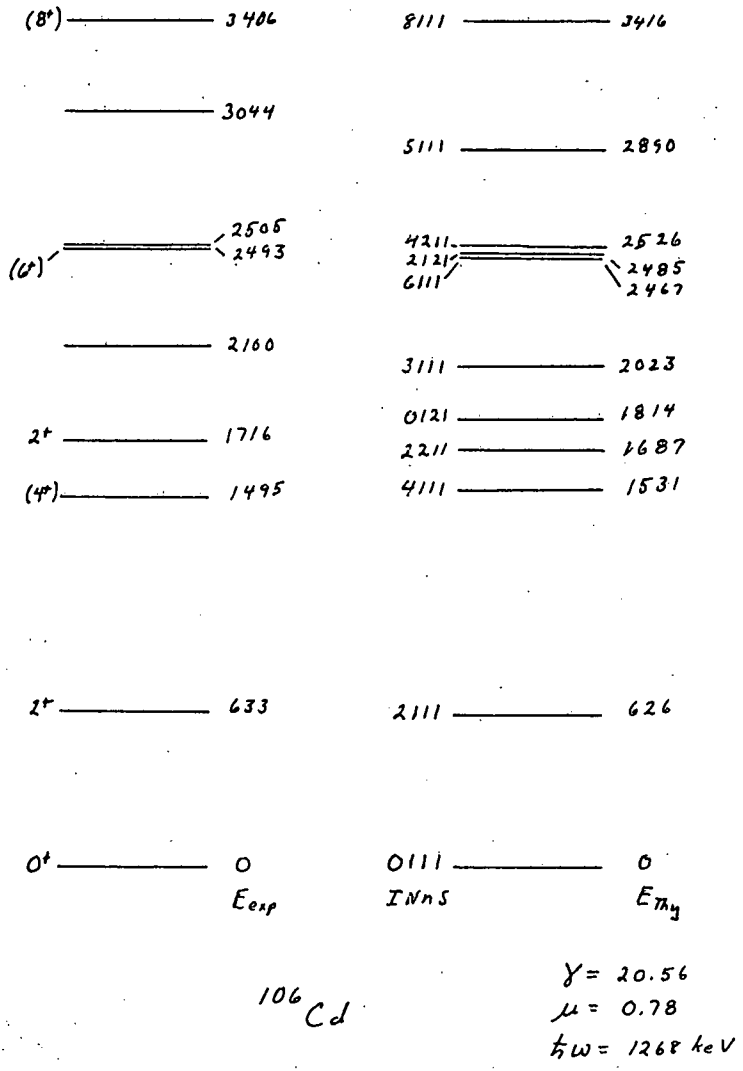

Figure 12. Comparison between theory and experiment for ^{106}Cd.

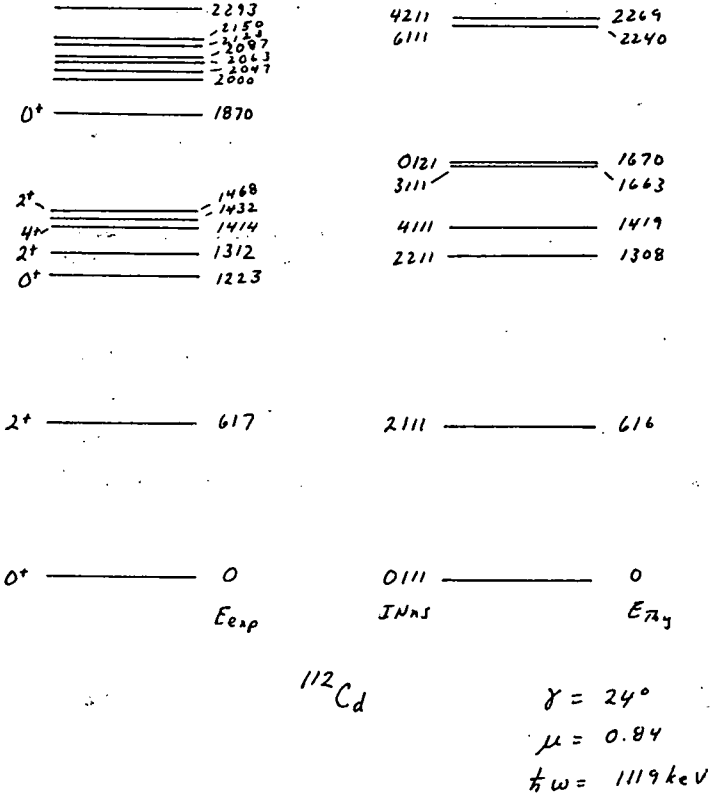

Figure 13. Comparison between theory and experiment for ^{112}Cd.

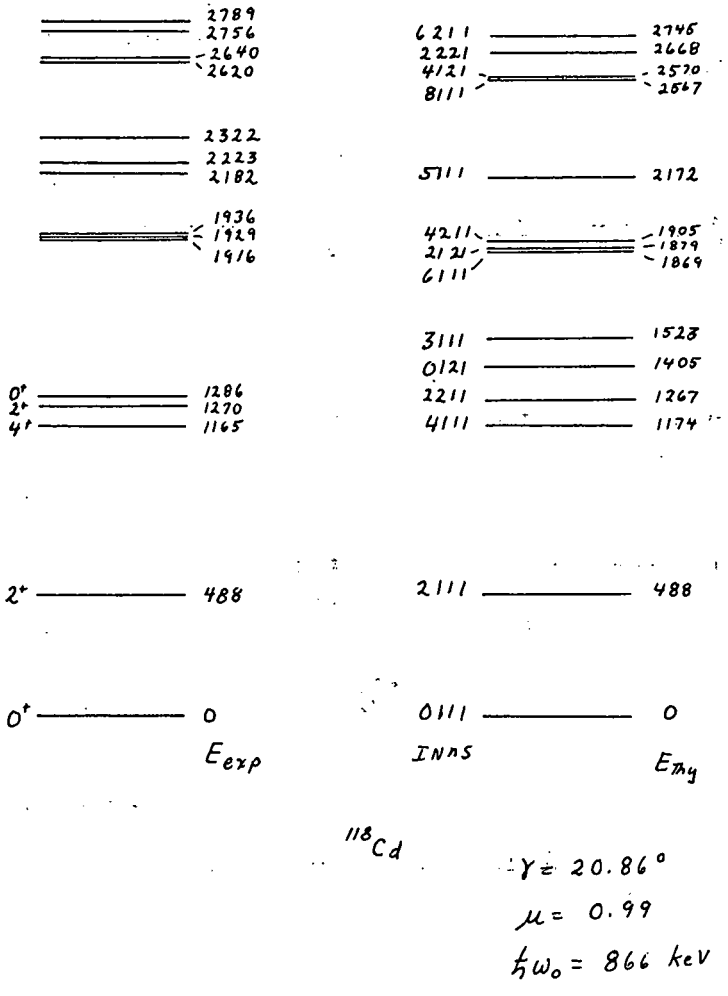

Figure 14. Theory and experiment for ^{118}Cd.

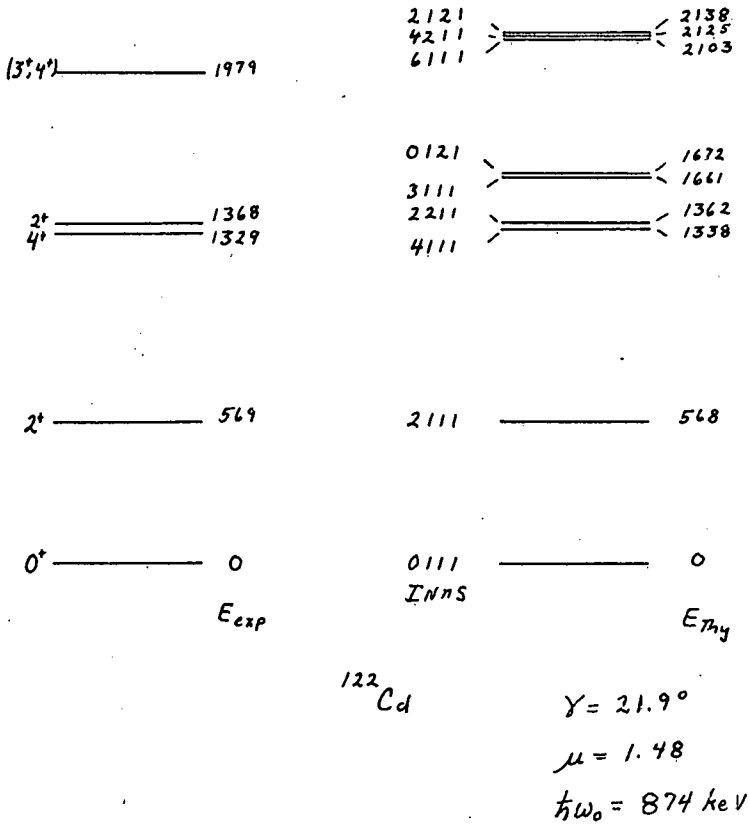

Figure 15. Theory and experiment for ^{122}Cd.

	106	108	110	112	114	116	
$\frac{BE2(2_i \rightarrow 2_1)}{BE2(2_1 \rightarrow 0)}$	0.54 / 0.58 ± 0.17	0.63 / 1.06 ± 0.32	0.86 / 0.92 ± 0.28	0.93 / 1.10 ± 0.33	0.91 / 1.05 ± 0.32	0.75 / 0.97 ± 0.29	Theory / Exp
$\frac{BE2(4_1 \rightarrow 2_1)}{BE2(2_1 \rightarrow 0)}$	1.88 / 1.0 ± 0.3	1.89 / 0.6 ± 0.2	1.88 / 1.4 ± 0.2	1.86 / 1.8 ± 0.2	1.88 / 1.8 ± 0.2	1.88 / 1.6 ± 0.4	
$\frac{BE2(2_2 \rightarrow 2_1)}{BE2(2_2 \rightarrow 0)}$	8.7	9.6 / 10 ± 3	14 / 24 ± 8	22 / 33 ± 8	15 / 33 ± 10	11 / 19 ± 6	

Figure 16. BE2 ratios for the Cd isotopes.

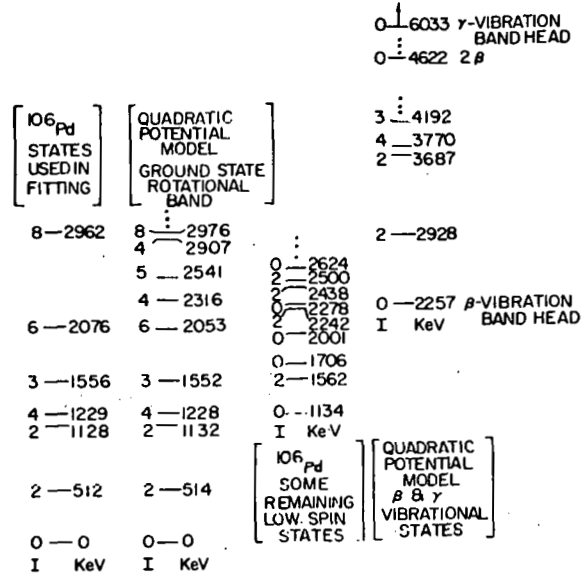

Figure 17. Application of the quadratic potential model to ^{106}Pd. The experimental levels used in determining the parameters are shown at the left. Some of the other experimental levels are also indicated as well as the model predictions.

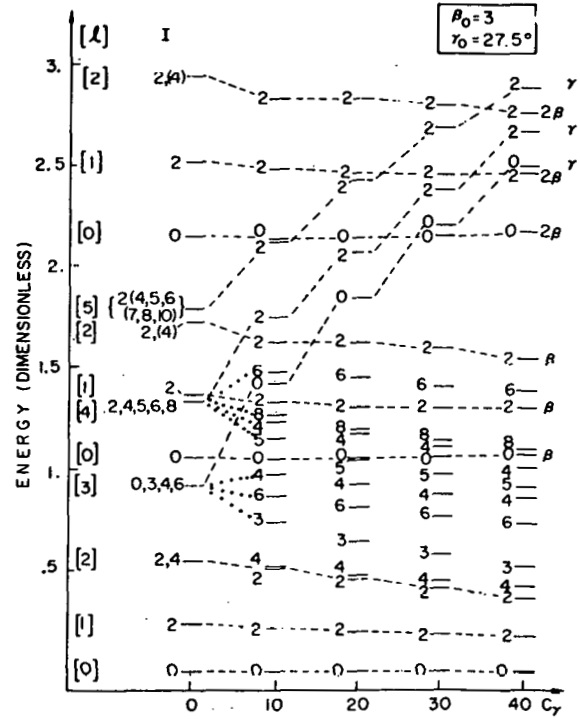

Figure 18. Development of selected levels of the quadratic potential model. At $C_\gamma = 0$, ℓ is a good quantum number and is listed in square braces. The development is not shown for levels whose spins are placed in parentheses. The (0,2,2) states of the ground state, γ-vibrational, and first two β-vibrational states are traced with dashed lines.

TWO SIMPLE-MINDED ATTACKS

$|108\rangle = \theta^\dagger|106\rangle \qquad |104\rangle = \tilde{\theta}|106\rangle \qquad \theta^\dagger\tilde{\theta}|106\rangle = |106\rangle$

$E = 16634 - 15767 = 867$ keV

	$E(\theta^\dagger\theta)$	E^{1st}	By Scaling to 104
104	994	1333	1333
106	867	1134	1163
108	810	1052	1066
110	879	946	1179

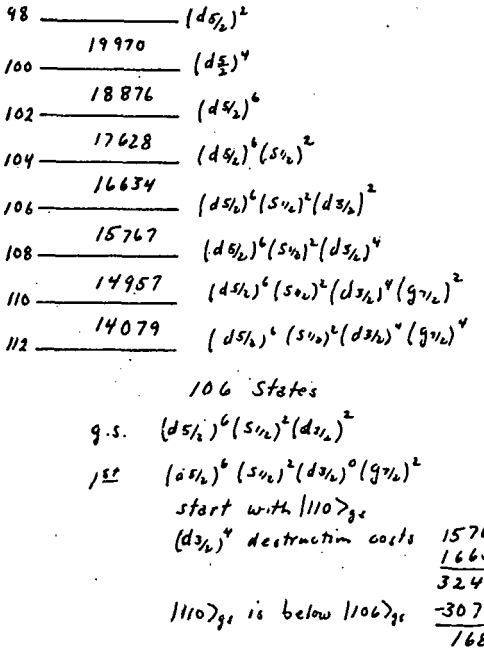

106 states

g.s. $(ds_{5/2})^6(s_{1/2})^2(d_{3/2})^2$

1st $(ds_{5/2})^6(s_{1/2})^2(d_{3/2})^0(g_{7/2})^2$

start with $|110\rangle_{gs}$

$(d_{3/2})^4$ destruction costs 15767 + 16634 = 32401

$|110\rangle_{gs}$ is below $|106\rangle_{gs}$ −30718

1683 keV

2nd $(ds_{5/2})^6(s_{1/2})^0(d_{3/2})^4$ 17628 − 15767 = 1861 keV

3rd $(ds_{5/2})^6(s_{1/2})^0(d_{3/2})^2(g_{7/2})^2$ 2676 keV

4th $(ds_{5/2})^4(s_{1/2})^2(d_{3/2})^4$ 3109 keV

$$\begin{pmatrix} 1683-\Delta & \delta \\ \delta & 1861-\Delta \end{pmatrix} \rightarrow \begin{pmatrix} 1134 & 0 \\ 0 & 1706 \end{pmatrix}$$

$\Delta = 352$ keV

$\delta = 272$ keV

$$\begin{pmatrix} 2676-\Delta & \delta \\ \delta & 3109-\Delta \end{pmatrix} \rightarrow \begin{pmatrix} 2190 & 0 \\ 0 & 2890 \end{pmatrix}$$

Figure 19. Two simple approaches to the 0^+ sequence heads.

Pd	C (keV)	G (keV)	1st Sequence (keV) Thy	1st Sequence (keV) Exp	2nd Sequence (keV) Thy	2nd Sequence (keV) Exp	
102	-2084	644	3157		4697		extrapolation
104	-1674	632	1340	1333	2283		extrapolation
106	-930	620	1128	1133	1708	1706	fitted
108	-112	608	955	1052	1436	1314	fitted
110	-595	597	946	946	1473	1472	fitted
112	-1042	587	622		1419		extrapolation
114	-1492	576	1190		2205		extrapolation

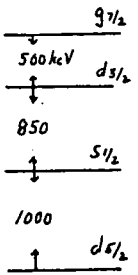

$$V_{ij} = C\, b^{-4} \left[r_i^2 Y_2(i)\; r_j^2 Y_2(j) \right]^0 - G\,(2J_j+1)\,\delta_{ij}$$

Figure 20. Zero coupled pair calculations for the Pd isotopes.

Proceedings of the Brookhaven National Laboratory Workshop on ISOL Systems, Oct. 31-Nov. 1, 1977

Studies of ^{12}Be and Other Off-Stability Nuclei*

David E. Alburger

Brookhaven National Laboratory, Upton, New York 11973

Abstract

In collaboration with the Tandem Van de Graaff staff at the University of Pennsylvania the reaction ^{10}Be(t,p)^{12}Be at E_t = 12 MeV has been used to study the properties of ^{12}Be. The first excited state of ^{12}Be has been found to lie at 2.110 ± 0.015 MeV and to have J = 2 from p,γ angular correlation measurements. Using a chopped beam the search for delayed neutrons from the decay of ^{12}Be was negative. However, the decay curve for β rays can be fitted only if a half-life component of about 25 msec for ^{12}Be is included along with the activities ^{12}B, ^{9}Li, and ^{8}Li known to be present. A review of the search for new T_z = +5/2 isotopes in the s-d shell at the Brookhaven Tandem Van de Graaff is presented and recent results on the T_z = +3 nucleus ^{34}Si, formed in the ^{18}O(^{18}O,2p)^{34}Si reaction, are outlined. Utilizing new ion-source techniques to form a beam of ^{9}Be ions the reaction ^{48}Ca(^{9}Be,pn)^{55}V has been used to find and study the new isotope ^{55}V of 6 sec half-life. The extension of these techniques to higher Z may be possible although recent studies of heavy-ion reactions indicate that the cross sections may be very small.

*Research supported by the Department of Energy under Contract No. EY-76-C-02-0016.

I. Introduction

The search for new isotopes and the study of their properties is very useful for testing the predictions of various theoretical models. Spectroscopic information on levels, spins, parities, and lifetimes can be compared with shell model predictions, for example. Mass values of nuclei far from the line of stability can test the theoretical predictions of the Garvey-Kelson formulation or others such as the modified shell model. The measured values of masses provide new input information for refining the predictions of masses even farther from stability.

In the present paper two experimental programs are discussed, the first being a series of investigations of the nucleus ^{12}Be and the second a review of earlier work on $T_z = +5/2$ nuclei in the s-d shell at Brookhaven and new results on ^{34}Si and ^{55}V both found recently using heavy-ion reactions at the Tandem Van de Graaff.

II. Studies of ^{12}Be

A. Background

^{12}Be is a $T_z = +2$ nucleus that lies 3 neutrons away from the only stable Be isotope. Its ground state has analogs in ^{12}B at 12.71 MeV and in ^{12}C at 27.61 MeV as indicated in Fig. 1. Studies[1] of the ^{14}C(p,t)^{12}C and ^{14}C(p,^{3}He)^{12}B reactions showed that the second T = 2 state in both ^{12}B and ^{12}C lies about 2 MeV above the first T = 2 state, but the t and ^{3}He angular distribution data, while seeming to favor J = 0 for the upper state, were not definitive. Meanwhile Barker[2] has predicted that the second T = 2 state in A = 12 should have J = 0.

The most straightforward way to settle the question of the spin of the second T = 2 state is to form the first excited state of ^{12}Be using the

^{10}Be(t,p)^{12}Be reaction. Since the ground state of ^{12}Be is even-even and there-

e must necessarily have $J^{\pi} = 0^{+}$ then the first excited state can decay by γ-ray emission only if $J \neq 0$. If γ rays are emitted in the decay, then a measurement of the p,γ angular correlation can establish the spin.

Two previous experiments have been performed that have measured the mass of ^{12}Be but have given conflicting evidence for the position of the first excited state. Using the ^{7}Li(^{7}Li,2p)^{12}Be reaction, Howard, Stokes, and Erkkila[3] found a mass excess of 24.95 ± 0.10 MeV for ^{12}Be and weak evidence for an excited state at 0.81 ± 0.10 MeV. In the other experiment Ball et al.[4] studied the reaction ^{14}C(^{18}O,^{20}Ne)^{12}Be and obtained a ^{12}Be mass excess of 25.05 ± 0.05 MeV in agreement with the Los Alamos result, but they found that the ^{12}Be first-excited state is at 2.09 ± 0.05 MeV with no evidence for a state at 0.81 MeV.

Only one experiment has been reported on the decay of ^{12}Be. Using GeV proton bombardment of various targets Poskanzer, Reeder, and Dostrovsky[5] reported a delayed neutron activity having a half-life of 11.4 ± 0.5 msec which was attributed to ^{12}Be decay. A β-ray branching of 7% to neutron-emitting states was estimated. However, the assignment was based in part on the assumed particle-instability of ^{11}Li, and it was shown shortly afterwards by Poskanzer and others[6] that ^{11}Li is not only particle stable but branches 61% to delayed neutron-

tting states and has $T_{1/2}$ = 8.5 msec. The assignment of ^{12}Be was thereby placed in doubt. If ^{12}Be were a delayed neutron emitter it should be relatively easy to detect the neutrons and to measure the half-life by forming it in the ^{10}Be(t,p)^{12}Be reaction.

B. ^{10}Be(t,p)^{12}Be Coincidence Experiments

Experiments on the ^{10}Be(t,p)^{12}Be reaction were made possible through the unique combination of ^{10}Be targets that had been fabricated at Brookhaven by

D. R. Goosman and the triton beam produced recently at the University of Pennsylvania Tandem Van de Graaff. Staff members at Penn who collaborated in this work include D. P. Balamuth, H. T. Fortune, J. M. Lind, L. Mulligan, K. C. Young, R. Middleton, and R. W. Zurmühle.

The spectrometer used for the p,γ coincidence measurements has been described previously.[7] Protons are detected at 0° by magnetic deflection onto a position-sensitive counter and γ rays in four NaI(Tℓ) crystals at various angles around the target. The ^{10}Be target was a 94% enriched sample of ^{10}BeO 100 μg/cm^2 thick deposited on a 1.0-mg/cm^2 thick Pt backing. This was bombarded with a 12-MeV beam of tritons.

Figure 2 shows the singles and coincidences proton spectra from which the energy of the ^{12}Be first excited state is measured to be 2.110 ± 0.015 MeV. The coincidence γ-ray spectrum in Fig. 3 immediately demonstrates that J ≠ 0 and in Fig. 4 the angular correlation clearly establishes J = 2 for this excited state.

C. β Decay Experiments on ^{12}Be

A fast chopper, consisting of a rotating disk with slots, was set up on the main beam line of the Penn Tandem Van de Graaff in order to investigate the delayed activity following the ^{10}Be + t bombardment. The ^{10}BeO target had a thickness of 600 μg/cm^2 on a thick Pt backing and this was placed in a 2.5-cm dia. glass target chamber. A 12-MeV triton beam activated the target.

In the first test a ^{3}He proportional counter was placed a few cm from the target and the entire target-detector assembly was surrounded with paraffin blocks. Counts due to thermalized neutrons were multiscaled following each beam burst on the target. The sequence totaled about 475 msec consisting of 35 msec of bombardment, a wait of 10 msec, and counting at 0.8 msec per channel for 500 channels. Delayed neutrons were observed, but the decay curve exhibited only a

single component corresponding to the 178-msec decay of ^{9}Li formed in the ^{10}Be(t,α)^{9}Li reaction. An upper limit of about 1% was estimated for possible branching of ^{12}Be to delayed neutron-emitting states, assuming ^{12}Be has a half-life in the 10-30 msec range.

By changing to a 7.5-cm dia. by 5-cm thick plastic scintillator placed next to the glass target chamber, the decay of β rays was studied using the same timing regime. One expects 20-msec ^{12}B from the ^{10}Be(t,n)^{12}B reaction, ^{9}Li of 178 msec as mentioned above, and 0.8 sec ^{8}Li from the ^{9}Be(t,α)^{8}Li reaction. The resulting decay curves for β-ray biases of 3 and 6 MeV could not be fitted assuming only these three components but fits were satisfactory if a fourth component of about 25 msec was also assumed to be present. The initial intensity of the 25-msec activity would be about 1/3 that of the ^{12}B and 1/4 that of the ^{9}Li. The latter ratio agrees within a factor of 2 with the relative (t,p) and (t,α) cross sections on ^{10}Be from multi-gap spectrograph measurements (see below). Hence it is tentatively proposed that ^{12}Be has a half-life of about 25 msec.

D. Multi-gap Spectrograph Measurements

Several exposures in the Penn multi-gap magnetic spectrograph were made on the ^{10}Be + t reaction at E_t = 15 MeV in order to measure the ground-state Q-value in the (t,p) reaction, and therefore the mass of ^{12}Be, as well as the locations of excited states. These same exposures allow a study of the ^{10}Be(t,α)^{9}Li reaction to be made and relative (t,p) and (t,α) cross sections to be determined.

At the present time the analysis of the multi-gap data is not yet completed. Qualitative observations indicate no excited states in ^{12}Be below the 2.110-MeV state reported above. A rough measurement of the relative (t,p) and

(t,α) cross sections is also mentioned above.

It is expected that a mass value will be obtained for ^{12}Be that will have an accuracy of ∿ ± 10 keV.

III. The Search for New Isotopes at Brookhaven

A. The program on T_z = +5/2 Nuclei in the s-d Shell

When the Tandem Van de Graaff facility was brought into operation at Brookhaven National Laboratory in 1970 a general program was planned on the study of radioactive isotopes that could be produced in heavy-ion reactions. A target-transfer or "rabbit" system[8] was constructed for this purpose and as an initial test the production and study of ^{20}O formed in the ^{18}O(^{18}O,^{16}O)^{20}O reaction was carried out. The technique consisted of activating a target of $Ta_2{}^{18}O_5$ clamped on the rabbit, transferring it to a shielded area, and counting γ and β radiations with Ge(Li) and plastic detectors. Half-lives could be measured by storing data in successive time bins in a computer. A timer-programmer[9] designed and built at Brookhaven was particularly useful in all of this work.

In addition to the ^{20}O numerous weak activities were found to be produced in the ^{18}O + ^{18}O reaction with $E_{^{18}O} \tilde{=}$ 42 MeV. The most interesting outcome of this first study was the observation of three γ rays that decayed with a 6-sec half-life and could not be attributed to any known activity. It was subsequently determined[8] that the new isotope ^{33}Si was being formed in the ^{18}O(^{18}O,2pn)^{33}Si reaction. The decay scheme was established and the mass was found from the end-point of β rays entering a plastic scintillator in coincidence with γ rays. Comparisons of the decay scheme were made with the shell model, while the mass excess, established with an accuracy of ± 50 keV, was compared with the Garvey-Kelson mass formulation and shown to differ by 420 keV from the prediction.

The ^{33}Si β spectrum in coincidence with γ rays is shown in Fig. 5.

After realizing the potentialities of heavy-ion reactions for producing new isotopes, a program was set up on the $T_z = +5/2$ nuclei from ^{21}O to ^{35}P as indicated in the portion of the chart of nuclei shown in Fig. 6. Collaborators in this work included D. R. Goosman, C. N. Davids, and J. C. Hardy. In order to form the activities, various reactions were used as indicated in Table I. For the work on ^{25}Ne a gas transfer system was used instead of the rabbit.

To summarize the extensive results of these investigations the new isotopes ^{23}F, ^{29}Mg, ^{31}Al, ^{33}Si, and ^{35}P were established along with their properties including mass values. Masses, half-lives, and spectroscopic properties were also measured for ^{25}Ne and ^{27}Na which had meanwhile been discovered at other laboratories. Four attempts were made to find ^{21}O without success. The decay schemes of these new isotopes in general agreed quite well with the predictions of the shell model but the mass excesses exhibited a systematic departure from the Garvey-Kelson mass formulation as shown in the upper part of Fig. 7. Meanwhile, new theoretical calculations of these masses using a modified shell model have been carried out by Wilcox et al.[10] As may be seen in the lower part of Fig. 7, the agreement of these predictions with experimental values is very much better. A new value for the ^{21}O mass excess has recently been measured by Ball et al.[11] bringing its value down by 1.2 MeV in line with the others in the lower part of Fig. 7.

B. The Discovery of ^{34}Si

Several other weak γ rays (429, 1179, and 1608 keV) in the delayed spectrum following the $^{18}O + ^{18}O$ reaction remained unassigned until recently. It was suspected that these γ rays belonged to the decay of the $T_z = +3$ nucleus

^{34}Si produced in the ^{18}O(^{18}O,2p)^{34}Si reaction, but this could not be proved since the energy levels of the daughter nucleus ^{34}P were not known. However, a recent study[12] at Los Alamos of the ^{34}S(t,^{3}He)^{34}P reaction established the energies of five excited states of ^{34}P, the first two states being at 423 ± 10 keV and 1605 ± 10 keV.

In collaboration with A. M. Nathan a new investigation[13] of activities from the ^{18}O + ^{18}O reaction was undertaken. The techniques were similar to those used earlier. Comparison of the three un-assigned γ-ray energies with the ^{34}P levels mentioned above identified the activity as ^{34}Si; the resulting decay scheme is shown in Fig. 8. The half-life of ^{34}Si is 2.77 ± 0.20 sec as obtained from the data shown in Fig. 9. Finally, the mass was measured from the end point of β rays in coincidence with γ rays giving a mass excess of -19850 ± 300 keV. This agrees within 200 keV with the predictions of two shell-model calculations.

C. Investigation of ^{55}V

The extension of isotope searches to somewhat higher Z has been made possible by the voltage upgrading of the Tandem Van de Graaff at Brookhaven and by the recent development of new ion-source techniques. Middleton[14] has shown that moderately intense beams of negative hydrides such as BeH^- or CaH^- can be produced by the introduction of ammonia vapor into a UNIS-type source. These beams have the advantage over a beam such as BeO^- in that a larger proportion of the energy of the BeH^- ion residues in the Be atom prior to stripping after the first stage of acceleration.

In collaboration with E. K. Warburton, A. M. Nathan, and J. W. Olness, a search was made for the previously unknown nucleus ^{55}V formed in the ^{48}Ca(^{9}Be,pn)^{55}V reaction. Following the methods described above, the decay

scheme of ^{55}V was established[15] as shown in Fig. 10. The ^{55}V half-life was found to be 6.54 ± 0.15 sec and its mass excess of 49152 ± 100 keV is in exact agreement with a modified shell-model calculation.

D. Unsuccessful Isotope Searches

Although quite a few new isotopes have been found and studied in the program at the Brookhaven Tandem Van de Graaff there have been some unsuccessful searches that should be discussed. The four experiments on ^{21}O were mentioned above. Other activities, the reactions used, and the type of radiation measured are summarized in Table II. In all cases there is information on levels in the daughter nucleus which would presumably allow the identification to be made. The failure to observe any of these activities can be attributed either to cross sections too low to permit the characteristic radiations to be observed above the background, or to β decay leading mostly to the ground state of the daughter nucleus. Due to the presence of so many different activities produced in these heavy-ion reactions it is generally impossible to identify a particular activity unless there is a reasonable amount of β-ray branching to an excited state, at least using the methods at our disposal. Mass and Z separation of the products would of course be a great help in sorting out the exotic nuclei formed in heavy-ion reactions. Thus the discovery and study of the isotopes listed in Table II poses a challenge for the future.

Future extension to higher Z

With the present availability of higher terminal voltages on the MP Tandem Van de Graaffs at Brookhaven and the new ion-source techniques mentioned above, tentative plans have been made to investigate off-stability nuclei at higher Z utilizing techniques similar to those discussed above. A schematic representation of the situation is illustrated in Fig. 11. This shows that,

due to the curvature of the line of β stability on a plot of Z versus N, the compound nucleus in the $^{40}Ca + ^{40}Ca$ reaction, i.e. ^{80}Zr, lies on the proton-rich side of the valley of stability. It might be possible to produce various new isotopes in that region, particularly since the MP-7 Tandem accelerator now operates at 14 MV on the terminal and can produce Ca beams well above the Coulomb barrier for the Ca + Ca reaction.

There have been some very recent time-of-flight experiments by Wegner[16] and others at Brookhaven that have unfortunately indicated very low cross sections for producing exotic nuclei in this region. Using the reaction $^{40}Ca + ^{35}Cl$ to reach the neutron-deficient side of the valley and $^{48}Ca + ^{37}Cl$ to reach the neutron-excess side, Wegner's group has looked for the production of off-stability isotopes. Preliminary analysis suggests that the compound nuclei quickly boil off particles returning the final nucleus close to, or in the valley of stability. The final outcome of these experiments may influence the direction of the programmatic search for new radioactive isotopes. But even if cross sections are small it should be pointed out that the detection of delayed radiations is a sensitive way to find new isotopes.

References

1. D. Ashery, M. S. Zisman, G. W. Goth, G. J. Wozniak, R. B. Weisenmiller, and J. Cerny, Phys. Rev. C13, 1345 (1976).
2. F. C. Barker, J. Phys. G: Nucl. Phys. 2, L45 (1976).
3. H. H. Howard, R. H. Stokes, and B. H. Erikkila, Phys. Rev. Lett. 27, 1086 (1971).
4. G. C. Ball, J. G. Costa, W. G. Davies, J. S. Forster, J. C. Hardy, and A. B. McDonald, Phys. Lett. B49, 33 (1974).
5. A. M. Poskanzer, P. L. Reeder, and I. Dostrovsky, Phys. Rev. 138, B18 (1965).
6. A. M. Poskanzer, S. W. Cosper, E. K. Hyde, and J. Cerny, Phys. Rev. Lett. 17, 1271 (1966). See also, R. Klapisch, C. Thibault-Philippe, C. Detraz, J. Chaumont, R. Bernas, and E. Beck, Phys. Rev. Lett. 23, 652 (1969).
7. R. W. Zurmühle, P. F. Hinrichsen, C. M. Fou, C. R. Gould, and G. P. Anatassiou, Nucl. Instr. and Methods 71, 311 (1969).
8. D. R. Goosman and D. E. Alburger, Phys. Rev. C5, 1252 (1972); ibid. C6, 825 (1972); D. R. Goosman, C. N. Davids, and D. E. Alburger, ibid C8, 1324 (1973).
9. G. E. Schwender, D. R. Goosman, and K. W. Jones, Rev. Sci. Instr. 43, 832 (1972).
10. K. H. Wilcox, N. A. Jelley, G. J. Wozniak, R. B. Weisenmiller, H. L. Harney, and J. Cerny, Phys. Rev. Lett. 30, 866 (1973).
11. G. C. Ball, W. G. Davies, J. S. Forster, and H. R. Andrews, Bull. Am. Phys. Soc. 21, 579 (1976).
12. F. Ajzenberg-Selove, E. B. Flynn, S. Orbesen, and J. W. Sunier, Phys. Rev. C15, 1 (1977).
13. A. M. Nathan and D. E. Alburger, Phys. Rev. C15, 1448 (1977).

14. R. Middleton, private communication.

15. A. M. Nathan, D. E. Alburger, J. W. Olness, and E. K. Warburton, Phys. Rev. C (in course of publication).

16. H. E. Wegner, private communication.

Table I. Compound reactions making T_z = +5/2 nuclides in the s-d shell.

Nuclide	Reaction	Nuclide	Reaction
^{21}O	$^{10}Be(^{13}C,2p)^{21}O$	^{29}Mg	$^{18}O(^{13}C,2p)^{29}Mg$
	$^{9}Be(^{18}O,\alpha 2p)^{21}O$		$^{14}C(^{18}O,2pn)^{29}Mg$
^{23}F	$^{18}O(^{7}Li,2p)^{23}F$	^{31}Al	$^{18}O(^{18}O,\alpha p)^{31}Al$
	$^{10}Be(^{18}O,\alpha p)^{23}F$		$^{15}N(^{18}O,2p)^{31}Al$
^{25}Ne	$^{9}Be(^{18}O,2p)^{25}Ne$	^{33}Si	$^{18}O(^{18}O,2pn)^{33}Si$
^{27}Na	$^{11}B(^{18}O,2p)^{27}Na$	^{35}P	$^{18}O(^{19}F,2p)^{35}P$

Table II. Summary of unsuccessful isotope searches.

Isotope	Reaction	Measurement
^{15}B	$^{10}Be(^{7}Li,2p)^{15}B$	n
^{17}C	$^{10}Be(^{9}Be,2p)^{17}C$	γ
^{19}N	$^{10}Be(^{11}B,2p)^{19}N$	n,γ
^{21}O	$^{10}Be(^{13}C,2p)^{21}O$	γ
	$^{9}Be(^{18}O,2p\alpha)^{21}O$	γ
^{26}Ne	$^{10}Be(^{18}O,2p)^{26}Ne$	γ
^{30}Mg	$^{14}C(^{18}O,2p)^{30}Mg$	γ

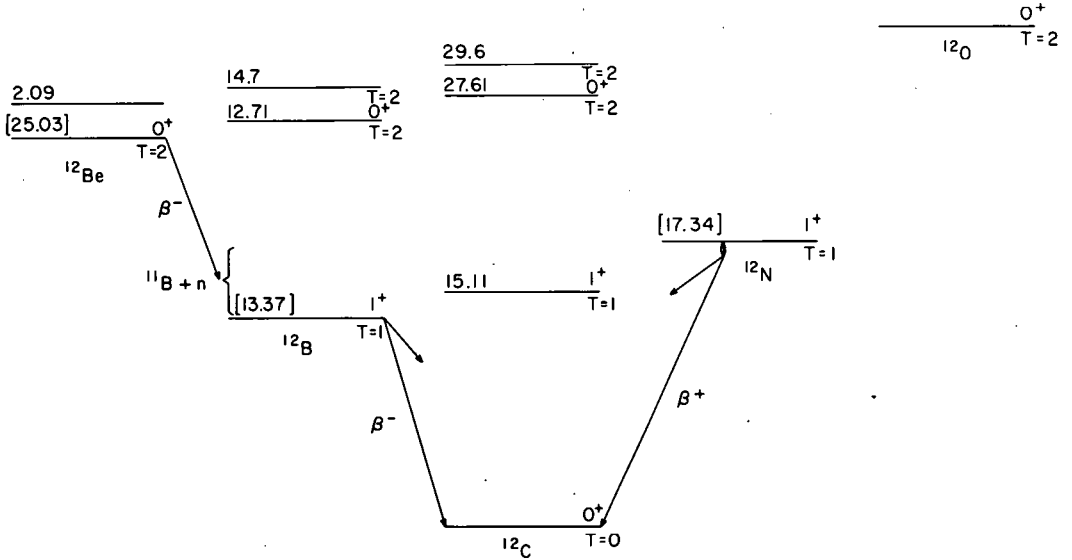

Figure 1. The T = 2 isospin quintet in A = 12 showing the positions of the second T = 2 states in ^{12}Be, ^{12}B, and ^{12}C.

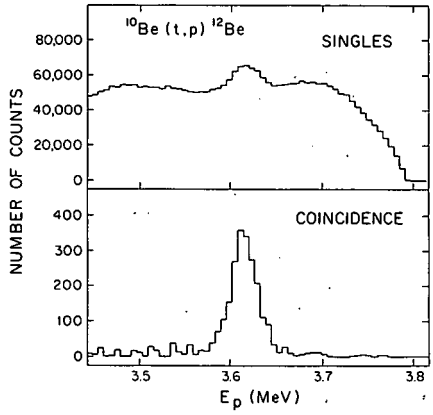

Figure 2. Top: singles proton spectrum from the ^{10}Be(t,p)^{12}Be reaction near the excited level at $E_{exc.}$ = 2.110 MeV; Bottom: same spectrum with the additional requirement of a p,γ coincidence.

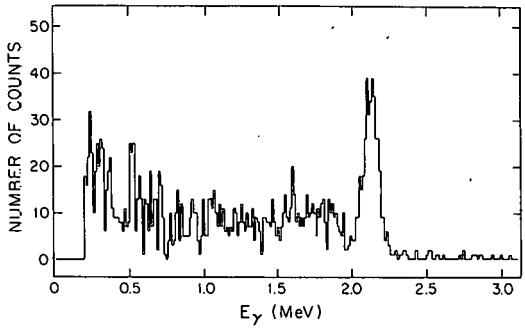

Figure 3. Gamma-ray spectrum from the decay of the ^{12}Be 2.110-MeV level in coincidence with protons.

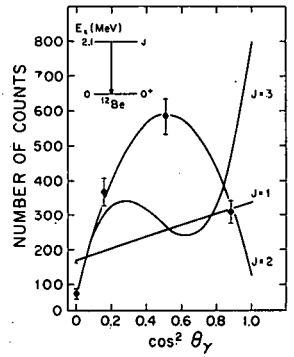

Figure 4. Angular correlation of the γ rays from the 2.110 → 0 MeV transition in ^{12}Be. The curves are best fits for the spins shown.

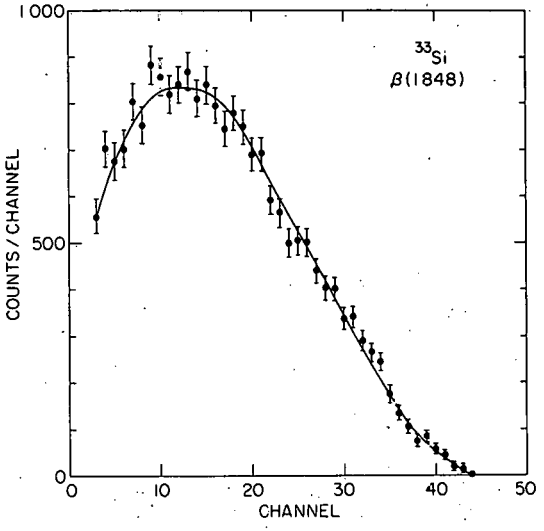

Figure 5. β-ray spectrum of ^{33}Si in a plastic scintillator in coincidence with 1848-keV γ rays. The solid curve is a calibration fit using a known ^{23}Ne activity that has a nearby β end-point energy.

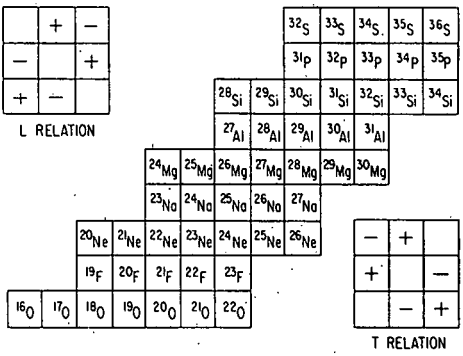

Figure 6. Region of the table of elements including the eight "exotic" $T_z = +5/2$ nuclei from ^{21}O to ^{35}P investigated at Brookhaven. According to the transverse (T) and longitudinal (L) relations of the Garvey-Kelson mass formulation the sum of the three (+) masses should equal the sum of the three (-) masses. Thus the masses of all 8 of the $T_z = +5/2$ nuclei can be predicted using the T relation.

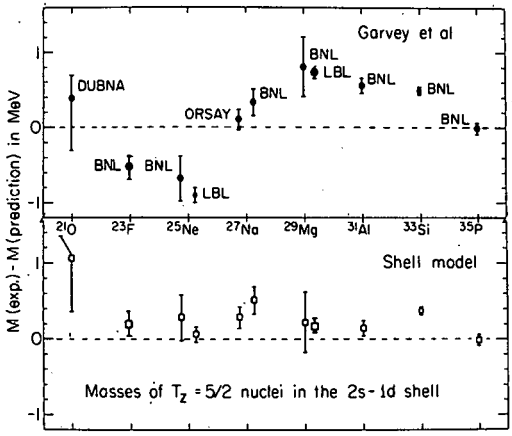

Figure 7. Upper part - differences between experimental masses and those predicted by the Garvey-Kelson transverse relation for the $T_z = +5/2$ nuclei in the 2s-1d shell. Lower part - similar comparison of experimental masses with shell-model calculations. Recent measurements have lowered the ^{21}O value by 1.2 MeV bringing it in line with the others (see text).

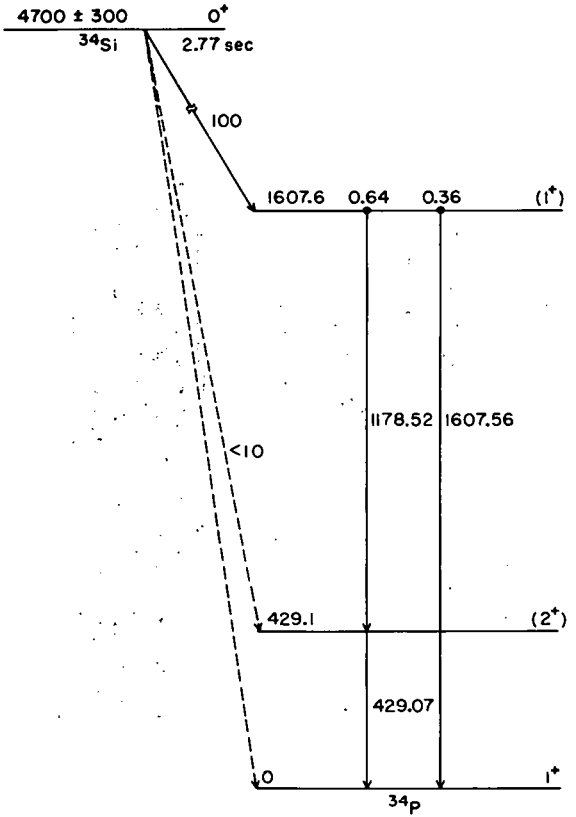

Figure 8. Decay scheme of ^{34}Si.

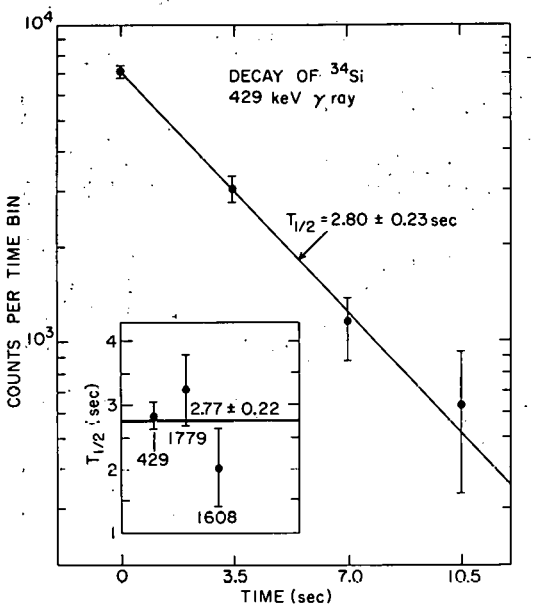

Figure 9. Half-life data on the decay of ^{34}Si γ rays.

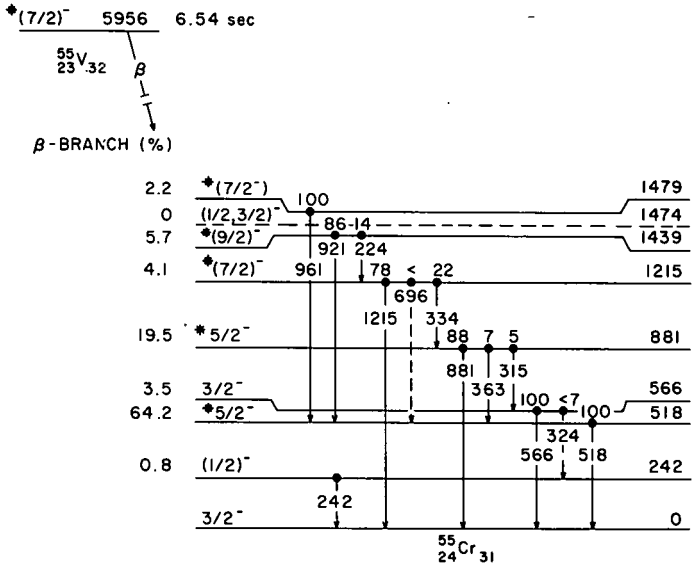

Figure 10. Decay scheme proposed for ^{55}V.

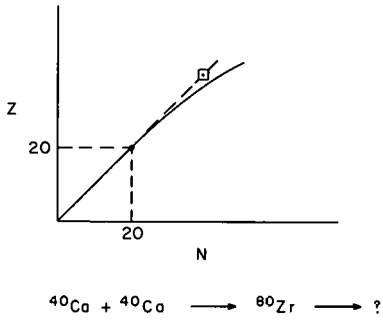

Figure 11. Schematic representation of the manner in which the $^{40}Ca + ^{40}Ca$ reaction can reach the region of proton-rich nuclei in the vicinity of ^{80}Zr.

THIS PAGE

WAS INTENTIONALLY

LEFT BLANK

Some Recent Experiments at ISOLDE

J.C. Hardy

Atomic Energy of Canada Limited, Chalk River Nuclear Laboratories, Chalk River, Ontario KOJ 1JO, Canada

My personal experience with on-line isotope separators (ISOL) encompasses only two instruments: one presently under construction at Chalk River and one at CERN, which has been in successful operation for about 10 years. I had originally intended to divide this talk equally between them both, but while listening to the talks yesterday and this morning I modified my plan somewhat.

So far at this meeting ISOLDE has received very little attention. Considering that for the past decade ISOLDE has been the most successful and prolific on-line isotope separator in the world, this appears to me a rather serious omission, and I have altered the emphasis of my talk in order to counterbalance this unfortunate impression. In doing so I must emphasize that I am not in any way an expert on nor a representative of ISOLDE; I am simply a satisfied user, having recently spent a very pleasant sabbatical leave there. Of the many experiments on the floor there I shall describe two that I was actually involved with, in the hopes that these will highlight some of the general qualities of the facility.

First, though, in order not to shorten the shrift too drastically for the Chalk River separator, I should like to outline its properties and expectations.

I. The Chalk River ISOL

The Chalk River ISOL[1] differs from most others, which like ISOLDE and TRISTAN are of the so-called Scandinavian design, in following the higher current Orsay approach[2,3]. This involves the use of an $n=\frac{1}{2}$ double-focussing magnet, and the elimination of all electrostatic focussing elements in order to achieve ion beam currents of up to 20 mA - compared with $\lesssim$ 500 μA from a Scandinavian machine. In other important respects, such as resolution and enhancement factor, the beam properties of both types are expected to be comparable.

As anyone familiar with on-line separators will realize, we did not make this choice because we expected such high currents of exotic nuclei. However, because our separator will be on-line with a heavy-ion accelerator (the Chalk River upgraded MP tandem) we shall frequently use a helium jet[4] to transport recoil nuclei from the target position to the separator's ion source. Although much of the helium gas can be skimmed away en route, the demands on the system are far less stringent if the separator itself can bear a relatively high current of helium without degrading the overall beam quality.

The layout of the separator and nearby tandem beam lines is shown in Fig. 1. The location of the ion source near the convergence of two beam lines will permit operation either in the helium-jet mode as described, the target being in the 47.1° beam line, or with the tandem beam impinging - via the 21.7° line - directly on a target placed in or near the ion source itself. Note also that following magnetic separation, the ion beam corresponding to a selected mass may be further transported, here electrostatically,

to a shielded counting area in target room 2. In the first phase of development only the central transport line will be built, but future flexibility can be ensured by adding two more lines, for which provision has already been made.

The current status of the project is that the mechanical assembly is well advanced with vacuum tests now in progress. All electrical components should be in our hands within a few months and first off-line tests are scheduled for early spring.

II. ISOLDE

We must now make a change of scale. This is not just a change from the scale of the uncompleted instrument just described but from the scale of any other existing on-line separator. The extent of the change should be evident from a look at Fig. 2, which is a drawing of the present ISOLDE facility. There are at least nine experimental stations used by over 100 physicists and chemists from a half dozen countries - not counting the overseas visitors.

I have not the time to even begin describing in detail the properties of the separator or the myriad experiments undertaken there. Instead, let me mention two features in particular that are recently developed and perhaps least familiar to you: 1) the production of neutron-rich isotopes and 2) the use of targets with very short release times.

The bombardment of a thick (14 g/cm^2) uranium target with a 1 μA beam of 600 MeV protons yields a prolific variety of neutron-rich nuclei through fission. Figure 3 shows the numbers of atoms per second actually observed at ISOLDE for the isotopes of caesium. For perspective, I should tell you

A=133 is the stable caesium isotope, and even at A=144, the heaviest one shown on the figure, a beam of $\sim$ 1 pA is produced. Thus, useful experiments can be performed on even heavier-mass isotopes. Of course, with a lanthanum target, light caesium isotopes have been produced routinely at ISOLDE (through spallation reactions) for many years. Isotopes have been observed all the way down to the proton drip line at A=114, and from A=123 to A=132 the separated beams are each above 1 nA!

Considerable advances have also been made recently on the development of refractory targets from which nuclear reaction products can be released rapidly[7]. One example appears in Fig. 4, which shows the fractional activity of ^{41}Ar observed from a vanadium carbide target as a function both of temperature and of the time delay after bombardment ceased. At 2100°C it is evident that most of the argon is released from the target material within a few seconds of its production.

As an illustration of the usefulness of these high yields and short release times, let me describe one experiment performed last year on a light argon isotope. Prior to that time the most neutron-deficient nuclei (i.e. those with the most negative T_z values) whose decays had been studied were those, such as ^{33}Ar, with $T_z = -3/2$. Despite numerous attempts to observe them, the production cross sections of $T_z = -2$ nucleides were simply too small to permit their decay to be observed. With the improved target techniques at ISOLDE, though, we succeeded in detecting[8] β-delayed protons from the decay of the $T_z = -2$ nucleus ^{32}Ar. The proton spectrum is shown in Fig. 5 together with the spectrum from the decay of ^{33}Ar, which was used for calibration and as a means of tuning the separator. The production rate of 75 msec ^{32}Ar was about 1 atom per 5 seconds.

The decay scheme appears in Fig. 6. The observed proton peak corresponds to the superallowed $0^+ \rightarrow 0^+$ β-transition that populates the lowest T=2 state in ^{32}Cl. From the measured proton energy, the mass excess of the T=2 state was determined to be -8295.6 ± 5.2 keV, and this result together with the known masses of three other members of the same isobaric multiplet yielded an accurate test for a cubic term in the isobaric multiplet mass equation for A=32: the coefficient of such a possible term was determined to be 0.5 ± 2.5 keV.

Argon-32 is at the very limits of particle stability so, even at ISOLDE, its production rate is too low to permit any experiments more complex than the singles counting of delayed protons. However, a separator need not be used exclusively for prospecting in such remote regions. The high yields available nearer stability make possible experiments of quite considerable complexity, which at ISOLDE include atomic beam magnetic resonance studies, on-line mass spectrometry and laser spectroscopy[5]. These are marvelously elegant experiments, but as a non-participant I am not the right person to describe them to you. Instead, I should like to describe another experiment that relied on high separator yields to produce a result that would otherwise have been inaccessible.

Krypton-73 is five neutrons away from the lightest stable isotope of krypton, ^{78}Kr. It decays by electron capture to states in ^{73}Br, some of which are unstable to proton emission. It is possible to measure the lifetimes of these particle-unstable states by comparing their decay time with the filling time of a vacancy in the atomic K shell. Any nucleus (with atomic number Z) that decays by electron capture to excited states in the

daughter (Z-1) produces simultaneously a vacancy in an atomic shell (see Fig. 7). If those excited states are unstable to proton emission, the energy of the X-ray emitted with the filling of the atomic vacancy will depend upon whether the proton has already been emitted (in which case the X-ray would be characteristic of a Z-2 element) or not (a Z-1 element). If the nuclear and atomic lifetimes are comparable, then the K_α X-rays observed in coincidence with protons will lie in two peaks whose relative intensities uniquely relate one lifetime with another.

This technique has previously been applied only once[9]: to the decay of ^{69}Se. That experiment was performed without isotope separation and, even though the production mode - ^{40}Ca(^{32}S,2pn)^{69}Se - is rather favourable, data collection was plagued by an extremely high rate of β-rays from other competing activities. Without their removal, the extension of these measurements to other, less accessible, nuclei proved to be impracticable.

The spectrum of coincident X-rays from the decay of ^{73}Kr, observed in 8 hours of counting at ISOLDE[10], is shown in Fig. 8. The corresponding proton spectrum appears in Fig. 9a together with a simplified decay scheme. The statistics are virtually identical to the earlier ^{69}Se data[9], which took about 40 hours - and a vastly more complicated experimental set-up - to obtain.

Statistical model calculations of the type described in ref[11] have been applied to the ^{73}Kr decay, and quite reasonable agreement with the experimental proton spectrum is evident. Agreement with the average level lifetimes is also quite satisfactory as can be seen in Fig. 9b, which is a plot of the ratio of Se X-rays (measured in coincidence with protons)

relative to those from As, given as a function of coincident proton energy. Since level lifetimes are related to level densities[9,11], this comparison between theory and experiment was used, in a single parameter fit, to determine the level density parameter a, with the result $a = 9.8\ \mathrm{MeV}^{-1}$. This is consistent with the results for mass-69 and with general expectations[12].

I have briefly described these two experiments in the hopes of conveying some flavour of the physics already possible with an on-line separator. My belief is that this type of physics easily justifies a modest proliferation of facilities, but one must appreciate at the same time that reactor-based separators no longer seem to offer unique advantages, even in the production of neutron-rich nuclei, compared with the best of the accelerator-based facilities. The real measure of success lies in the development of a sophisticated target/ion source technology, and it is in this direction that a new facility will have to set its sights.

III. Pandemonium

Having touted the value of ISOL physics, it is only fair that I conclude with a few cautionary remarks. These arise from another study we performed last year at CERN[13], this time on β-delayed γ-rays from the decay of ^{145}Gd.

The γ-ray spectrum we obtained appears in Fig. 10. It is qualitatively the same as previously published experimental data[14] for ^{145}Gd, and is also typical of the γ-ray spectra easily observed with an ISOL. Why this should be remarkable is explained by the fact that Fig. 10 was recorded without a Ge(Li) detector and, for that matter, without a real nucleus. Instead, we

created a fictional nucleus and then simulated its decay numerically, using the statistical principles known to circumscribe nuclear excitation and decay[15,16]. Since the existence of this nucleus, which we named Pandemonium, was confined to the functioning of a computer program, we could on the one hand know the Pandemonium β-transition rates exactly, while on the other hand generate for analysis a simulated spectrum of β-delayed γ-rays. We could then test whether transition rates extracted in the usual way from the (simulated) experimental data agree or not with the true rates.

The spectrum of Fig.10 was processed in a standard manner using the peak analysis program SAMPO[17]. A portion of the γ-ray spectrum appears again in Fig. 11 where the shaded photopeaks indicate the γ-rays detected by the program. The arrows mark the peaks actually present, but undetected. It should be emphasized that this is not a defect of the analysis program but is a fundamental fact that as the density of states increases, most γ-rays will be in principle undetectable by any peak-finding technique.

More important than the missing peaks is the amount of missing intensity, which is illustrated in figure 12. In total, for the case shown, 14% of the γ-ray intensity above 1.7 MeV is undetected in a peak analysis, and only ∿ 35 out of ∿ 1000 γ-rays are identified. If the number of counts had been a factor of 10 less, 45% of the intensity would have been lost. In the light of these results, every complex β-decay scheme that is based on γ-ray peak analysis and intensity balances must now be regarded as doubtful. In such schemes, the β-decay feeding to each level is assumed to be the difference between the total γ-ray intensity depopulating the level and that

seen feeding it. If significant γ-ray intensity remains unobserved, these differences are incomplete and the derived β-decay branching ratios, for all but the strongest transitions, could be wrong by orders of magnitude.

One must conclude then that the complexity of transitions apparently revealed by Ge(Li)-detector spectroscopy, in conjunction with an on-line isotope separator, may in fact only mislead if treated with the same biases that we use in assimilating the simpler decays seen nearer stability. Instead, we must seek new techniques better suited to the data observed. In my view these new techniques must lie not in the direction of level-by-level spectroscopy but rather in a statistical approach to strength distributions. This approach itself is, of course, not new but it is for the moment divorced from the mainstream of nuclear spectroscopy. It may well be that ISOL studies of nuclei far from stability will provide the necessary experimental link to statistical spectroscopy, matching the theoretical link that is already well on the way[18].

REFERENCES

1) Designed and assembled by a Chalk River (W. Perry, H. Schmeing and myself) and Orsay (J. Camplan and B. Rosenbaum) collaboration.

2) R. Meunier, J. Camplan, J-L. Bonneval, J-L. Daban-Hauroc, D. Deboffle, D. Leclercq, M. Ligonniere and G. Moroy, Nucl. Instr. & Meth. 139 (1976) 101.

3) P. Paris, V. Berg, A. Caruette, J. Obert, J.C. Putaux and J.L. Sarrouy, Nucl. Instr. & Meth. 139 (1976) 251.

4) H. Schmeing, V. Koslowsky, M. Wightman, J.C. Hardy, J.A. MacDonald, T. Faestermann, H.R. Andrews, J.S. Geiger and R.L. Graham, Nucl. Instr. & Meth. 139 (1976) 335.

5) Article in CERN Courrier No. 1/2 January/February 1977, pg. 15.

6) H.L. Ravn, to be published (private communication).

7) L.C. Carraz, I.R. Haldorsen, H.L. Ravn, M. Skarestad and L. Westgaard, CERN preprint, submitted to Nucl. Instr. & Meth.

8) E. Hagberg, P.G. Hansen, J.C. Hardy, A. Huck, B. Johson, S. Mattsson, H.L. Ravn, P. Tedemand-Petersson and G. Walter, Phys. Rev. Lett. 39 (1977) 792.

9) J.C. Hardy, J.A. Macdonald, H. Schmeing, H.R. Andrews, J.S. Geiger, R.L. Graham, T. Faestermann, E.T.H. Clifford and K.P. Jackson, Phys. Rev. Lett. 37 (1976) 133.

10) E. Hagberg, P.G. Hansen, J.C. Hardy, P. Hornshøj, B. Jonson, S. Mattsson, P. Tedemand-Petersson and P. Asboe-Hansen, to be published

11) J.A. Macdonald, J.C. Hardy, H. Schmeing, T. Faestermann, H.R. Andrews, J.S. Geiger, R.L. Graham and K.P. Jackson, Nucl. Phys. A288 (1977) 1.

12) J.W. Truran, A.G.W. Cameron and E. Hilf. International Conference on Properties of Nuclei far from Stability, CERN report 70-30 (1970) 275.

13) J.C. Hardy, L.C. Carraz, B. Johson and P.G. Hansen, Phys. Lett. 71B (1977) 307.

14) R.E. Eppley, W.C. McHarris and W.H. Kelly, Phys. Rev. C3 (1971) 282.

15) J.E. Lynn, The Theory of Neutron Resonance Reactions (Clarendon Press, Oxford, 1968).

16) B. Johson, E. Hagberg, P.G. Hansen, P. Hornshøj and P. Tedemand-Petersson, Proc. 3rd Int. Conf. on Nuclei Far From Stability, CERN report 76-13 (1976) 277.

17) J.T. Routti and S.G. Prussin, Nucl. Inst. & Meth. 72 (1969) 125.

18) J.P. Draayer, J.B. French and S.S.M.Wong, Annals of Physics 106 (1977) 472 and 503.

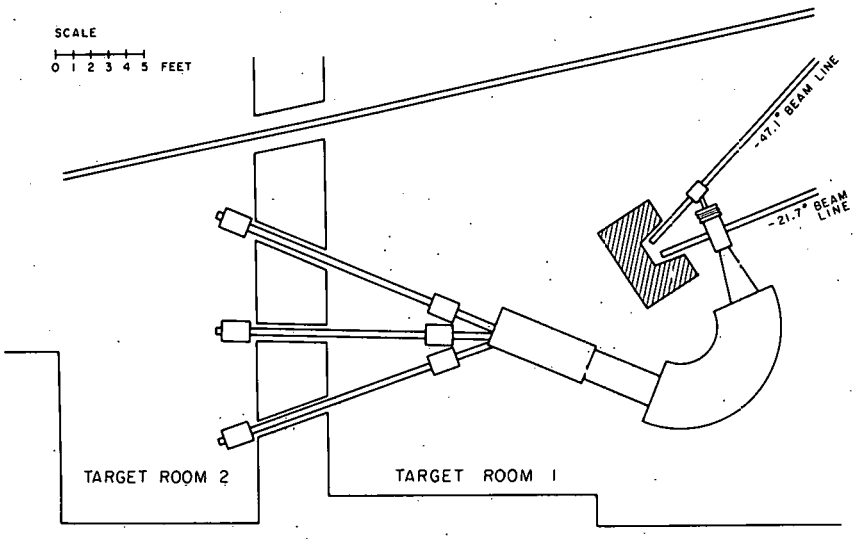

Figure 1. Layout of the Chalk River on-line isotope separator and the neighboring tandem beam lines.

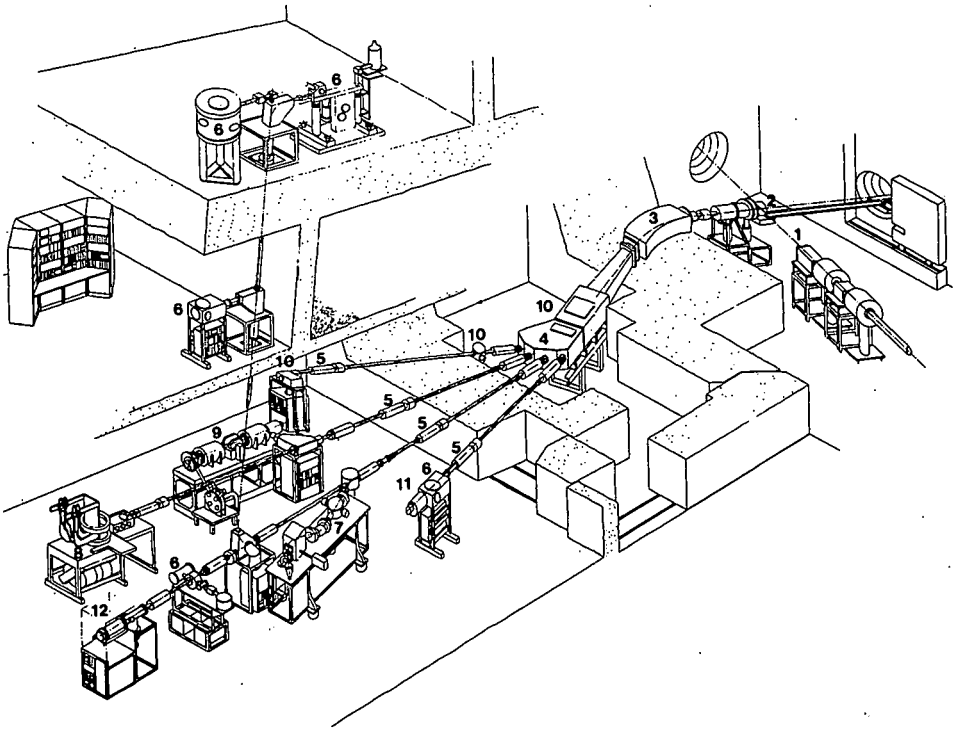

Figure 2. Perspective view of the isotope separator, ISOLDE. The 600 MeV proton beam (1) from the CERN synchro-cyclotron is focused on the target ion source unit (2). A beam of radioactive ions is formed by a 60 kV acceleration stage and is mass analyzed in a magnet (3). Individual masses are then selected by electrostatic deflection in the switchyard (4) and distributed through the external beam-lines (5) to the various experiments. These are: (6) Nuclear spectroscopy (α, β, γ) (7) High resolution mass spectrometer (8) Optical pumping and laser spectroscopy (9) Atomic beam magnetic resonance (10) Collection of radioactive sources for off-line work (hyperfine interactions in solids, determination of shifts in X-ray energies, targets for nuclear reaction studies) (11) Beta delayed particles (12) Range measurements of ions in gases. From Ref. 5.

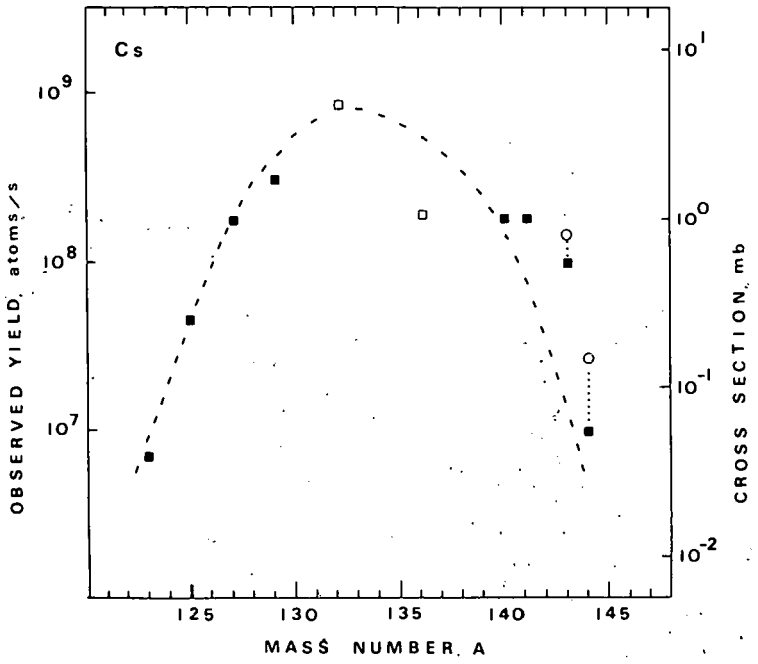

Figure 3. Observed yields (plotted as squares) of separated beams of Cs isotopes corresponding to a 1μA beam of 600 MeV protons impinging on a 14 g/cm^2 uranium target (in the form of impregnated graphite cloth) at 2050°C. The open squares are shielded isotopes; open circles are yields corrected for decay losses in the separator. The dashed curve is the result of a calculation based on measured fission yields. From Ref. 6.

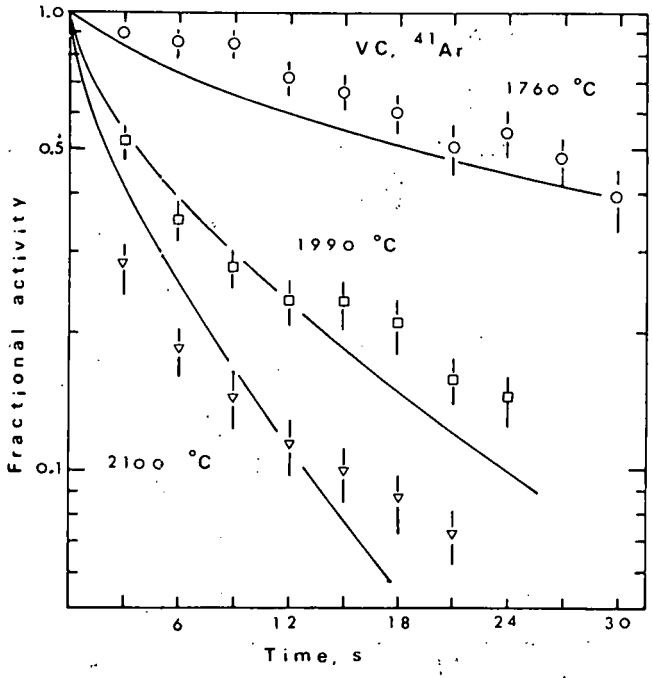

Figure 4. The observed activity of ^{41}Ar produced from a vanadium-carbide target bombarded by 600 MeV protons. The abscissa corresponds to the length of time between the cessation of bombardment and the period of observation[6]). The curves are labelled by the target temperature.

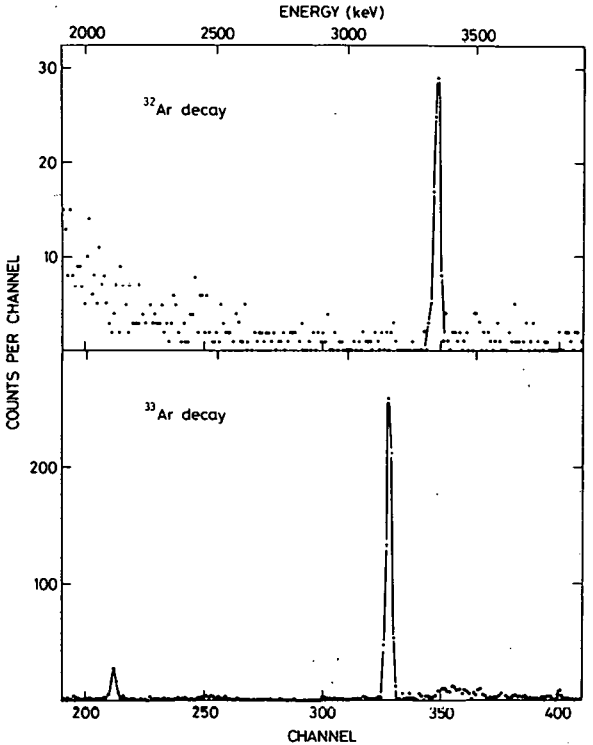

Figure 5. Energy spectra of delayed protons observed following the decays of ^{32}Ar and ^{33}Ar. From Ref. 8.

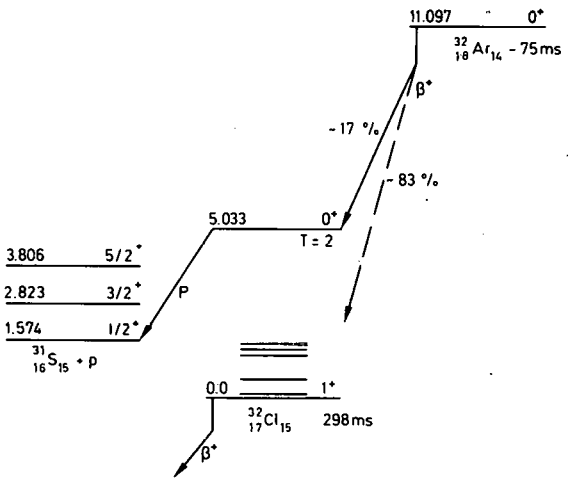

Figure 6. Decay scheme of ^{32}Ar. From Ref. 8.

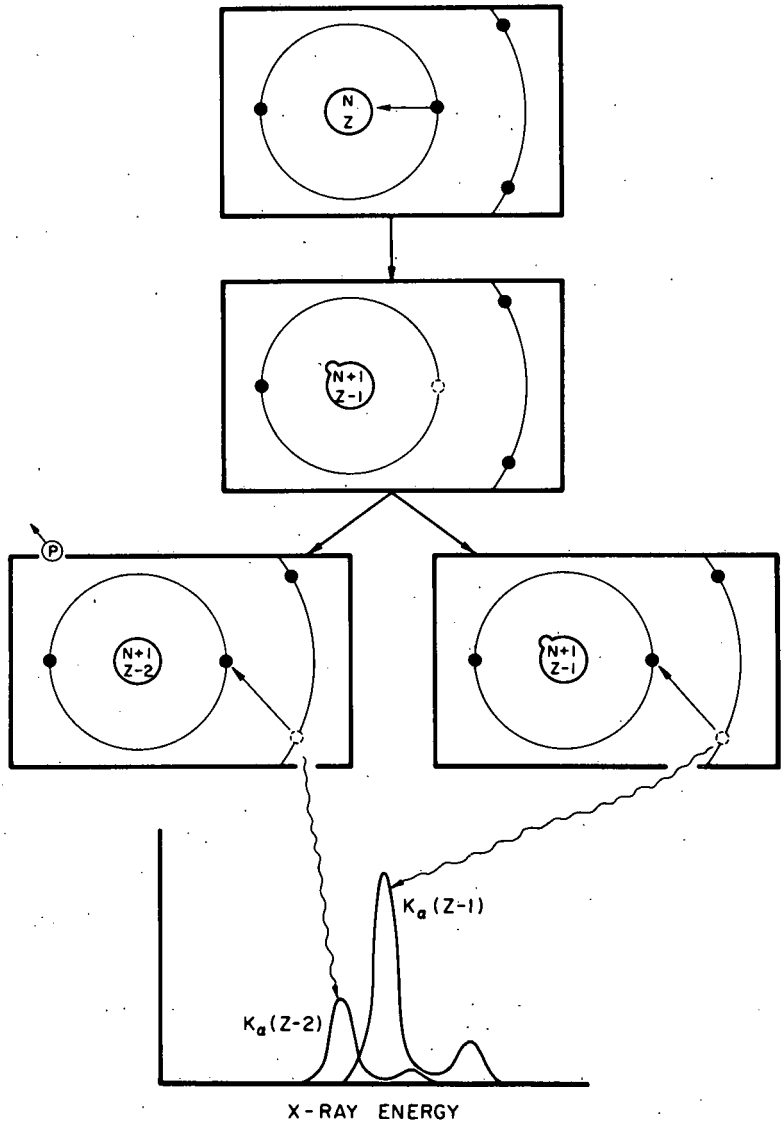

Figure 7. Pictorial representation of the p-X coincidence technique for lifetime measurements on proton unstable states produced by electron capture.

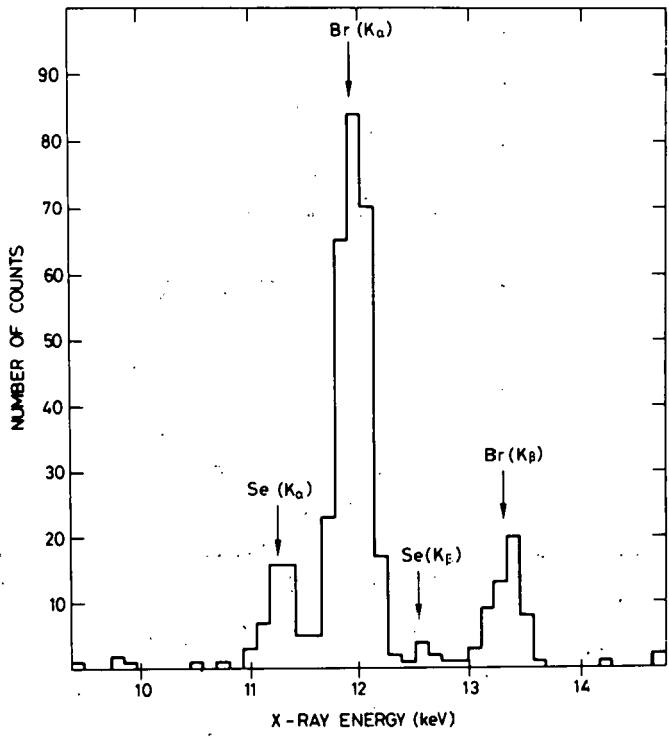

Figure 8. Spectrum of x-rays observed in coincidence with all delayed protons from the decay of ^{73}Kr.

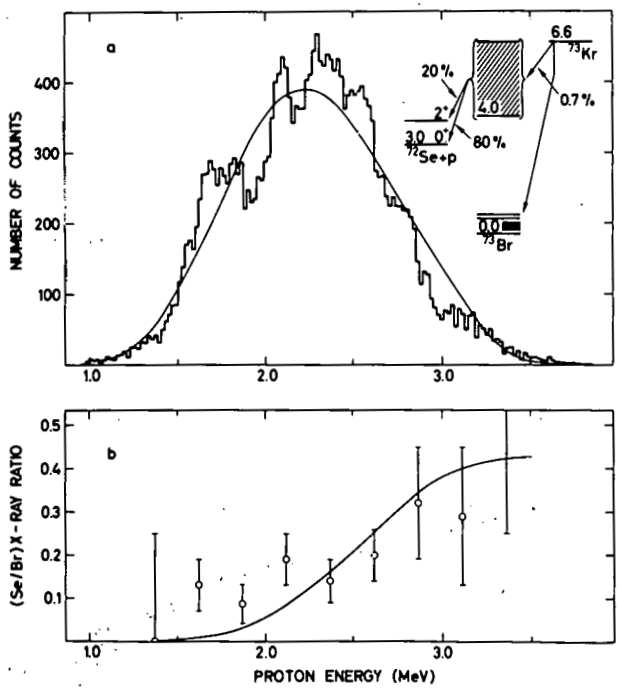

Figure 9. a) Spectrum of protons observed following the decay of ^{73}Kr; a simplified decay scheme appears as the inset. b) Ratio of coincident Se x-rays relative to those from As, plotted as a function of coincident proton energy. The smooth curves in (a) and (b) are the results of statistical model calculations.

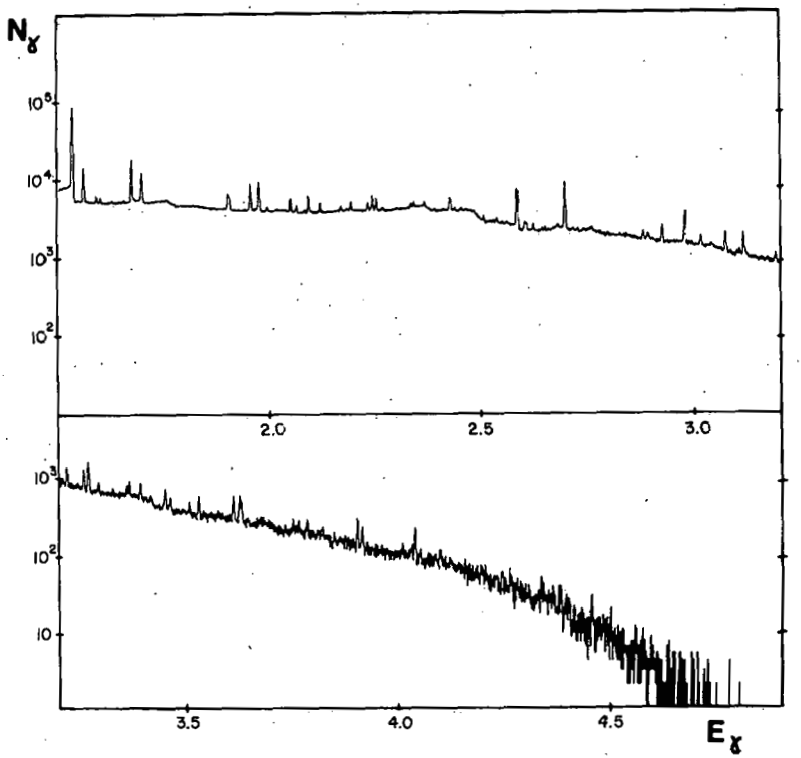

Figure 10. Computer simulated γ-ray spectrum corresponding to the fictional decay of Pandemonium, which in this application has been assigned the mass and atomic number of ^{145}Gd. From Ref. 13.

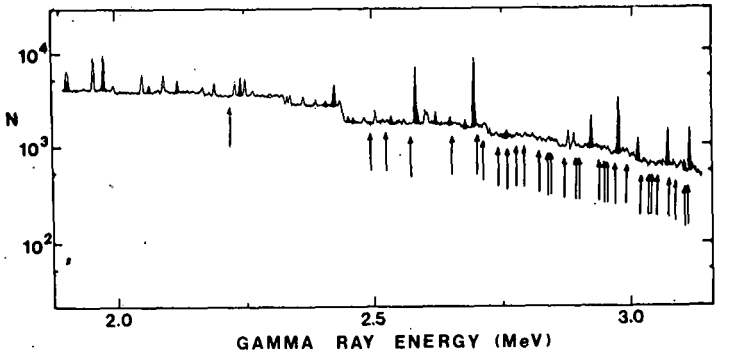

Figure 11. Part of the γ-ray spectrum of figure 1. The photopeaks identified in the analysis are shaded; those that are present but unidentified are indicated by arrows.

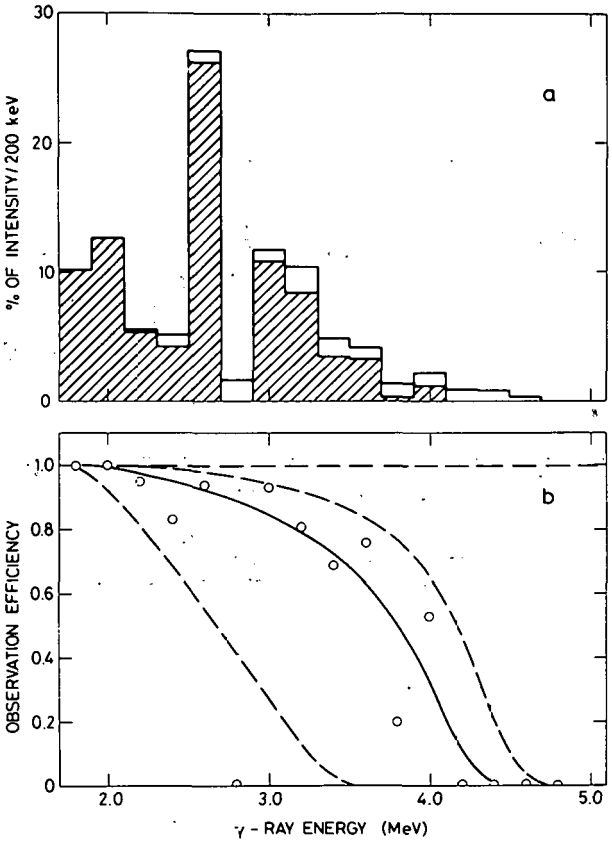

Figure 12. a) Observed and true γ-ray intensity (shaded and unshaded histograms respectively) for the data of figure 9 plotted in intervals of 200 keV of γ-ray energy. The ordinate is scaled to give a total of 100% true intensity above 1.7 MeV. b) The circles correspond to the data in fig. 2a expressed as an "observation efficiency" for the detection of γ-ray intensity. The solid line is drawn simply to indicate the trend of the results. The two dashed curves show the corresponding trends for one tenth and ten times the counting statistics. Note that $E_{\gamma_{max}} = Q_{EC}$=5.0 MeV. From ref. 13.

Contribution to the Isotope Separator On-line Workshop, Brookhaven, 31 October - 1 November 1977, to be published as BNL Report.

Recent Developments and Results with the GSI On-line Separator at the UNILAC.

E. Roeckl, R. Kirchner, O. Klepper, G. Nyman[+], W. Reisdorf
GSI Darmstadt, Postfach 110541, 6100 Darmstadt 11,
Federal Republic of Germany

ABSTRACT

The GSI mass separator facility on-line to the heavy-ion accelerator UNILAC was applied for separation of neutron-deficient isotopes from ^{40}Ar and ^{58}Ni induced fusion reactions. A status report on the facility is given with particular emphasis on separation parameters such as overall efficiency and release time for isotopes in the tin region ($46 \leq Z \leq 55$). Examples for current experiments are the measurement of isotopic distributions of evaporation residues in comparison with predictions from evaporation calculations, and production of very neutron-deficient isotopes of tellurium, iodine, and xenon via ^{58}Ni induced reactions on ^{58}Ni and ^{63}Cu targets. The new isotopes identified in this region, including the island of the α emitters ^{108}Te, ^{109}Te, ^{110}I and ^{111}I, are discussed within the framework of mass β-strength-function systematics, in view of extending the search for neutron-deficient isotopes at the proton drip line.

Darmstadt - 21 October 1977

[+]Present address: Department of Physics, Chalmers University of Technology, 40220 Göteborg, Sweden.

1. Introduction.

For studying nuclei far away from stability the method of on-line mass (and isotope) separation is playing an important role, in particular if short-lived nuclei are investigated and if production cross sections are small compared tc dominant reaction channels. The Cargèse Conference (1), for instance, has recently demonstrated the variety of applications of on-line separators.

At this workshop we want to report on the status of the GSI mass separator facility on-line to the heavy-ion accelerator UNILAC. Emphasis will be put on experimental techniques, the merits (and limitations) of which may be of interest tc other projects. The ion source (2), its on-line connection to a target position of the UNILAC, the general layout of the separator facility as well as introductory on-line measurements (3) have been published elsewhere. An artist's view of the present status of the separator is shown in Fig. 1. It includes single and telescope detector-arrays for particle decay-spectroscopy inside the collector tank, and a switchyard becoming operational beginning of 1978. Essential modifications were made in the target ion-source area as will be described in Section 2 together with recent ion-source development. In Section 3 resulting separation parameters such as overall efficiencies, and release times are presented as obtained using ^{40}Ar and ^{58}Ni ions as projectiles. To illustrate the application of an on-line separator for reaction studies, measurements of isotopic distributions and excitation functions of evaporation residues from fusion reactions are discussed in Section 4. Based on these results a search for very neutron deficient trans-tin isotopes via fusion reactions of ^{58}Ni ions with ^{58}Ni and ^{63}Cu targets was started, the results of which are given in Section 5.

2. Target ion-source system.

The heart of the whole facility is the ion source developed by R. Kirchner (5) which proved to hold the promising features found in

preceeding off-line and on-line parameter investigations (2,3,4,5). The present target ion-source system, shown in Fig. 2, includes a number of improvements made without any major change of the target ion-source housing (3,4).

As the target life-time at high UNILAC-beam intensities was reasonably long only if the beam was not too well focused on target, a careful defocusing procedure had to be performed at the beginning of each on-line run: The beam was initially focused onto a tantalum screen close to the target to give a wide circular beam spot. This first step was controlled by monitoring the charge deposited by the beam on the insulated screen, and by watching the beam spot on the tantalum screen via a TV camera positioned in front of the 13° magnet. Subsequently, the screen was removed to enable beam entrance through a 7 mm diameter collimator, which was insulated to allow current measurements, into a Faraday cup supplied with electrostatic eletron-suppression. If the beam was well centered and within the useful intensity range, the Faraday cup was finally removed delivering the beam through the same 7 mm collimator to the target. Here it usually caused a visible (red glowing) spot which was monitored via the TV camera mentioned above. Moreover, the Faraday cup was switched into its beam position regularly during an experiment in accordance with the respective irradiation-counting cycle.

So far, refractory metal targets of 0.7 to 5.1 mg/cm^2 thickness and 10 mm effective diameter were used as self-supporting foils mounted in a water-cooled holder. Targets of Sc, Fe, Ni, Cu, Ge, Y, Rh, Dy, Lu, Ta, and Pt lasted over periods of a few hours until a maximum of 18 hours at intensities of up to 10^{12} particles/sec for 5.9 MeV/u ^{40}Ar and $2 \cdot 10^{11}$ particles/sec for 5.0 MeV/u ^{58}Ni, copper being the less and germanium the most sensitive target material. Under these conditions both the 50 µg/cm^2 carbon heat-shield mounted between ion source and target, and the

0.9 mg/cm^2 tantalum window of the ion source were comparatively long-lived.

On-line tests of various catchers were carried out using the catcher position at the "downstream" opening [3,4] of the ion source. According to results from these tests, to be described in Section 3, another configuration was chosen (see Figs. 1 and 2), in which the reaction recoils are implanted directly into the tantalum capsule cathode or into a tantalum foil wrapped around the capsule. The "downstream" opening was equipped with an additional electron bombardment heater. The new configuration enables higher catcher temperatures of about 2500°C (the coldest part of the ion source - the outlet plate - being at about 1500°C), and reduces the distance between target and catcher to 16.5 mm.

Except for occasional production of alkali isotopes by surface ionization, the ion source was operated in FEBIAD (forced electron beam induced arc discharge) mode on krypton, xenon, respectively. In addition to general performance controls such as mass marking and optimizing of line shape, the overall efficiency of the separation was regularly checked during an on-line experiment by using calibrated krypton or xenon leaks.

The dependence of ionization efficiency and line shape on emission orifice diameter was investigated [6] off-line at a small Scandinavian-type mass separator, its dispersion perpendicular to the central beam is 8.5 mm/%. Fig. 3 shows line shapes measured by a 20 µm-diameter scanner pin for emission orifice diameters of 0.1 mm, 0.3 mm, and 0.6 mm. The ion source was operated for yielding maximum resolving power (in contrast to efficiency-optimizing on-line operation), the overall efficiencies being 0.6, 1.5, 5.2% for the examples given in Fig. 3. The complete dependence of mass resolving power on ionization efficiency and orifice diameter is given in Fig. 4 for xenon. For on-line operation, an emission orifice diameter of 0.6 mm seems to represent a reasonable compromise.

It is striking to note that for the conventional mass separator, used here, a mass resolving power of 10 000 could be reached. This may mean that direct mass measurements of nuclei far away from stability may come within reach also for non-alkali elements.

The FEBIAD characteristics - low operation pressure, low ion-beam intensity (typically nA), and low cross contamination - suggest that direct ion-detection by a secondary-eletron multiplier may be feasible. Fig. 5 shows the mass spectrum measured with a secondary-electron multiplier in the mass range 70-95. We conclude that only surface-ionization mode guaranties clean mass spectra (except for alkali, alkaline earth, and rare earth peak), whereas the FEBIAD mode clearly has the "peak-at-every-mass" problem. There is hope for improvement by using higher-purity material. On the other hand, the mass spectrum of Fig. 5 exemplifies again the good line-shape obtained with this ion source, resulting in a total contamination of less than 10^{-5} down to less than 10^{-8} with increasing distance from the "strong" krypton lines.

3. Release properties.

For on-line tests in the tin region, reactions of 4.8 to 5.9 MeV/u ^{40}Ar beams on copper, germanium, and yttrium targets were used. Regarding the wide distribution of evaporation residues (compare Section 4) and the low degree of elemental discrimination to be expected from a hot catcher, inside a plasma ion-source, beta-gamma decay spectroscopy was generally necessary to decompose the different isotopes present within a mass-separated sample.

The overall efficiency η of the separation process was determined as ratio between source strength n of separated sample and primary production rate n_{Target}. n is determined from decay measurements using known intensities of characteristic gamma-rays, while n_{Target} follows from cross-section calculated by the ALICE code [7,8]. Because of the uncertainty in the latter prediction, η can only be considered as a rough guess.

With a graphite catcher in the "downstream" opening of the ion source and catcher temperatures up to 2000°C, η amounted up to about 10% for cesium, several percent for antimony and iodine, and was lower for tellurium and xenon. The efficiencies for these elements remained the same (within a factor of 2) for different types of graphite felt, solid graphite, and tantalum. It was therefore decided to simply use the tantalum capsule-cathode as catcher. Due to the higher temperature of about 2500°C, η increased considerably for almost all elements mentioned above. There still remains the fact that overall efficiencies determined on-line are lower than values for stable species (see Fig. 4). Our preliminary conclusion is that the deficit can be explained by slow and/or incomplete release of implanted recoils from the catcher.

In addition to Te, I, Xe, Cs also isotopes of Pd, Ag, Cd, In, Sn have been separated in useful yields. The refractory palladium, which has a melting point of 1550°C and reaches a vapor pressure of 760 torr at 3020°C, represents a special surprise. The attractive separation-properties in this region with $46 \leq Z \leq 55$ has led us to the search for very neutron-deficient trans-tin isotopes to be described in Section 5. It is to be expected that chemical homologues would also be suitable for on-line separation, which is supported for the region $28 \leq Z \leq 37$ by separation tests on Br, Kr, Rb and for the region $78 \leq Z \leq 87$ by experiments on Bi, Po, At, Fr.

The release-time measurement for 2.4 min ^{117}I, shown in Fig. 6, yields a short-lived half-time component of 2-3 sec, whereas tellurium is released much slower (half-time about 40 sec). It is evidently the short-lived release component, which enabled the detection of 0.69 sec ^{110}I - the most short-lived isotope observed so far at the GSI separator.

4. Isotopic distributions and excitation functions.

An extension of the introductory on-line tests, which were to yield optimum release-parameters, lead quite naturally to measurements of

isotopic distributions as shown in Fig. 7. Such distributions were then compared with predictions from evaporation calculations with the aim of both understanding evaporation after compound-nucleus formation and testing the respective computer code as a **predictive** tool.

As can be seen from Fig. 7, there is qualitative agreement between experiment and predictions from a modified version (7) of the ALICE code (8). The fitting procedure results in η values between 0.5 and 7% for this particular run with a graphite-felt catcher at 1500 to 2000°C.

It is interesting to use the evaporation code for investigating different heavy-ion target-projectile combinations and beam energies in view of capabilities of producing neutron-deficient isotopes, and to compare to high-energy proton reactions. Taking mass-separated cesium as an example, the isotopic distribution from 600 MeV protons on a lanthanum target peaks near stability at a few 10^{10} atoms/sec (or 1 Curie in saturation), and reaches a level of 1 atom/sec for ^{114}Cs (9). Reactions of ^{40}Ar on ^{89}Y cannot compete, disregarding the smaller width of the isotopic distribution, as peak rates do not exceed a few 10^{5} atoms/sec (or 10 μC in saturation) which represents a limit also for other elements with our present target, catcher and ion-source technology. It is more promising, of course, to try to produce more neutron-deficient compound nuclei such as ^{124}Ce (via ^{32}S on ^{92}Mo), ^{121}La (via ^{58}Ni on ^{63}Cu), or ^{116}Ba (via ^{58}Ni on ^{58}Ni) even if emission of several protons and/or alpha particles decreases the initial proton-to-neutron ratio. For the reaction ^{58}Ni on ^{58}Ni, which will be discussed further in Section 5, an intensity of about 50 atoms/sec was estimated for the mass-separated ^{114}Cs beam of a recent experiment. It should be mentioned here, however, that this qualitative comparison just gives the present status which will almost certainly change according to technical development going on at different laboratories.

For determination of isotopic distributions in the mass range 114 to 124 from reactions of ^{40}Ar with ^{89}Y, β-γ spectroscopy was performed with a tape station positioned in the focal plane of the separator for collection of a selected mass. After sufficient statistics has been accumulated, the tape carriage was moved into another mass-beam. As stability of UNILAC beam and separator efficiency were not controlled regularly during the scan, the experimental source-strength distributions have to be considered preliminary. In order to test the stability of the separator performance and the feasibility of measuring reliable isotopic distributions and excitation functions, respectively, $^{164}Dy(^{40}Ar,xn)^{204-x}Po$ reactions were investigated recently at 4.2 to 5.8 MeV/u incident ^{40}Ar-energy. At a given UNILAC-beam energy three polonium isotopes were detected simultaneously by three alpha detectors mounted in the collector tank. The UNILAC-beam intensity was monitored by regular current measurements, the separator efficiency was controlled via a calibrated xenon leak (compare Section 2). Preliminary results from this test experiment are shown in Fig. 8. The shift of experimental excitation functions with respect to predictions from evaporation calculation (7,8) support qualitatively earlier conclusions of Le Beyec et al. (10). Without going into any discussion of this shift here, we note the following advantages of the mass-separator method for measuring excitation functions:

-1- Unambiguous mass assignment.
-2- Sensitivity to low cross sections (e.g. wings of distributions accessible down to less than 1/300 of peak height).
-3- Sufficient long-term stability (drifts in UNILAC beam intensities and separator efficiency can be corrected for).

5. Search for neutron-deficient isotopes

Based on the qualitative agreement between experiment and evaporation calculations (7,8) for a series of ^{40}Ar-induced reactions, and neglecting the energy shift mentioned above, reactions of ^{58}Ni ions on ^{58}Ni and ^{63}Cu targets seemed to be promising for production of neutron deficient transtin isotopes. First results on these reactions were published recently (11)

and are reviewed here only briefly.

Qualitative agreement (see Fig. 9) between experiment and prediction manifests itself in the identification of the nine new isotopes $^{108-110}Te$, $^{110-114}I$, ^{114}Xe. (The tellurium assignments remove a long-standing discrepancy in the literature.) The identification was accomplished by beta, gamma or X-ray spectroscopy (12) or by particle counting (13). Examples of particle spectra accumulated at mass 110 and mass 111, respectively, are displayed in Fig. 10.

^{108}Te, ^{109}Te, ^{110}I, and ^{111}I form a new island of alpha emission above the shell closure at Z=50. From comparing (13) the experimental alpha energies and other mass-differences far from stability with mass predictions, the mass formula of Jänecke and Eynon (14) was chosen as a preliminary basis for the following conclusions. According to the calculated proton-drip line (14), the isotopes 0.69 sec ^{110}I - 17 neutrons away from stable ^{127}I - and 0.7 sec ^{114}Cs - 19 neutrons away from stable ^{133}Cs - represent the last bound isotopes of iodine and cesium, respectively (see Fig. 9). Beta strength-function systematics (16), which is plotted in Fig. 11 as derived from Q-value predictions (14) and half-life measurements from this work and from the literature, allows the extrapolation towards beta-decay half-lives of more neutron-deficient isotopes. Of special interest are the half-life predictions of 0.5 sec for ^{109}I and of 0.1 to 0.2 sec for ^{113}Cs, since both isotopes represent candidates for Coulomb-delayed proton emission from ground states (or proton radioactivity), a phenomenon, which may become accessible to experiment within the near future.

References:

(1) Proceedings of the 3rd International Conference on Nuclei far from Stability, Cargèse, Corsica (France), 19-26 May 1976, published as CERN 76-13 (1976).

(2) R. Kirchner and E. Roeckl, Nucl. Instr. Meth. 133 (1976) 187.

(3) K.H. Burkard, W. Dumanski, R. Kirchner, O. Klepper and E. Roeckl, Nucl. Instr. Meth. 139 (1976) 275.

(4) R. Kirchner and E. Roeckl, Nucl. Instr. Meth. 139 (1976) 291.

(5) R. Kirchner, Thesis (Mainz University, 1976), published as GSI-Report GSI P-1-76 (1976).

(6) R. Kirchner, Contribution to the International Conference on Low Energy Ion Beams, Salford, Great Britain, September 5-8, 1977, Proceedings to be published in Institute of Physics Conference Series No. 38 (1978).

(7) W. Reisdorf, unpublished.

(8) F. Plasil and M. Blann, Phys. Rev. C11 (1975) 508.

(9) H.L. Ravn, L.C. Carraz, J. Denimal, E. Kugler, M. Skarestad, S. Sundell and L. Westgaard, Nucl. Instr. Meth. 139 (1976) 267.

(10) Y. Le Beyec, R.L. Hahn, K.S. Toth and R. Eppley, Phys. Rev. C14 (1976) 1038.

(11) R. Kirchner, O. Klepper, G. Nyman, W. Reisdorf, E. Roeckl, D. Schardt, N. Kaffrell, P. Peuser and K. Schneeweiß, Phys. Letters 70B (1977) 150.

(12) G. Nyman, R. Kirchner, O. Klepper, W. Reisdorf, E. Roeckl, N. Kaffrell and K. Schneeweiß, to be published.

(13) O. Klepper, R. Kirchner, G. Nyman, W. Reisdorf, E. Roeckl, D. Schardt, K. Wien and R. Faß, to be published.

(14) J. Jänecke and B.P. Eynon, Atomic Data and Nuclear Data Tables 17 (1976) 467.

(15) B. Jonson, E. Hagberg, P.G. Hansen, P. Hornshøj and P. Tidemand-Petersson, CERN Report 76-13 (1976) p.277.

(16) P.G. Hansen, Advances in Nucl. Phys. 7 (1976) 159.

(17) W. Seelmann-Eggebert, G. Pfennig, H. Münzel, Chart of Nuclides, 4th edition, 1974, Gesellschaft für Kernforschung, Karlsruhe.

(18) The ISOLDE Collaboration, to be published.

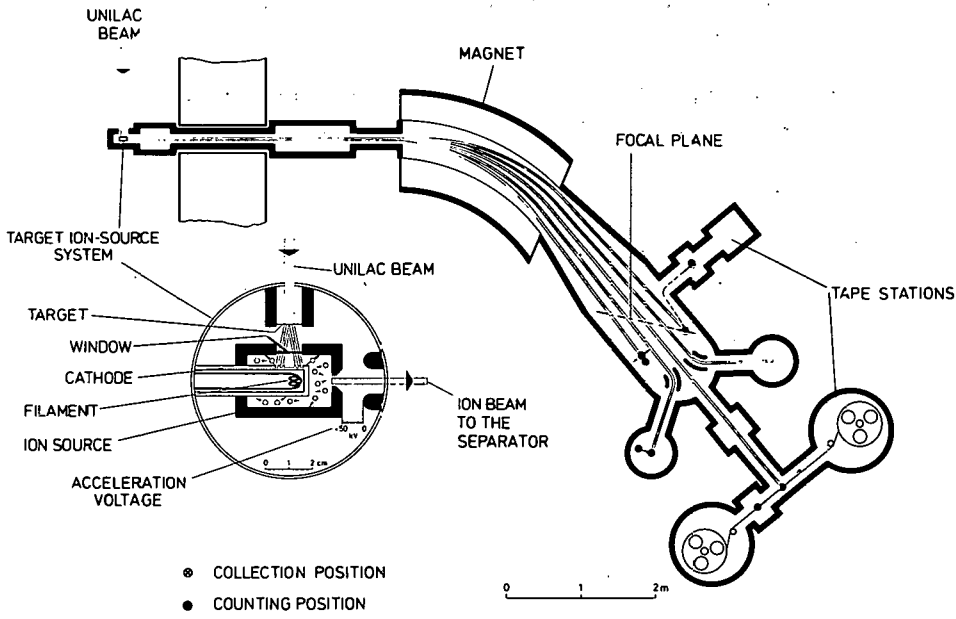

Figure 1. Layout of the GSI mass separator facility on-line to the heavy-ion accelerator UNILAC.

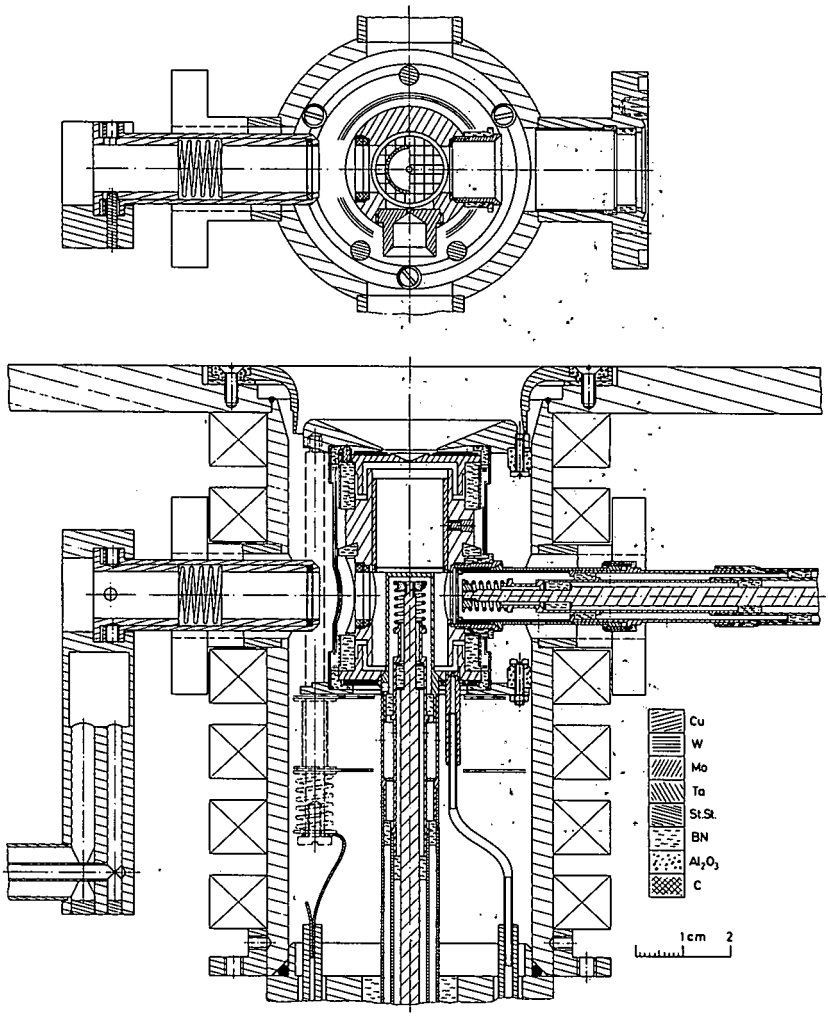

Figure 2. Cross-sectional view of the target ion-source system. The UNILAC beam enters from the left side, beam-diagnostic instruments (screen, collimator, Faraday cup) are not shown.

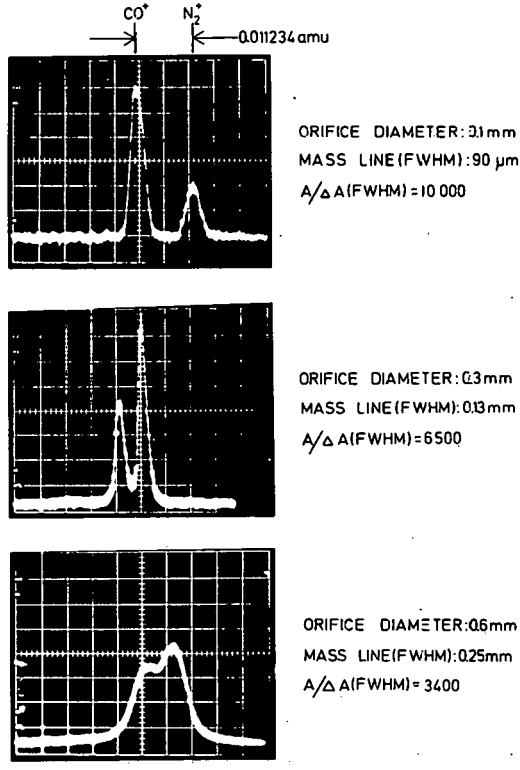

Figure 3. Separation of the isobaric doublet at mass 28, using the FEBIAD ion source with different emission-orifice diameters operated for maximum resolving power. Separator parameters: Single gap acceleration, acceleration voltage 40 kV (stability $2 \cdot 10^{-5}$), no collimation, transmission 95%, dispersion perpendicular to central beam 8.5 mm/%, scanner pin diameter 20 μm. Vacuum: Injector chamber $8 \cdot 10^{-7}$ torr, second lens and dispersion chamber $5 \cdot 10^{-6}$ torr, collector chamber $2 \cdot 10^{-6}$ torr.

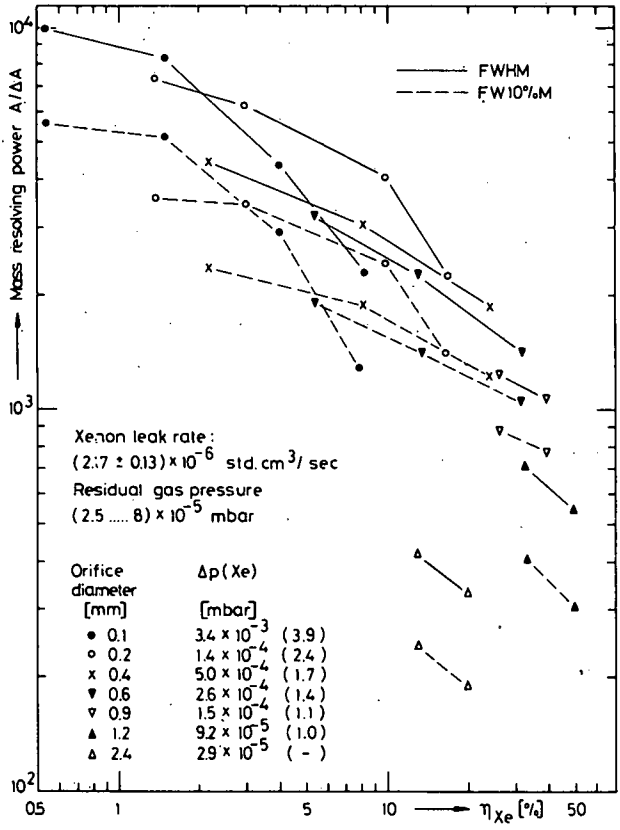

Figure 4. Mass resolving power versus ionization efficiency for xenon obtained with the FEBIAD ion source. Δp (Xe) is the observed xenon partial pressure in the discharge chamber for the respective orifice diameter. Acceleration voltage 40 kV. Relative error: ±7% for η, ±2% up to ±5% for A/ΔA.

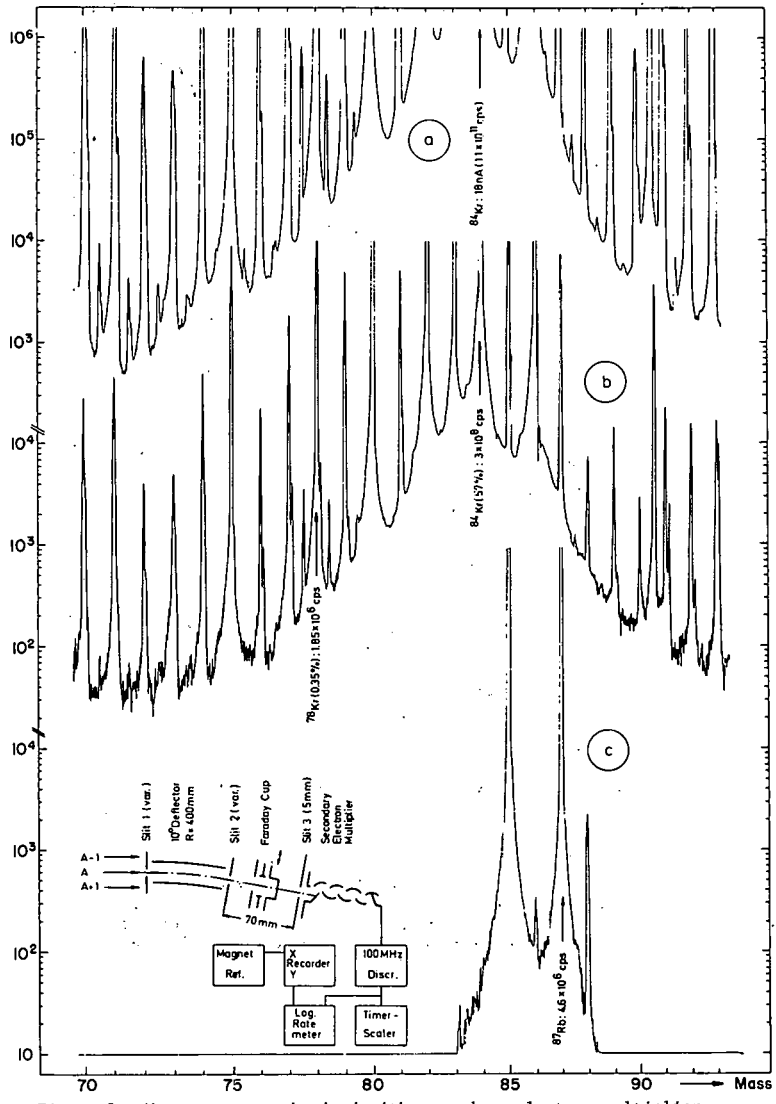

Figure 5. Mass spectrum obtained with secondary electron multiplier. (a) Integral scan for FEBIAD mode: 90% beam transmission through slit 1 and 2. (b) Differential scan for FEBIAD mode: Peak intensity reduced to ∿ 1/300 by slit 1. (c) Integral scan for surface ionization mode: Slits as in (a). Only rubidium and strontium peaks are seen, absence of statistical fluctuations in background indicates counting rates of less than 10 cps. Experimental conditions: Orifice diameter 0.4 mm, krypton partial pressure 1.1 x 10^{-5} mbar in the discharge chamber, krypton efficiency 14%, acceleration voltage 40 kV. Average source temperature 1800°K in FEBIAD mode and 1600°K in surface ionization mode; cathode temperature 2600°K. For more details see Ref. 6.

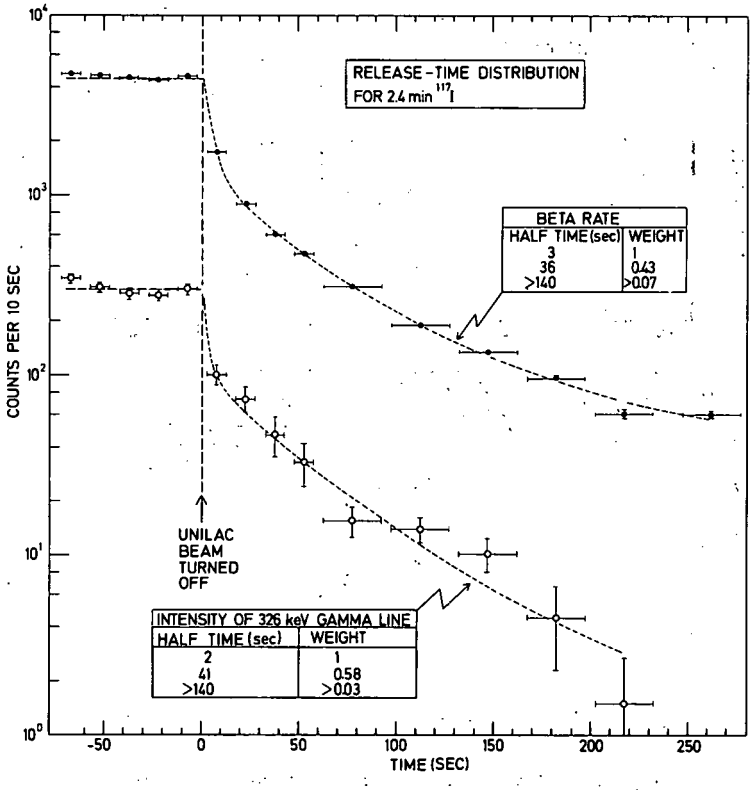

Figure 6. Release-time distribution for 2.4 min ^{117}I recoils from ^{89}Y(^{40}Ar, 4p8n) reactions and a tantalum catcher at 2500°C. A tape station stopped the mass-separated beam at mass 117 in the collector tank during a preselected time-interval and moved the collected sample subsequently into a detector position where beta counting in a plastic scintillation detector and gamma spectroscopy in a Ge(Li) detector were performed simultaneously. While such collection-transport-counting cycles were repeated, the UNILAC beam was switched off. The resulting release-time distribution was fitted by a sum of exponentials, the half-time components and respective weights are given as insets.

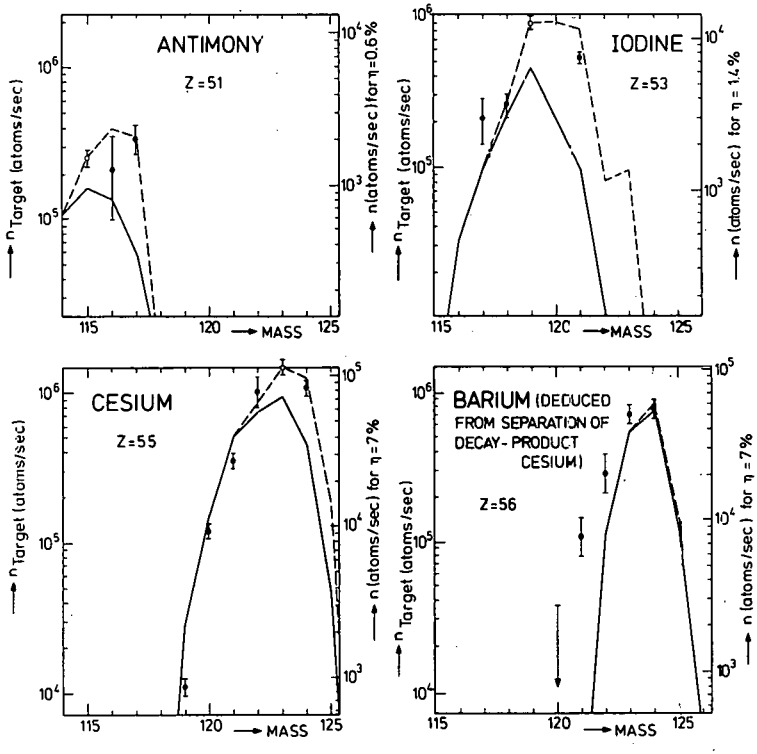

Figure 7. Isotopic distributions of antimony, iodine, cesium, and barium evaporation-residues from 5.9 MeV/u ^{40}Ar induced reactions on ^{89}Y. Experimental source strengths n of mass-separated samples are given as points. Calculated primary-production rates n_{Target} are drawn as solid lines for the independent cross section, dashed lines include cumulative effects. Experiment and calculation were fitted to each other by normalizing at one isotope (open point) for each element. The scaling factors correspond to overall efficiencies η. As barium was not released from the catcher, n was deduced via the decay-daughter cesium.

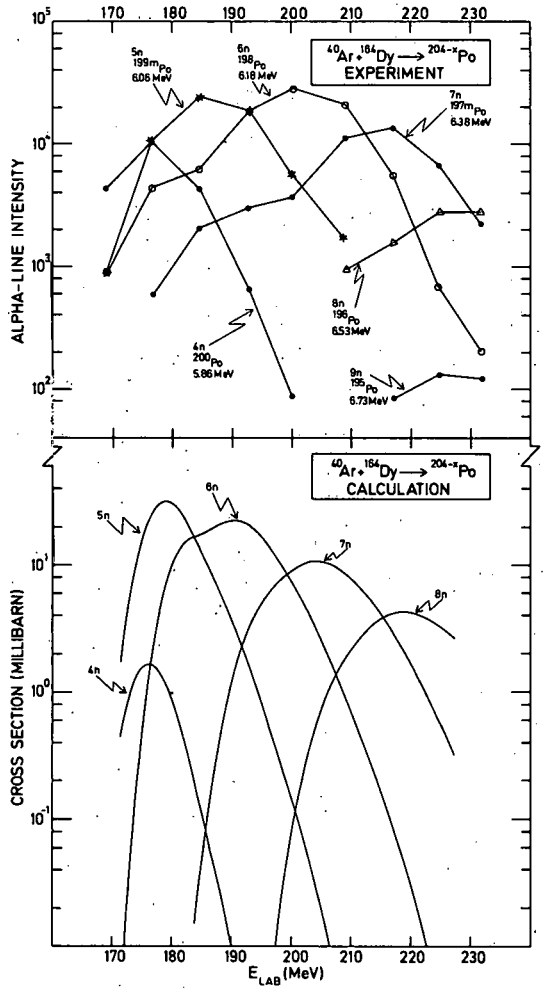

Figure 8. Excitation functions for the reaction ^{164}Dy (^{40}Ar, xn)$^{204-x}Po$. Calculations shown were made using a modified version (7) of the ALICE code (8). Experimental alpha-line intensities represent a preliminary evaluation with only approximate corrections for instabilities of the UNILAC beam and the corresponding activity fluctuations, the accuracy of the data obtained in this way is estimated to ±30%. Moreover, corrections for isotopic target-impurities and for energy spread of ^{40}Ar beam are not included. In order to use the alpha intensities as a relative cross-section measure, the alpha-branching ratio ought to be taken into account.

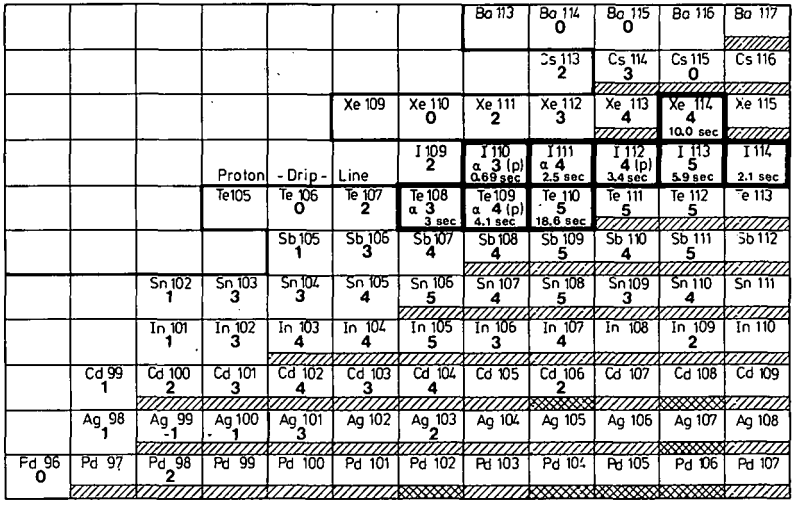

Figure 9. Part of the chart of nuclides showing production rates calculated by the ALICE code for a 290 MeV ^{58}Ni beam of $2 \cdot 10^{11}$ particles/sec incident on a 3.1 mg/cm^2 ^{58}Ni target (corresponding to excitation energies of the compound nucleus ranging from 50 to 80 MeV). The one-digit numbers below the isotope symbols indicate the order-of-magnitude of the production rate; 5, for example, stands for a range between 10^5 and 10^6 atoms/sec produced in the target. Hatched areas mark isotopes unambiguously identified in the literature. Cross-hatched areas mark stable isotopes. The new isotopes $^{108-110}Te$, $^{110-113}I$, ^{114}Xe (from ^{58}Ni on ^{58}Ni) and ^{114}I (from ^{58}Ni on ^{63}Cu) as identified in the present work are given with their measured half-lives and particle activities in heavily outlined boxes.

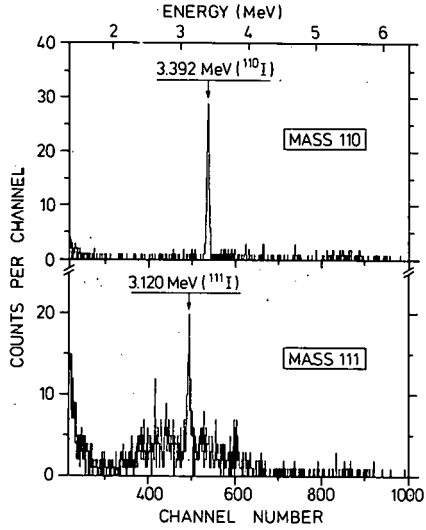

Figure 10. Particles spectra measured by means of a 300 mm^2, 300 µm thick surface barrier detector mounted at the collector position of the windmill system with a solid angle of 5% of 4π. The upper spectrum was accumulated at mass 110 during 1118 collection periods of 2.0 sec each. Both the 3.39 MeV alpha line ($T_{1/2}$ = 0.68 sec) and the "background" of delayed protons (0.70 sec) are assigned to ^{110}I. The lower spectrum was accumulated at mass 111 during 851 collection periods of 5.0 sec each. The 3.12 MeV alpha line (2.3 sec) is assigned to ^{111}I, the delayed protons (19 sec) to ^{111}Te. Protons and α particles were discriminated by means of ΔE-E telescope counting the same samples after a 90° rotation of the windmill wings.

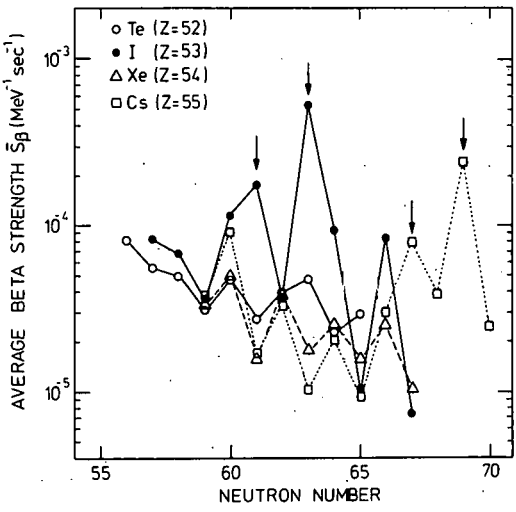

Figure 11. Average β strength functions $\bar{S}_\beta$ versus neutron number for neutron-deficient isotopes of Te, I, Xe, and Cs. Only cases with Q-C>2 MeV are plotted. Half-lives are from refs. (15,17) and from the present work except for ^{114}Cs (0.7 sec) and ^{115}Cs (1 sec) (18). In case of isomerism the ground-states hald-life was used (17). Competition with other decay modes was neglected (b=o), since the branching ratios for alpha decay observed in ^{108}Te, ^{109}Te, ^{110}I, and ^{111}I are expected to stay below 10%. For the apparently high average beta strength of the isotopes ^{114}I, ^{116}I, ^{112g}Cs and ^{124}Cs marked by arrows see ref. (11).

Fast Ion Beam Spectroscopy at the Marburg Separator.

oehle; H.Huehnermann; G.Kroemer; Th.Meier; H.Wagner; W.Walcher
Fachbereich 13, Philipps University, D-3550 Marburg, Renthof 5

Summary.

Fast ion beam spectroscopy of Xe and Ba has been performed at the Marburg off-line separator to determine the optical hyperfine structure and the isotope shift by means of a tunable laser. A reduction of the Doppler broadening of the spectral lines according to the calculations of Kaufman was observed. The error limits for the hyperfine splitting factors A and B and for the isotope shifts were in the order of 0.05 mK (~1.5 MHz). On-line measurements on Ba seem possible for an ion current of 10^5 ions/s with 100 counts per second at the detector in resonance.

Introduction:

The Marburg separator constructed by Walcher 1937 [1] has been used since its start in connection with optical hyperfine structure (hfs) and isotope shift measurements (is). The sensitivity of the classical measuring technique using a Schüler hollow cathode and Fabry-Perot interferometer has been increased considerably e.g. by introducing photon counting technique at the detector. The amount of material necessary for one experiment decreased from mg-quantities to ng-quantities. Thus we were able to include radioactive isotopes with half lives down to 5 days in our studies. The fast ion beam spectroscopy proposed by Kaufman [2] seemed to be especially suited for on-line work with short lived isotopes and therefore we investigated it experimentally with regard to line width, sensitivity and precision on xenon [3], barium [4] and now (in progress) lanthanum. Some related studies have been performed by other groups [5], [6], [7], [8].

The experiments

Fig.1 gives a schematical drawing of the experimental setup. Laser beam and mono-isotopic ion beam (here $^{129}Xe^{+}$) intersect in the focal plane of the separator. This range is observed by a photomultiplier. Ion energies were about 20 keV. A hollow cathode ion source was used for Xe and Ba, a surface ion source of the Johnson type for Ba and La. The laser beam is produced by a dye laser (Spectra Physics 580) which is pumped by a 5 W argon laser. The transition induced by the laser in the ion beam starts from a metastable ion state A in fig.2 and goes to the level D (λ = 605 nm). The fluorescence light has a wave length of 529 nm. The current of the photomultiplier as a function of the frequency scan of the laser is given in fig.3 for $^{129}Xe^{+}$. We observe a hfs pattern of three well separated components. For $^{131}Xe^{+}$ (see fig.4) only 7 of 9 components are to be seen.

The direct beam. Besides using a separated ion beam it is possible to use the direct beam without separation. Fig.5 gives the experimental setup with Ba while fig.6 shows the measured curve which contains the spectral lines for the most abundant Ba isotopes. The distances between lines of different isotopes are mainly given by the different Doppler shifts (due to the different velocities) and partly by the (atomic) isotope shifts.

Line width. Measuring the spectral lines in beam direction reduces the line widths ccnsiderably as shown in fig.7. The broad lines are se obtained in a Xe-gas discharge, the narrow ones are those ...m the fast ion beam experiment. Kaufman [2] has calculated that the broadening by Doppler effect of the spectral lines is reduced in the same measure as the differences in velocities which are reduced due to the acceleration by a factor

$$R = \frac{1}{2}\sqrt{\frac{kT}{eU_a}} \quad ; \qquad \begin{array}{l} kT \text{ thermal ion energy } \sim 0.1 \text{ eV} \\ eU_a \text{ acceleration energy } \sim 20 \text{ keV} \end{array}$$

$$(R \sim \frac{1}{900})$$

To observe the reduced line width the laser light has to be parallel to the ion beam (downstream) or antiparallel (upstream).

We estimate the contributions to the line width for Ba as follows:

contributions:	$\Delta\nu$
natural line width	$\sim$ 20 MHz
reduced Doppler broadening	$\sim$ 1 MHz
line width of laser	$\sim$ 10 MHz
high voltage ripple $\sim$ 1 V_{ss}	$\sim$ 15 MHz
ion beam divergence	$\sim$ 5 MHz
total line width estim.	$\sim$ 30 MHz
line width observed	$\geq$ 35 MHz

Power broadening. Fig.7 shows the influence of laser power on the line shape and height in a direct Ba^+-beam experiment. We observe above 16 mW a saturation and at 36 mW laser power even a dip in the ... shape while the half width increases with laser power. We cannot yet explain this phenomenon but it has to be taken care of in order to obtain narrow lines.

Sensitivity. To obtain a high sensitivity you have to reduce first the background light arriving at the photomultiplier. It results from a) reflected laser light; b) from the glowing ion source; c) radiation from the residual gas molecules after collisions with the ions.

Light with a frequency different from the observed transition is effectively reduced by a narrow band filter in front of the photomultiplier. Therefore reflected laser light is easily eliminated.

The influence of the ion source is only observed in direct beam experiments not with a separated ion beam. Gas radiation is reduced by reduction of the residual gas pressure and by eliminating ion beams not to be measured which may be done with separated beams. For a 10 nA Ba^+-beam ($6 \cdot 10^{10}$ ions/s) we obtained $2 \cdot 10^5$ counts per second at the detector.

The efficiencies of the different steps is estimated as follows

Process	efficiency
Production and transport of metastable ions	0.2
Excitation of the metastable ions in the observation region	0.1
Distribution on different hfs components	0.5
Transmission of the filter for the fluorescence light	0.7
Quantum efficiency of the photomultiplier	0.3
Solid angle of acceptance for the photomultiplier	0.003
Total efficiency	$\sim 10^{-5}$

By increasing the angle of acceptance and some smaller changes we hope to increase the efficiency by a factor of about 100, i.e. for an ion current of 10^5 ions/s a counting rate of 100 counts per second should be achieved.

These values would allow on-line operation on line a reactor. The time lag and the resulting limitation on the life times of the studied nuclei is only given by the on-line separation.

Application: Fast ion beam spectroscopy can be used to measure the nuclear spin I, the hyperfine structure splitting factors A,B, the isotope shift $\Delta\nu_{IS}$, and the mass of the ion m_i. I is calculated from the hfs pattern. A,B are calculated from the frequency differences of the hfs components. Our error is about 1.5 MHz and results from high tension instability and non-linearity of the laser scan. $\Delta\nu_{IS}$ is calculated from the frequency differences of identical transitions from different isotopes. Our error is in the order of 1.5 MHz. m_i has not been measured by us. You need large laser scans and preci-

sion measurements of the acceleration voltage according to Kaufman.

clusion: Our studies show that fast ion beam spectroscopy is well ted for on-line work with short lived nuclei. The precision of measurement is good and may be improved further by better stabilization of acceleration voltage and the laser. We are now building an on-line separator at the TRIGA-reactor at Mainz with a He-jet system. Beside other applications the separator will be used for fast ion beam spectroscopy.

Thank is due to Prof. M.Elbel for his assistance. The optical research has been supported by the Bundesminister für Forschung und Technologie while separator work has been subsided by the Gesellschaft für Schwerionenforschung Darmstadt.

[1] W.Walcher, Z.f.Physik 108 (1938) 376
[2] S.L.Kaufman, Opt.Comm. 17 (1976) 309
[3] Th.Meier et al., Opt.Comm. 20 (1977) 397
[4] C.Hoehle et al., Z.f.Physik A (1977) in press
[5] W.H.Iving et al., Phys.Rev.Lett. 36 (1976) 1488
[6] R.A.Holt et al., Phys.Rev. A 15 (1977) 2293
[7] K.R.Anton et al., Verh.DPG VI 12 (1977) 506
[8] M.Dufay et al., Phys.Rev.Lett. 37 (1976) 1678

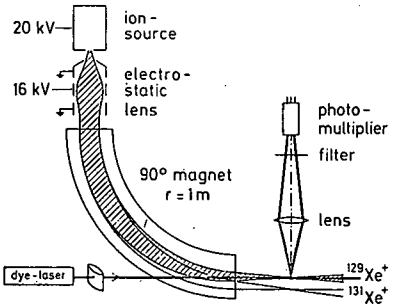

Figure 1.

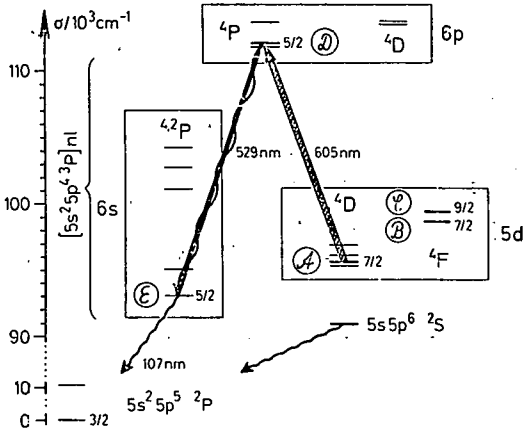

Figure 2.

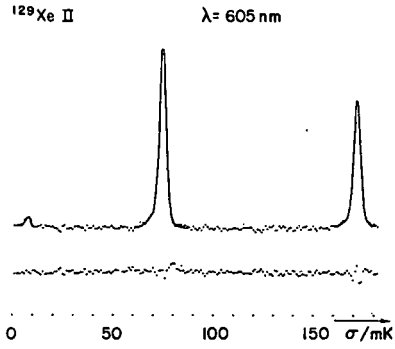

Figure 3.

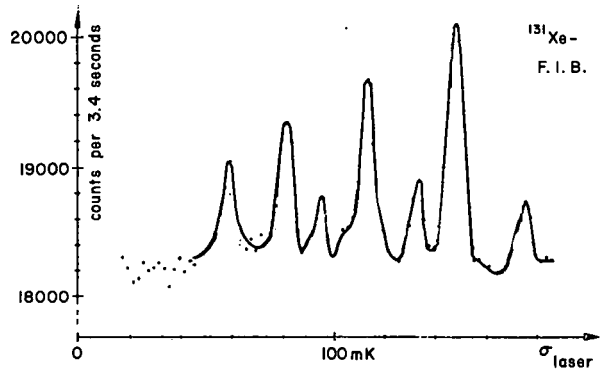

Figure 4.

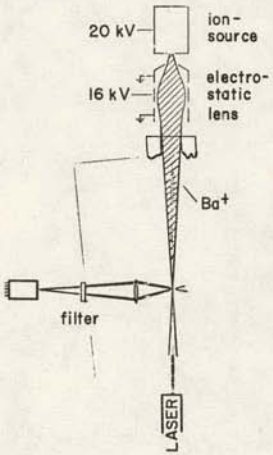

Figure 5.

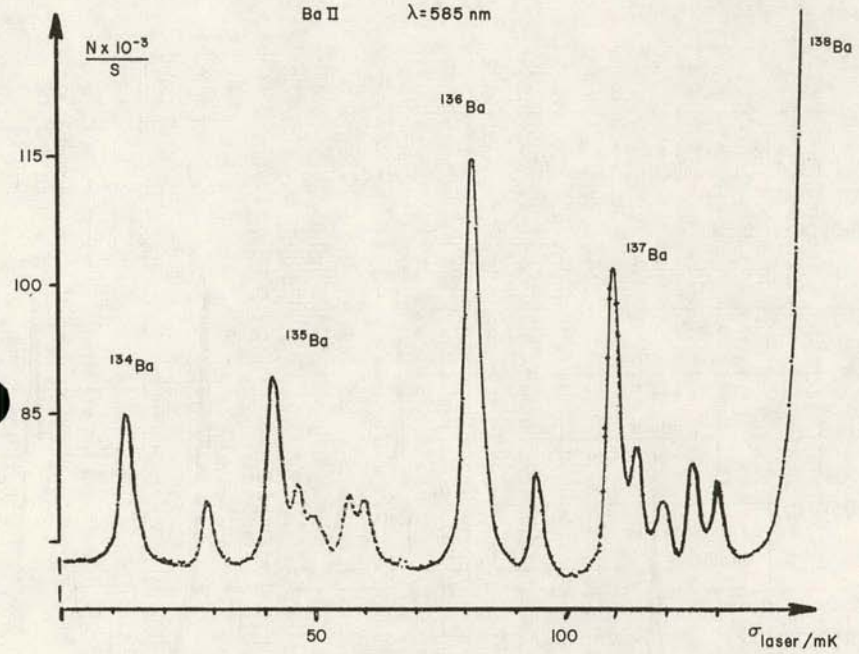

Figure 6.

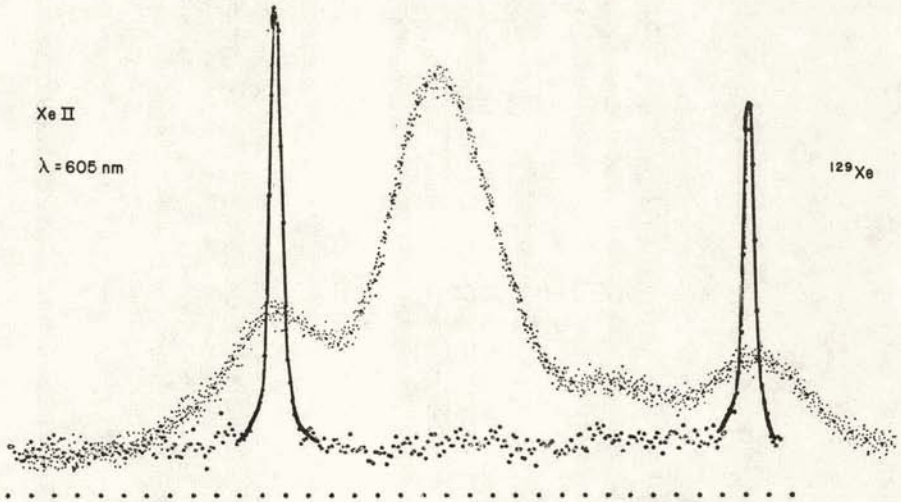

Figure 7.

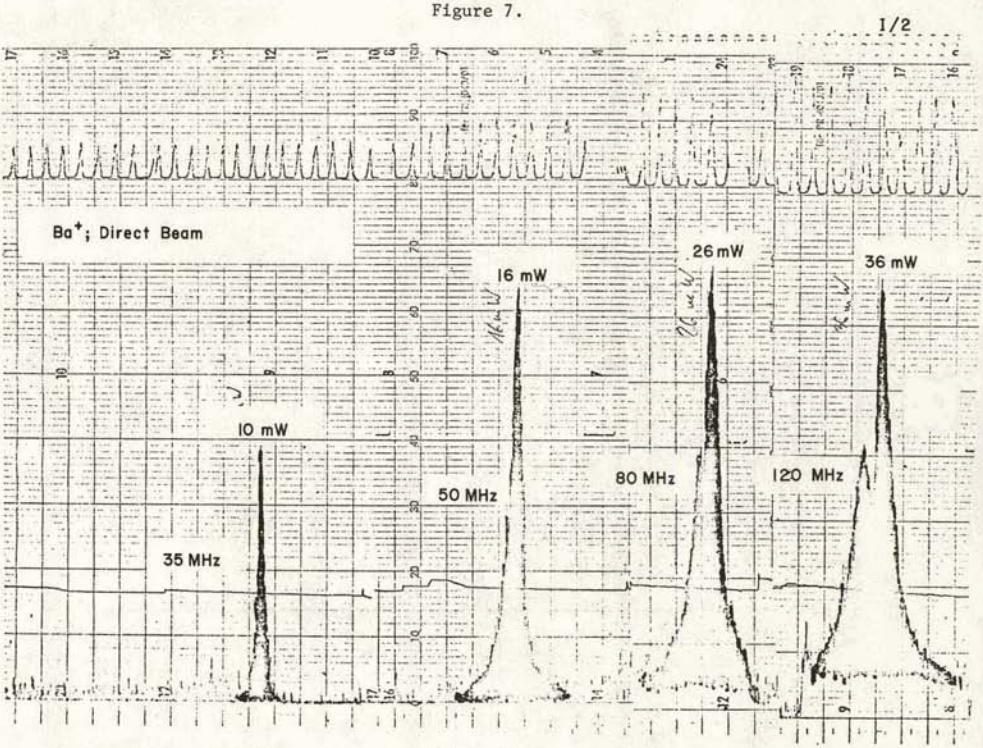

Figure 8.

LIST OF PARTICIPANTS

r. D. A. Alburger
Brookhaven National Laboratory, Department of Physics, Upton, NY 11973

Dr. R. A. Anderl
E G & G Idaho, Inc., P.O. Box 1625, Idaho Falls, ID 83401

Dr. M. Blume
Brookhaven National Laboratory, Department of Physics, Upton, NY 11973

Prof. D. S. Brenner
Clark University, Department of Chemistry, Worcester, MA 01610

Dr. J. L. Burnett
U. S. Department of Energy, Division of Nuclear Sciences, Washington, D.C. 20545

Dr. H. K. Carter
Oak Ridge National Laboratory, P.O. Box X, Oak Ridge, TN 37830

Dr. R. F. Casten
Brookhaven National Laboratory, Department of Physics, Upton, NY 11973

Prof. J. Cerny
University of California, Department of Chemistry, Berkeley, CA 94720

Dr. R. E. Chrien
Brookhaven National Laboratory, Department of Physics, Upton, NY 11973

Dr. Y. Y. Chu
Brookhaven National Laboratory, Department of Chemistry, Upton, NY 11973

Ms. J. A. Cizewski
Brookhaven National Laboratory, Department of Physics, Upton, NY 11973

Prof. J. M. D'Auria
Simon Fraser University, Department of Chemistry, Burnaby, B.C. V5A 156 Canada

Dr. E. der Mateosian
Brookhaven National Laboratory, Department of Physics, Upton, NY 11973

Dr. B. J. Dropesky
Los Alamos Scientific Laboratory, P.O. Box 1663, Los Alamos, NM 87545

Prof. C. L. Duke
Grinnell College, Department of Physics, Grinnell, IA 50112

Prof. D. D. Fossan
State University of New York at Stony Brook, Department of Physics, Stony Brook, NY 11794

Dr. G. Friedlander
Brookhaven National Laboratory, Department of Chemistry, Upton, NY 11973

Prof. J. B. Garg
State University of New York at Albany, Department of Physics,
Albany, NY 12222

Prof. M. Gartner
Iowa State University, Department of Physics, Ames, IA 50011

Prof. R. Gill
Iowa State University, Department of Physics, Ames, IA 50011

Dr. G. Goldhaber
Brookhaven National Laboratory, Department of Physics, Upton, NY 11973

Prof. G. W. Greenlees
University of Minnesota, Department of Physics, Minneapolis, MN 55455

Dr. R. C. Greenwood
E G & G Idaho, Inc., P.O. Box 1625, Idaho Falls, ID 83401

Prof. H. C. Griffin
University of Michigan, Department of Chemistry, Ann Arbor, MI 48109

Dr. J. C. Hardy
Atomic Energy of Canada, Ltd., Chalk River Nuclear Laboratory,
Chalk River, Ontario, K0J 1J0 Canada

Dr. P. Haustein
Brookhaven National Laboratory, Department of Chemistry, Upton, NY 11973

Dr. R. L. Heath
E G & G Idaho, Inc., P.O. Box 1625, Idaho Falls, ID 83401

Dr. E. A. Henry
Lawrence Livermore Laboratory, P.O. Box 808, Livermore, CA 94550

Prof. J. C. Hill
Iowa State University, Department of Physics, Ames, IA 50011

Dr. A. Huck
Centre de Recherches Nucleaires, 17 Rue Becquerel, 67037 Strasbourg,
France

Dr. J. Hudis
Brookhaven National Laboratory, Department of Chemistry, Upton, NY 11973

Dr. M. Huyse
Instituut voor Kern- en Stralingsfysika, Leuven University, Celestijnenlaan
200 D, B-3030 Heverlee, Belgium

Dr. W. R. Kane
Brookhaven National Laboratory, Department of Physics, Upton, NY 11973

Dr. S. Katcoff
Brookhaven National Laboratory, Department of Chemistry, Upton, NY 11973

Dr. M. J. Kenny
A.A.E.C. Research Establishment, Private Mailbag, Sutherland 2232, N.S.W. Australia

Prof. T. A. Khan
McMaster University, Tandem Accelerator Laboratory, Hamilton L8S 4M1, Ontario, Canada

Dr. O. Kistner
Brookhaven National Laboratory, Department of Physics, Upton, NY 11973

Prof. J. Lee
McGill University, Department of Physics, Montreal, Quebec, Canada

Prof. D. A. Lewis
Iowa State University, Department of Physics, Ames, IA 50011

Prof. T. K. Li
Iowa State University, Department of Physics, Ames, IA 50011

Dr. H. I. Liou
Brookhaven National Laboratory, Department of Physics, Upton, NY 11973

Ms. C. M. McCullagh
Brookhaven National Laboratory, Department of Physics, Upton, NY 11973

Dr. R. A. Meyer
Lawrence Livermore Laboratory, P.O. Box 808, Livermore, CA 94550

Prof. J. W. Mihelich
University of Notre Dame, Department of Physics, Notre Dame, IN 46556

Prof. R. A. Naumann
Princeton University, Department of Chemistry, Princeton, NJ 08540

Dr. J. M. Nitschke
Lawrence Berkeley Laboratory, Physics Division, Berkeley, CA 94720

Dr. Z. J. Parsa
New Jersey Institute of Technology, Department of Physics, 323 High St. Newark, NJ 07102

Prof. R. F. Petry
University of Oklahoma, Department of Physics, Norman, OK 73019

Prof. S. Prussin
University of California, Department of Nuclear Engineering, Berkeley, CA 94720

Dr. R. S. Raghavan
Bell Laboratories, Murray Hill, NJ 07974

Dr. P. L. Reeder
Battelle Pacific Northwest Laboratories, Richland, WA 99352

Dr. C. W. Reich
E G & G Idaho, Inc., P.O. Box 1625, Idaho Falls, ID 83401

Prof. L. Riedinger
University of Tennessee, Department of Physics, Knoxville, TN 37916

Prof. E. Roeckl
GSI Darmstadt, Postfach 110541, 6100 Darmstadt 11, Federal Republic of Germany

Dr. N. P. Samios
Brookhaven National Laboratory, Department of Physics, Upton, NY 11973

Prof. H. A. Schuessler
Texas A & M University, Department of Physics, College Station, TX 77843

Dr. P. Sen
Institute of Physics, A/105 Saheed Nagar, Bhubaneswar 751 007, India

Dr. G. J. Smith
Brookhaven National Laboratory, Department of Physics, Upton, NY 11973

Dr. E. H. Spejewski
Oak Ridge National Laboratory, P.O. Box X, Oak Ridge, TN 37830

Prof. G. D. Sprouse
State University of New York at Stony Brook, Department of Physics, Stony Brook, NY 11794

Dr. M. L. Stelts
Brookhaven National Laboratory, Department of Physics, Upton, NY 11973

Dr. P. C. Stevenson
Lawrence Livermore Laboratory, P.O. Box 808, Livermore, CA 94550

Dr. W. L. Talbert, Jr.
Los Alamos Scientific Laboratory, MS-560, P.O. Box 1663, Los Alamos, NM 87545

Prof. V. K. Tikku
State University of New York at Albany, Department of Physics, Albany, NY 12222

Dr. K. S. Toth
Oak Ridge National Laboratory, P.O. Box X, Oak Ridge, TN 37830

Prof. J. P. Vary
Iowa State University, Department of Physics, Ames, IA 50011

Prof. H. Wagner
Physialisches Institut, Phillips Universitat, D-355 Marburg, Lahnberge, Federal Republic of Germany

Prof. W. B. Walters
University of Maryland, Department of Chemistry, College Park, MD 20742

Dr. R. A. Warner
Battelle Pacific Northwest Laboratories, Richland, WA 99352

Dr. J. Weneser
Brookhaven National Laboratory, Department of Physics, Upton, NY 11973

Dr. S. L. Whetstone
U. S. Department of Energy, Division of Physical Research, Washington, D. C. 20545

Prof. S. A. Williams
Iowa State University, Department of Physics, Ames, IA 50011

Prof. F. K. Wohn
Iowa State University, Department of Physics, Ames, IA 50011

Dr. J. L. Wood
Georgia Institute of Technology, School of Chemistry, Atlanta, GA 30332

Dr. K. D. Wunsch
Institut Laue-Langevin, B.P. 156 Centre de Tri, 38042 Grenoble Cedex, France

Prof. E. F. Zganjar
Louisiana State University, Department of Physics, Baton Rouge, LA 70803